MICROSCALE EVALUATION OF DE NOVO ENGINEERED WHOLE CELL BIOCATALYSTS

Leonardo Rios Solis

A thesis submitted for the degree of
Doctor of Philosophy
to
University College London

Department of Biochemical Engineering
University College London
Torrington Place
London
WC1E 7JE
2012

‘I, Leonardo Rios Solis, confirm that the work presented in this thesis is my own. Where information has been derived from other sources, I confirm that this has been indicated in the thesis.’

ABSTRACT

Biocatalysis has emerged as a powerful tool for the synthesis of high value optically pure compounds. With advances in synthetic biology, it is now possible to design *de novo* non-native pathways to perform non-natural chiral bioconversions. However these systems are difficult to assemble and operate productively, severely hampering their industrial application.

The purpose of this study was to develop a microscale toolbox for the rapid design and evaluation of synthetic pathways, in order to increase their operational productivities and speed-up their process development.

The first aim of this work was to establish a microscale platform to accelerate the evaluation of different variants of transketolase (TK) and transaminase (TAm), in order to design and construct a *de novo* pathway for the one-pot synthesis of chiral amino alcohols. The second aim was to develop a microscale methodology to rapidly establish the complete kinetic models of the selected TKs and TAms, which would allow efficient operation of the one-pot synthesis. The third aim was to scale-up the production of the biocatalyst to pilot plant, while controlling and maintaining the desired level of expression of each enzyme. Finally the fourth aim of this project was to scale-up and simulate the complete one-pot syntheses to preparative scale, while predicting and applying the best reaction strategies and reactor configurations.

The experimental microscale toolbox was based on 96 microwell plates with automation capacities, where the one-pot syntheses of the diastereoisomers (2*S*,3*S*)-2 aminopentane-1,3-diol (APD) and (2*S*,3*R*)-2-amino-1,3,4-butanetriol (ABT) were designed and performed with final product yields of 90% and 87% mol/mol respectively. For the synthesis of ABT and APD, the wild type *E. coli* TK and the engineered D469E TK were identified as the best candidates respectively, and both enzymes were paired with the TAm from *Chromobacterium violaceum.*

A microscale methodology for kinetic model establishment was developed based on programmable non linear methods. The TAm step was found to be the bottleneck of the multi-step syntheses, due to the high a Michaelis constant of intermediate substrate erythrulose for the synthesis of ABT, and the low catalytic constants for the synthesis of APD. Also the amino donor substrate was discovered to be toxic for the TAm, as well as causing side reactions, thus affecting the overall performance of the *de novo* pathway.

The production of the *E. coli* whole cells containing the *de novo* pathway were successfully scaled-up to pilot plant without losing catalytic activity. By manipulating the fermentation temperature and induction time of TAm, it was found the desired level of expression of each enzyme could be achieved.

Finally, the complete one-pot syntheses were simulated using the previously established microscale kinetic models, which were found to be predictive of preparative scale bioconversions. A reactor with fed-batch addition of the amino donor was predicted as the best operating strategy in each case. Using this strategy, the one-pot syntheses allowed up to a 6-fold increase in product yield (% mol/mol), while using concentrations one order of magnitude higher than previously published preparative scale data.

As a conclusion, this work is the first of its kind to develop such a microscale modelling toolbox, which is designed to exploit the synthetic potential of engineered and recombinant enzymes, in order to design, simulate and optimize *de novo* engineered pathways. This makes the results of this work an original contribution for the process development of synthetic pathways.

.

ACKNOWLEDGEMENTS

I would like to thank my supervisor Professor Gary J. Lye, for believing in me to carry out this project. I also thank him for his support and guidance which lead to the successful achievement of the aims of this project, and for making my PhD experience so enjoyable. I thank also Dr. Frank Baganz for his invaluable advice during the project, and for trusting me with new ideas to improve the quality of my research. I would also like to thank Dr Paul A. Dalby for his help and support any time I needed it.

I dedicate this thesis to my family, who are the most wonderful gift I have in my life: they are my best friends. I thank them for inspiring me to set high goals in my life, and for teaching me that above all, a high goal is to become a better man, and that to become a better man, you need to first help your other friends. I thank them also for inspiring me to fight for this PhD, and for never letting me feel alone, even if half a world was separating us.

Following those principles, I want to thank Patty Morris and Homam Al-bahrani, who started with me this PhD adventure, and at the end they became more than friends: they are part of my family nowadays. I thank them for all the fun we had together in lab, promoting unlimited collaborations between protein engineering, microfluidics and microscale multi-step synthesis, while organizing parties in the office and singing like rock stars in the lab. I thank them also for all the good moments we had outside the lab, from trips to the end of the world, to the endless nights in the pub or the typical football games in Wednesday´s nights. But especially I thank them for supporting me in the difficult times, when I did even have to ask to receive a cheerful hand.

A special mention with all my gratitude goes to Chuanjie and Murni, who showed me how invaluable they are as friends. I thank them for all the collaborative research we did together, making the hard times in the lab become funnier times.

I would like to thank Akin Odeleye for been such a fantastic student, and for his important contributions in doing part of the pilot scale fermentations.

I would like to thank Armando Cázares for his important contributions synthesizing my products and substrates standards, as well as helping me to purify and analyse them.

Also, I acknowledge and would like to thank Nihal Bayir and Jian Hao for his important contributions in the kinetic modelling studies.

Finally, I would like to thank all the members and ex members of the BiCe group including Chris Grant, Raha Faharomi, Maria Francisca Villegas, Dawid Dreszcz, Panyupa Pankhong, Amana Halim, Subhas Pradhan, Sandro Matosevic among many others for all the inspiring discussions in the lab meetings relating with this project, as well as for making the lab environment so cheerful and motivating.

CONTENTS

LIST OF FIGURES

LIST OF TABLES

NOMENCLATURE AND ABBREVIATIONS

A260	Absorbance at 260 nm
ABT	(2S,3R)-2-amino-1,3,4-butanetriol
AP	Acetophenone
APD	(2*S*,3*S*)-2-aminopentane-1,3-diol
BRENDA	Braunschweig Enzyme Database
c	Protein concentration in mol L^{-1}.
CO_2	Carbon dioxide
CV20205	*Chromacterium Violaceum* 20205
d_B	Width of baffle (mm)
d_i	Diameter of impeller (mm)
DNA	Deoxyribonucleic acid
DOT	Dissolved oxygen tension (%)
d_T	Diameter of vessel (mm)
ε	Extinction coefficient
E. coli	*Escherichia coli*
EDTA	Ethylenediaminetetraacetic acid
ee	Enantiomeric excess
E_{iTAm}	Transaminase concentration
E_{iTK}	Transketolase concentration
E-PLP	Transaminase –PLP complex
E-PMP	Transaminase –PMP complex
EtOA	Ethyl alcohol
F	Feed rate (L hr^{-1}),
FeedRate	Feeding rate of MBA solution (L min^{-1})
λ	Path length equal to 1 cm
g	Gram
GA	Glycoaldehyde
g_{DCW}	Grams of dry cell weight
HEPES	N−2−hydroxyethylpiperazine−N'−ethanesulphonic acid
His_6-tag	6x histidine- tagged

HPA	Hydroxypyruvate
HPLC	High pressure liquid chromatography
IPA	Isopropylamine
IPTG	Isopropyl β-D-1-thiogalactopyranoside
K_1	Equilibrium constant of the first half reaction of transaminase
K_2	Equilibrium constant of the second half reaction of transaminase
K_{ABT}	Michaelis-Menten constant of ABT
K_{ABT}	Michaelis-Menten constant of APT
K_{AP}	Michaelis-Menten constant of AP
kDa	Kilo Dalton
K_{eq}	Equilibrium constant
K_{ERY}	Michaelis-Menten constant of ERY
k_f	Catalytic rate constant for the forward reaction
K_{GA}	Michaelis-Menten constant of GA
K_{HPA}	Michaelis-Menten constant of HPA
K_{iABT}	Inhibition constant of ABT
K_{iAP}	Inhibition constant of AP
K_{iAPD}	Inhibition constant of APD
K_{iERY}	Inhibition constant of ERY
K_{iGA}	Inhibition constant of GA
K_{iHPA}	Inhibition constant of HPA
K_{iMBA}	Inhibition constants of MBA
K_{iPA}	Inhibition constant of PA
K_{iPKD}	Inhibition constant of PKD
K_{MBA}	Michaelis-Menten constant of MBA
K_{PA}	Michaelis-Menten constant of PA
k_r	Catalytic rate constant for the reverse reaction
L	Litre
LB	Luria Bertrani
lGM	Phosphoglucomutase
MBA	Methybenzylamine
MBAFeed	Concentration of MBA in the feed
MeOH	Methanol
Mg	Magnesium
mg	Milligram
min	Minute

mL	Millilitre
mM	Millimolar
mmol	Millimol
NaOH	Sodium Hydroxide
Ni	Nickel
OD_{600}	Optical density at 600 nm
PA	Propionaldehyde
PK	Pyruvate kinase
PKD	(S)-1,3-dihydroxypentan-2-one
PLP	Pyridoxal 5´phospahte
pmol	Picomol
PMP	Pyridoxamine phosphate
PP	Pyrophsphate-binding domain
PPG	Polypropylene glycol
R_i	kinetic reaction rate of compound i (mM min^{-1})
RO	Reverse osmosis
rpm	Revolutions per minute
SA	Static surface area
SDS-PAGE	Sodium dodecyl sulfate polyacrylamide gel electrophoresis
t	Time
TAm	Transaminase
TFA	Trifluoroacetic acid
TK	Transketolase
TPP	Thiamine pyrophosphate
TRIS	Tris(hydroxymethyl)aminomethane
U	Units of enzyme activity (µmolmin^{-1})
µ	Specific growth rate (h^{-1})
UDP	Uridine 5'-diphosphate
UDPGE	UDP-galactose
µL	Microlitre
µm	Micrometer
μ_{max}	Maximum specific growth rate (h^{-1})
µmol	Micromole
UTP	Uridine 5'-triphosphate
UV/Vis	Ultra violet / visible
v	Reaction rate (mmol/min)
V	Volume (L)

V.fluvialis	*Vibrio Fluvialis*
v/v	Volume by volume
Vol	Working reaction volume (L)
V_W	Total well volume
Wt	Wilde type
x	Cell biomass (g_{DCW} L^{-1}),
Y	Yield of cell mass per unit of carbon source of glycerol (g g^{-1})
ω-TAm	ω-transaminase

1. INTRODUCTION AND AIMS OF THE PROJECT

> The chemist who designs and completes an original and aesthetically pleasing multi-step synthesis is like the composer, artist or poet who, with great individuality, fashions new forms of beauty from the interplay of mind and spirit (*Elias James Corey, Nobel lecture, 1990*).

1.1. Introduction to multi-enzyme catalysis

Enzymes have demonstrated their usefulness for chemical organic synthesis due to their moderate reaction conditions, reduced environmental impact, and their high chemo-, regio- and stereo-selectivity (Whitesides & Wong, 1985; Straathof et al., 2002; Woodley, 2008). In many cases, enzymes have emerged as the only tool to achieve the direct preparation of optically active compounds, resulting in many commercial applications

where the key feature is the enzymatic asymmetrical synthesis (Schmid et al., 2001; Breuer et al., 2004).

Conventional biocatalytic process development has focused on single reactions and their optimization (Murzin, 2008). Nevertheless, Nature did not design enzymes to be used in isolation, instead living beings have evolved effective multi-enzymatic strategies to synthesize and build complex structures from simple substrates (Roessner & Scott, 1996b). Enzymes working in cascades lead to important advantages to the cells in terms of storage and consumption of energy. It also enables them to minimize metabolic waste, make a reversible reaction irreversible, avoid the purification step of intermediates, and minimize inhibition or toxic effects of metabolites by keeping their concentration low among many other benefits (Bruggink et al., 2003; Schultheisz et al., 2008).

It was not until the late 1980s, with the discovery of the polymerase chain reaction, and the further development of metabolic engineering tools, that scientists started to mimic the exquisite multi-step efficiency shown by enzymes in Nature (Chotani et al., 2000). This has led to the successful investigation of multi-step, metabolically engineered pathways towards application as pharmaceutical production platforms (Burkart, 2003).

Nowadays, it is possible to design *de novo* non-native engineered pathways in heterologous hosts, to carry out specific non-natural bioconversions producing chiral compounds, difficult to obtain by existing biosynthetic pathways or chemical synthesis (Roessner & Scott, 1996; Prather & Martin, 2008; Martin et al.,2009; Dalby et al., 2009) .

This has led to the rapid expansion of molecular pathway construction, creating opportunities for the synthesis of a broad range of fine chemicals and pharmaceutical intermediates (Wilkinson and Bachmann, 2006). However, those opportunities have been rarely applied beyond laboratory scale, because such *de novo* engineered pathways are difficult to assemble, model, scale-up and operate productively (Meyer et al., 2007). In order to overcome those complexities, recent advances in protein engineering (Hibbert et

al., 2005; Dalby et al., 2009), microscale high-throughput methods (Lye et al., 2003; Micheletti & Lye, 2006), and modelling tools for biochemical processes (Chou & Voit, 2009; Sin et al., 2009) can be applied to facilitate the rational design of such systems. This would enable to harvest the potential of *de novo* pathways, leading to a greater integration of such systems in industrial scale synthesis (Lye et al., 2002).

1.2. Classification of multi-enzymatic processes

A multi-step enzymatic process uses two or more enzymes via parallel, cascade, or network configurations to achieve a desired synthesis (Findrik, 2009). Several classifications have been proposed for multi-enzymatic processes, depending on the nature of the biocatalyst (living cell, artificial cell, lysate, pure enzymes etc), the number of enzymes, vessels or recovery steps, integration with other type of catalysts (enzymatic, chemo-enzymatic etc), the purpose of the extra steps (equilibrium shift, cofactor regeneration, deracemization etc) among many other categories (Schilling et al., 1999; Bruggink et al., 2003; Hailes et al., 2007; Murzin, 2008). In this work, a simplified version of the classification proposed by Santacoloma et al., (2011) has been followed, and is represented in Figure 1.2.

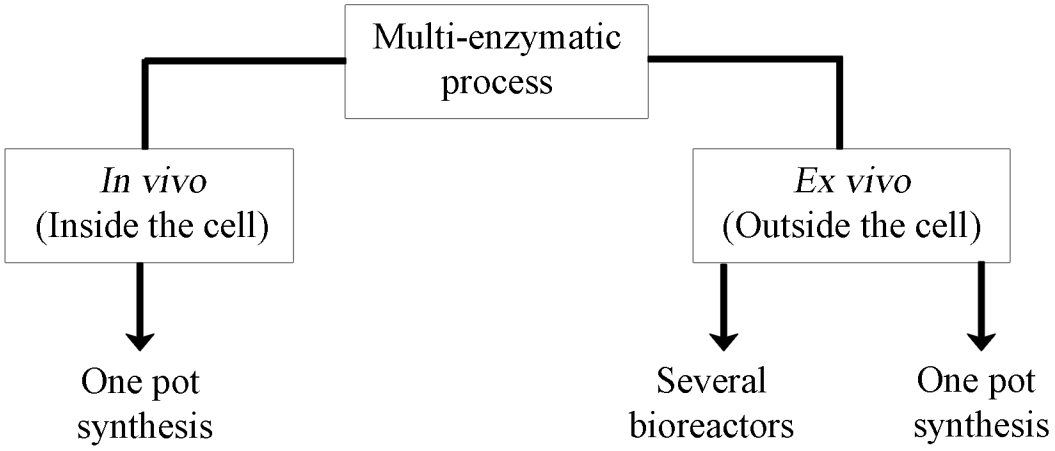

Figure 1.1. Classification of a multi-enzymatic process. Figure modified from Santacoloma et al., (2011).

In the first hierarchy, the multi-enzymatic processes have been classified as *in vivo* when the biocatalytic steps are carried out inside a living cell, and *ex vivo* when the reactions take place outside the cell.

Depending on the characteristics of the process and degree of compatibility of each enzyme, an *in vitro* multi-enzymatic synthesis can be operated in multiple or single reactors. For an *in vivo* synthesis, the metabolic pathway inside the cell cannot be separated into individual reactions, therefore is not feasible to carry out the process in more than one reactor (Findrik, 2009; Santacoloma et al., 2011). Those systems where a bioconversion is carried out using two or more enzymes in a single bioreactor are referred as "one-pot" synthesis, and the next sections will focus on this type of multi-step bioconversions.

1.2.1. One-pot synthesis

The traditional step-by-step approach to convert a starting material **A** into a final product **D** is using a single reactor for each enzymatic bioconversion step, in which intermediate products **B** and **C** would be isolated and purified for each conversion step (Figure 1.2a) (Bruggink et al., 2003). Such systems present the disadvantages of low overall yields due to loses in each separation step, higher capital investment, longer reaction times, laborious recycle loops and large amounts of waste produced in each downstream outlet (Findrik, 2009). In contrast, in a multi-enzymatic one-pot synthesis, a starting material **A** is converted by a set of enzymes in a single vessel to produce the final product **D** without separation of intermediates **B** and **C** (Figure 1.2b) (Sheldon, 2008).

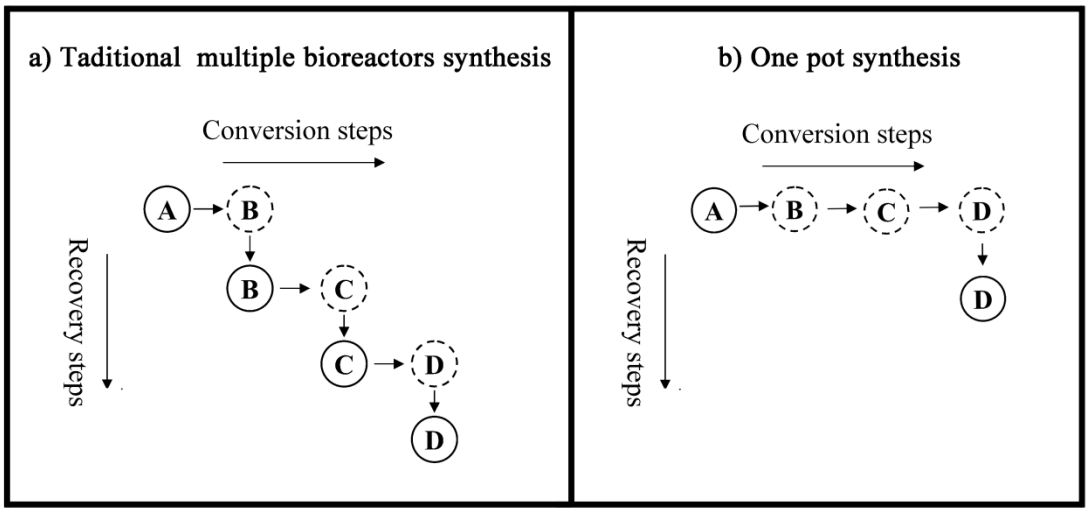

Figure 1.2. Configurations of a multi-step synthesis. (a) Traditional multiple bioreactors syntheses used in industry which involves a recovery step after each bioconversion. (b) One-pot synthesis as it is done in the cells which involves coupled reactions without intermediate recovery steps. Figure adapted from Bruggink et al., (2003) and from Sheldon, (2008).

In such one-pot processes, all the enzymes working together can be exploited simultaneously, leading to a reduction in the global reaction time, a decrease in the concentration of toxic intermediates, an improvement in the half life of the enzymes, an increase in the overall yield of the reaction, in addition to a considerable reduction in downstream processing and operation costs (Ingram et al., 2007; Murzin, 2008; Findrik, 2009; Kalaitzakis & Smonou, 2010).

However, the one-pot multi-step synthesis offers many challenges, given that each enzyme may have disparate optimal conditions; therefore optimum global conditions need to be identified, usually at the expenses of the most favourable kinetic steps in order to alleviate bottlenecks (Murzin, 2008). Non-beneficial side reactions between different promiscuous enzymes and the intermediates that occur as a result, diminish the final yield and severely affect the global economic performance of the process (Schmid et al., 2001; Pollard & Woodley, 2007). In addition, the global rate of the steps should be harmonized, avoiding the accumulation of toxic intermediates due to a fast reaction step,

as well as the substrate "starving" of another step, diminishing the benefits of the sequential operation (Roessner & Scott, 1996; Murzin, 2008).

Many different one-pot syntheses have tackled those initial challenges, and have been successfully demonstrated at laboratory scale with different objectives like *in situ* cofactor regeneration (Chenault et al., 1998; Schultheisz et al., 2008; Van Hecke et al., 2009), deracemization (Caligiuri et al., 2006; Koszelewski et al., 2009) and cascade biocatalysis (Ingram et al., 2007; Chi et al., 2008). A very complete review has been made by Bruggink et al., (2003) covering multi-step one-pot synthesis using pure enzymatic, chemoenzymatic, homogeneous and heterogeneous catalytic reactions, highlighting the many options and tools available for the synthetic scientist to design one-pot process. In the following sections, the main advantages about *in vivo* and *ex vivo* multi-enzymatic one-pot synthesis will discussed and relevant examples will be given; special emphasis will be given to the *in vivo de novo* pathways.

1.2.1.1. *Ex vivo* one-pot synthesis

When an enzyme is taken out the cell to perform a specific function, the process is considered *ex vivo*. Therefore, the application of several isolated enzymes in a single vessel can be viewed as a multi-step *ex vivo* synthesis (Roessner & Scott, 1996). *Ex vivo* processes can make use of catalysts in different forms, such as the trapping or enzymes in polymeric microcapsules (artificial cells) (Chang, 1988; Chi et al., 2008), immobilized enzymes (Sheldon, 2007; Matosevic et al., 2011) or cellular extracts and purified enzymes (Li et al., 1993; Woodley, 2006).

Using all those different forms of biocatalysts, elegant one-pot syntheses have been achieved, including an 8 enzyme one-pot synthesis of N-acetyllactosamine, involving the required regeneration of uridine 5'-diphosphate as shown in Figure 1.3 (Wong et al., 1982).

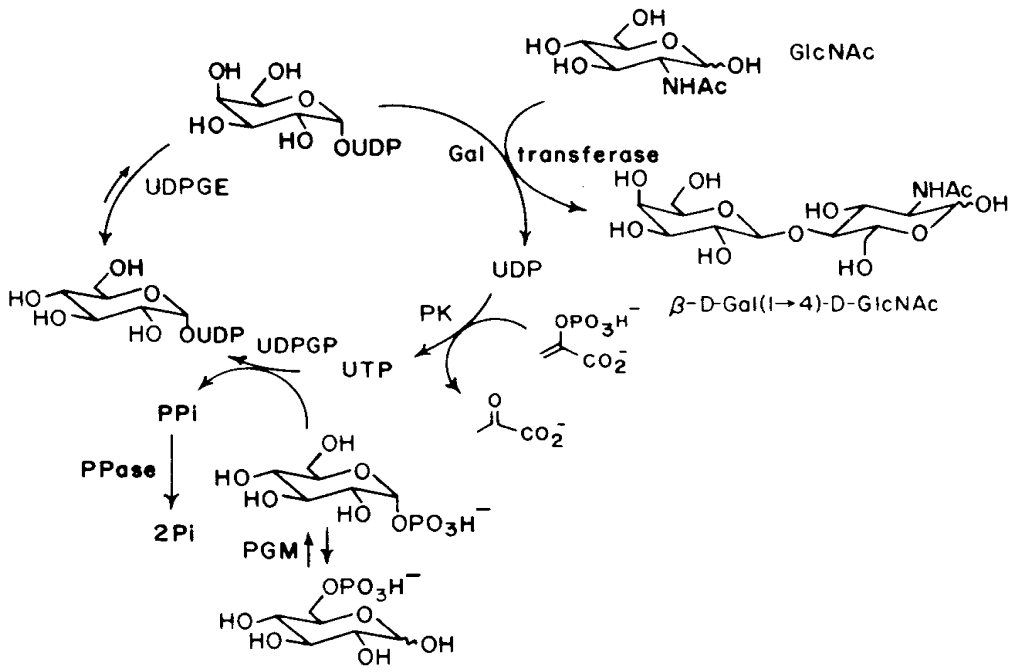

Figure 1.3. Multi-step synthesis of N-acetyllactosamine. Abbreviations: UDP: uridine 5'-diphosphate; UTP: uridine 5'-triphosphate; UDPGE: UDP-galactose 4'-epimerase; Gal transferase: galactosyl transferase; UDPGP: UDP-glucose pyrophosphorylase ; lGM: phosphoglucomutase; PK: pyruvate kinase; β-D-Gal(1→4)-D-GlcNAc: N-acetyllactosamine. Figure adapted from Wong et al., (1982).

A 12 step one-pot synthesis of a precursor of vitamin B12 has been achieved using purified cells, reaching an individual yield higher than 90% for each step, leading to an overall 20% yield mol/mol (Roessner et al., 1994; Scott, 1994; Roessner & Scott, 1996b). Of special interest is the 8 enzyme one-pot synthesis of riboflavin, where 6 enzymes performed synthetic steps and 2 were involved in cofactor regeneration achieving a final yield of 35% mol/mol (Rumisch et al., 2002).

The previous syntheses demonstrated the potential of *ex vivo* multi step one-pot synthesis. While it requires the isolation of the enzymes, *ex vivo* systems are not hampered by mass transfer limitations caused by the cell wall, they can work at conditions toxic for a cell such as high substrates or solvent concentrations, and avoid the cellular metabolic

pathway interference, which may compete for substrates (Roessner & Scott 1996a; Schultheisz et al., 2008; Santacoloma et al., 2011). Apart from its potential in synthesis, *ex vivo* systems are ideal for protein function identification due to the flexibility that they offer to the scientist to manipulate the enzymes, substrates and intermediates without any cellular background (Kajiwara et al., 2006).

The main drawback for *ex vivo* one-pot synthesis is that the cost associated to purify the enzymes usually does not allow scaling up the process beyond research scale (Rozzell, 1999; Meyer et al., 2007). It has been estimated that for a commercial process, a metric defined as cost of product/cost of gram of enzyme should be at least 1000 for a purified enzyme compared to 15 using a whole cell system, reflecting the difference in costs for each biocatalyst form (Pollard & Woodley, 2007). Immobilization will play an important role in lowering the associated costs of purification by recycling the enzyme (Sheldon, 2007; Tufvesson et al., 2010).

In vivo biocatalysis is a solution that can reduce the cost of production of the several enzymes involved in a multi-step synthesis; this type of system will be studied in more detail in Section 1.2.3.

1.2.1.2. *In vivo* one-pot synthesis

In vivo biocatalysis is considered the cheaper alternative for multi-step synthesis, because it has the potential to synthesize of all the desired enzymes within a single host, without any further processing (Woodley, 2006). With the advances in fermentation technology, using fed-batch strategies can allow cell cultures to easily reach bacterial densities of 50 to 100 g L^{-1} with up to 40% of the total protein being the desired enzyme (Lee, 1996; Shiloach & Fass, 2005). New trends in fermentation for biocatalyst production using *Pichia Pastoris* as the host cells could increase the yield of the cell density and the desired enzymes by 1 order of magnitude (Payne et al., 1997; Macauley-Patrick et al., 2005).

In addition, *in vivo* biocatalysis has the potential advantages of increasing the stability of the enzymes, especially for membrane bounds proteins or enzymes that require accessory cellular systems, as well as enabling easy regeneration of expensive cofactors, including sources of reducing equivalents and ATP among others (Wilkinson & Bachmann, 2006; Tufvesson et al., 2010).

Nevertheless, optimizing an expression system for *in vivo* biocatalysis is not straightforward, and many variables can have an impact on the production efficiency, like the choice of the vector, inducer system, medium composition, and growth conditions among others (Thiry & Cingolani, 2002). *In vivo* systems are generally more complex than their *ex vivo* counterparts, due to the complexity of the cellular metabolic network that is still present during the biocatalysis, therefore they present more challenges to be assembled and operated efficiently (Tyo et al., 2007). Special care needs to be taken to avoid side reactions, and a certain 'insulation' of the cellular metabolism can be obtained through the overexpression of the target genes relative to the background (Meyer et al., 2007). New approaches to minimize the harmful interference of the cellular metabolism include the use of reduced genomes, like the *E. coli* minima genome project (Pósfai et al., 2006).

Advances in metabolic engineering over the past 25 years have resulted in the engineering of microorganisms for the production of high value products for industrial scale (Burkart, 2003). Successful examples are the production of antibiotics (Li & Townsend, 2006; Rokem et al., 2007) or amino acids (Lee et al., 2007; Sprenger, 2007) using native engineered hosts. New tools of metabolic engineering have allowed the complete expression of heterologous pathways in new hosts with better growth and protein expression characteristics (Pfeifer, 2001; Carter et al., 2003).

Those previously mentioned examples show how *in vivo* one-pot synthesis using the metabolic engineering tools have become a reality (Tyo et al., 2007). Those examples focused on the manipulation and optimization of existing natural pathways. However in

order to take advantage of the full potential of the *in vivo* synthesis, it is necessary to shift towards the design of new *de novo* engineered pathways for both natural and unnatural compounds (Prather & Martin, 2008). The necessity arises due to the fact that the number of compounds of commercial interest greatly outnumbers the available characterized natural pathways and enzymes (Martin et al., 2009). From a top 12 list of biochemical targets highlighted by the U.S Department of Energy, only half had a known biochemical synthetic route (Werpy, 2004).

Prather & Martin (2008) classified synthetic engineered pathways not fully recruited from a single source in three categories as described in Figure 1.4. In the first category, different pathways can be gathered from different microorganisms and combined in a single host. Secondly, pathways can also be modified to produce new non-natural compounds. Lastly, by combining the previous two approaches, which are the recruitment of biosynthetic components from different sources and the modification of those components for new catalytic capabilities, lead to the third approach commonly known as *de novo* pathway design, which will be discussed with more detail in the next section 1.2.3.1.

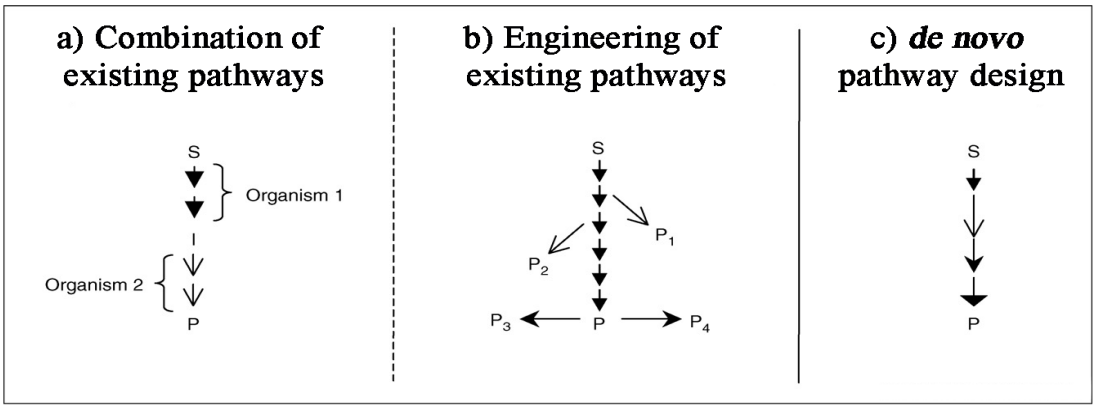

Figure 1.4. Strategies for pathway design to perform one-pot *in vivo* synthesis. (a) The pathway from S to I is from one organism while from I to P is from another. (b) New products P_i are produced from modifications or extensions of an existing pathway. (c) Each step in the pathway is proposed independently. This work will focus especially in this approach. Figure adapted from Prather & Martin (2008).

1.2.1.3. *De novo* pathway design

The essence that distinguishes a *de novo* pathway from the previously mentioned engineered pathways is that its design begins from scratch, without relying upon any natural precedent (Tyo et al., 2007; McArthur & Fong, 2010). Its creation involves linking unrelated enzymes towards the synthesis of unnatural compounds of high value. In theory, this approach offers incredible opportunities to synthesize a wide range of compounds, by taking advantage of the natural diversity of enzymes across species (Ferrer et al., 2005). Nevertheless, several big challenges and obstacles remain to be solved for *de novo* pathway design, due to the complete unnatural characteristic of the pathway, which may result in no natural set of enzymes capable to integrate it (Sprenger, 2007) . Therefore protein engineering tools emerges as a solution to compensate for the lack of natural enzymes to catalyze unnatural substrates (Dalby et al., 2009).

Few successful examples of *de novo* pathways exist nowadays which have solved this challenge, like the synthesis of the energetic material precursor 1,2,4-butanetriol, were multiple enzymes from *Pseudomonas fragi* and *putida* combined with native *E. coli* enzymes were screened to successfully design the *de novo* the pathway (Niu et al. 2003). Also several biofuels like isobutanol and 2-phenylethanol were successfully synthesized using a *de novo* pathway, by screening and exploiting the promiscuity of several enzymes of *Lactococcus lactis* and *E. coli* (Lee et al., 2008). An example of a *de novo* pathway used engineered enzymes of *Porphyromonas gingivalis* combined with *E. coli* enzymes, allowing the synthesis of 3-hydroxypropionic acid (Brazeau et al., 2006). A last elegant example involved the combination of an engineered pyruvate decarboxylase and 2-isopropylmalate synthase, which allowed the synthesis of a broad range of unnatural alcohols (Zhang et al., 2008).

In the previous examples, the objective of designing a *de novo* pathway was to find the best combination of enzymes that could work together *in vivo* to produce a new desired compound. Those enzymes could be wild type or engineered, and theoretically many

possibilities will exist, therefore tools that would allow the identification and characterization of the different enzymes to select the best combination is a central challenge of *de novo* pathway design (McArthur & Fong, 2010). High throughput microscale instrumentation combined with protein engineering and mathematical models would create a powerful tool to rapidly solve those problems. Those tools will be discussed in the Section 1.3.

1.3. Microscale high-throughput experimentation

Establishing an industrial biocatalytic bioconversion is usually a slow process compared with the traditional chemical routes (Yazbeck et al., 2004). This is due to the necessity to screen a large set of biocatalyst libraries in order to identify the appropriate enzymes, followed by large amount of data that needs to be collected at each stage of the process development (Lye et al., 2003; Fernandes, 2010). New strategies that could handle a large quantity of experiments in order to test all the different enzymes are necessary. High-throughput microscale techniques offer the potential to overcome those problems by considerably speeding up the process development with a minimum quantity of materials and time (Micheletti & Lye, 2006). The key advantages of such techniques are: (Lye et al., 2002, Lye et al., 2003).

- Rapid evaluation of large enzyme libraries.
- Reduction in the quantity of materials including expensive enzymes and substrates required for process development.
- Rapid generation of early data for process design and models establishment predictive of larger scale operations.
- Early identification of the optimum reaction conditions and reactor configurations.
- Capacity to automate the complete bioprocess.
- Promotion of a rapid and efficient translation from discovery to pilot plant scale.

The majority of the microscale bioprocesses studies have been performed on microwell systems of different geometries and sizes with scales ranging from 20 to 2000 μL (Doig et al., 2002). Figure 1.5 shows the dimensions of 3 standard size microwell bioreactors.

Although the use of microscale techniques has been heavily used since the last 2 decades for screening purposes, it is only recently that studies on fundamental engineering aspects have been performed, including mass and heat transfer phenomena and scaling up techniques (Zhang et al., 2008; Marques et al., 2009; Barrett et al., 2010).

Of special interest is the liquid mixing in such small reactors, which behave different from larger scale processes in terms of the importance of diffusion and convection (Matosevic et al., 2008). Orbital shaking of microwell plates has been found to be the most efficient way to promote mixing, and several studies have been conducted to determine the critical speed to assure an uniform mixing (Micheletti et al., 2006). These studies have lead to a better understanding of the reaction conditions and engineering principles of the microscale tools, allowing the establishment of key parameters for efficient scale-up (Islam et al., 2008) .

Recent studies have also focused on the quantification of enzyme kinetics using microscale tools (Lye et al., 2002). Of special interest is a study of a whole cell cyclohexanone monooxygenase performing the oxidation of bicyclic ketones to synthesize chiral lactones (Doig et al., 2002). In that work, the authors were able to characterize the oxygen mass transfer behavior under different reaction conditions and microwell geometries, as well as determining accurately substrate inhibition parameters.

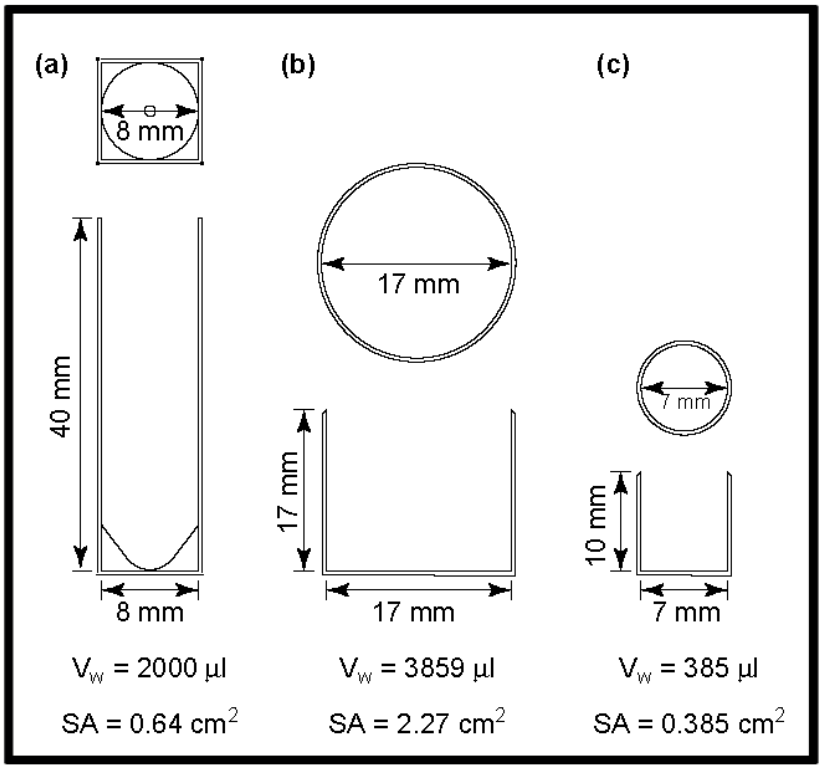

Figure 1.5. **Diagram representation of individual microwell formats: (a) 96-deep square well format; (b) 24-round well format; (c) 96-round well format. V_W represents the total well volume; SA represents the static surface area available for gas–liquid mass transfer. Figure adapted from Doig et al., (2002).**

Several other works describe quantitative methods for the determination of Michaelis - Menten parameters following spectrophotometrically the change in pH of the reaction through the use of pH dependent colorimetric dye. This method could be applied to any reaction that produce an acid or a base, but special care must be taken to avoid inaccuracies in the kinetic data collected, due to effect of the pH change in the behaviour of the enzyme (John & Heinzle, 2001; Truppo et al., 2009) .

The use of microscale techniques combined with analytical tools such as HPLC (high-performance liquid chromatography) for the reliable determination of kinetic parameters has been demonstrated using cellular extracts, pure and immobilized enzymes (Chen et

al., 2008; Matosevic et al., 2011). Of special interest is the work from Chen et al., (2009), where a full kinetic model was established using automated microscale tools, evaluating key parameters such as substrate and product inhibition.

Therefore microscale bioprocessing techniques emerge as an ideal tool that can be used to study and evaluate the different components of a complex bioprocess such as a *de novo* pathway, in order to generate quantitative data early on to better inform the process design, as will be discussed in the next Section 1.3.1 .

1.3.1. Microscale processing techniques for *de novo* pathway design

Microscale high-throughput would allow for the evaluation of each the *de novo* pathway, allowing the determination of the best enzyme candidate of each step under the global conditions of the one-pot synthesis.

Therefore, a retro-biosynthetic approach, similar to the one used in organic chemistry to design the synthesis target compounds, could be applied to design the *de novo* pathway (Prather & Martin, 2008). The approach would consider the bioconversion of functional groups rather than considering entire structures or initial substrates (Yazbeck et al., 2004). This retro-biosynthetic approach offers the challenge to be able to take advantage of the huge diversity of enzymes across species and also the engineered ones.

Nevertheless a methodology is necessary to be able to cope with the expanded possibilities of synthesis that *de novo* pathways offer, and microscale techniques emerge as a powerful tool to assist in that aspect. Figure 1.6 shows the proposed retro-biosynthetic methodology to design a *de novo* pathway, where microscale instrumentation plays a crucial role.

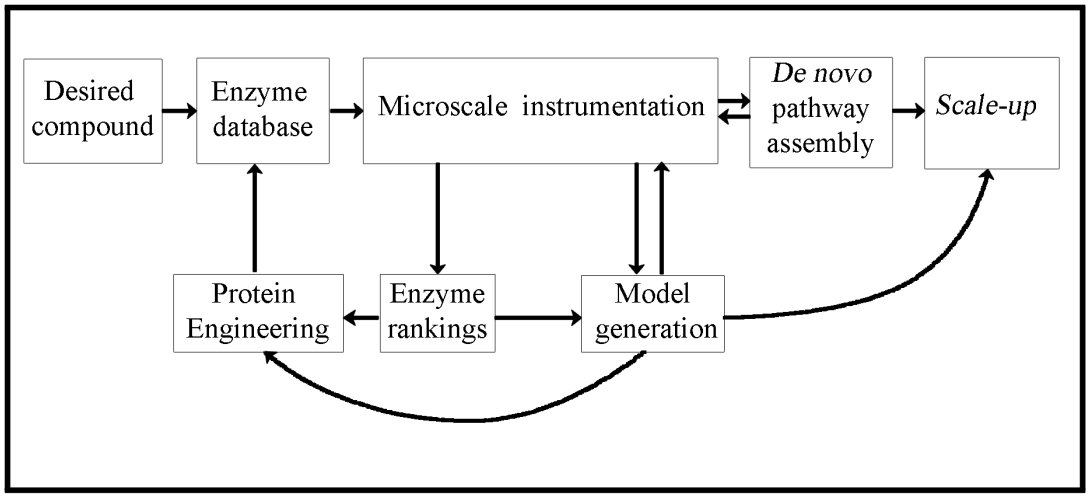

Figure 1.6. Methodology proposed in this work to design and optimize a *de novo* pathway for rapid process development.

Starting from a desired compound with specific functional groups, an enzyme recruitment step needs to be performed selecting many potential candidates for each individual reaction that needs to be performed. The recruitment could be made from databases like BRENDA (Schomburg et al., 2004) or SWISE PROT (Wu et al., 2006), or from specific previously developed libraries gathered in a particular laboratory. Using the high-throughput microscale tools, all the candidates could be evaluate under a defined set of conditions, and rankings could be given to each set of enzymes depending on their performance. Those "rankings" would inform in the identification of the best candidates for each reaction step, and also in the early determination of steps where new rounds of protein engineering were necessary.

Further characterization of the selected enzymes could be rapidly achieved due to the nature of the high-throughput platform, in order to develop mathematical models to predict and characterize the kinetic behaviour of each selected enzyme. This would have a considerable impact in the assembly of the *de novo* pathway, where cellular resources and physical space limit the overexpression of all the enzymes in a single cell (Tyo et al., 2007). Therefore the determination of the catalytic steps where strong overexpression

needs to be achieved to overcome the slower kinetic rate is necessary, at the expenses of the expression of the most kinetically fast enzymes.

The scalable nature of the microscale tools discussed in Section 1.3 would allow predicting larger scale operations. Hence the performance of the *de novo* pathway under many scenarios and reactor configurations could be analyzed. This would speed up the determination of the best reaction conditions, which would translate in a faster process development to manufacturing scale. The development of such models will be review in Section 1.4.

1.4. Modelling of biocatalytic processes.

Mathematical models are tools that contain information of a process in order to describe its behaviour under a limited set of physical conditions (Jimenez-Gonzalez & Woodley, 2010). For biocatalytic processes, they usually consist on differential and non-linear algebraic equations that describe the mass balance of substrates, intermediates and products as well and the different reaction rates (Meyer et al. 2007). Apart from promoting fundamental process understanding, such models can predict the outcomes under different scenarios and reactor configurations, enabling substantial time saving for the identification of the optimum reaction conditions (Chou & Voit, 2009; Santacoloma et al.,2011).

Sin et al., (2009) classified the models developed in biocatalysis according to their scope in the following categories:

- Enzyme: models aims to understand the molecular structure of the enzyme, explaining the interaction of the enzyme-substrate at a molecular level, leading to the prediction of the stereo-selectivity of an enzyme catalyzed conversion.
- Reaction: kinetic models describing reaction mechanism and reaction rate based on detectable and controllable inputs like concentration, pH and temperature.

- Reactor configuration: kinetic models describing the reaction rates and final outcomes in different reactor configurations. Those models include mass balance as well as transport phenomena conditions.
- Process: models allowing the analysis of the global performance of a process, including the interaction between different unit operations.

An illustrative representation of the different scopes of each type of model has been shown in Figure 1.7.

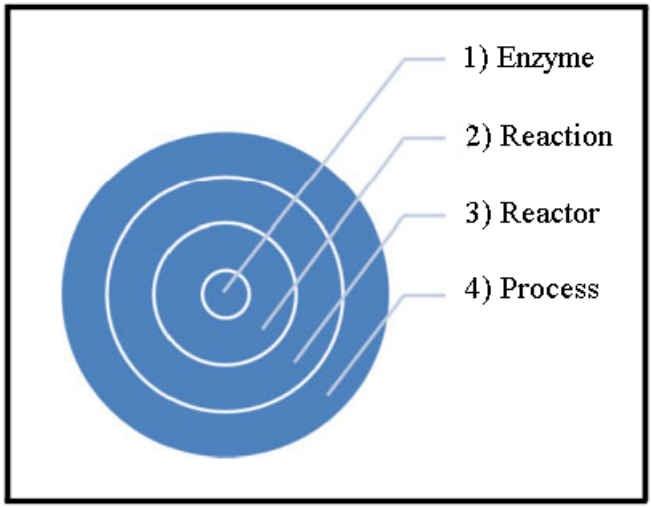

Figure 1.7. Representation of different models applied in biocatalysis categorized in the order of increasing scope: (1) intrinsic properties of the enzyme, (2) reaction kinetics, (3) reactor kinetics, and (4) process dynamics. Figure adapted from Sin et al., (2009).

Each model scope and the combinations of them can have their own increasing complexities. Nevertheless the more complex the model is, the more time and resources it will consume to be established(Sin et al., 2009). This can hamper the overall objective of establishing the models which is to speed up process development (Law et al., 2008). Therefore simplifications of the models need to be done, in order to speed up the design of a *de novo* pathway. For example, in the early screening procedure of the individual enzymes using the microscale techniques described in Figure 1.6; simple models describing the specific activity of the different enzymes could be used as the rankings for

decision making tools. Also, those simplified models could quickly permit the selection of appropriate reaction conditions for the overall one-pot synthesis.

When a potential candidate has been selected, the model complexity should be increased to establish the reaction kinetic model. The objective of the model would be to understand possible bottlenecks of the step (in order to inform subsequent protein engineering rounds), as well as to predict different scenarios to determine the best reaction conditions. The kinetic model developed in this step should not necessarily be very accurate in the enzyme scope level, as obtaining a complete understanding of the interaction of the enzyme-substrate at a molecular level would be time consuming, without necessarily bringing much extra information to impact in the decision making.

To finalize, when the kinetic models of the different steps have been established, they should be compared in order to identify the major bottleneck of the reaction, which will define the overall rate of the one-pot synthesis. Reactor models should be used to determine the best reaction configuration that would benefit each individual step. The reactor configuration should be selected to overcome the previously major detected bottleneck step of the reaction.

Therefore a global reaction model should be constructed which should integrate all the kinetic models and the selected reactor configuration. This model should enable to predict the global performance of the one-pot synthesis as well as the different simultaneous interactions between the different catalytic steps. In a one-pot synthesis, there is still room to modify different reaction conditions and configurations over the time of the bioconversion. For example, switching from a batch mode to a fed-batch transformation or changing the pH to switch on and off different enzymes could bring benefits (Schoevaart et al., 2000). The possibility to manipulate those conditions with perfect timing in order to optimize the overall one-pot synthesis only becomes a possibility due to the establishment of the different kinetic models.

1.4.1. Strategies to establish biocatalytic kinetic models

Figure 1.8 describes the general steps followed to establish kinetic mathematical models for bioprocesses (Sin et al., 2009).

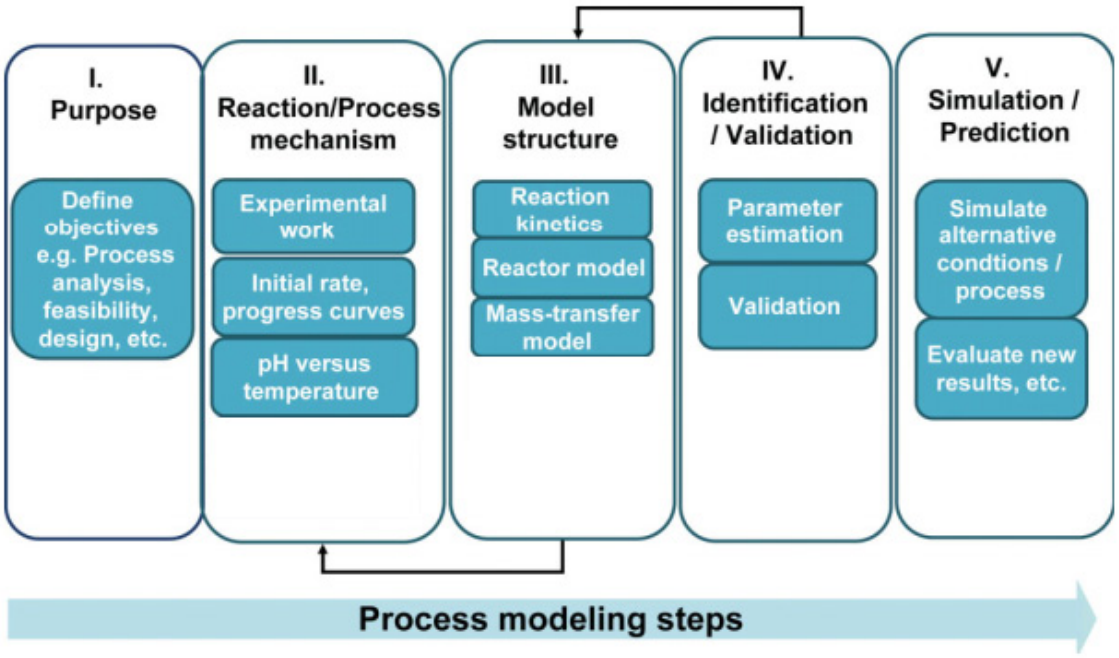

Figure 1.8. General common steps involved in the establishment of biocatalytic mathematical models, arrows indicate feedback loops between steps. Figure adapted from Sin et al., (2007).

This procedure should be applied to the "model generation" section represented in Figure 1.6. After establishing the objective of the model which will define the scope of mathematical model (reaction level scope for selected enzyme candidates) (Figure 1.7), experimental work should be planned and performed in order to establish the model structure and its corresponding parameters.

Traditional approaches were based on simplification of the kinetic models to linear plots, like the Lineweaver-Burk method, where the kinetic parameters could be successively determined using experimental initial rates (Lineweaver & Burk, 1934; Eisenthal & Crosnish-Bowden, 1974). Those methods have been found to be theoretically undesirable, because they distort the error weight after linearization of the equations, as

well as presenting large errors in the initial rate determination (Dowd & Rigss, 1965; Ranaldi et al., 1999). In addition, those methods require a large amount of experiments to establish all the kinetic parameters including inhibition constants, making them time consuming and unsuitable for the purpose of speeding up process development (Chen et al., 2008).

In order to overcome this problem, non-linear regression methods provide an alternative. In order to determine the kinetic parameters, those methods use optimization algorithms to fit a defined set of concentrations of substrates and products as a function of time, minimizing an objective function that punishes deviation between experimental and predicted data (Blackmond, 2005; Meyer et al., 2007).

The advantages of such techniques are that they consider the data of the full progress curves, in comparison to the initial rates used in the linear methods, therefore requiring much less experimentation. Also, they do not distort the error, are programmable and consequently faster and more reliable (Morbiducci et al., 2005; Chou & Voit, 2009).

However, the large number of parameters that needs to be estimated, and the highly non - linear nature of the equations can be difficult for the parameters determination (Gernaey et al., 2010). Initial estimates have been found to play a major role in the quality of the results using non-linear methods (Moros et al., 1996). Hybrid methods combining traditional initial rates experiments to identify a solution in the vicinity of the global minimum, with non-linear regression methods to determine the exact location of the global minimum have been successful (Katare et al., 2004; Chen et al., 2009).

Establishing a systematic model development methodology will be beneficial and necessary to design *de novo* engineered pathways for several reasons (Sin et al., 2009):

- Model development is more efficient, requiring less time and resources.

- Model development becomes a systematic routine, which can be easily applied to all the different enzymes of the *de novo* pathway.
- Following the same methodology, the comparison of the kinetic results of the different enzymes is more transparent.
- Communication and knowledge transfer among the members of a multidisciplinary team is facilitated.

Nowadays, there are practically no studies where full kinetic analysis and modelling of *de novo* engineered pathways have been performed. This is because such multi-step synthesis are usually focused on non natural substrates with several engineered enzymes in a same one-pot synthesis, which makes the process complex and requires large amount of experimentation to characterize (Murzin et al., 2008). By combining the advantages of high-throughput microscale instrumentation described in Section 1.3, with a systematic procedure for the establishment of kinetic models, and protein engineering, powerful toolboxes can be created to rapidly design and optimize *de novo* pathways as described in Figure 1.6.

In this work, the *de novo* synthesis of optically pure amino alcohols using a transaminase (TAm) and a transketolase (TK) was chosen as an example to demonstrate the applicability of the toolbox described in Section 1.3.1. In the next Section a state of the art of the *de novo* synthesis of amino alcohols will be given, as well as key information about the enzymes TK and TAm which integrate the pathway.

1.5. *De novo* pathway for the synthesis of amino alcohols

1.5.1. Relevance of amino alcohols

Due to the fact that the human body functions using chiral metabolites, the trend for new chiral pharmaceutical compounds is continuing to increase (Breuer et al., 2004). In 2000, 35% of intermediates were chiral and this number is expected to increase to 70% by 2010

(Pollard & Woodley, 2007). Therefore, it is not surprising that the main reasons for using biocatalysis is to perform synthetic steps with regio- and stereoselective properties (Schmid et al., 2001). Molecules with more than one chiral centre are compounds difficult to synthesize with organic chemistry, like the case of amino alcohols which are an ideal target for multi-step synthesis (Hailes, 2009).

Chiral amino alcohols are of great interest to the pharmaceutical and fine-chemical industries, since they are used as building blocks for several commercial optically pure compounds. For example they are necessary in the synthesis of protease inhibitors (Kwon & Ko, 2002), in particular the protein kinase inhibitor sphingosine (Smal & De Meyts, 1989), or the glycosidase inhibitor deoxymannojirimycin (Fuhrmann et al., 1984) and the HIV protease inhibitor Saquinavir (Kaldor et al., 1997). Optically pure amino alcohols are also used in the synthesis of detoxifying agents against antibiotics in the treatment for rice blast disease (Monache & Zappia, 1999) or serve as chiral starting material in the synthesis of various optically active molecules such as (S)-amphetamine (Rozwadoska, 1993) or broad spectrum antibiotics like chloramphenicol and thiamphenicol (Bhaskar, 2004; Boruwa et al., 2005).

The standard chemical synthesis route to produce optically pure amino alcohols is usually complex, requiring many steps in order to obtain the final product, resulting in low overall productivities (Hailes *et al*., 2009; Smithies *et al*., 2009). Using the retro-biosynthetic approach discussed in Section 1.3.1, TAm was selected to perform the amino group addition (Ingram et al., 2009), because of its superior features in asymmetric synthesis with high stereoselectivity and no need for cofactor recycling (Stewart, 2001). For the chiral alcohol, TK was selected because it could enable asymmetric synthesis of ketols with high stereoselectivity and no need of cofactors recycling (Ingram et al., 2009), in addition that it allowed to perform carbon-carbon bond formation, enabling the synthesis of complex molecules from simpler achiral starting substrates (Turner, 2000). The principal characteristics of TK and TAm will be summarized in sections 1.5.2 and 1.5.3.

1.5.2. Transketolase

1.5.2.1. Introduction to transketolase

Transketolase is an enzyme that catalyses a carbon-carbon bond formation by transferring a C_2 moiety (1,2-dihydroxyethyl group) between a ketose sugar and an aldose sugar (Sprenger et al., 1995) (Figure 1.9). The enzyme requires thiamine pyrophosphate (TPP) and Mg^{2+} as cofactors to perform the synthesis (Morris et al., 1996) .

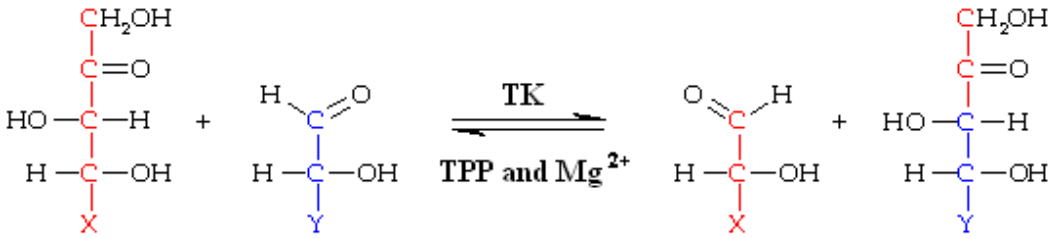

Figure 1.9. General reaction scheme of the carbon-carbon bon formation catalyzed by transketolase. A 1,2-dihydroxyethyl group is transferred between a ketose (red carbon skeleton) and an aldose (blue carbon skeleton). X and Y could be variable groups.

In vivo, the enzyme creates a link in conjunction with transaldose between the non-oxidative branch of the pentose phosphate pathway and glycolysis. The reactions it catalyze are the conversion of D-xylulose-5-phosphate and D-ribose-5-phosphate to D-sedulose-7-phosphate and D-glyceraldehyde-3-phosphate (Figure 1.10a); and the conversion of D-xylulose-5-phosphate and D-erythrose-4-phosphate to D-fructose-6-phosphate and D-glyceraldehyde-3-phosphate as shown in Figure 1.10b (Sprenger et al., 1995). In plants and photosynthetic bacteria, transketolase is also found in the Calvin cycle where it catalyzes the reverse reaction of the previously mentioned conversions (Schenk et al. 1998)

Ex vivo, several transketolases have been found to accept a wide range of substrates, making it ideal to integrate de novo pathways. Of particular interest is the use of β-hydroxypyruvate (HPA) as keto donor so that CO2 is released as a side product, making the reaction irreversible (Figure 1.10c) (Mitra & Woodley, 1996). Using HPA as a substrate, the specific activity of the TK of *E. coli* has been found to be 6 and 30 times higher than the yeast or spinach activities (Sprenger & Pohl, 1999), in addition the TK of *E. coli* can form carbon–carbon bonds between a broader range of substrates including hydroxylated and unphosphorylated compounds (Pohl et al., 2004).

The feasibility of the production of the enzyme at larger scale has been demonstrated up to 1000 litres (Hobbs et al., 1996). The clarified cell extract these authors obtained contained about 230 U/ml of the enzyme, which represented about 40% of the total cell protein. Those results make the *E. coli* TK a very good candidate for industrial catalysis (Turner, 2000) and to be part of a *de novo* pathway for the synthesis of amino alcohols.

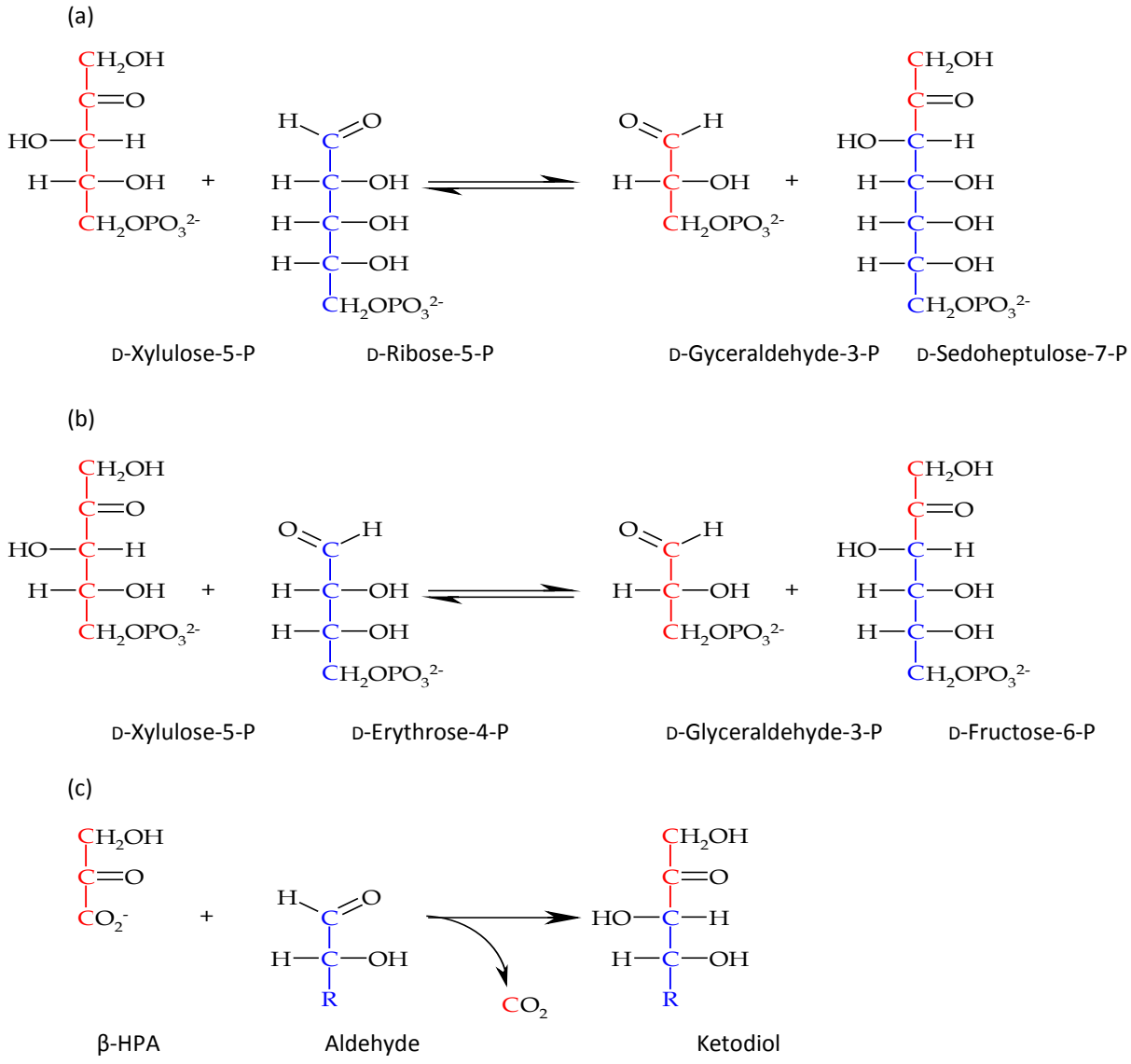

Figure 1.10. Reactions catalyzed by TK in vivo and ex vivo. Reactions (a) and (b) are reversible reactions that occur *in vivo* in the pentose phosphate pathway and Calvin cycle. Reaction (c) is used *ex vivo* where β-HPA is used as the keto donor to make the reaction irreversible by releasing CO_2.

1.5.2.2. Structure of transketolase

The *E. coli* TK is homodimer with a subunit molecular weight of 72 kDA. The active sites of each subunit are located at the interface between the two identical components of the homodimer. The thiamine diphosphate cofactor is also situated at the interface

between these two subunits (Sprenger et al., 1995) . Figure 1.11 shows the ribbon structure of the enzyme.

Figure 1.11. Ribbon structure of the *E. coli* transketolase homodimer. One monomer is coloured blue and the other is colored grey. Figure Created from the PDB structure file 1QGD using PyMOL Molecular Graphics System (DeLano, 2002) on World Wide Web http://www.pymol.org

Each subunit of TK is composed by three domains as can be seen in Figure 1.12. The amino-terminal, or PP-domain, consists of a five-stranded parallel β-sheet with α-helices on both sides. The second domain, the Pyr-domain, is a six-stranded parallel β-sheet, sandwiched between α-helices. Both domains are involved in binding TPP and therefore have an important role in catalysis. The carboxy-terminal domain or C-domain contains a mixed β-sheet with four parallel and one antiparallel strand, it does not contribute any amino acids to the active site and its function remains unclear (Muller et al., 1993; König et al.,1994).

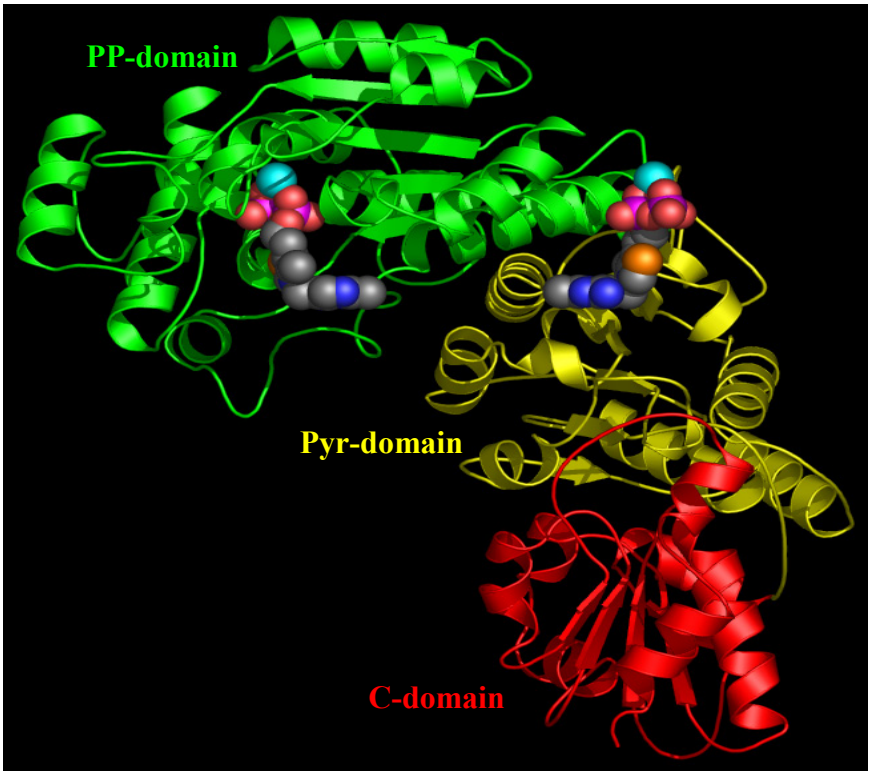

Figure 1.12. Ribbon structure of a single subunit of *E. coli* transketolase. Two TPP molecules, which bind to the PP- and Pyr-domains are shown as spherical space-filling models. The divalent metal ion Mg^{2+} binding to TPP required for catalytic activity is highlighted in cyan. Figure created from the PDB structure file 1QGD using PyMOL Molecular Graphics System (DeLano, 2002) on World Wide Web http://www.pymol.org.

1.5.2.3. Kinetic mechanism of transketolase

The kinetic mechanism of TK follows a ping pong bi-bi ordered mechanism, which can be described as two half reactions which are represented in a condensed way in Figure 1.13 (Sayar et al., 2009). Using HPA as the keto donor and any aldehyde (**AL**) as keto acceptor, in the first half reaction, **HPA** binds the enzyme (**E**) in the (through the cofactor TTP) and is cleaved releasing CO_2, while forming a covalently bound active intermediate, the 2-α-carbanion of 1,2-dihydroxyethyl-TPP (**F**). In the second half of the reaction, the 2-α-carbanion (**F**) suffers a nucleophilic attack by the aldehyde (**AL**),

forming the second product, a ketose with an extended 2 carbon skeleton (**K**) while releasing the enzyme in its original form (**E**).

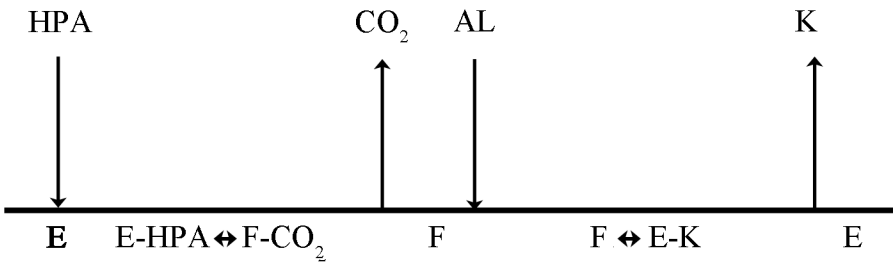

Figure 1. 13. Representation of the ping pong bi-bi ordered mechanism followed by TK using HPA as keto donor and any aldehyde (AL) as keto acceptor. E represents the enzyme in its original form, K is the enzyme in its activated form, HPA is hydroxypyruate, and K is the final ketose product.

The reaction mechanism at a molecular level is shown in figure 1.14 (Wikner et al., 1997). For modelling purposes, this is a fine example of the different scopes that a model can cover as illustrated in Figure 1.7. Using the mechanism in Figure 1.13 would be appropriate for developing models at reaction level, while using the mechanism represented in Figure 1.14 would be necessary to develop a more complex model at enzyme level. Although the model resulting from the Figure 1.14 would give more information, due to time limit constrains of process development, all the kinetic models to design and optimize the *de novo* pathway will be done in this work at the reaction level scope.

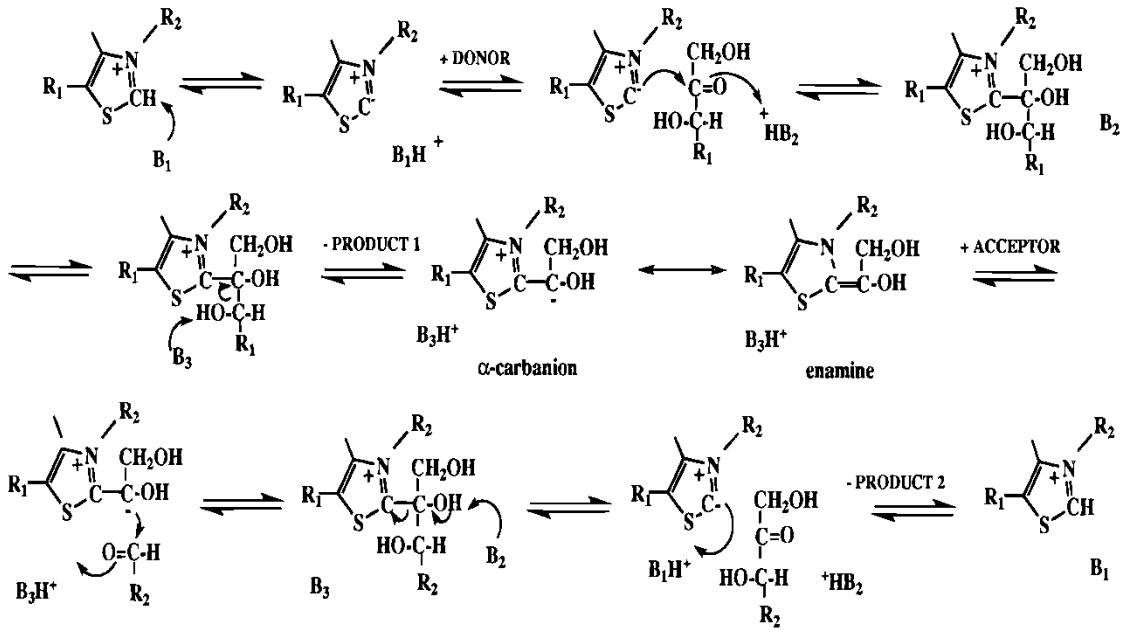

Figure 1.14. Molecular scheme of the TK ping pong bi-bi ordered kinetic reaction mechanism. B1-B3 represents catalytic groups involved in the proton transfer steps during the reaction. Figure adapted from Wikner et al., (1997).

1.5.2.4. Applications of transketolase in multi-step synthesis

Due to the high demand of carbon-carbon bon formation with stereoselective properties, TK has been applied in several multi-step syntheses to produce compounds of high value (Turner, 2000). For example, TK has been employed in a chemoenzymatic reaction to produce 6-deoxy-L-sorbose, which is a precursor of furanol that is used as a fragrance component in the food industry (Hecquet, 1996) . In this bioconversion, HPA was prepared from L-serine through the use of serine glyoxylate aminotransferase. The aldehyde 4-deoxy-L-threose which would be the keto acceptor of TK was produced through the microbial isomerisation of 4-deoxy-L-erythrulose using whole cells of *Corynebacterium equi* or *Serratia liquefaciens*. TK was finally used to perform a carbon-carbon bond formation between 4-deoxy-L-threose and HPA, thus yielding 6-deoxy-L-sorbose (L Hecquet 1996).

TK has also been applied for the synthesis of the unnatural sugar 4-deoxy-D-fructose 6-phosphate through another multi-step chemoenzymatic synthesis shown in Figure 1.15 (Guérard et al., 1999). (*R,S*)-1,1-diethoxy-3,4-eqoxybutane (**1**) was resolved using an epoxide hydrolase from *Aspergillus niger* in order to give (*S*)-epoxide (**2**) with a yield of 30% and >98% enantiomeric excess. This epoxide was converted into the corresponding phosphorylated (S)-aldehyde (**3**) (via a phosphate inorganic treatment followed by acidic hydrolysis). The aldehyde was then reacted with (**4**) L-erythrulose in the presence of the *S. cerevisiae* TK. This generated 4-deoxy-D-fructos 6-phosphate (**5**) with a yield of 52%. The glycolaldehyde (**6**) that was released was reduced *in situ* using yeast alcohol dehydrogenase and catalytic NADH.

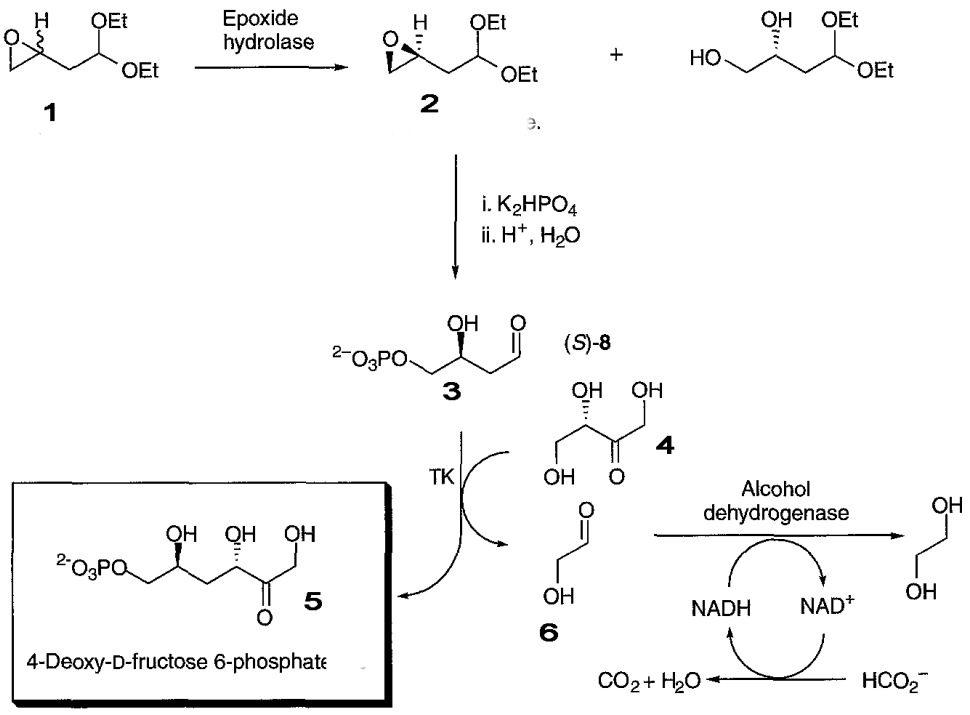

Figure 1.15. Chemoenzymatic multi-step synthesis of 4-deoxy D-fructose 6-phosphate using an epoxide hydrolase and *S. cerevisiae* TK. Figure adapted from Hecquet (1996) and Tuner (2000).

Another example of using TK in a multi step synthesis involved the synthesis of D-xylulose 5-phosphate where TK was combined with an aldolase and isomerise to obtain a final yield of 82 % mol/mol (Zimmermann et al., 1999).

1.5.3. Transaminase

1.5.3.1. Introduction to transaminases

A transaminase or an aminotransferase is included in the class of enzymes like the acid dehydrogenases (Brunhuber & Blanchard, 1994) or the amine dehydrogenases ((Hyun & Davidson, 1995) that convert a carbonyl group to an amino group as shown in Figure 1.16. The enzyme needs the cofactor pyridoxal 5´ phosphate (PLP) to catalyze the reaction .(John, 1995)

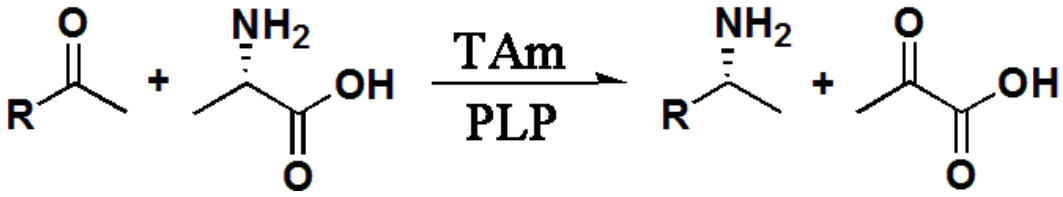

Figure 1.16. General reaction scheme of a TAm reaction where an amino group is transferred to a carbonyl group.

In vivo, TAms are one of the key enzymes for the formation of desired amino acids at the expense of the catabolism of proteins. The main aim of a transaminase reaction within amino acid metabolism is to collect the amino groups from several different amino acids in the form of mainly L-glutamate (L-alanine in a lesser degree) (Lombardo et al., 1989; Davies, 1961) . This L-glutamate then functions as an amino group donor for biosynthetic anabolism or for the nitrogen excretion pathway (Urea Cycle) (Stitt et al., 2001).

Ex vivo, several transaminases with broad range of substrate specificity have been identified (Taylor et al., 1998). This has lead to their increasing industrial application for the synthesis of either natural or unnatural D- or L-amino acids (Stewart, 2001) .

1.5.3.2. Classification of transaminases

The classification of the different TAms has been done through sequence homologies, this classification corresponded with the structural classification of the substrates utilized by the enzymes according to the position of the amino group transferred with respect to the carboxyl group of the substrate. Therefore the TAms have been divided in four groups. Groups I, III, and IV are comprised of α-TAm whilst the ω-TAm make up Group II (Mehta et al., 1993; Mehta & Christen, 1994). The ω-TAm has the potential to access a range of substrates not accepted by the α-TAm, as the need for an α-amino acid or α-keto acid is not necessary (Shin & Kim, 1999; Koszelewski et al., 2010a). Several ω-TAm have been reported to show catalytic activity towards primary and secondary amines which do not need to have a carboxylic group (Shin & Kim, 2001; Koszelewski et al., 2010).

The α-transaminases have been studied more extensively due to their potential in the industrial synthesis of amino acids (Stewart, 2001). However, in part due to the similarity between the products and substrates, low equilibrium constants have prevented their industrial use (Tufvesson et al., 2011).

The synthetic potential of several ω-TAms have been studied, including ω-TAms from *Klebsiella pneumoniae*, *Bacillus thuringiensis* JS64, *Vibrio fluvialis* JS17, and *Arthrobacter sp* among others (Shin & Kim, 1997; Shin & Kim, 2001; Iwasaki et al., 2006; Yun & Kim, 2008). Among them, the ω−TAm from *Vibrio fluvialis* showed the best performance for kinetic resolution and asymmetric synthesis of chiral amines (Shin & Kim ,2001). The enzyme showed high selectivity towards (*S*)−enantiomers such as (*S*)−α−methylbenzylamine (MBA), and was capable of convert a broad range of ketones, making it ideal for asymmetric synthesis (Shin et al., 2003). Nevertheless the enzyme suffered from strong product and substrate inhibition, and different studies using *in situ* product removable have been developed. Examples are using a biphasic media (Shin &

Kim, 1997) (Shin & Kim, 1999b), a reduced pressure system (Yun et al., 2004) , or membrane reactors (Shin et al., 2001) among others .

1.5.3.3. Structure of transaminase

Figure 1.17 shows the ribbon structure of the homodimeric TAm from *Vibrio Fluvialis*, where each subunit had a molecular weight of 50 kDA.

.

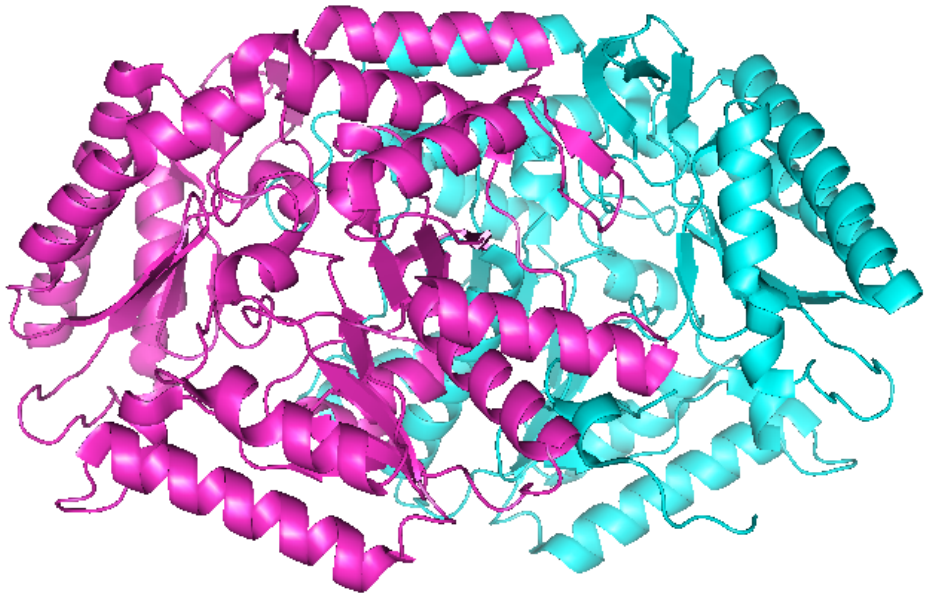

Figure 1. 17. Ribbon structure of homodimeric TAm from *V. fluvialis* JS17. Figure created from the PDB structure file 1qgd using PyMOL Molecular Graphics System (DeLano, 2002) on World Wide Web http://www.pymol.org.

An active site model of the TAm has been constructed (Figure 1.18) (Shin & Kim, 2002). This resulted in a two-binding site model, which contained two pockets, one large and one smaller, the latter one presenting a strong repulsion for a carboxlate, playing an important role in the substrate specificity and stereoselectivity. The large pocket showed a dual recognition mode for both hydrophobic and carboxyl groups, and corresponded to

a carboxylate trap, while the small pocket played the role of a side chain recognition site. (Shin & Kim, 2002).

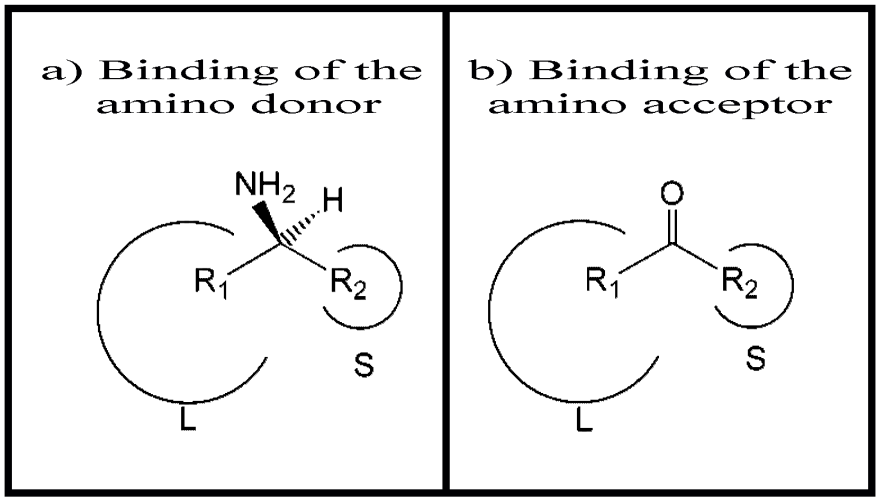

Figure 1.18. Two-Binding Site Model of TAm of *V. fluvialis* showing (a) the binding of the amino donor and (b) the binding of the amino acceptor. L and S denote large and small binding pockets respectively. Figure adapted from Shin & Kim (2002).

1.5.3.4. Reaction mechanism of transaminase

The TAm catalyzes the enzymatic amino transfer by a ping-pong bi–bi ordered mechanism analogue to the one of TK shown in Section 1.5.2.3 (Bulos & Handler, 1965) (Smith et al., 1998). The reaction mechanism is represented in Figure 1.19 where in the first half reaction, the amino donor (**AN**) binds to the enzyme and the amino group is transferred to the pyridoxal 5´phosphate (**EPLP**), which forms pyridoxamine 5-phosphate (**EPMP)**, and the respective keto product (**A**) is released. During the second half reaction, the EPMP transfers the amino group to the acceptor substrate (**B**) and EPLP is regenerated, while the new aminated compound is released (**B-N**) (Christen and Metzler, 1995).

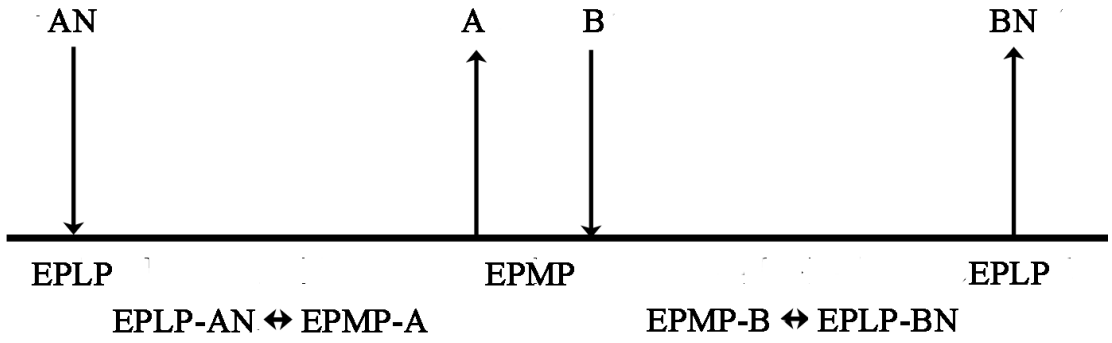

Figure 1.19. Schematic representation of the ping pong bi-bi ordered reaction mechanism used of TAm.

Some TAm have been reported to form "dead end complexes" between E-PLP or E-PMP and an incorrect substrate (for example an amino acceptor binding E-PLP or an amino donor binding E-PMP). Depending of the degree of inhibition that those abortive complexes could cause, they may need to be taken into account in the modelling of the reaction (Bulos & Handler, 1965; Shin & Kim, 1998).

1.5.3.5. Applications of TAm in multi-step synthesis

TAm has been used in many multi-step syntheses for chiral amine catalysis. The majority of the multi-step syntheses involving TAm have had as objective to overcome the low equilibrium constant which hampers the reaction (Talylor, 1998). A elegant example is the *in vivo* production of *L*-2-aminobutyric acid, where the overexpression of *E. coli* aromatic TAm, *E. coli* K12 threonine deaminase and *Bacillus subtilis* acetolate synthase was achieved in a single host to perform the one-pot synthesis (Figure 1.20) (Fotheringham et al., 1999). The threonine deaminase catalyzed the *in situ* formation of transaminase substrate, 2-ketobutyrate from *L*-threonine, while the synthase eliminated the pyruvate by-product which enabled to shift the equilibrium towards the forward reaction, which normally was 50% using the TAm individually.

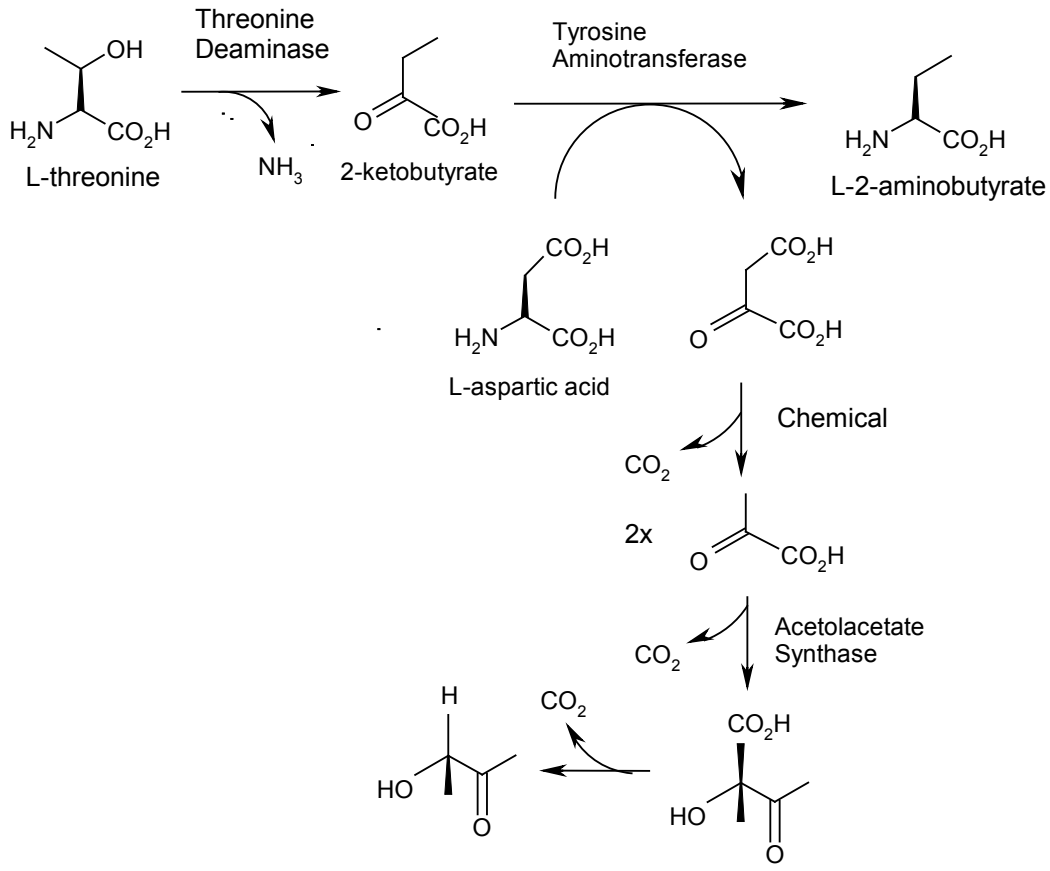

Figure 1. 20. Engineered multi-step pathway for the synthesis of L-aminoburyric acid. Figure adapted from Fotheringhan et al., (1999).

Also, combining an enzymatic transamination and dehydrogenation step *ex vivo*, it was possible to shift the equilibrium of the bioconversion to produce optically pure amines with yields higher than 90% (Figure 1.21) (Truppo et al., 2010) .

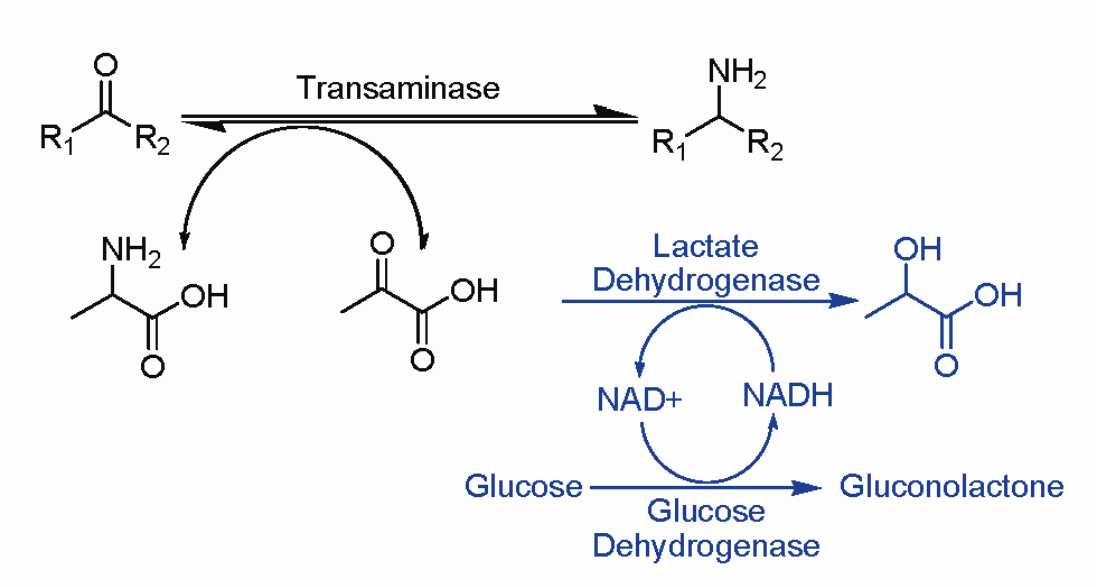

Figure 1.21. Synthesis of chiral amines combining an enzymatic transamination and dehydrogenation step in order to shift to equilibrium towards the forward reaction. Figure adapted from Truppo et al. (2010).

Recently, in our research group, the ω-TAm from *Chromobacterium violaceum* (TAm CV2025), was identified to be the best TAm for stereoselective ketodiol amination from a pool of 17 recombinant TAms (Kaulmann et al., 2007; Sayer et al., 2007). The enzyme had a molecular weight of 51 kDa and exhibited 38% sequence identity to the TAm from *V. fluvialis* studied in Section 1.5.3.3. It was also found to be a homodimer with a similar catalytic site as the TAm from *V. fluvialis* illustrated in Figure 1.18 (no crystal structure has been published). The CV2025 TAm was of special interest for the *de novo* pathway design of amino alcohols as the majority of the TAms cannot catalyse the conversion of ketodiols, which could be produced by TK. In the next section, a literature review of the state of the art of the *de novo* engineered pathways for the synthesis of amino alcohols will be discussed.

1.5.4. One-pot synthesis of chiral amino alcohols

The *de novo* pathway approach for the synthesis of amino alcohols was firstly demonstrated for the synthesis of the single syn-diastereoisomer (2*S*,3*R*)-2-amino-1,3,4-butanetriol (ABT) (Ingram et al., 2007). This was performed by using erythrulose (ERY) and glycolaldehyde (GA) as achiral substrates for TK, and (*S)*-(α)-methyl benzylamine as amino donor for the TAm, and by overexpressing the *E. coli* TK and the β-alanine-pyruvate TAm from *Pseudomonas aeruginosa* in a single *E. coli* host to perform the *in vivo* one-pot synthesis as shown in Figure 1.22. ABT is an important building block in the pharmaceutical industry, which for example has the potential to be used to synthesize the chiral core of the protease inhibitor drug Nelfinavir™ (Kaldor *et al.,* 1997).

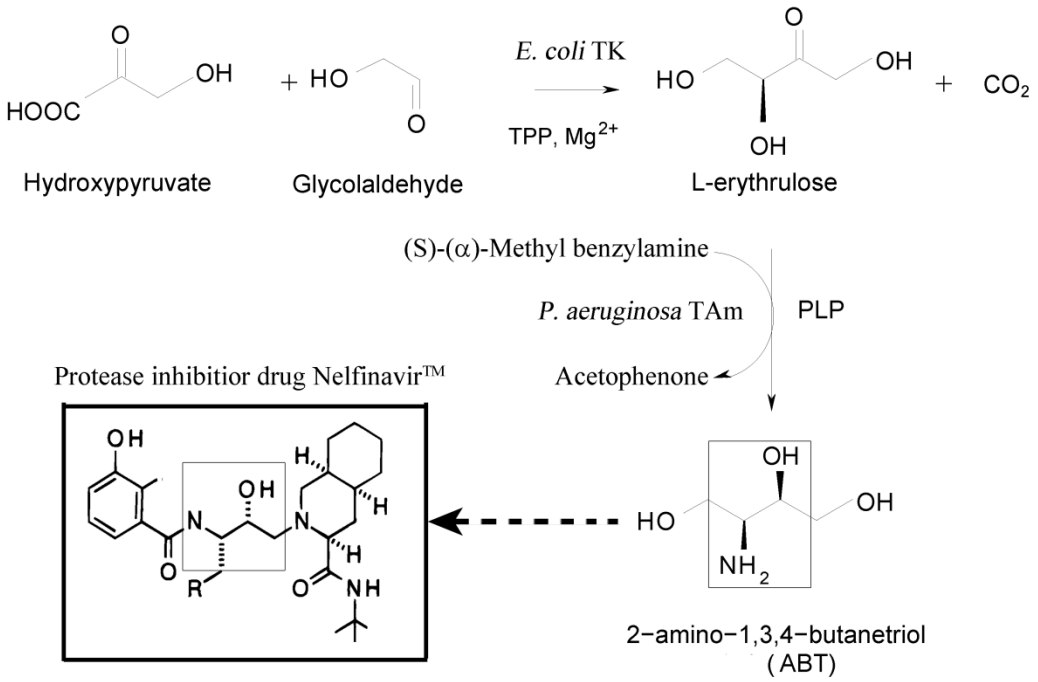

Figure 1.22. The synthesis of chiral amino alcohol 2-amino1,3,4-buntanetriol (ABT) from achiral substrates glycolaldehyde and hydroxypyruvate using a *de-novo* TK–TAm pathway. TPP is thiamine pyrophosphate and PLP is pyridoxal 5´phospahte.

The main limitation of this one-pot synthesis was the low activity of the β-alanine-pyruvate TAm causing a low overall yield of the reaction, as well as a lack of mathematical models to determine the best reaction conditions (Ingram et al., 2007).

Consequently, several libraries of engineered TKs and novel TAms have been constructed, which could be used as a recruitment source to design new *de novo* engineered pathways for amino alcohols with increased performance (Hibbert et al., 2007; Kaulmann et al., 2007; Hibbert, et al. 2008; Smith et al., 2008). Of special interest was one work where I collaborated, where the potential of different *E. coli* TK mutants to accept new substrates with high stereoselectivity was predicted using molecular modelling bioinformatic tools like direct docking (Full paper attached in Appendix XIV) (Cázares et al., 2010). The TK residue D469 was predicted to have a crucial role in accepting new substrates like propionaldehyde (PA), which could be a useful starting material for the *de novo* pathway of amino alcohols (Figure 1.23).

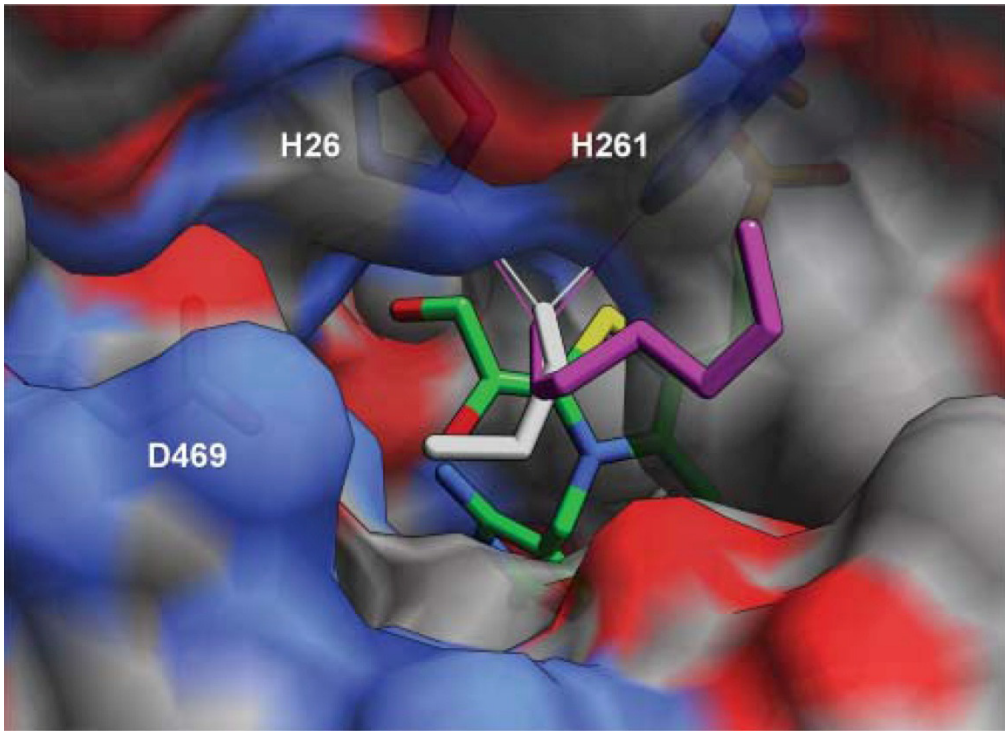

Figure 1.23. **Aldehydes propionaldehyde (grey) and butanaldehyde (magenta) docked into the TK active site containing the modelled TPP-enamine intermediate (green). A surface plot is shown with the key residues D469, H26 and H261 highlighted as sticks beneath the surface. Figure adapted from Cázares et al., (2010).**

Also, of great relevance was the identification and characterization of the CV2025 TAm, which showed great potential for amino alcohols synthesis as mentioned in section 1.5.3.5.

Recent work has shown that the synthesis of (2*S*,3*S*)-2-aminopentane-1,3-diol (APD) could be achieved in two separate TK and TAm bioconversions, where the *E. coli* TK mutant D469T and the CV2025 TAm enzymes were selected (Smith et al., 2010). Compounds like APD which contains the chiral 2-amino-1,3-diol moiety are an important class of pharmaceutical building blocks with their motif present in antibiotics, antiviral glycosidase inhibitors, and sphingolipids (Hailes *et al*., 2009). The synthesis was achieved by using HPA and PA as achiral substrates for the mutant D469T *E. coli* TK to synthesize the intermediate (*S*)-1,3-dihydroxypentan-2-one (PKD), and after a

purification step to isolate PKD, IPA was used as the achiral amino donor using the CV2025 TAm to synthesize APD with a final yield of 13% mol/mol respect to the initial TK substrates. The overall reaction pathway without including the separation and purification steps is shown in Figure 1.24.

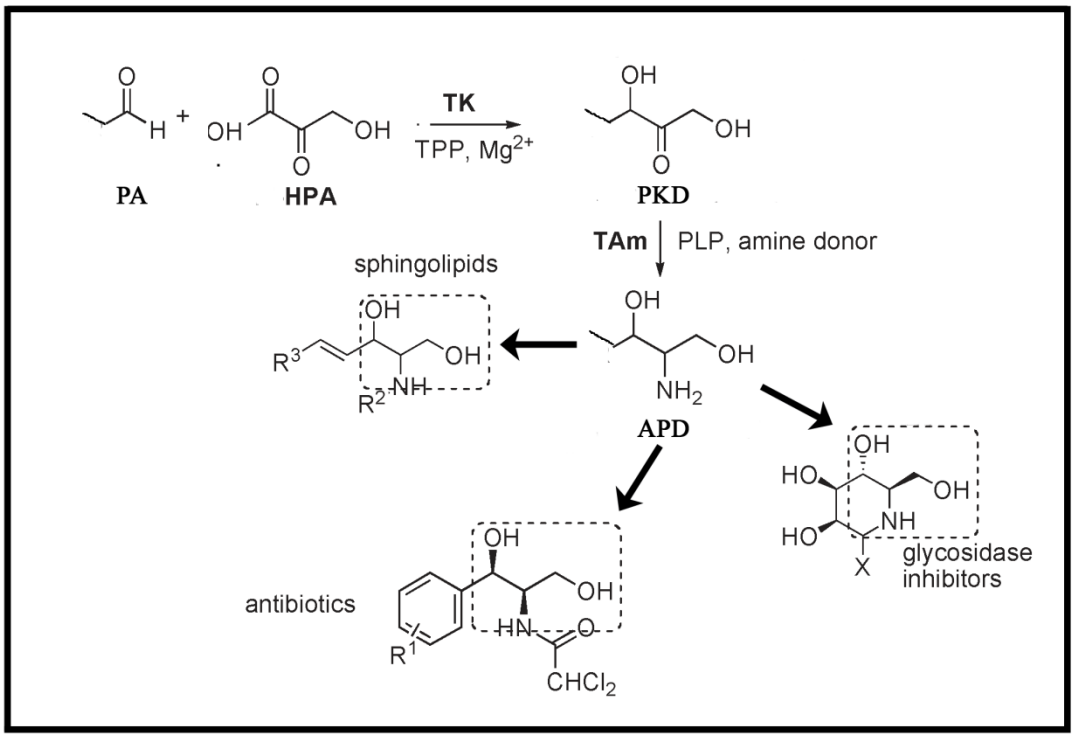

Figure 1.24. Two-step biocatalytic synthesis of 2-amino-1,3-diols using transketolase (TK) and transaminase (TAm). PA is propionaldehyde, HPA is hydroxypyruvate, TPP is thiamine pyrophosphate, PKD is (*S*)-1,3-dihydroxypentan-2-one, PLP is pyridoxal 5´phospahte and APD is of (2*S*,3*S*)-2-aminopentane-1,3-diol. Figure modified from Hailes et al., (2009).

In this case, the process required many downstream steps to isolate the TK product PKD prior to the TAm bioconversion as has been shown in the proposed manufacturing process by the authors in Figure 1.25.

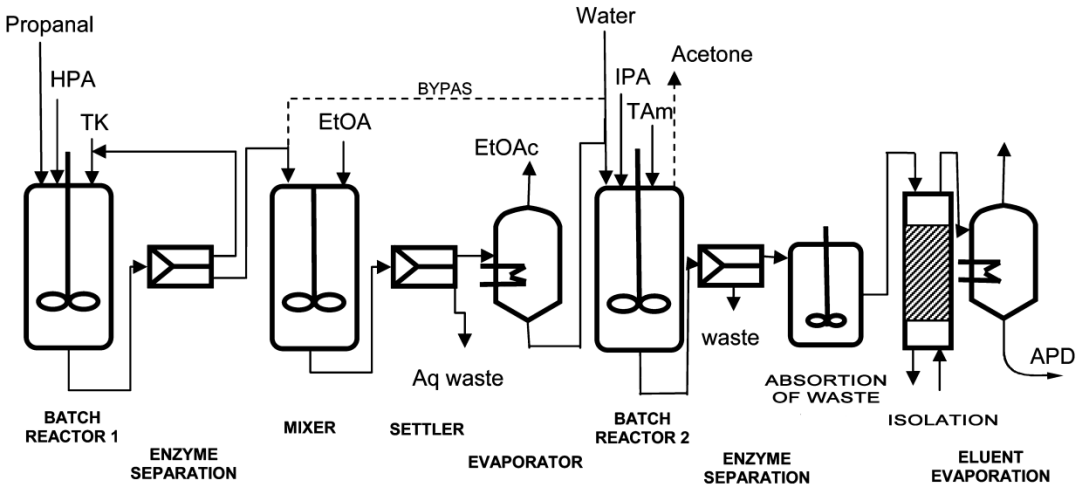

Figure 1. 25. **Hypothetical manufacturing process flow sheet for the large-scale, two-step TK D469T (batch reactor 1) and CV2025 TAm (batch reactor 2) biocatalytic synthesis and purification of (2*S*,3*S*)-2-aminopentane-1,3-diol (APD). HPA is hydroxypyruvate, IPA is isopropylamine and EtOA is ethyl alcohol. Figure adapted from Smith et al., (2010).**

During the purification steps, more than 30% mol/mol of the intermediate PKD was lost, apart from the use of large quantities of waste used in the downstream steps shown between the two reactors in Figure 1.25. Those problems could be potentially avoided by using a one-pot synthesis strategy, which could be designed combining microscale instrumentation with modelling tools, in order to select the best enzyme candidates and identify the best reaction conditions, allowing to achieve higher yields of the final product. As far as we know, no *de novo* engineered pathway has been designed, evaluated and completely modelled using high-throughput microscale tools which would be predictive of larger scale operations, increasing the challenge and impact of this work.

1.6. Aim and Objectives of the Project

To date most industrial bioconversion processes have focused on single-step enzymatic transformations primarily for the synthesis of pharmaceuticals and chiral intermediates. As described in Section 1.2.1.2, however, the *de novo* construction of multi-step enzymatic synthesis in whole cell biocatalysts provides a number of advantages. These include atom-efficient bioconversions in a single vessel potentially increasing space-time yields and reducing the production costs of complex syntheses for a wider range of products. Nevertheless, multi-step enzymatic systems have been relatively poorly explored (Section 1.2.1.3). In contrast to single enzyme systems they display higher levels of complexity, making them more difficult to construct and time consuming to characterize and model.

Microscale bioprocessing techniques, as described in Section 1.3, offer the potential to speed up the early characterization and optimization of biocatlaytic processes and the design and scale-up of bioprocess unit operations. The linkage of microscale experimentation with numerical approaches (Micheletti et al., 2006, Chen et al., 2008) further enables modelling and simulation of different biocatalyst and process options.

The aim of this project is therefore to design and characterize whole cell *E. coli* biocatalysts containing *de novo* engineered, multi-step enzymatic pathways for the synthesis of chiral amino alcohols. In particular a generic "toolbox" approach will be highlighted in order to simulate and optimize multi-step enzymatic syntheses using high-throughput microscale methods that are predictive of larger scale operating conditions. The enzymes transketolase (Section 1.5.2) and transaminase (Section 1.5.3), which do not naturally work in series, were selected in order to exemplify options for the one-pot synthesis of chiral amino-alcohols (Section 1.5.4) which are of special interest for the pharmaceutical industry (Section 1.5.1). In order to achieve this aim the primary objectives of the project are summarized below.

- The initial objective was to establish a microscale "toolbox" for the rapid evaluation of different variants of TK and TAm for the one-pot synthesis of a range of amino-alcohols. This required the construction of *de novo* engineered pathways that were based on a double transformed *E. coli* expression system, which combined with the microscale high-throughput experimentation, enabled systematic evaluation of different pairs of enzymes with different substrates under a range of reaction conditions. The results of this work are presented and discussed in Chapter 3.

- The next objective was to be able to model and simulate the bioconversion reactions. In particular the TAm step was identified as the bottleneck of the multi-step synthesis (Chapter 3) and so this work focused on a methodology to elucidate and determine the TAm kinetic parameters. The kinetic parameters for the TAm mediated synthesis of ABT and APD were thus determined based on a novel numerical approach and microscale experimentation. As shown in Chapter 4 this enabled simulation of the TAm bioconversion under a broad range of substrates concentrations facilitating selection of the best reaction conditions. The results of this work are presented and discussed in Chapter 4.

- The next objective was to scale-up the production of the biocatalyst, while obtaining a desired TK-TAm expression that would match the kinetic properties determined in Chapter 4. Here different fermentation conditions to manipulate the TK and TAm expression levels within the *E. coli* biocatalyst were studied. The best conditions were then used to scale-up the fermentation from shake flasks to a 7.5 litre fermentor, and the kinetic properties of the larger and small scale biocatalyst were compared. The results of this work are presented and discussed in Chapter 5.

- The last objective was to illustrate successful scale-up and predictive modelling of selected one-pot syntheses. The scale-up and modelling of the complete one-pot TK-

TAm synthesis of APD and ABT were successfully performed from µl to preparative scale, demonstrating the capacity of the microscale tools to speed up the development of multi-step synthetic processes. Finally, the best reactor configurations were determined and applied to optimize the *de novo* one-pot synthesis of chiral amino alcohols. The results of this work are presented and discussed in Chapter 6.

- Finally, in Chapter 7, the generic outcomes of this work are highlighted and suggestions for future work are presented.

2. MATERIALS AND METHODS

2.1. MATERIALS

2.1.1. Reagents and suppliers

Molecular biology enzymes were obtained from New England Bio-laboratories (NEB, Hitchin, UK). Nutrient broth and nutrient agar were obtained from Fisher Scientific (Leicestershire, UK). Competent *E. coli* BL21-Gold (DE3) cells were obtained from Stratagene (Amsterdam, NL). Primers and oligonucleotides were purchased from Operon (Cologne, DE). All other reagents were obtained from Sigma-Aldrich (Gillingham, UK) unless noted otherwise and were of the highest purity available. Reverse osmosis (RO) water was used in all experimental work.

2.1.2. Media preparation

All batch *E. coli* fermentations were performed using LB-glycerol medium the contents of which are described in Table 2.1.

Table 2. 1. Composition of the LB-glycerol medium used in all batch *E. coli* fermentations.

Component	Concentration (g L^{-1})
Yeast extract	5.0
Tryptone	10.0
NaCl	10.0
Glycerol	10.0

The different components of the media were measured out and dissolved in RO water to 1 L. The pH of the media was adjusted to pH 7 with a solution of 1 M NaOH when necessary. The medium was then autoclaved at 121 ^{o}C for 20 min for sterilization.

2.1.3. Luria Bertrani agar plates

LB-agar was prepared by adding 15 g L^{-1} of agar to LB-glycerol medium as described in Table 2.1. The LB-agar preparation was then autoclaved at 121^{o}C for 20 min. Once cooled down to between 40-50 °C, 30 mL of media was poured into each standard size Petri dish (Fisher Scientific, UK).

2.1.4. Antibiotic solutions

The antibiotics ampicillin and kanamycin were dissolved individually in RO water to a concentration of 150 mg mL^{-1}. The solutions were then sterilized by passing them slowly through a 0.2 µm filter (Fisher Scientific, UK) and aseptically transferred into previously sterilized 1.5 mL Eppendorf tubes and stored at -20 °C. The antibiotics were added to either LB-glycerol medium or to LB-agar before the start of any culture. Ampicillin was used when growing cells with plasmid pQR412 for TK expression (Section 2.3.1) at a concentration of 150 µg mL^{-1} and kanamycin was used for growing cells with plasmid pQR801 for TAm expression (Section 2.3.3) at a concentration of 150 µg mL^{-1}. For double transformed cells containing both plasmids pQR412 and pQR801, a concentration of 50 µg mL^{-1} of each antibiotic was used (Section 2.4.2).

2.2. MOLECULAR BIOLOGY TECHNIQUES

2.2.1. DNA extraction and quantification

A QIAprep spin miniprep kit (Qiagen, Crawley, UK) was used to obtain plasmid DNA from host *E. coli* cells, and the method was carried out following the techniques

described by the supplier. The concentration of DNA was determined by measuring absorbance at 260nm (A260) using a NanoDrop™ 1000 UV/vis spectrophotometer (Thermo Fisher Scientific, Waltham, MA, USA). DNA concentrations were calculated internally by the spectrophotometer by considering that 1.0 A260 unit of double-stranded DNA was equivalent to 50 ng μL^{-1}. Protein contamination was estimated from the A260/A280 ratio. Readings were blanked with the same buffer solution used for DNA elution.

2.2.2. Restriction digests and agarose gels

Analytical restriction digests were performed for four hours at 37^{o}C in the recommended restriction buffer, according to the enzyme used and following the manufacturer's protocol. To analyze the different DNA fragments, agarose DNA gels were run on 1% w/v agarose gels with 1X TBE buffer. Molecular weight markers were lambda DNA cleaved with *pst*1 or a 1 KB ladder (NEB, Hitchin, UK) while staining was performed with ethidium bromide.

2.2.3. Preparation of competent cells

Competent cells were prepared in house from *E. coli* BL21-Gold (DE3) (Stratagene (Amsterdam, NL) cells cultured in 250 mL shake flasks containing 20 mL of LB-glycerol medium and 20 mM $MgCl_2$ at 37^{o}C, 250 rpm to an optical density of 0.5 (Section 2.9.2). Cells were harvested by centrifugation and chilled on ice for 30 minutes. Resuspension was carried out in 75 mM $CaCl_2$ and the cells were re-pelleted by centrifugation. This was carried out three times. Following the final centrifugation cells were suspended in 75 mM $CaCl_2$ with 15 % v/v glycerol. Cells were then aliquoted and either placed on ice for immediate transformation or stored at -80^{o}C.

2.2.4. Transformation of cells by heat shock technique

E. coli BL21-Gold (DE3) cells were used to carry out heat-shock transformations. Competent cells were either prepared in house (Section 2.2.3) or purchased commercially. Cells were first thawed on ice and 50 µL aliquots transferred into 15 mL pre-chilled Falcon tubes. A sample of 1.5 µL of a single plasmid or a mixture of two plasmids with a total concentration of 50 ng μL^{-1} of DNA was added to cells in each tube which were then mixed gently and incubated on ice for 30 minutes. The cells were then heat shocked in a 42 ^{o}C water bath (Grant Instruments, Cambridge, UK) for 30 seconds and immediately placed on ice for 5 minutes. A volume of 0.9 mL of preheated (37 ^{o}C) LB-glycerol media was added to each Falcon tube and the cells were incubated at 37 ^{o}C for 1 h with shaking at 220 rpm in a SI 50 orbital shaker (Stuart Scientific, Redhill, UK). Finally 100 µL of transformed cells were uniformly spread on LB-agar plates with the corresponding antibiotic resistance (Section 2.1.4.) and left to incubate at 37^{o}C overnight.

2.2.5. Master glycerol stocks

To prepare master stock cultures a single colony was picked from the plates containing the desired transformed cells expressing either single enzymes or pairs of enzymes (Section 2.2.4). This was then inoculated into a sterile 250 mL shake flask containing 25 mL of LB-glycerol medium with the corresponding antibiotic(s). When the culture reached an OD of 0.5 at 600 nm (Section 2.9.2), 400 µL aliquots of cell broth were mixed aseptically in sterilized 1.5 mL Eppendorf tubes with 200 µL of a 50% v/v filter sterilized glycerol solution. The aliquots were then frozen and stored at -80 ^{o}C and were used throughout the rest of this project.

2.3. PLASMIDS

2.3.1. Transketolase plasmid pQR412

Plasmid pQR412 (11.2kb) contained the complete *E. coli* TK gene, *tktA,* with its native promoter and an N-terminal His6-tag as constructed previously (Ingram *et al.,* 2007). The plasmid was provided by Professor John Ward (Institute of Structural and Molecular Biology, UCL) and it was assembled using the expression vector pMMB67HE (8.8kb), which has a RSF1010 origin of replication, the *tac* promoter, the Lac repressor and codes for resistance to ampicillin (Figure 2.1). Even if the plasmid contained the inducible *tac* promoter, the expression of the *E. coli tktA* was constitutive because of the presence of its native promoter (Ingram *et al.*, 2007).

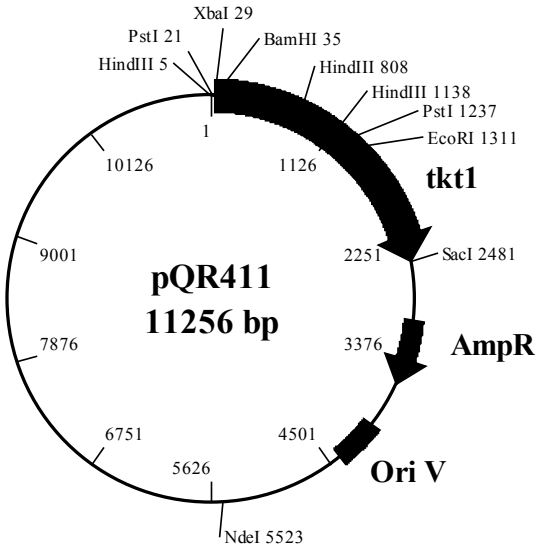

Figure 2.1. Structure of the plasmid pQR412. Image obtained from Ingram *et al.* (2007).

2.3.2. Site directed mutagenesis of TK

Site direct mutagenesis on the TK gene was performed using the Quikchange kit (Stratagene, Amsterdan, NL) following the supplier's instructions. The primers used for the TK mutagenesis were the following:

D469T: TCGGTCTGGGCGAA**ACT**GGGCCGACTCACCAG
D469E: TCGGTCTGGGCGAA**CAA**GGGCCGACTCACCAG

The resulting plasmid was transformed into commercially competent *E. coli* BL21-Gold (DE3) cells as described in Section 2.2.4.

2.3.3. Transaminase plasmid pQR801

Plasmid pQR801 contained the complete *Chromobacterium violaceum* 2025 TAm gene with an N-Terminal His6-tag (GenBank accession no. NP_901695) and was synthesized in a previous work (Kaulmann *et al.,* 2007). The plasmid was provided by Professor John Ward (Institute of Structural and Molecular Biology, UCL) and was constructed using the expression vector pET29(a)+ (5.3kb), which contained an inducible T7 promoter, the Lac repressor and codes for resistance to kanamycin.

2.3.4. Plasmids sequencing

DNA sequencing was performed by the sequencing service of the UCL Wolfson Institute for Biomedical Research. 12 μL of DNA sample were given to the service at a concentration of 100 ng μL^{-1} in 1.5 mL Eppendorf tubes. Three main custom primers were used to sequence the *E. coli* TK gene which were the following:

TKN 5'-GATCCAGAGATTTCTGA-3';
TKmedSeq 5'-GTATGAAAGGCGAAAT GCCG TCTGACT-3'
TKC 3'-CAAAAGAACTGCTGTAA-5'.

Two main primers were used to sequence the CV2025 TAm gene which where the following:

T7: 5' - GTA ATA CGA CTC ACT ATA GGG C - 3'
T7term: 5' - GCT AGT TAT TGC TCA GCG G - 3'

Primers were prepared at a concentration of 5 pmoles L^{-1}. Results were analyzed using Bioedit software available on the internet (www.mbio.ncsu.edu/BioEdit/bioedit.html).

2.4. SHAKE FLASK FERMENTATIONS

2.4.1. TK shake flask fermentations

Competent *E. coli* BL21-Gold (DE3) cells were transformed with the plasmid pQR412 using the heat shock technique (Section 2.2.4) and were then grown in LB-agar plates in the presence of ampicillin (150 ug mL^{-1}). Using a single colony from the agar plates, an overnight culture of the transformed cells was then inoculated in a 100 mL shake flask (10 mL working volume) containing LB-glycerol broth as described in Table 2.1 again with the addition of ampicillin. Growth was performed at 37 ^{o}C with orbital shaking at 250 rpm using an SI 50 orbital shaker during 8 hr (Stuart Scientific, Redhill, UK). The total volume of this culture was used to inoculate a 1 litre shake flask (100 mL working volume) which was left to grow for 8 hours. The cells were harvested and following the removal of broth using a Universal 320R centrifuge (Buckinghamshire, UK) for 10 min at 5000 rpm, they were resuspended in 50 mM TRIS buffer, pH 7.5 unless otherwise noted. The cells were either used immediately for whole cell bioconversions (Section 2.8.1) otherwise they were stored at -20 ^{o}C following the removal of broth by centrifugation.

2.4.2. TAm and TK-TAm shake flask fermentations

The double transformation of *E. coli* BL21-Gold (DE3) cells with the plasmid pQR801 and pQR412 or the single transformation of the cells with plasmid PQR801 and the inoculum preparation were performed as described in Section 2.4.1, except that 150 µg mL^{-1} of kanamycin were used for the single transformed cells and 50 µg mL^{-1} of both kanamycin and ampicillin were used for the double transformed strain. To construct the double transformed biocatalyst, 50 µL of competent *E. coli* BL21-Gold (DE3) cells were double transformed with a 1.5 µL solution of plasmids pQR412 and pQR801 (50 µg mL^{-1}

total plasmid concentration) using the heat shock technique described in Section 2.2.4. After inoculation of a 1 litre shake flask (100 mL working volume), when the OD_{600} reached a value of 0.8-1.0, Isopropyl *β-D-1*-thiogalactopyranoside (IPTG) was added to final concentration of 0.2 mM. After 4 hr induction, the cells were harvested and following the removal of broth by centrifugation, they were suspended in 50 mM HEPES buffer, pH 7.5 unless noted otherwise and used for whole cell bioconversions, otherwise they were stored at -20 ^{o}C following the removal of broth by centrifugation.

2.5. LABORATORY AND PILOT SCALE FERMENTATIONS

2.5.1. 2 L Adaptive Biosystems batch fermentation

A 2 L fermentor (Adaptive Biosystems, London, England), was used to grow *E. coli* BL21(DE3) Gold double transformed cells with plasmids pQR412 and pQR801 and also single transformed cells with plasmid pQR801 (1.4L working volume). The vessel was equipped with two 6 bladed Rushton turbine impellers and four baffles equally spaced. It also comprised a thermocouple, a pH probe, and a polarographic oxygen probe (Ingold Messtechnik, Urdorf, Switzerland). All probes were steam sterilisable.

The vessel was filled with 1.26 L of LB-glycerol media and all the probe calibrations and pre-sterilization procedures were performed following the manufacturer's instructions. The fermentor was sterilized as a complete unit in an autoclave at 121^{o}C for 20 min and after the media was cooled down the corresponding antibiotic (Section 2.1.4) and pre-sterilized antifoam, polyethylene glycol (PPG) to a final concentration of 0.2 g L^{-1}, was added.

The fermentor was then inoculated with 140 mL of previously grown overnight shake flasks cultures as described in Section 2.4.2. The pH was set at 7.0 and was controlled with the addition of 85% v/v H_3PO_4 (acid) and 28% NH_4OH v/v (base). The oxygen and carbon dioxide content in the exhaust air were measured on-line by a TanDem gas

analyzer (Adaptive Biosystems, London, England). Temperature was automatically controlled via cold water circulation in the external jacket of the bioreactor and maintained at 30 or 37°C using a heating jacket. The stirrer was set at a speed of 1200 rpm with an aeration rate of 2 L min^{-1}. Ingoing air was sterilized by passage through a 0.2 μm membrane filter and dispersed in the vessel at the base of the lower turbine with a ring sparger. The fermentor was linked to Biodirector proprietary control software to control and monitor online the temperature, DOT, speed impeller and pH. Additionally, the fermentation was monitored by taking regular OD_{600} measurements as described in Section 2.9.2.

2.5.2. 7.5 L New Brunswick batch fermentation

Batch fermentations were carried out in a 7.5 L fermentor (BioFlo 110, New Brunswick, Hertfordshire, UK) with a working volume of 5 L. The fermentor had an aspect ratio of 1.79:1 and comprised two six-bladed dual Rushton-type impellers (59 mm, di/dt = 0.25) and four equally spaced baffles. The Temperature was monitored by a thermocouple and automatically controlled at 30 or 37^{o}C via cold water circulation in the external jacket of the fermentor in addition to a heating jacket. The pH was measured by a Ingold gel filled pH probe (Ingold Messtechnik, Urdorf, Switzerland) and was controlled with the addition of 85% v/v H3PO4 (acid) and 28% NH4OH v/v (base). DOT was monitored by a polarographic oxygen electrode (Ingold Messtechnik, Urdorf, Switzerland) and was set to be maintained at 30% through a cascade control of the impeller speed. Ingoing air was sterilized by passage through a membrane filter and dispersed in the vessel at the base of the lower turbine with a ring sparger and the flow rate was 5 L min^{-1}.

The vessel was filled with 4.5 L of LB-glycerol media and all the probe calibrations and pre-sterilization procedures were performed following the manufacturer instructions. The fermentor was then sterilized as a complete unit in an autoclave at 121^{o}C for 20 min, and after the media was cool down, the corresponding antibiotic (Section 2.1.4) and sterilized antifoam PPG was added to a final concentration of 0.2 g L^{-1}.

The fermentor was then inoculated aseptically with five 100 mL shake flasks cultures previously grown overnight as described in Section 2.4.2. The progress of the fermentation was monitored as in Section 2.5.1. Data was logged by on-line measurements of DOT, pH, temperature and speed of the impeller using the BioCommand software (BioFlo 110, New Brunswick, Hertfordshire, UK) as well as by taking regular OD_{600} measurements as described in Section 2.9.2.

2.5.3. Fed-batch fermentations

Both the 2 L and 7.5 L fermentors described above were also used to perform fed-batch fermentations. This was performed in order to minimize the accumulation of toxic by-products of an exponentially growing culture by maintaining a limited growth carbon source, in order to achieve higher biomass and protein expression yields (Shiloach & Fass 2005). This protocol described in this work follows a simple glycerol-supplementation method where cells were first grown in batch mode as described in Section 2.5.1 and 2.5.2, in a medium containing 10 g L^{-1} glycerol. After the initial glycerol was consumed, which was detected by a sharp rise in the DOT, indicative of reduced oxygen consumption and thus of glycerol becoming limiting, the culture was supplemented using a Watson Marlow 501U pump (Cornwall, UK) with an increasing feed rate of pre-sterilized medium containing 10 g L^{-1} of NaCL, 10 g L^{-1} of yeast extract, 20 g L^{-1} of tryptone and 500 g L^{-1} of glycerol. The feeding rate was calculated according to Equation 2.1 (Bernard & Payton 2001) and was modified every hour:

$$F = \frac{\mu V x}{Y[Gly]} \qquad \text{Equation 2.1}$$

where F is the feed rate (L hr^{-1}), μ is the specific target growth rate (hr^{-1}), V is the fermentor volume (L), x is the cell biomass (g_{DCW} L^{-1}), Y is the yield of cell mass per unit of carbon source of glycerol (g g^{-1}), and [Gly] is the concentration of glycerol in the feed solution (g L^{-1}). A value of 80% of the maximum growth rate obtained in the batch cultures (Sections 2.5.1 and 2.5.2) was used for μ and n standard estimate for Y of 0.3 g g L^{-1} was applied to calculate the feed rate using Equation 2.1 (Bernard & Payton 2001) .

2.6. BIOCATALYST PREPARATION

2.6.1. Whole cell and lysate forms

Fresh cells where always used for whole cell bioconversions and were obtained as described in Section 2.4.1 and Section 2.4.2. When a cell-free lysate was needed, the cells were sonicated with a Soniprep 150 sonicator (MSE, Sanyo, Japan) using 10 seconds on/off at 10 μm amplitude for 10 cycles. Cells were placed on ice to stop overheating during the sonication. The sonicated lysate was then centrifuged at 5000 rpm in Falcon tubes for 5 min to remove cell debris, and the clarified supernatant was finally aliquoted into 1.5 mL Eppendorf vials to be stored at -20 ^{o}C and used within 1 month. Prior to the initiation of a bioconversion, the frozen lysates (300μL) were thawed in a water bath at 30^{o}C for typically 10 min and then immediately incubated with cofactors.

2.6.2. Purified enzymes (His_6-tag purification)

The *E. coli* TK and CV2025 TAm expressed from plasmids pQR412 and pQR801 respectively both have an N-terminal His6-tag (Section 2.3.1 and 2.3.3) to facilitate rapid single-step purification using a His Bind Quick 900 cartridge (EMD Biosciences, Darmstadt, Germany). The cartridges were purchased packed with a pre-charged cellulose matrix with tethered Ni^{2+} complex immobilised on Nα,Nα-Bis [carboxymethyl]-L-lysine (NTA). The composition of all buffers used for the enzyme purification procedure is shown in Table 2.2, the pH of all buffers was 7 for TK and 7.5 for TAm. After equilibration of the cartridge with 10 mL binding buffer, the purification was performed loading the lysate solution prepared as described in Section 2.6.1, following the loading of the sample, the cartridge was washed with 20 mL wash and 10 mL binding buffer. Elution was carried out with either strip or elution buffer depending whether or not the beads needed to be regenerated.

Table 2.2. His6-tag enzyme purification buffers used in Section 2.6.2.

Buffer	Components
Binding	500 mM NaCl, 20 mM Tris-HCl, 5 mM imidazole
Wash	50 mM Tris-HCl
Strip	50 mM EDTA, 50 mM Tris-HCl
Elution	1 M imidazole, 500 mM NaCl and 20 mM Tris-HCl

Following the elution, in order to remove free EDTA and EDTA-nickel complexes from the elution buffer, the enzyme solution was dialyzed against 500 mL of 50 mM TRIS buffer at pH 7.0 or 50 mM HEPES pH 7.5 for TK and TAm solutions respectively. The buffer exchange was performed using a flat packed semi-permeable membrane with a molecular weight cut-off of 14,000 Da (BioDesign, Carmel, NY, USA). The membrane was left overnight at 4^{o}C with gentle magnetic stirring. The purity of the dialyzed enzymes was determined by SDS-PAGE as described in Section 2.9.5. The dialyzed enzyme solution was stored in the fridge at 4°C for a period of up to 2 weeks before use.

2.7. SYNTHESIS OF SUBSTRATES AND PRODUCTS

2.7.1. Chemical synthesis of hydroxypyruvate

Hydroxypyruvate (HPA) was synthesized by reacting bromopyruvic acid with LiOH following a previously described method (Morris *et al*., 1996). The details of the synthesis were as follows: bromopyruvic acid (0.06 mol) was dissolved in 100 mL water followed by careful addition of aq. LiOH (1M) until a stable pH of 9 was reached. At no time during the addition was the pH allowed to exceed 9. The reaction mixture was then adjusted to pH 5.0 by addition of glacial acetic acid and concentrated under vacuum to

approximately 20 mL. Following refrigeration at -20^{o}C overnight, the crude product was washed with ethanol and then suspended in 50 mL ethanol at 25^{o}C for 30 min. After filtration the solid product was dried under vacuum to give a white or slightly yellowish powder (expected yield is 2-4 g per batch) which was stored at -20^{o}C.

2.7.2. Enzymatic synthesis of PKD

PKD was synthesized in a 100 mL scale bioconversion with 300 mM HPA, 350 mM propionaldehyde (PA), 9 mM $MgCl_2$, 2.4 mM thiamine pyrophosphate (TPP), pH 7.0 and 30% v/v of D469E TK lysate (final TK concentration of 0.3 mg mL^{-1}). The reaction was stirred for 10 hours at room temperature in a sealed flask and the pH was maintained at 7.0 using a 718 STAT Titrino pH controller (Metrohm Ion Analysis, Switzerland). The solution was dried on silica and purified by column chromatography (ethyl acetate: hexane, 1:1) to yield PKD as a colourless oil that crystallized on standing. The PKD *ee* was determined as described in Section 2.9.6.

2.7.3. Chemical synthesis of ABT product standard

The chemical synthesis of ABT was performed as described by Ingram *et al*. (2007). Briefly *L*-erythrulose (4 g, 33 mmol), was suspended in acetone:dimethoxypropane 9:1 v/v (30 mL) and p-toluenesulfonic acid (catalyst) was added. The mixture was stirred at room temperature under N_2 for 3 h during which time the reaction mixture became homogeneous. The reaction was monitored by TLC using a 2:1 v/v, ethyl acetate:hexane running solvent.

Sodium acetate (0.5 g) was added and the reaction stirred for a further hour before the mixture was filtered and concentrated to dryness. The residue was purified by flash chromatography on silica gel (ethyl acetate/hexane 1:2 v/v) to yield the desired 3,4-*O*-isopropylidene acetal.

To an aliquot of the produced acetal (487 mg, 3.02 mmol) in methanol (10 mL) was added benzylamine (660 μL, 6.04 mmol) and then sodium cyanoborohydride (570 mg, 9.06 mmol). The pH was adjusted to pH 6.0 using acetic acid and the reaction was stirred at room temperature for 6 hours. The reaction was monitored by TLC (1:1, ethyl acetate:hexane). The mixture was concentrated under vacuum and the residue partitioned between dichloromethane (100 mL) and sodium hydrogen carbonate (aq, sat) (100 mL) with vigorous stirring.

Solid sodium carbonate was added to the suspension in small portions to ensure that the final pH of the aqueous layer was 9. The layers were then separated, the aqueous phase was extracted with further dichloromethane (two times 100 mL) and the organic phases combined and concentrated to dryness. The residue was purified by flash chromatography on silica gel (ethyl acetate/hexane 1:1 v/v then neat ethyl acetate) to yield the desired amine as a 1:1 mixture of diastereomers.

To a solution of the previously produced amine (200 mg, 0.80 mmol) in MeOH (5 mL) was added drop wise 1 M HCl (aq) to give a mixture that gave a dark red colour to moist litmus paper. The reaction was stirred at room temperature and was monitored by TLC (1:1 v/v, ethyl acetate:hexane). After 2 h the reaction was complete and the mixture concentrated to dryness to yield the crude amine as the hydrochloride salt. This residue was re-dissolved in MeOH (5 mL) and hydrogenated (balloon pressure) in the presence of palladium on carbon (10% wt/wt, 100 mg) at room temperature overnight. The catalyst was removed by filtration and the solvent removed under vacuum to yield 2-amino-1,3,4-butanetriol as a 1:1 mixture of *threo* and *erythro* diastereomers.

2.7.4. Enzymatic synthesis of ABT and APD

The enzymatic synthesis of APD was performed in a 100 mL scale bioconversion with 200 mM PKD, 0.2 mM PLP and 30% v/v of CV2025 TAm lysate (final enzyme concentration of 0.3 mg mL^{-1}). To this mixture, a solution of 300 mM IPA (pH 7.5) was added in a fed batch mode using a P-1 peristaltic pump (Pharmacia Fine Chemicals,

Uppsala, Sweden) with a volume rate of 2.1 mL hr^{-1} for 48 hr until the total volume of the reaction was approximately 200 mL. The temperature of the TAm catalyzed reaction was maintained at 30°C using a circulating water bath (Grant Instruments, Cambridge, UK), and the pH was kept at 7.5 by the automatic addition of 1 M NaOH using a 718 STAT Titrino pH controller (Metrohm Ion Analysis, Switzerland).

After the bioconversion, the enzyme was spun down (5000 rpm, at 4 °C for 15 min) and the mixture was additionally filtered through a 0.2 μm sterile filter. 50 g of Amberlite IRA-410 resin (Sigma-Aldrich, Gillingham, UK) were added to the reaction mixture for 1 hr, and the resin was then removed by filtration. The remaining aqueous mixture was then passed through 80 g of an Isolute SCX-2 ion exchange column (Biotage, Uppsala, Sweden), and the column was washed with 400 mL of methanol. The column was then eluted with 500 mL 4 M NH_3 and the eluent was evaporated to yield the desired product. The enzymatic synthesis of ABT was performed the same way as the one for APD, expect that ERY was used instead of PKD as initial substrate.

2.7.5. Synthesis of derivatizing reagent

The derivatizing agent 6-aminoquinolyl-*N*-hydroxysuccinimidyl carbamate (AQC) was synthesized 'in house' according to a previously published protocol (Cohen & Michaud, 1993). Di(*N*-succinimidyl)carbamate (3 g, 6 mmol), was refluxed in 25 mL of dry acetonitrile. Dropwise addition of a 6-aminoquinoline (1.5 g, 5 mmol) solution in dry acetonitrile was carried out over 45 minutes. Following a further 30 minutes reflux, concentration was carried out to half the original volume. The solution was stored at –20°C overnight. The crystals were then filtered off and stored *in vacuo*.

2.8. BIOCONVERSION KINETICS

2.8.1. Microscale experimental platform

All microscale bioconversions were performed in a glass 96-well, flat-bottomed microtiter plate with individual wells having a diameter of 7.6 mm and height of 12 mm unless noted otherwise (Radleys Discovery Technologies, Essex, UK). The microplate was covered with a thermo plastic elastomer cap designed to work with automated equipment (Micronic, Lelystad, Netherlands).

All the bioconversions were performed using 300 µL total volume at 30 ^{o}C unless noted otherwise, and orbital shaking was provided at 300 rpm with a Thermomixer Comfort shaker (shaking diameter of 6 mm, Eppendorf, Cambridge, UK). TK single step reactions were performed in 50 mM TRIS buffer and the concentration of cofactors $MgCl_2$ and thiamine pyrophosphate (TTP) were 9 mM and 2.4 mM respectively for all reactions.

TAm single step reactions and all the two step syntheses were carried out in 50 mM HEPES buffer pH 7.5 unless noted otherwise and the concentration of TAm cofactor pyridoxal-5-phosphate (PLP) was 0.2 mM in all cases. The whole cell suspension or lysate with the cofactor solutions were always added first in the corresponding well and left to incubate for 20 min at 30 ^{o}C, prior to initiation of the reaction by addition of the substrate solutions.

Preliminary experiments showed that the initial cofactor incubation helped to ensure all expressed TK or TAm was in the active holo-form. This practice also enabled more consistent measurement of specific activity results, by avoiding initial non linear reaction kinetics believed to be caused in some cases by the binding of the enzyme and cofactors.

Aliquots of 20 µL were taken at various time intervals and quenched with 180 or 380 µL of a 0.1% v/v trifluoroacetic acid (TFA) solution for TK and TAm experiments respectively. They were then centrifuged for 5 min at 5000 rpm and transferred into an

HPLC vial for further analysis. The specific activities were determined as the amount of PKD, ERY, AP, APD and ABT formed per unit of time normalized by the amount of enzyme used in the reaction. The specific activity was based on the measured mass of TAm or TK present in each bioconversion. For whole cell experiments, it was calculated based on 50% of the dry cell weight of the cells being protein (Watson, 1972), combined with the measured result of the percentage of TK and TAm by SDS-PAGE analysis described in Section 2.95.

2.8.2. Preparative scale bioconversions

Bioconversions at preparative scale (volumes from 30 to 120 mL) were performed in a 150 mL titration vessel with thermostat jacket (Metrohm Ion Analysis, Switzerland). Temperature was maintained at 30^{o}C using a circulating water bath (Grant Instruments, Cambridge, UK), mixing was achieved using a magnetic stirrer at 300 rpm, and the pH was maintained at pH 7.5 unless noted otherwise by the use of an automated addition of 1 M NaOH using a 718 STAT Titrino pH controller (Metrohm Ion Analysis, Switzerland). For preparative scale fed batch reactions, a peristaltic P-1 pump (Pharmacia Fine Chemicals, Uppsala, Sweden) was used to add the desired substrate solution over time. Sampling procedures were performed in the same way as in Section 2.8.1.

2.9. ANALYTICAL METHODS

2.9.1. Dry cell weight (DCW) measurement

1.5 mL aliquots of cell suspension were added to pre-dried and pre-weighed 2.2 mL Eppendorf tubes which were then centrifuged at 13,000 rpm for 5 minutes (Eppendorf AG, Germany). The supernatant was discarded and the vials were left to dry at 90^{o}C for 24 hours. The biomass concentration in g_{DCW} L^{-1} of the culture could then be calculated.

2.9.2. Optical density measurements for biomass quantification

Optical density measurements were performed at a wavelength of 600 nm (OD_{600}) using an Ultraspec 4000 variable wavelength spectrophotometer (Pharmacia Biotech, USA). A small aliquot of *E. coli* BL21 culture medium was taken from the shake flask cultures of the bioreactors and diluted with RO water so that the optical density measurement was between 0.1-0.8 absorbance units. A calibration curve relating the OD_{600} measurement from a serial dilution of broth sample to the corresponding g_{DCW} L^{-1} measurement was constructed and is shown in Appendix I. The calibration relationship determined was that 1 unit of (OD_{600}) was equal to 0.4 g_{DCW} L^{-1}. This relationship was unaltered for cells transformed with TK, TAm or the double transformed cells.

2.9.3. Bradford assay for lysate total protein quantification

Protein concentrations of the lysates were obtained using the Bradford assay method (Bradford, 1976) following the instructions of a commercial protein assay kit (Bio-Rad Laboratories Inc., Hemel Hempstead, UK). The protein concentration was calibrated against a bovine serum albumin standard curve which was generated for each assay (Appendix II). Absorbance measurements at 595 nm were carried out on an ATI Unicam UV/VIS spectrophotometer (Spectronic, Leeds, United Kingdom).

2.9.4. Purified enzyme quantification by UV absorbance.

The quantification of pure enzyme concentration was performed by UV absorbance at 280 nm using an ATI Unicam UV/VIS spectrophotometer (Spectronic, Leeds, United Kingdom). Readings were blanked with the appropriate buffer solution. Absorbance measurements were converted to protein concentration using the Beer-Lambert law:

$$A = \varepsilon\lambda c \qquad \text{Equation 2.2}$$

where A was the absorbance at 280 nm, ε was the extinction coefficient previously determined as 93,905 $M.cm^{-1}$ for TK (Martinez-torres et al., 2007) and 78,000 $M.cm^{-1}$ for TAm (Matosevic, 2009) , λ was the path length equal to 1 cm, and c was the protein concentration in mol L^{-1}.

2.9.5. SDS-PAGE electrophoresis

SDS-PAGE for protein analysis was carried out on a Mini-Protean II system (Bio-Rad Laboratories Inc., Hemel Hempstead, UK) using 8% w/v Tris-Glycine comercial gels (1.5 mm, 10 well, Invitrogen, Paisley, UK). Clarified lysate or pure enzyme solutions were mixed (1:1) with 2X protein sample buffer (Sigma-Aldrich, UK) and heated to 99^{o} C in a PCR machine (Techne LTD, Cambridge, UK) for 10 min. Samples were subsequently loaded onto the gel using 20 µL per well. A range of 15 to 20 µg of total protein was applied per lane to avoid saturation of the bands.

The gel was stained with 50 mL of Coomassie Blue staining solution containing 0.1% (w/v) Coomassie Blue R-250, 40% (v/v) methanol and 10% (v/v) acetic acid and it was microwaved for 1 minute. After washing the Coomassie Blue solution, the gel was de-stained overnight with a solution 10% acetic acid and 40% v/v methanol. All gels were visualized and quantified (where appropriate) on a Gel–Doc–it bioimaging system with Labworks 4.5 software (Bioimaging systems, Cambridge).

2.9.6. HPLC methods

Separation and quantification of PKD, ERY and HPA was performed on a Dionex HPLC system (Camberley, UK) with a Bio-Rad Aminex HPX-87H reverse phase column (300 x 7.8 mm, Bio-Rad Labs., Richmond, CA, USA), controlled by Chromeleon client 6.60 software . The system comprised a GP50 gradient pump, a FAMOS autosampler, an LC30 chromatography column oven and an AD20 UV/Vis absorbance detector. The HPLC method used has been described previously (Chen *et al*., 2008).

Separation and quantification of MBA, AP, APD and ABT was performed on an integrated Dionex ultimate 3000 HPLC system (Camberley, UK) with an ACE 5 C18 reverse phase column (150mm×4.6 mm, 5 µm particle size; Advance Chromatography Technologies, Aberdeen, UK) controlled by Chromeleon client 6.60 software. The HPLC

method has been reported elsewhere (Kaulmann *et al*, 2007). To analyse ABT and APD, the samples were derivatized by addition of an excess of 6-aminoquinolyl-*N*-hydroxysuccinimidyl carbamate. The derivatizing reagent was synthesized in house as described in Section 2.7.5, and the HPLC method used has been described previously (Ingram *et al*, 2007).

The enantiomeric excess (*ee*) of the ketodiols was determined by derivatization via dibenzoylation for satisfactory peak resolution by chiral HPLC. This was performed on a Varian Prostar instrument equipped with a Chiracel AD chiral column (Daicel; Chiral Technologies Europe, France, 25 cm × 0.46 cm) and a mobile phase of n-hexane/2-propanol solvent mixture (90:10 v/v) was used. The method has been described in more detail elsewhere (Cázares *et al*., 2010). The *ee* of ABT and APD was determined by first derivatizing the amino alcohol to the respective benzoate form. The assay was performed against the four diastereomer samples of the benzoate synthesized as described elsewhere (Smith *et al*., 2010) using chiral HPLC: Chiracel-OD column (Daicel); mobile phase, isopropanol/hexane (5:95); flow rate, 0.8 mL/min, detection, UV 210 nm.

Figure 2.2 shows examples of HPLC profiles for the chiral separation and *ee* determination of (3*S*)-1,3-dihydroxypentan-2-one (*S*-PKD) and (3*R*)-1,3-dihydroxypentan-2-one (*R*-PKD), as well as the HPLC profiles for the detection and quantification (non chiral) of APD , HPA, ERY, PKD, AP and MBA. The standard graphs for all of the above methods can be found in Appendix III.

2.9.7. LC−ECI−MS analysis

Liquid chromatography-electrospray ionisation-mass spectrometry (LCESI –MS) was performed on an Agilent 1100 Series System with a Finnigan LTQ mass spectrometer. Operating conditions of the ESI interface in positive ion mode: capillary temperature 300◦C, capillary voltage 9V, spray voltage 4.5 kV, sheath gas 80, auxiliary gas 30, and sweep gas 0 arbitrary units. Results are shown in Appendix XII.

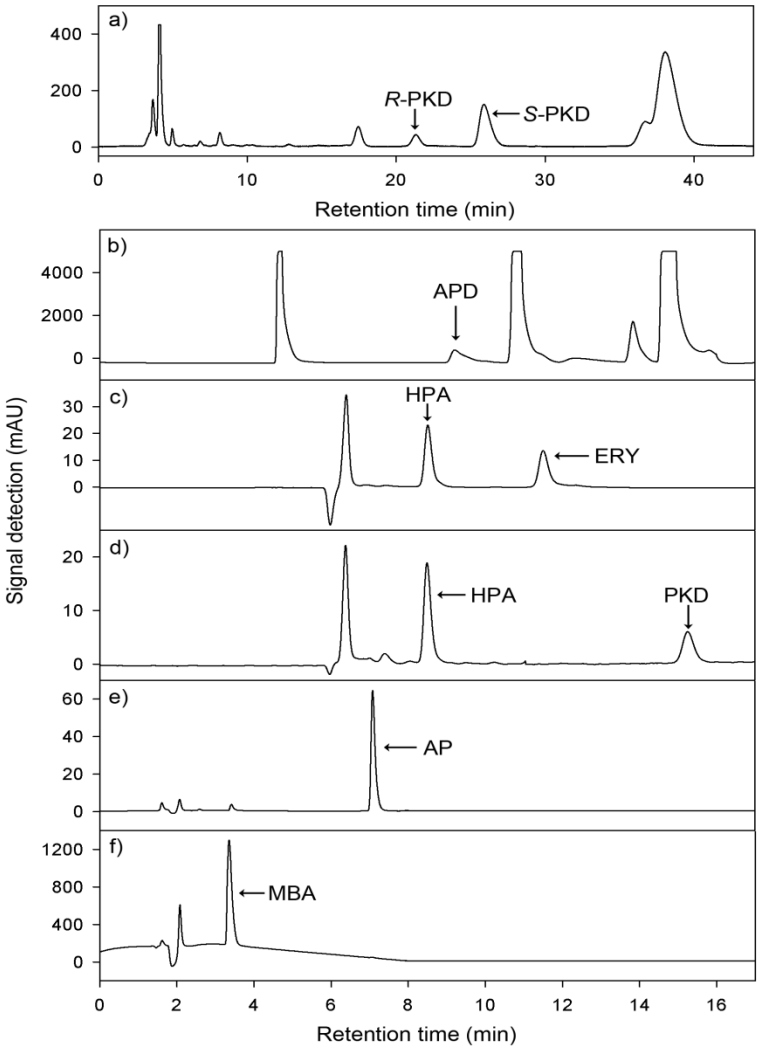

Figure 2.2. HPLC profiles from different reaction mixtures obtained as described in Section 2.8.1 for (a) the chiral separation and *ee* determination of (3*S*)-1,3-dihydroxypentan-2-one (*S*-PKD) and (3*R*)-1,3-dihydroxypentan-2-one (*R*-PKD), and for the detection and quantification (non chiral) of (b) APD, (c) HPA and ERY, (d) HPA and PKD, (e) AP and (f) MBA. HPLC conditions and sample preparation as described in Section 2.9.6.

3. EVALUATION OF DE NOVO TK-TAM PATHWAYS IN A WHOLE CELL BIOCATALYST†

3.1. INTRODUCTION

As described in Section 1.2.3.1, it is now possible to design *de novo* non-native pathways in heterologous hosts, to carry out specific non-natural bioconversions producing chiral compounds difficult to obtain by existing biosynthetic pathways or chemical synthesis (Burkart, 2003; Roessner and Scott, 2003; Prather and Martin, 2008; Dalby *et al.*, 2009).

The *de novo* design of synthetic pathways has recently been demonstrated for the sequential two-step reaction of carbon-carbon bond formation using a transketolase (TK) enzyme, followed by a transaminase (TAm) as described in Section 1.5.4 for the synthesis of ABT (Scheme 3.1) (Ingram *et al.*, 2007).

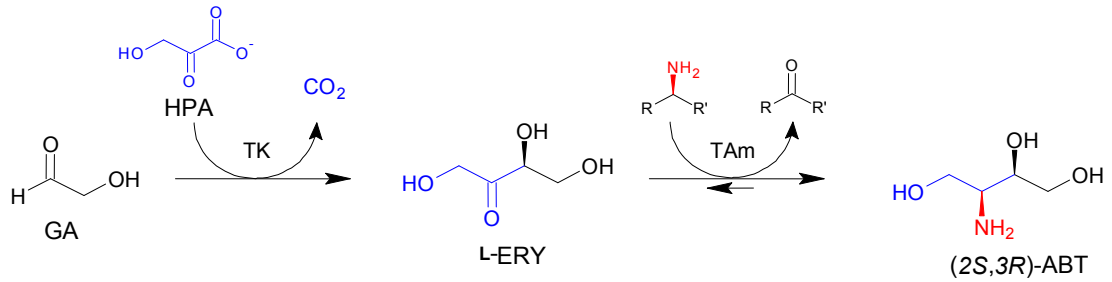

Scheme 3.1. Reaction scheme of the *de-novo* TK-TAm pathway for the synthesis of chiral amino alcohol (2*S*,3*R*)-2-amino-1,3,4-butanetriol (ABT), from achiral substrates glycolaldehyde (GA) and hydroxypyruvate (HPA).

† The results presented in this chapter have been published as: Rios-Solis L., M. Halim, A. Cázares, P. Morris, J. M. Ward, H. C. Hailes, P. A. Dalby, F. Baganz, and G. J. Lye. 2011. A toolbox approach for the rapid evaluation of multi-step enzymatic syntheses comprising a "mix and match" *E. coli* expression system with microscale experimentation. *Biocat and Biotrans*. 29:192-203.

However, in that work, low yields were achieved due to the low specific activity of the TAm from *Pseudomonas aeruginosa*. Recently, new libraries of engineered and recombinant TKs and TAms have been built (Hibbert et al., 2007, Kaulmann et al., 2007, Hibbert et al., 2008, Cázares et al., 2010). Those libraries have the potential to be applied to improve the performance of the *de novo* pathway, as well as expanding its synthetic potentials to chiral 2-amino-1,3-diol like APD (Scheme 3.2), which are an important class of pharmaceutical building blocks as described in Section 1.5.4.

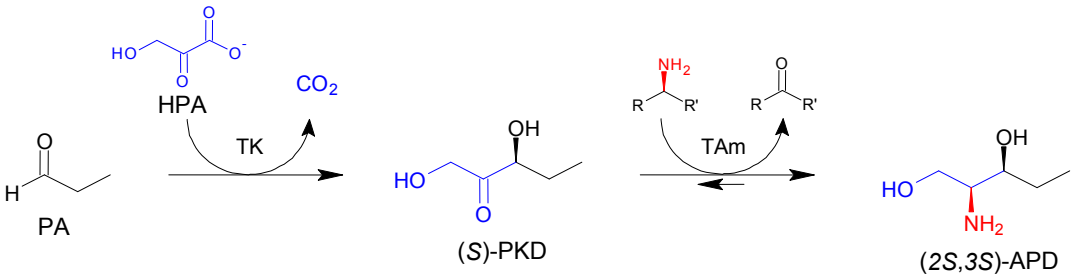

Scheme 3.2. Reaction scheme of the *de-novo* TK-TAm pathway for the synthesis of chiral amino alcohol (2*S*,3*S*)-2-aminopentane-1,3-diol (APD) from achiral substrates propionaldehyde (PA) and hydroxypyruvate (HPA).

Nevertheless as described in Section 1.3.1, the design and assembly of synthetic pathways is a complex process, and a methodology is necessary to be able to cope with the expanded possibilities of synthesis that *de novo* pathways offer. In particular testing several pairs of enzymes, under different reaction conditions can be time consuming. Also the evaluation of kinetic data is necessary in order to determine the compatibility and the bottlenecks of the one-pot synthesis. Developing a microscale "toolbox" to be able to do this quickly and with minimal cost emerge as a powerful solution to optimize *de novo* pathways.

3.2. AIM AND OBJETIVES

The aim of this chapter is to establish a microscale "toolbox" for the rapid evaluation of different variants of TK and TAm for the one-pot synthesis of a range of amino-alcohols. The approach will involve the construction of *de novo* engineered pathways that are based on a double transformed *E. coli* expression system, which combined with the microscale high-throughput platform and the gathering of kinetic data, could enable systematic evaluation of different pairs of enzymes with different substrates under a range of reaction conditions. The key objectives of this chapter are thus:

- Construction of various *de novo* engineered TK-TAm pathways based on a double transformed *E. coli* expression system and previously constructed TK and TAm libraries.

- Evaluation of cell growth kinetics and protein expression profiles in shake flasks for cells containing different *de novo* TK-TAm pathways.

- Determination of appropriate reaction conditions for various multi-step syntheses, evaluating the compromises to made from each enzyme-substrate combination.

- Determination of the best TK candidate for the synthesis of PKD and ERY and the best TAm candidate for the synthesis of APD and ABT.

- Demonstration of the microscale toolbox approach by achieving the one-pot syntheses of ABT and APD using the most appropriate forms of TK-TAm expressing biocatalysts.

3.3. RESUTLS

3.3.1. Biocatalyst production (TK-TAm)

In order to separately regulate expression of the TK and TAm enzymes in *E. coli*, a dual plasmid system was selected to facilitate the "mix and match" approach first proposed by Hussain & Ward (2003). This was based on two plasmids with different origins of replication and antibiotic resistance genes that would enable the rapid evaluation of different variants of TK and TAm (Section 2.3.1 and 2.3.3).

The verification that the double transformations were successful was performed by running DNA agarose and SDS PAGE gels as described in Section 2.2.2 and 2.9.5. To establish the metabolic burden of the two plasmids on the host cells, five different whole cell biocatalysts were initially generated and evaluated in shake flask fermentations. Growth kinetics were obtained with cultures of *E. coli* BL21-Gold (DE3) containing either no plasmid, the single TK or TAm gene expressing plasmids, or both the TK and TAm plasmids, in each case either induced or non induced. The results are shown in Figure 3.1.

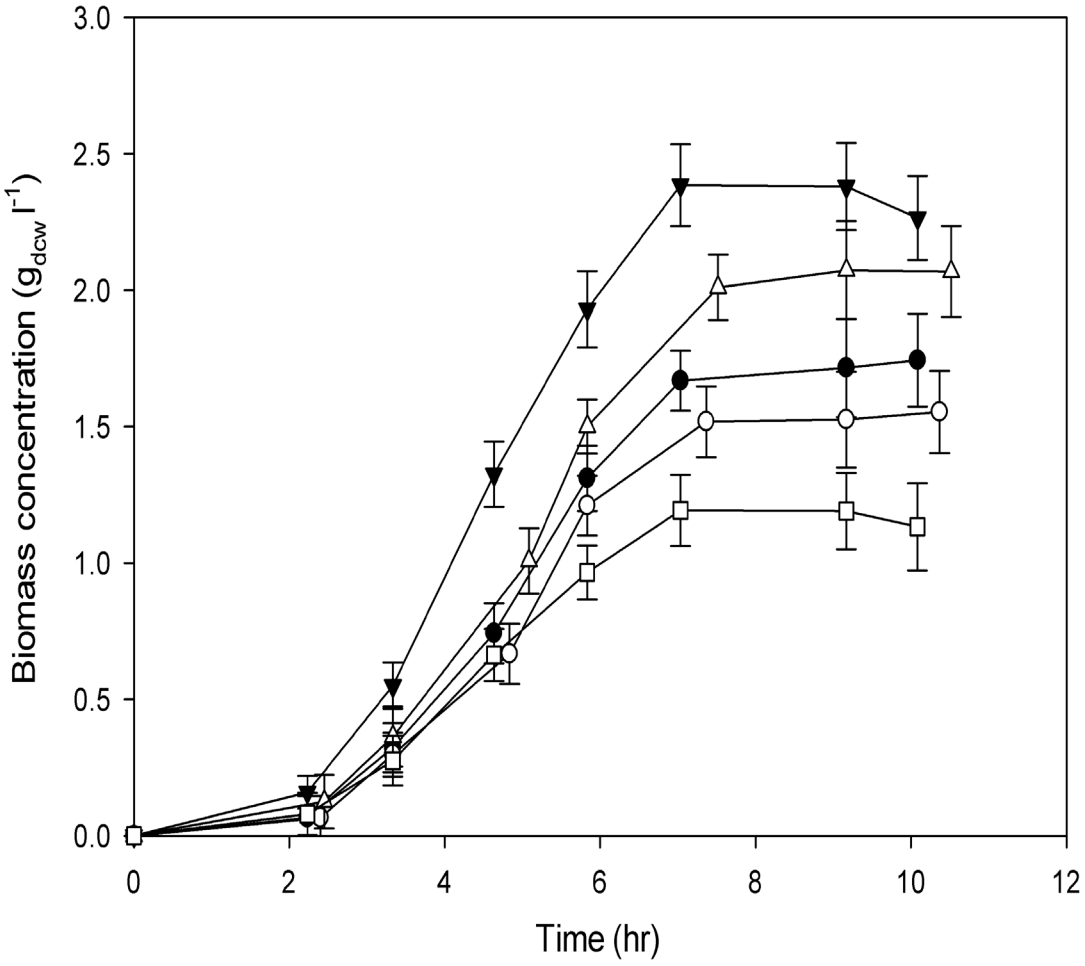

Figure 3.1. **Shake flask fermentation kinetics for *E. coli* BL21-Gold (DE3) grown in LB-glycerol medium at 37 °C with (▼) untransformed cells, and cells transformed with (Δ) pQR412 (TK), (●) pQR801 (CV2025 TAm), (o) double transformed uninduced strain with pQR801 and pQR412, (□) double transformed strain induced with 0.2 mM IPTG after 6 hours of cell growth. Fermentations performed as described in Section 2.4. Error bars represent one standard deviation about the mean (n=3).**

Single transformed strains with plasmid pQR412 (TK) or pQR801 (TAm) reached biomass concentrations of 2.1 and 1.8 $g_{DCW}\ l^{-1}$ respectively. These were 12.5% and 25% less than for the non transformed strain respectively. The double transformed and induced strain obtained a final biomass concentration of 1.2 $g_{DCW}\ l^{-1}$, representing nearly a 50% decrease compared with the non transformed strain. This decrease in growth, however, was compensated by the increase in enzyme synthesis which was expected due to the metabolic burden caused by the maintenance and expression of two plasmids.

In terms of enzyme expression levels, TK and TAm (induced with IPTG) in the single transformed cells were found to represent 20% and 40% w/w of the total protein respectively. For the double transformed strain, the TK concentration diminished compared to the single TK plasmid strain, and after inducing at a biomass concentration of 1 $g_{DCW}\ l^{-1}$ for 4 hours, the final enzyme expression of TK and TAm represented 8% and 36% w/w of the total protein. No difference in growth or enzyme expression was found by using engineered TKs D469T and D469E in the double transformed catalyst. Figure 3.2 shows the SDS-PAGE gel from cell extracts expressing individually TK and TAm and also for the double transformed biocatalyst.

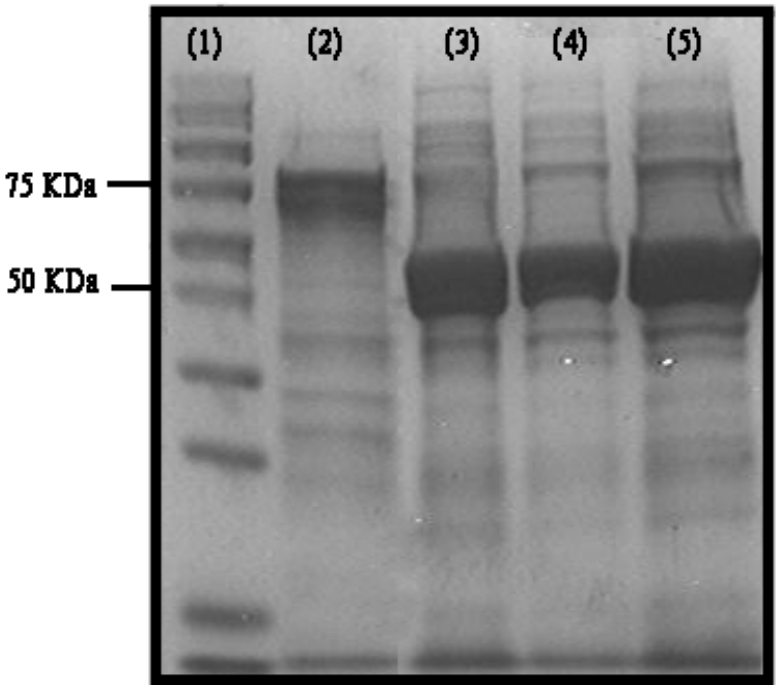

Figure 3.2. **SDS-PAGE gels showing expression of TK and TAm in cellular extracts of *E. coli* BL21(DE3)-Gold cells. Lane 1 is protein marker, lane 2 is cellular extracts with single plasmid pQR412 (TK), lane 3 is the cellular extracts with single plasmid pQR801, lane 4 and 5 are cellular extracts of double transformed cells with plasmid pQR412 (TK) and pQR801 (TAm). Biocatalysts produced as described in Figure 3.1 and Section 2.4. Molecular weight of TK is 73 kDa (Section 1.5.2.1) and molecular weight of TAm is 51 kDa (Section 1.5.3.1.)**

Because of the significantly lower activity of the TAm compared to the TK *(*Chen *et al*., 2006; Ingram *et al*., 2007), this method of induced expression of TK and TAm was considered acceptable and was used to prepare all the biocatalysts for the later two-step bioconversions performed in Section 3.7.

3.3.2. Considerations for one-pot TK-TAm synthesis

The use of multi-step enzymatic syntheses necessarily requires some compromises to be made regarding the optimum reaction conditions for each enzyme. This is particularly acute with isolated enzymes but can be alleviated, to some extent, by the use of whole cell biocatalysts. In order to rapidly collect the necessary data that will enable informed compromises to be made, all the following experiments have been performed using the microscale tools described in Section 2.8.1. This allowed an efficient and accelerated selection of the global reaction conditions that would be use in the one-pot syntheses (Section 3.7).

Optimum conditions reported for the *in vitro* TK-catalyzed synthesis of ERY was pH 7.0 using TRIS buffer at 25 ^{o}C (Hibbert *et al*., 2007; Ingram *et al*., 2007). Here, for PKD synthesis using whole cells with *E. coli* TK D469E, the optimum pH was found to be in the range pH 6.5-7 as shown in Figure 3.3. This value was similar to the optimum pH of 7.0 reported the E. *coli* TK D469T for the synthesis of PKD (Chen et al., 2008).

For the CV2025 TAm the optimum temperature reported for the synthesis of amino alcohols was 37^{o}C (Kaulmann *et al.*, 2007; Smith *et al*., 2010). The optimum pH for the whole cell TAm synthesis of ABT was found in this work to be pH 7.5 (Figure 3.4). This pH was in agreement with the pH of 7.5 found using the CV2025 TAm for the synthesis of APD (Smith et al., 2010).

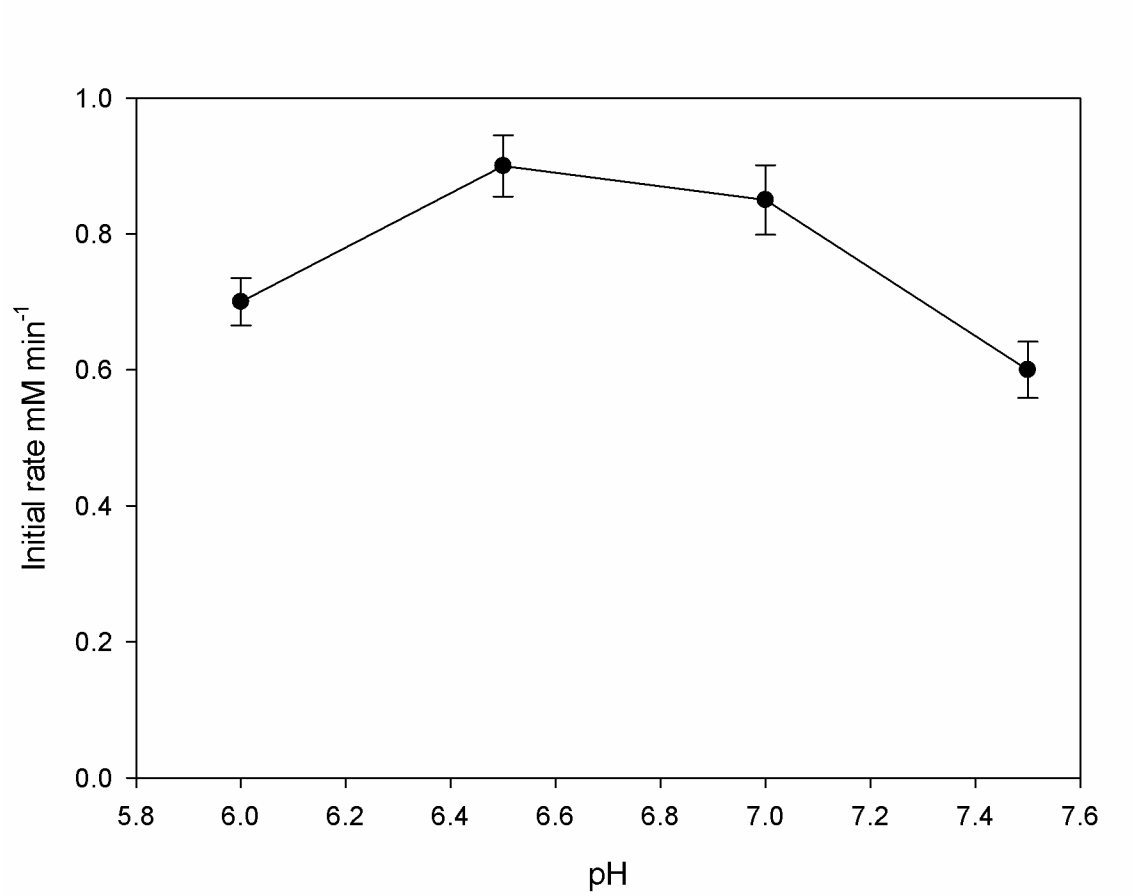

Figure 3.3. Effect of pH on the initial rate of PKD production by whole cells of *E. coli* expressing TK D469E. Reaction conditions: [PA] and [HPA] were 50 mM, 25°C; 300 rpm in 50 mM TRIS-HCL buffer ; total volume of 300 ul in 96 glass microplate. Bioconversions performed as described in Section 2.8.1. Error bars represent one standard deviation about the mean (n=3).

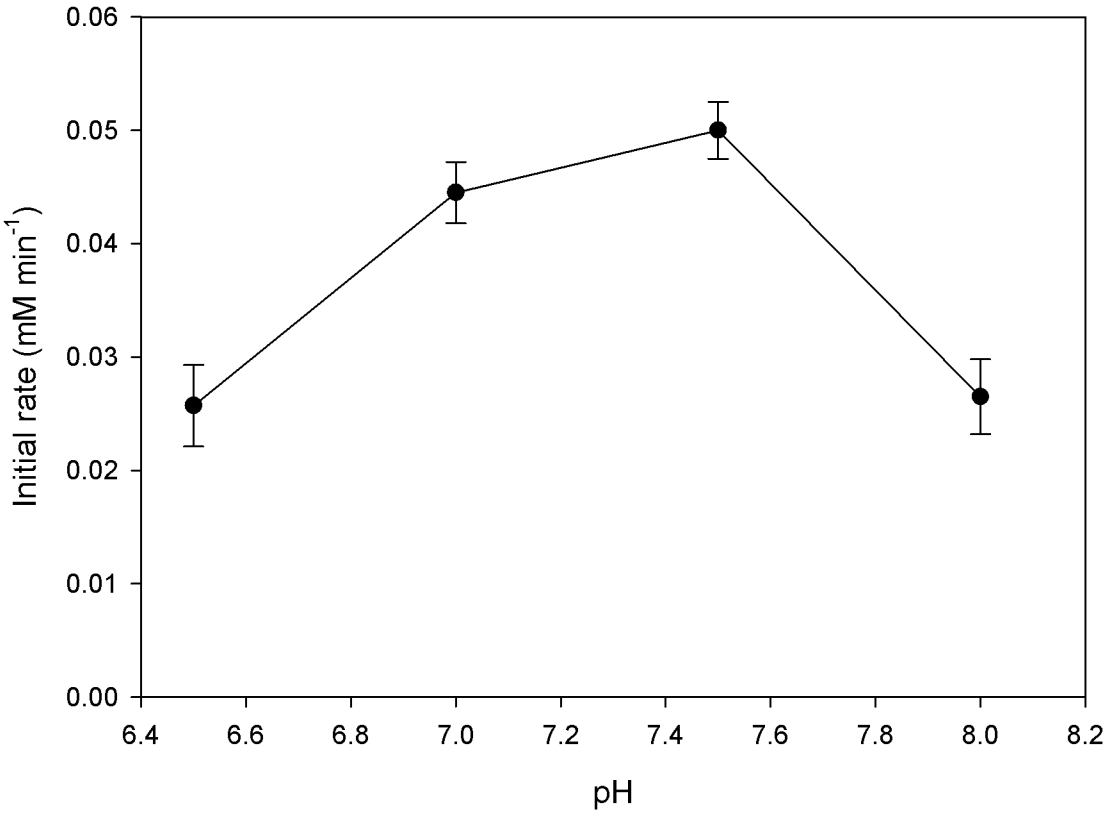

Figure 3.4. Initial rate of ABT production by whole cell TAm in function of pH. [MBA] and [ERY] were 50 mM, 37°C; 300 rpm in 50 mM HEPES buffer ; total volume of 300 ul in 96 glass microplate. Bioconversions performed as described in Section 2.8.1. Error bars represent one standard deviation about the mean (n=3).

Given the different optimum conditions for TK and TAm, a number of compromises on selected reaction conditions needed to be made. In order to evaluate these compromises, the synthesis of 10 mM ABT using MBA as amino donor was used as a reference reaction (Scheme 3.1). TK bioconversions in the presence of the working concentration of the TAm cofactor PLP demonstrated that this did not have any effect on the TK reaction. The same finding was obtained for the effect of TPP and Mg^{2+} on the TAm bioconversion (data not shown). Reactions of TK carried at a pH of 7.5 showed a decrease of TK activity of 33% as shown in Figure 3.3, nevertheless this pH was selected for subsequent studies considering the generally higher activity of TK compared to TAm (Figures 3.3 and 3.4).

In terms of reaction temperature, a control reaction using a lysate of untransformed *E. coli* BL21-Gold (DE3) showed that at 37 ^{o}C up to 50% of the HPA substrate was consumed by non-specific side reactions after 2 hours (Figure 3.5). In contrast at 30 ^{o}C, less than 5% of HPA was consumed over the same time.

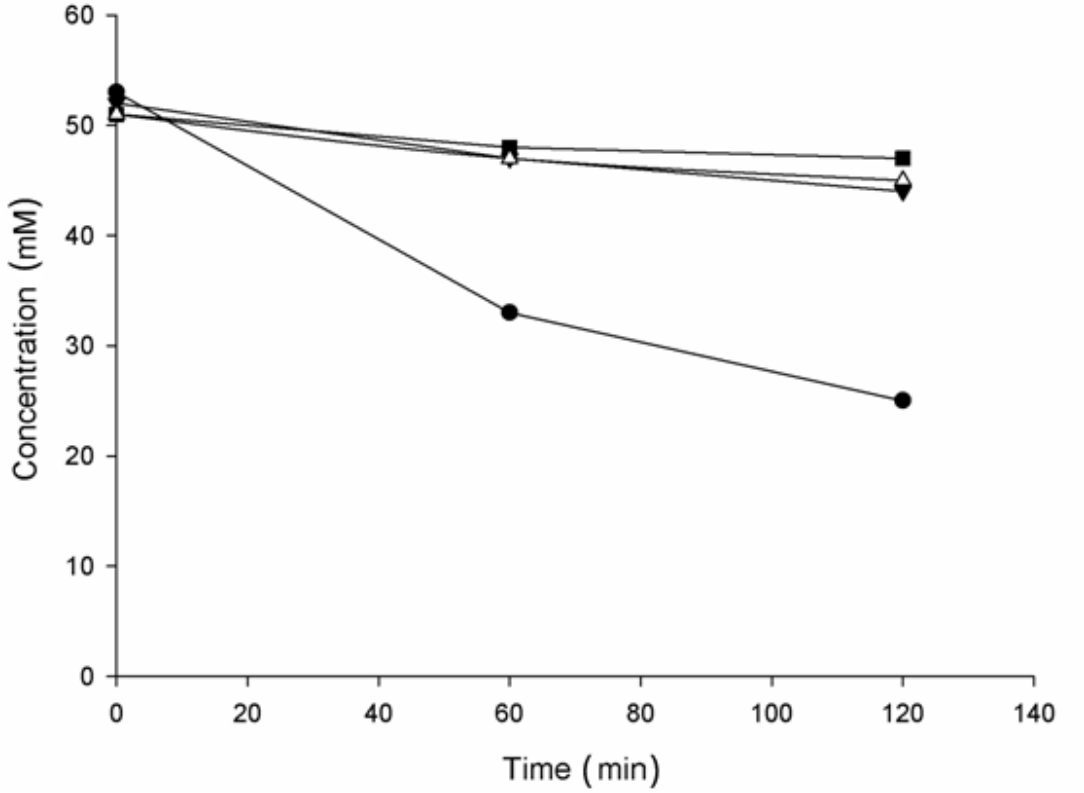

Figure 3.5. Non-specific consumption of reactatnts by TK *E. coli* cells at 37°C incubated only with (●) HPA, (▲) ERY, (■) PKD and (Δ) HPA at 30°C. Initial concentration of compound was 50 mM; total concentration of protein in the whole cell was 1 mg mL^{-1}, 300 rpm; 300 µl total reaction volume in 96 covered polystyrene microwell; pH 7.0 in 50 mM TRIS buffer. Control experiments performed as described in Section 2.8.1.

Consequently the TK-TAm reactions were performed at 30 ^{o}C to avoid non-specific HPA metabolism. With regards to buffer selection, control experiments using TRIS and phosphate buffer inhibited the CV2025 TAm compared to HEPES buffer (Figure 3.6).

It has been reported that HEPES buffer catalyzes biomimetic reactions between HPA and aldehydes at 37 ^{o}C (Smith *et al*., 2006), nevertheless at 30 ^{o}C, control experiments showed that less than 5% of HPA was lost by the biomimetic activity of 50 mM HEPES after two hours (data not shown). Based on all these considerations, the reaction conditions selected for the *in vitro* evaluation of the different TK-TAm variants were 30 ^{o}C and pH 7.5 in 50 mM HEPES buffer.

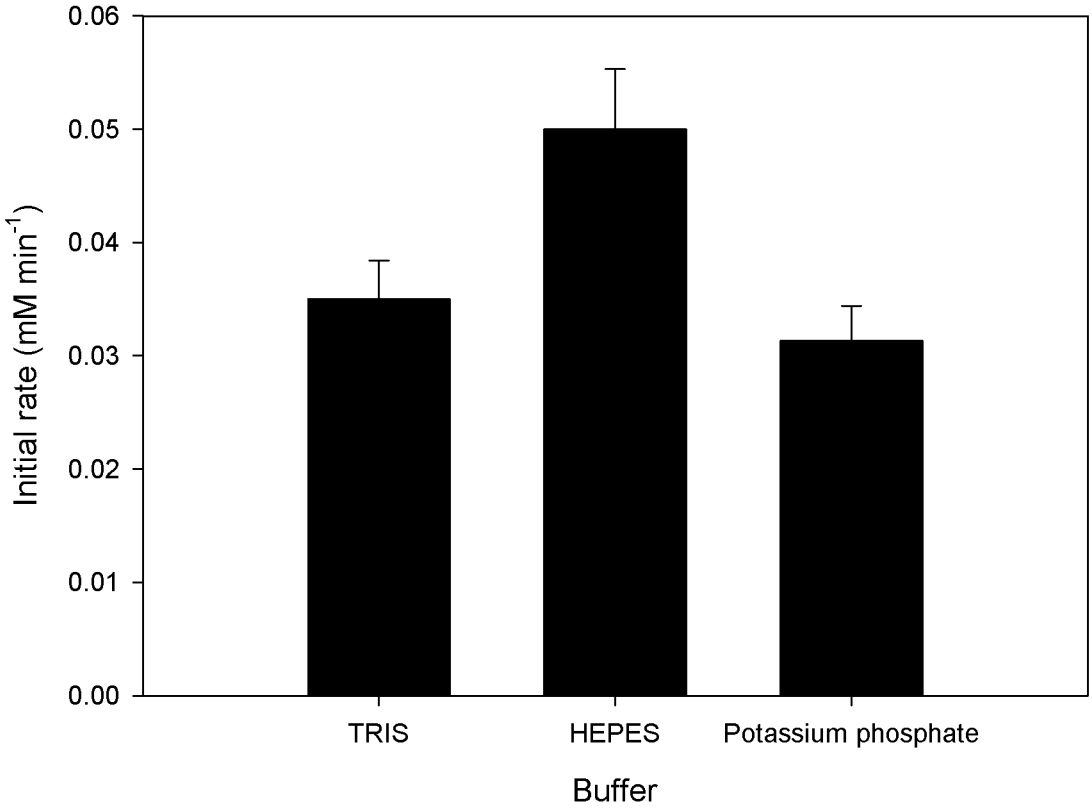

Figure 3.6. Effect of buffer composition on initial rate of ABT production by TAm in whole cell form. [MBA] and [ERY] were 50 mM, TAm was 0.3 mg mL^{-1}, 37^{o}C; 300 rpm in 50 mM of each buffer ; total volume of 300 ul in 96 glass microplate. Bioconversions performed as described in Section 2.8.1. Error bars represent one standard deviation about the mean (n=3).

3.3.3. Bioconversion with TK

Both the TK and TAm bioconversions were initially studied individually under conditions suitable for later two-step reactions (Section 3.4). Information on specific activities, *ee* and final yields gathered from those experiments would then enable to successfully "mix and match" the best pair of enzymes to synthesize specific amino alcohols.

Initial TK kinetics experiments showed that the activities and final yields obtained with *E. coli* TK lysates and whole cells were similar (Appendix IV), therefore data reported here for TK bioconversions were performed only with lysates containing the different TK variants. From TK mutant libraries developed previously (Hibbert et al., 2008; Smith et al., 2008, Cázares et al.,2010), the TK variants D469E, D469T and the wild type TK were selected as candidates due to their catalytic potential for the synthesis of ERY and/or PKD. Using HPA, the TK reactions were irreversible due to the release of CO_2 as a side product (Mitra & Woodley, 1996), and yields of more than 90% mol/mol were obtained using concentrations up to 300 mM of HPA and the aldehyde GA or PA (data not shown). In contrast, TAm reaction yields were severely hampered in concentrations higher than 10 mM using MBA as amino donor (Appendix VI), hence initial TK bioconversions studies were performed at this lower concentration.

Figure 3.7 shows the kinetics of ketodiol production for different combinations of TKs and aldehyde acceptors. The quantified activities, yields and measured *ee* values are summarized in Table 3.1.

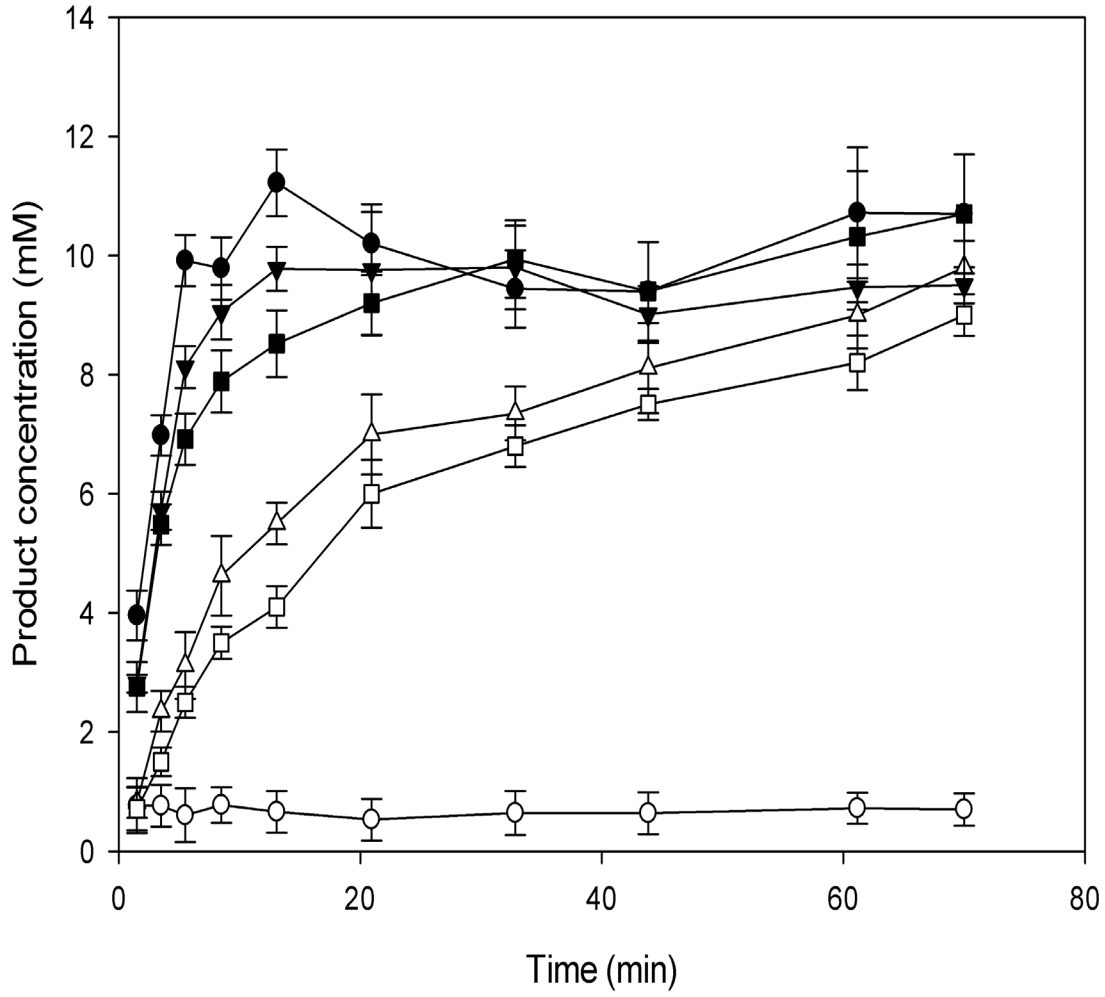

Figure 3.7. **Bioconversion kinetics showing ketodiol synthesis using different TK lysates and aldehyde acceptors: (●) ERY with wild type TK, (▼) ERY with D469T TK, (■) ERY with D469E TK, (Δ) PKD with D469T TK, (□) PKD with D469E TK, (○) PKD with wild type TK. Reaction conditions: 10 mM [HPA] and 10 Mm [GA] or [HPA], 2.4 mM TTP, 9 mM Mg^{2+}, 0.3 mg mL^{-1} TK, pH 7.5 in 50 mM TRIS, 30 ^{o}C. Bioconversions performed as described in Section 2.8.1. Error bars represent one standard deviation about the mean (n=3).**

Table 3.1. **Measured specific activities, product yields and *ee* for the TK lysate catalyzed bioconversions shown in Figure 3.7. The specific activities were determined as described in Section 2.8.1.**

TK variant	Aldehyde	Initial specific activity[a,c] (µmol min^{-1} mg^{-1})	*ee* (%)	Final conversion[b] (%mol/mol)
Wild type	GA	6.62 ± 0.13	>95	100
Wild type	PA	< 0.1	nd[d]	< 1
D469T	GA	5.13 ± 0.43	85	95
D469T	PA	1.98 ± 0.27	64	98
D469E	GA	4.96 ± 0.39	nd	100
D469E	PA	1.49 ± 0.26	>90	90

[a]The initial specific activity is based on the measured mass of TK in each bioconversion.
[b]Final conversion was determined at t=70 min.
[c] The error of the specific activity represents one standard deviation about the mean (n=3).
nd = not determined

The wild type TK was selected for ERY synthesis because it presented the highest activity and *ee* of 6.6 µmol min^{-1} mg^{-1} and >95% respectively. Gyamerah & Willetts (1997) obtained an activity of 13.2 µmol min^{-1} mg^{-1} for the same HPA and GA reaction using wild type *E. coli* TK. This was in agreement with the work described here considering the differences in concentration of substrates used.

For the synthesis of PKD, the highest activity was 1.98 µmol min^{-1} mg^{-1} using the TK mutant D469T, while no activity after 70 min of reaction was detected using the wild

type enzyme. The *ee* of PKD obtained with TK D469E was >90%, compared to a 64% *ee* of D469T. Due to the importance of the *ee* in the synthesis of optically pure amino alcohols, the TK mutant D469E was selected even though it had a 25% lower activity than D469T. The D469E mutation is in the pyrimidine binding domain of TK, and is assumed to enable activity towards PA because it replaces the original interaction of Asp with the C-2 hydroxyl group of GA, by creating a specific interaction between the Glu and the methyl group of the new substrate (Hibbert et al., 2008; Cázares et al., 2010).

3.3.4. Bioconversions with TAm

Single step TAm bioconversions focused on the CV2025 TAm as it had already been shown to be the best candidate for amino alcohol synthesis among several other transaminases cloned in previous work (Kaulmann *et al*., 2007). The comparison of *in vitro* and *in vivo* catalytic activity of CV2025 TAm had not previously been reported, so it was investigated here where a whole cell TAm biocatalyst was compared with a lysate for the synthesis of a number of ketodiols.

Figure 3.8 shows product formation kinetics using either MBA or IPA as amino donors and PKD as amino acceptor. Due to the volatility of IPA, an excess concentration of 100 mM IPA was initially used instead of 10 mM MBA to compensate for any loss due to evaporation. The results of activities and final yields of both amino alcohols are summarized in Table 3.2.

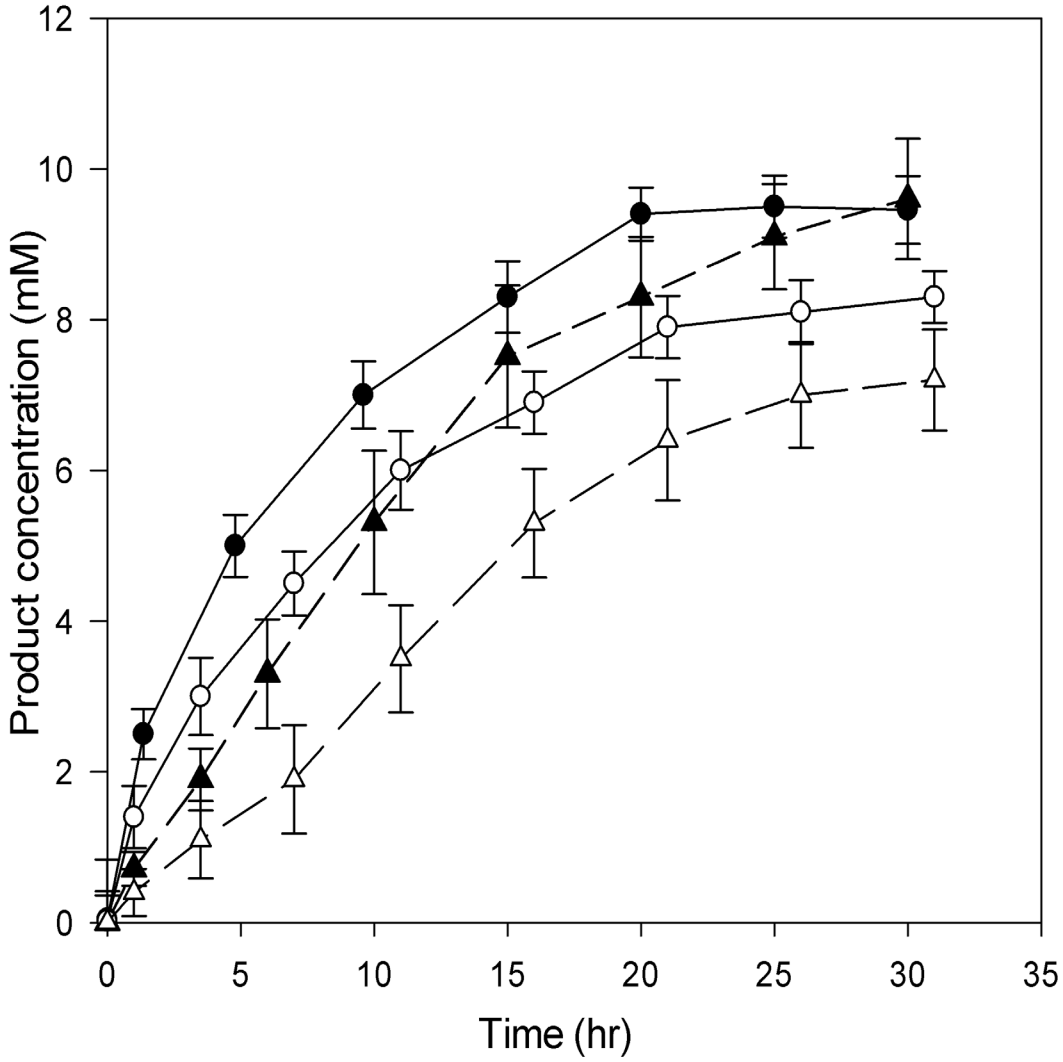

Figure 3.8. **Bioconversion kinetics showing APD synthesis using CV2015 TAm in either lysate or whole cell form with different amino donors: (●) whole cell with MBA, (▲) whole cell with IPA, (○) lysate with MBA, (Δ) lysate with IPA. Reaction conditions : 10 mM [MBA] or 100 mM [IPA], 10 mM [PKD], 0.2 mM PLP, 0.3 mg mL^{-1} TAm, pH 7.5 in 50 mM HEPES, 30 ^{o}C. Bioconversions performed as described in Section 2.8.1. Error bars represent one standard deviation about the mean (n=3).**

Table 3.2. Measured specific activities and product yields for the TAm catalyzed conversion of PKD and ERY. The specific activities were determined as describe in Section 2.8.1.

Biocatalyst form	Amino donor	Amino acceptor	Initial specific activity[a,c] (µmol min^{-1} mg^{-1})	Final conversion[b] (%mol/mol)
Whole cell	MBA	PKD	0.074 ± 0.006	95
Lysate	MBA	PKD	0.034 ± 0.003	83
Whole cell	IPA	PKD	0.029 ± 0.0035	96
Lysate	IPA	PKD	0.015 ± 0.003	75
Whole cell	MBA	ERY	0.096±0.005	92
Lysate	MBA	ERY	0.045±0.003	86
Whole cell	IPA	ERY	0.035±0.05	91
Lysate	IPA	ERY	0.026±0.04	71

[a]The specific activity was based on the measured mass of TAm present in each bioconversion. For whole cell experiments, it was calculated based on 50% of the dry cell weight of the cells being protein (Watson, 1972), and SDS-PAGE analysis that showed that 40% of the protein was TAm.

[b]Yield was determined at t=30 hours.

[c] The error of the specific activity represents one standard deviation about the mean (n=3).

The CV2025 TAm showed a 4 fold increase in yield and a 40 fold improvement in specific activity (Figure 3.8 and Table 3.2) compared to initial work with a β-alanine-pyruvate transaminase from *Pseudomonas aeruginosa* (Ingram *et al*., 2007).

The final yield of ABT of 92 and 86 % mol/mol using whole cell and lysates respectively improved the previously reported values of 14-22% mol/mol (Kaulmann *et al*., 2007).

The quantitative conversion of the reaction observed in Figure 3.8 and Table 3.2 was in agreement with the equilibrium constants obtained for a similar transamination of pyruvate with MBA using the ω-transaminase from *Bacillus thuringiensis* JS64, showing that the forward reaction was thermodynamically more favourable than the reverse reaction (Shin & Kim, 1998).

Smith *et al*., (2010) obtained a 93% mol/mol yield for the synthesis of APD with the CV2025 TAm using an excess of PKD (molar ratio of 1.5 PKD/IPA). In this work, the use of whole cells enabled to reach an almost complete conversion of the substrates with a final yield of 96 % mol/mol without having to use an excess of the chiral ketodiol.
Nevertheless, working with higher concentrations severely inhibited the bioconversion as shown in Figure 3.9, which illustrates the kinetics of TAm production of APD using initial equimolar concentration of substrates of 50 mM PKD with IPA or MBA as amino donors.

After 40 hours, the final yields were 52 and 23 % using IPA and MBA respectively, underlying the strong inhibition caused by MBA. This inhibitory effect of MBA has also been reported in the literature with transaminases from *Klebsiella pneumonia* and *Vibrio fluvialis* (Shin and Kim, 1997; Yun *et al*., 2004). In this case the use of *in situ* product removal by ion exchange resins or coupled reactions could be a possible solution as has been shown by others (Truppo *et al*., 2010).

Analyzing the results of Table 3.2 and Figure 3.8, similar yields were obtained using ERY or PKD as substrates, but the specific activities using ERY were between 17% and 42% higher than those of PKD.

.

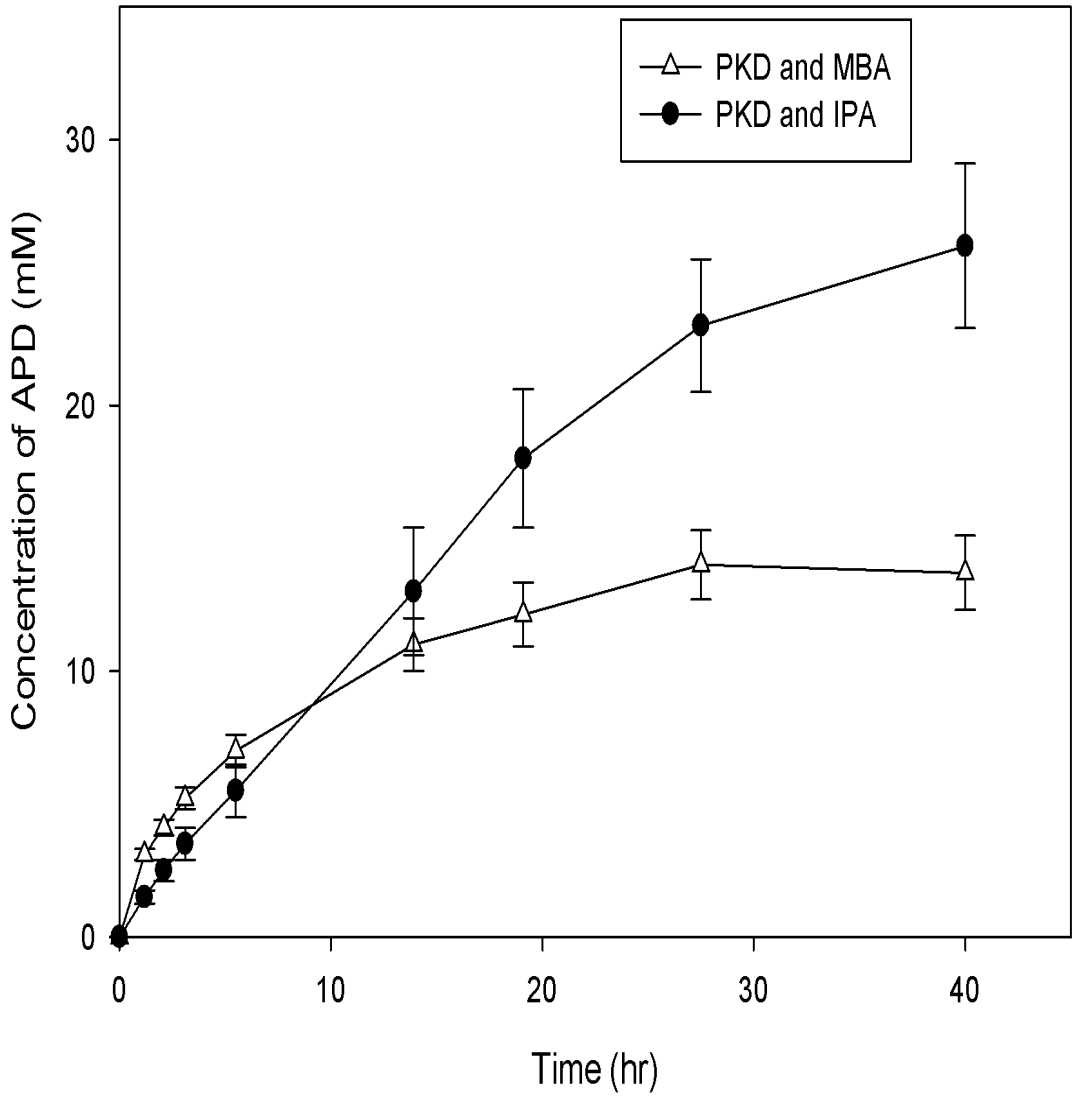

Figure 3.9. Bioconversion kinetics showing APD synthesis using CV2015 TAm in whole cell form with different amine donors: (●) 50 mM PKD and MBA and (Δ) 50 mM [PKD] and [IPA]. Reaction conditions: 0.2 mM PLP, 0.3 mg mL^{-1} TAm, pH 7.5 in 50 mM HEPES, 30 ^{o}C. Bioconversions performed as described in Section 2.8.1. Error bars represent one standard deviation about the mean (n=3).

For synthesis of both amino alcohol products, the whole cell biocatalysts performed better than the lysates demonstrating the beneficial effect of using TAm *in vivo* for these bioconversions. This phenomenon has also been reported in the literature, where higher yields using whole cell TAm biocatalysts have been attributed to better stability of the enzyme inside the cell (Shin & Kim 1997), to metabolism consumption of inhibitory compounds (Shin & Kim, 1999), or to the effect of the cell membrane in partitioning inhibitory components between the inside and outside of the cell (Yun *et al*., 2004).

In this work, the inhibitory product acetophenone (AP) was not further metabolized by the whole cells and MBA and AP where found to be more inhibitory than IPA and acetone (Figure 3.9). In contrast, when using TAm lysates lower yields were obtained using IPA (75 % and 71 % mol/mol for APD and ABT respectively) compared to MBA (83 % and 86 % mol/mol respectively). Addition of more enzyme and PLP after the initial reaction had stopped partially restored the biocatalytic activity, suggesting that the improved yield using whole cells could be attributed to an increase in stability of the enzyme.

Based on the results in Table 3.2, the whole cell TAm biocatalyst was selected for further study because of its superior performance compared to the lysate. IPA appears preferable as amine donor because of its advantages in terms of economy, downstream processing and reduced inhibition compared to MBA. However, both amine donors were evaluated for one-pot synthesis reactions in Section 3.7.

3.3.5. One-pot synthesis of amino alcohols

In order to achieve the one-pot synthesis of amino alcohols, two whole cell biocatalysts were constructed both with plasmid pQR801 expressing the CV2025 TAm, and with either pQR412 expressing the TK mutant D469E or the wild type variant for APD and ABT syntheses respectively.

The first one-pot synthesis of APD using MBA as amino donor gave a poor yield (15 % mol/mol) of amino alcohol after 20 hours but another product was detected by HPLC analysis after derivatizing the samples (Section 2.9.6). This compound was identified as serine, which was possibly produced by the transamination of HPA. To overcome this problem, MBA was subsequently added in fed batch mode after the TK reaction was complete. A typical reaction kinetic profile for this mode of operation is shown in Figure 3.10.

The volume added of the solution of MBA was equal to the volume of the reaction mixture; hence the original concentration of the reactants was diluted 2-fold after MBA addition. The first step comprising the TK reaction reached completion after 4 hours with a specific activity of 2.68 μmol min^{-1} mg^{-1}. The second step TAm reaction had a specific activity of 0.067 μmol min^{-1} mg^{-1} and reached a maximum APD yield of 90 % mol/mol after 21 hours of reaction with MBA. This measured activity was in agreement with the one found for the single TAm reaction (Table 3.2).

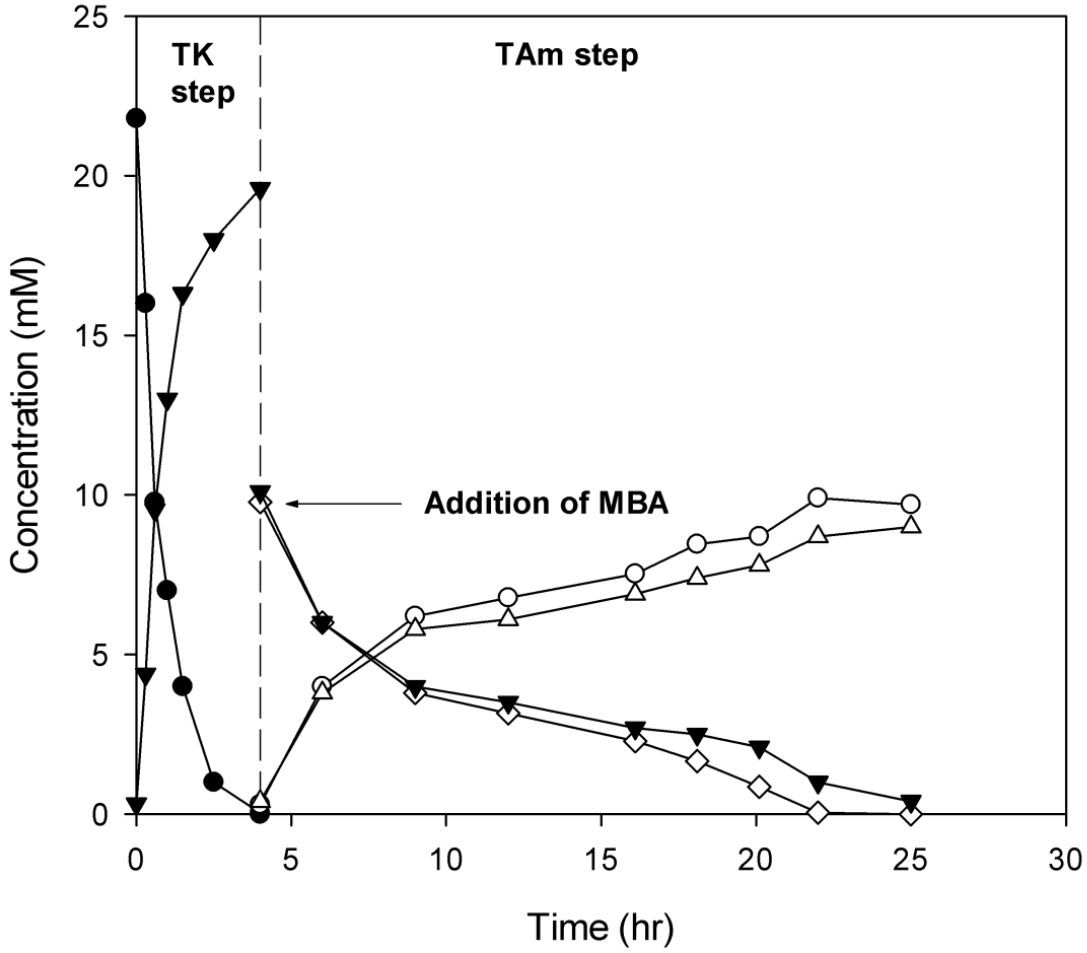

Figure 3.10. **Typical bioconversion kinetics for the sequential whole cell TK-TAm catalytic synthesis of APD with addition of amine donor (MBA) after 4 hours : (▼) PKD, (●) HPA, (Δ) APD, (◊) MBA and (o) AP. Reaction conditions (TK step): 20 mM [HPA] and [PA], 0.4 mM PLP, 2.4 mM TTP, 9 mM Mg^{2+}, 0.095 mg mL^{-1} TK, 0.43 mg mL^{-1} TAm, pH 7.5 in 50 mM HEPES, 30 ^{o}C. TAm step was initiated by adding MBA solution to reach a concentration of 10 mM which resulted in a 2 fold dilution of reactants. Bioconversions performed as described in Section 2.8.1.**

When using IPA as amine donor at the compromise temperature of 30 ^{o}C (Section 3.4), the TAm did not show any noticeable activity towards HPA, GA or PA over 5 hours. This was not the case at 37 ^{o}C, where activity towards TK substrates was detected in that period of time (data not shown). This suggested it was possible to perform the bioconversion of APD using IPA in a true one-pot synthesis at 30 ^{o}C as shown in Figure 3.11, were the TK reaction was completed after 5 hours, leading to a 90 % mol/mol yield of APD after 25 hours.

The specific activities of TK and TAm in the one-pot synthesis were 1.46 and 0.022 μmol min^{-1} mg^{-1} respectively, which were also in agreement with the corresponding TK and TAm specific activities for the single bioconversions (Table 3.1 and 3.2). Similar results were obtained for the one-pot synthesis of ABT using IPA as amine donor, reaching a final yield of 87 % mol/mol after 25 hours as shown in Figure 3.12.

The TK reaction for the ABT synthesis was completed in 1.5 hours instead of the 5 hours required for the APD synthesis. This was in agreement with the higher activity of the wild type TK enzyme towards ERY synthesis in comparison to the activity of the D469E variant towards PKD synthesis (Table 3.1).

The 87% mol/mol yield for ABT synthesis represented an improvement of 4-fold in yield in a quarter of the reaction time compared to previous work (Ingram *et al,* 2007). The 90 % mol/mol yield for APD represented a 7-fold improvement in a third of the reaction time compared to the previously reported two separated steps synthesis (Smith *et al.,* 2010).

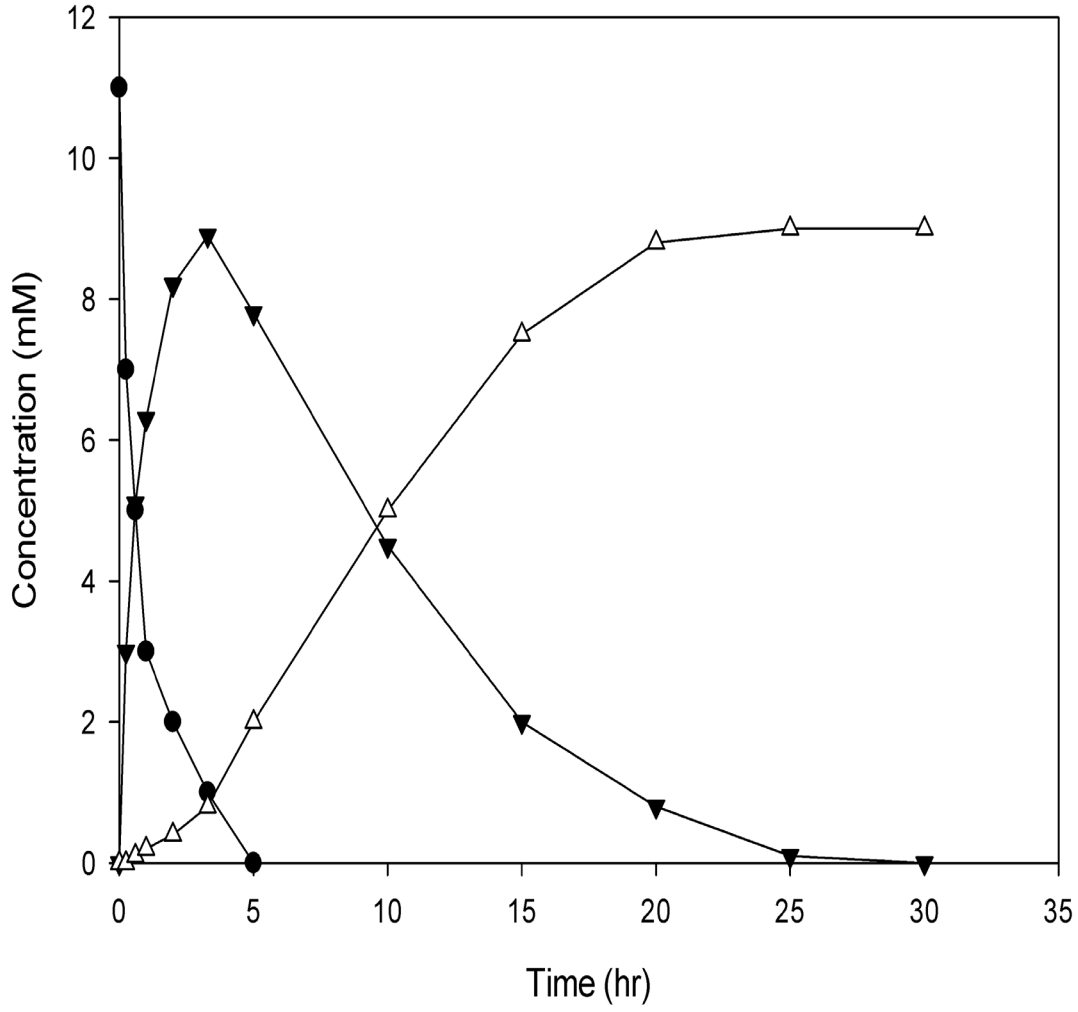

Figure 3.11. **Typical bioconversion kinetics for the one-pot, whole cell TK-TAm catalytic synthesis of APD using IPA as amine donor: (▼) PKD, (●) HPA, and (Δ) APD. Reaction conditions: 10 mM [HPA] and [PA], 100 mM [IPA], 0.2 mM PLP, 2.4 mM TTP, 9 mM Mg^{2+}, 0.095 mg mL^{-1} TK , 0.42 mg mL^{-1} TAm, pH 7.5 in 50 mM HEPES, 30 ^{o}C. Bioconversions performed as described in Section 2.8.1.**

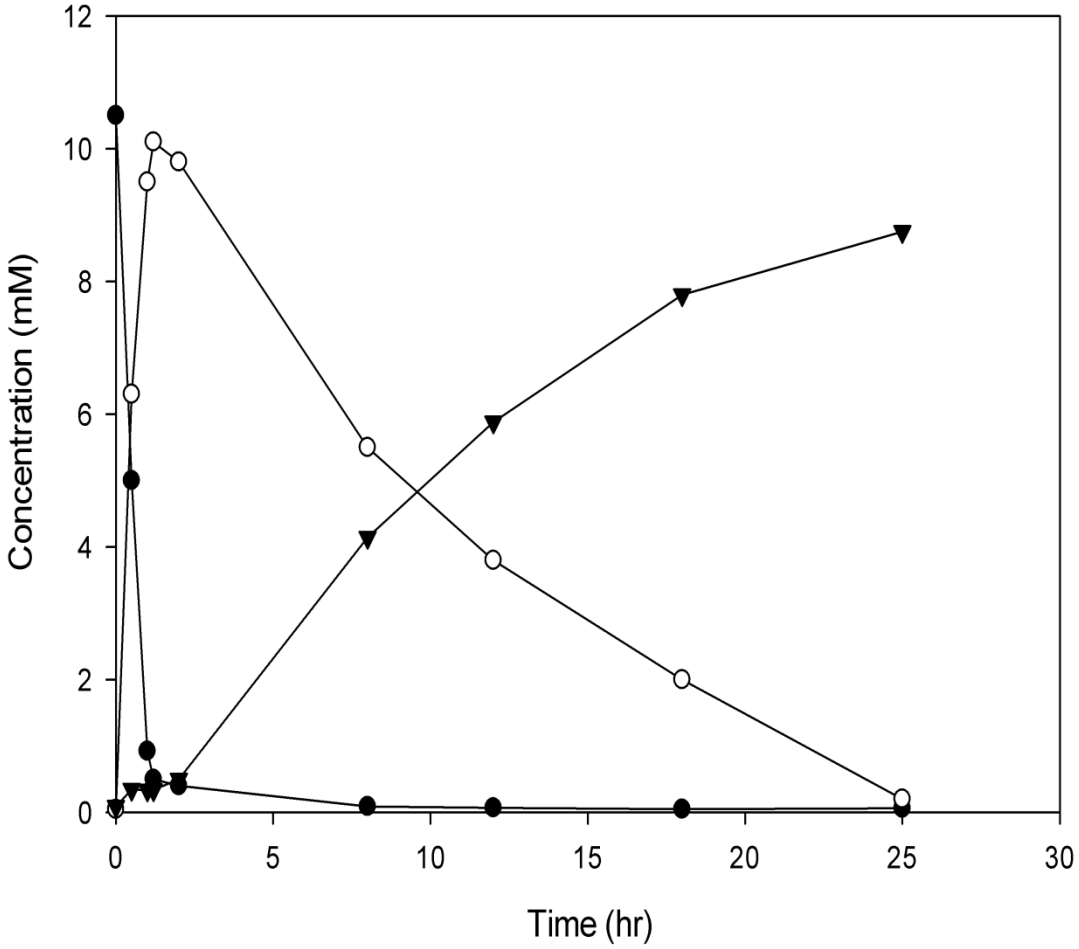

Figure 3.12. **Typical bioconversion kinetics for the one-pot, whole cell TK-TAm catalytic synthesis of ABT using IPA as amine donor: (▼) ABT, (●) HPA, and (o) ERY. Reaction conditions: 10 mM [HPA] and [GA], 100 mM [IPA], 0.2 mM PLP, 2.4 mM TTP, 9 mM Mg^{2+}, 0.095 mg mL^{-1} TK , 0.42 mg mL^{-1} TAm, pH 7.5 in 50 mM HEPES, 30 ^{o}C. Bioconversions performed as described in Section 2.8.1.**

3.4. SUMMARY

The work presented in this Chapter has shown that it is possible to rapidly evaluate and "mix and match" pairs of TK and TAm enzymes, in order to facilitate the design of the one-pot synthesis of various optically pure amino alcohols. The use of microscale experimentation (as described in Section 2.8.1) has enabled rapid collection of the reaction kinetic data, which was required to optimise overall reaction conditions (Figures 3.3 to 3.6), as well as selecting the best enzyme candidates (Figure 3.7 and 3.8). Together these two technologies comprise the experimental "toolbox" for the rapid evaluation of multi-step enzymatic synthesis of amino alcohols, that it was the aim of this Chapter to establish.

TK-TAm biocatalysts were successfully constructed (Figure 3.1), achieving a final enzyme expression of TK and TAm of 8% and 36% w/w of the total protein (Figure 3.2). The best reaction conditions were determined to be at 30^{o}C using a pH of 7.5 (Figure 3.3 to 3.6). The engineered TK D469E and the wild type TK were found to be the best candidates for the synthesis of APD and ABT respectively (Figure 3.7). Also, the CV2025 TAm was discovered to display better catalytic activity when used *in vivo* rather than *in vitro* (Figure 3.8). This lead to the design and construction of whole cell biocatalysts to perform the one-pot synthesis of the single diastereoisomers APD (Figure 3.11) and ABT (Figure 3.12). IPA was identified as a preferable amine donor compared to MBA for the one-pot syntheses, because side reactions with the initial TK substrates (catalysed by TAm) were negligible and higher yields could be obtained at higher concentrations (Figure 3.9). The TAm step was found as the bottleneck of the *de novo* pathway, due to its one order of magnitude lower specific activities compared to TK (Table 3.1 and 3.2), as well as been inhibited by higher concentrations of substrates (Figure 3.9). Therefore Chapter 4 was focused in obtaining the corresponding kinetic parameters in order to optimize the TAm bioconversion.

4. KINETIC MODELLING OF TRANSAMINASE SYNTHESIS OF CHIRAL AMINO ALCOHOLS[†]

4.1 INTRODUCTION

The ω-TAm from *C. violaceum* 2025 was shown in Chapter 3 to be a promising candidate to integrate the TK-TAm *de novo* pathway for the synthesis of chiral amino alcohols. Nevertheless it was also identified as the bottleneck of the one-pot synthesis presenting low specific activities and yields relative to the preceding TK bioconversion (Table 3.2).

The determination of the full TAm kinetic model would allow simulation of the conversion, enabling determination of the best reaction conditions, bioreactor design and integration within multi-step enzymatic syntheses (Chen et al., 2006; Sin et al., 2009; Santacoloma et al., 2011).

The determination of the required data for establishment of full kinetic models can be time and resource consuming, especially when using the traditional linear methods like the Lineweaver and Burk plot (Ranaldi 1999; Chen *et al*., 2009). This problem is further emphasised for non-natural bioconversions used in the pharmaceutical industry, that often present strong substrate and product inhibition (Yazbeck *et al.*, 2004), as commonly found with TAm bioconversions as described in Section 1.5.3.

Nonlinear regression methods can use programmable optimization algorithms to determine the kinetic parameters, consequently been less time and resource consuming (Blackmond, 2005).

[†] The majority of the results presented in this chapter have been submitted for publication as: L.Rios-Solis, N. Bayir, M. Halim., J. Hao, F. Baganz., G.J. Lye. Kinetic modeling of a transaminase to produce optically pure amino alcohols. *Biochem. Eng. J*. Submitted.

However, the determination of model parameters can suffer from global convergence problems, in particular the estimation procedure can be strongly dependent on the initial values of the parameters (Moros et al., 1996).

Hybrid methods combining traditional initial rates experiments to identify a solution in the vicinity of the global minimum, with non linear regression methods to determine the exact location of the solution emerge as an ideal solution to be integrated in the microscale toolbox (Katare et al., 2004; Chen et al., 2008).

4.2 AIM AND OBJECTIVES

Based on the discussion in Section 4.1 the aim of this Chapter is to develop a methodology to rapidly establish the TAm kinetic parameters in order to determine the optimum reaction conditions. The methodology was based on combining non linear numerical techniques (Katare et al., 2004; Morbiducci et al., 2005; Chou & Voit, 2009; Chen et al., 2008) with microscale experimentation (Lye et al., 2003; Micheletti & Lye, 2006). The approach will be exemplified for the TAm mediated synthesis of ABT as indicated in Scheme 3.1. The key objectives of this Chapter are thus:

- Extension of the non linear parameter estimation method first proposed by Chen et al., (2008) for application to equilibrium-controlled enzymatic reactions.
- Illustrate the new approach by determination of the apparent kinetic parameters of the TAm mediated synthesis of ABT using whole cells, which was found to be best biocatalyst form in Section 3.3.4.
- Validate the kinetic parameters obtained against additional experimental data.
- Identify main bottlenecks of the reaction.
- Identify the best reaction conditions for the synthesis of amino alcohols.

4.3 RESULTS

4.3.1 Model driven methodology for TAm kinetic parameters identification

In previous works (Chen *et al*. 2008; Chen *et al*. 2009), a microscale model driven methodology for determining the kinetic parameters of transketolase (TK) bioconversions was developed and validated for the synthesis of several ketodiols.
The method consisted in obtaining preliminary values of kinetic parameters on a step-by-step basis, reducing the number of estimated parameters to 3 or 4. These preliminary values where then used as initial guesses for a final parameter estimation step via nonlinear regression. Compared with the conventional linear plotting methods, this approach demonstrated to significantly reduce the number of experiments and materials required for kinetic parameter estimation, making it useful to rapidly simulate and optimize large scale bioconversions (Smith et al. 2010).

The TAm reaction is reversible and usually present strong substrate and/or product inhibition (Koszelewski et al., 2010), in addition the TAm model was only partially elucidated as described in Section 1.5.3.4, therefore the methodology should be able to test different kinetic models in order to determine the correct reaction mechanism.
However, the previous methodoliges were developed for TK bioconversions, which were irreversible and their kinetic model included less parameters and was already fully elucidated. Therefore several modifications had to be made to the original methodology, in order to enable the rapid and accurate elucidation of the Tam reaction model, as well as the determination of the kinetic parameters of a reversible reaction which may include strong substrate and/or product inhibition.

The methodology developed incorporates 5 main Steps as described in Figure 4.1 which are as follows:

1) Determination of the region of linear proportionality between the enzyme concentration and the initial rate.

2) Gathering of initial rate data for both forward and reverse reaction, testing of different kinetic models to elucidate the preliminary reaction pathway and determining the preliminary Michaelis and rate constants.
3) Determination of the stability of the enzyme under actual bioconversion conditions.
4) Determination of the preliminary values of equilibrium and inhibition constants through non linear regression of experimental progress curves.
5) Reconciliation of the parameters through a new round of non linear regression of the progress curves, using all the preliminary values of the kinetic parameters as initial guess for the final regression, and verification of the selected reaction pathway.

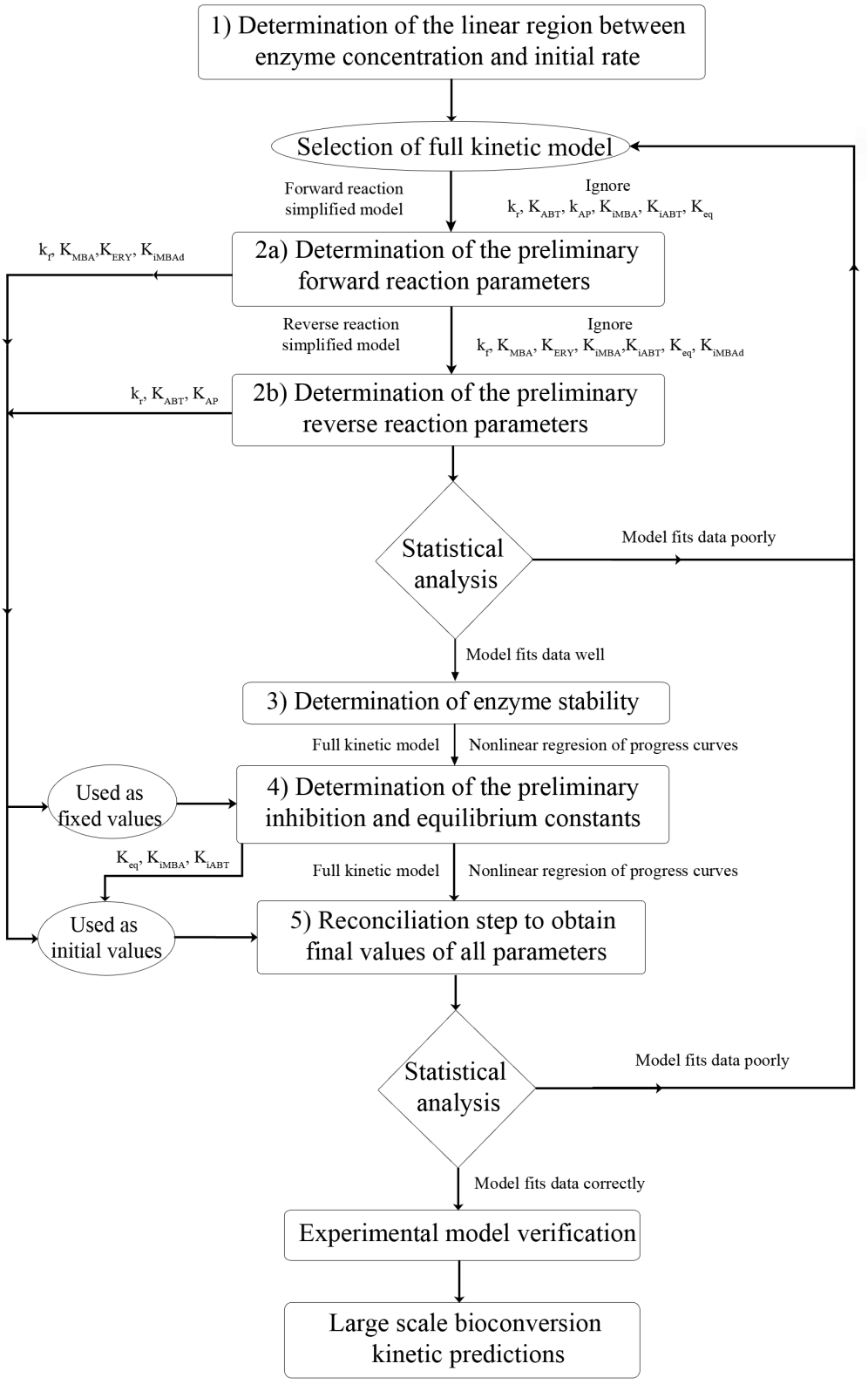

Figure 4.1. Schematic representation of the systematic procedure for rapid apparent kinetic parameter identification for an equilibrium controlled bioconversion such as the whole cell TAm mediated synthesis of ABT from ERY and MBA (Scheme 3.1).

In order to implement the procedure illustrated in Figure 4.1, a programme was developed using Matlab software (MathWorks, Natick, MA, USA) in order to automatically perform all the non linear regressions and statistical analyses. The complete Matlab code can be found in Appendix V.

The synthesis of ABT using MBA as amino donor was selected initially to develop the methodology in this chapter, because the analytical tools to follow the reaction were simpler and more established than using IPA as amino donor (Section 2.9.6).

4.3.2 Proportionality between reaction rate and enzyme concentration

As described in Figure 4.1, the first Step to obtain the kinetic parameters was to determine the region of linear proportionality between the TAm concentration in whole cell form and the initial reaction rate. This was necessary to ensure that any increase in enzyme concentration would contribute fully to the measured kinetics (Chen *et al.*, 2008). It is common that increasing the enzyme concentration in a reaction will not correspond to a proportional increase in the initial rate of the bioconversion; the reasons are usually mass transfer limitations or certain forms of inhibition (Law *et al*., 2006). The substrate concentrations used were 10 mM MBA and 50 mM ERY for each enzyme concentration and the linear relationship could be maintained up to a TAm concentration of 0.8 mg mL^{-1} as can be seen in Figure 4.2. This value was thus set as the upper limit for all subsequent experiments.

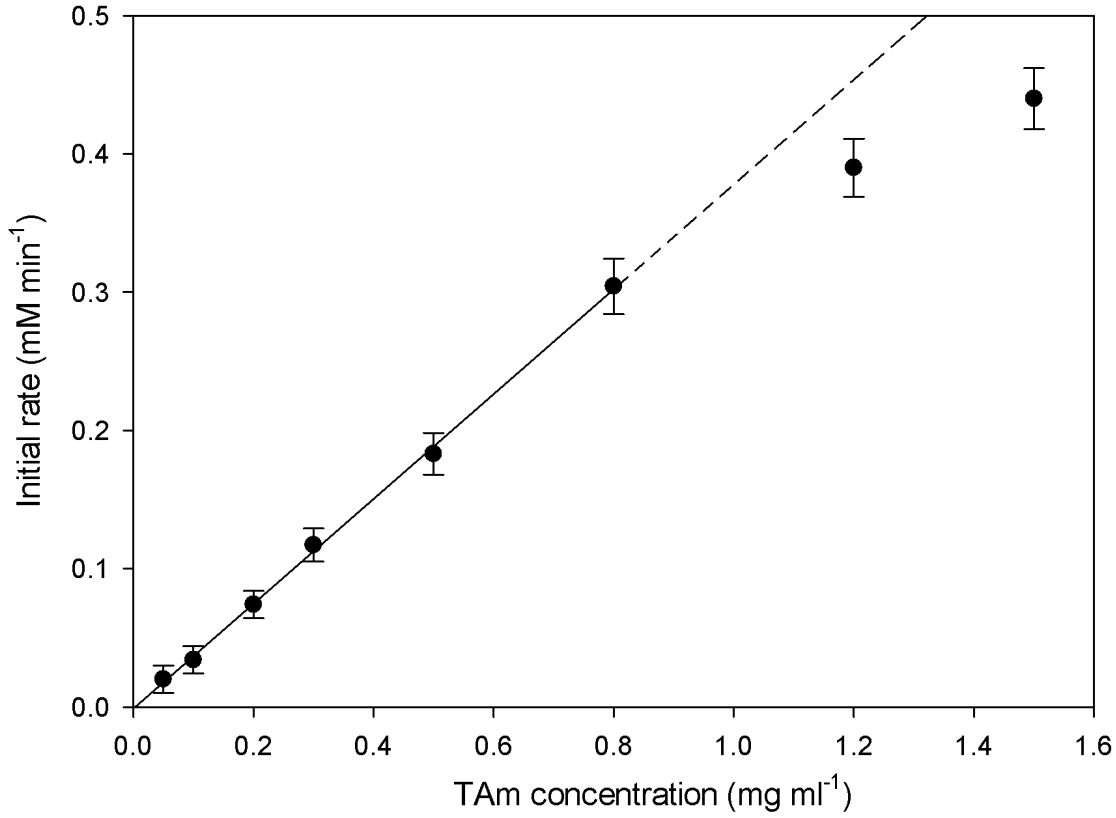

Figure 4.2. Apparent initial rate of ABT and AP TAm mediated synthesis (Scheme 3.1) as a function of TAm concentration in whole cell form. Reaction conditions: 10 mM [MBA] and 50 mM [ERY], 0.2 mM PLP, 30°C and pH 7.5 in 200 mM HEPES. Experiments performed as described in Section 2.8.1. Whole cells produced as described in Section 2.4.2. Solid line fitted by linear regression (R^2 0.99885). Error bars represent one standard deviation of the mean (n=3).

This upper limit result of 0.8 mg mL^{-1} was one order of magnitude lower when compared to other types of enzymes like TK (Chen *et al*., 2009). The observation of a lower limit of proportionality among transaminases has been reported before (Banks *et al.* 1959). A possible explanation is that the enzyme can show self-inhibition where an end amino group of one TAm molecule might bind the pyridoxal phosphate associated with the active site of another enzyme molecule (Ellis & Davies, 1961). In the case of whole cells mass transfer limitations across the cell wall might also be the cause (Ni & Chen, 2004; Woodley, 2006).

4.3.3 Kinetic model of TAm and initial rate experiments

In the second Step of the methodology described in Figure 4.1, a set of initial rate data varying the concentration of one substrate, while maintaining the other one fixed was obtained for both forward and reverse reactions (Scheme 3.1).

Figure 4.3 shows a plot of the measured initial reaction rate for the forward reaction as a function of varying concentrations of substrate ERY while maintaining the concentration of MBA fixed at 10 mM. A second plot is shown in Figure 4.3 for the variation of the concentration of MBA while maintaining ERY at 200 mM.

The same procedure was followed for the reverse reaction, where Figure 4.4 shows a plot of the measured initial reaction rate as a function of varying the concentration of substrate ABT, while maintaining the concentration of AP fixed at 35 mM. For AP this is close to the maximum solubility of 42 mM at 25^{o}C (Siegel, 2000). A second plot in Figure 4.4 shows the initial rate of the reverse reaction as a function of the variation of the concentration of AP while maintaining ABT concentration at 100 mM. The whole cell TAm concentration for all the experiments shown in Figures 4.3 and 4.4 was 0.2 mg mL^{-1}.

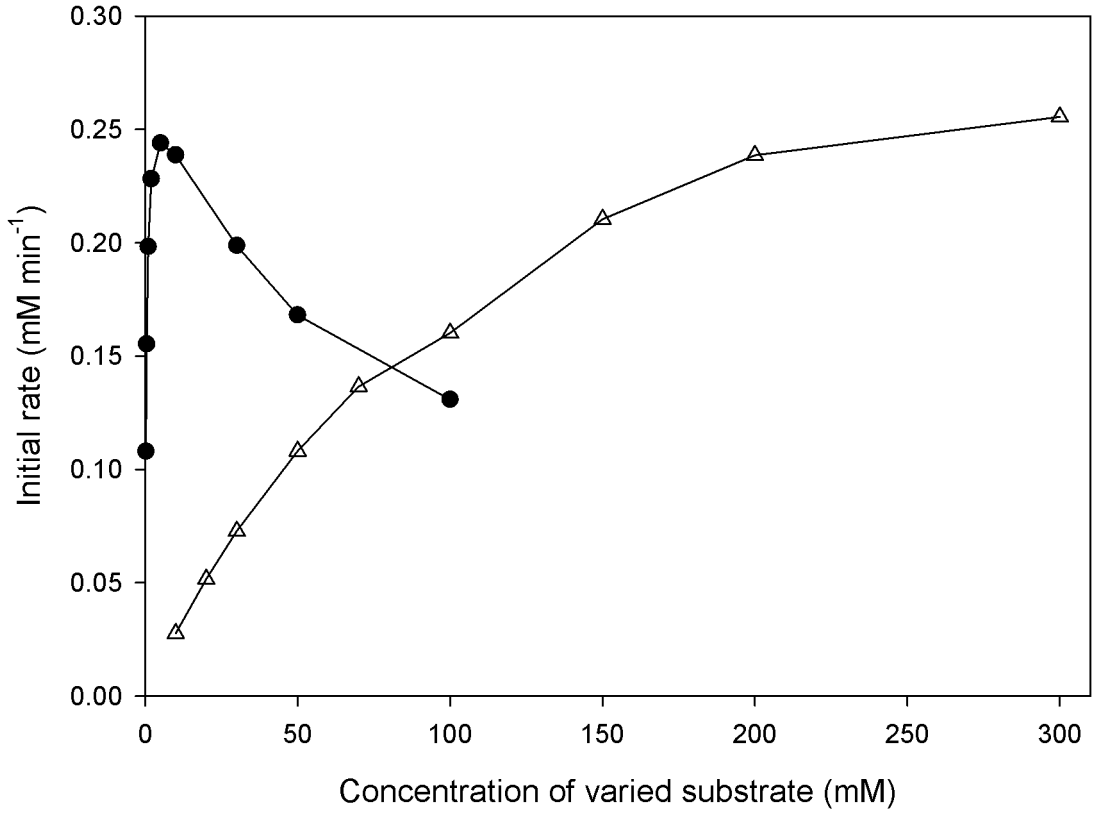

Figure 4.3. **Apparent initial rate of the forward TAm reaction for ABT and AP synthesis (Scheme 3.1) as a function of the substrate concentration. (●) [MBA] was varied while maintaining [ERY] fixed at 200 mM, (Δ) [ERY] was varied while maintaining [MBA] fixed at 10 mM. In all experiments 0.2 mg mL^{-1} of TAm in whole cell form was used with 0.2 mM PLP, 30^{o}C and pH 7.5 in 200 mM HEPES. Experiments performed as described in Section 2.8.1. Whole cells produced as described in Section 2.4.2.**

The reverse reaction was considerably slower compared to the forward reaction (Figure 4.3 and 4.4). This created some experimental difficulties to obtain the initial rate data using whole cells for the reverse reaction. The cause of those difficulties were the necessity to measure very small concentrations of MBA or ERY (in the order of 0.05 mM) which required very fine analytical detection tools with minimum noise. In addition, MBA and ERY in such small concentrations were easily consumed by side reactions of the whole cells.

To demonstrate that the products that were quantified were actually produced by the TAm bioconversion and not by whole cell side reactions, a set of experiments to obtain reverse initial reaction rates using pure TAm (see Section 2.6.2 for the purification procedure) were also performed and the results are shown in an extra plot in Figure 4.4.

Obtaining the reverse initial rates using pure enzyme eliminated the problems of whole cells side reactions and analytical noise, making the experimental procedure straight forward.

In Section 3.3.4 it was found that the TAm biocatalyst *in vivo* form was more stable than *ex vivo*. This stability effect was negligible for initial rate data, where both plots using TAm in pure and whole cell form showed a similar trend with the same order of magnitude of initial rates (Figure 4.4). This indicated that the bioconversion was not mass transfer limited using 0.2 mg mL^{-1} of TAm in whole cell form. Similar results were found for the initial rates of Figure 4.3 comparing lysates and whole cells (data not shown).

Because of the higher quality of data obtained with pure TAm and its similar initial rate behaviour compared with the whole cell biocatalyst (Figure 4.4), it was decided in this chapter to use the pure enzyme reverse kinetic data, in conjunction with the whole cell forward kinetic data to obtain the preliminary parameters of the reaction.

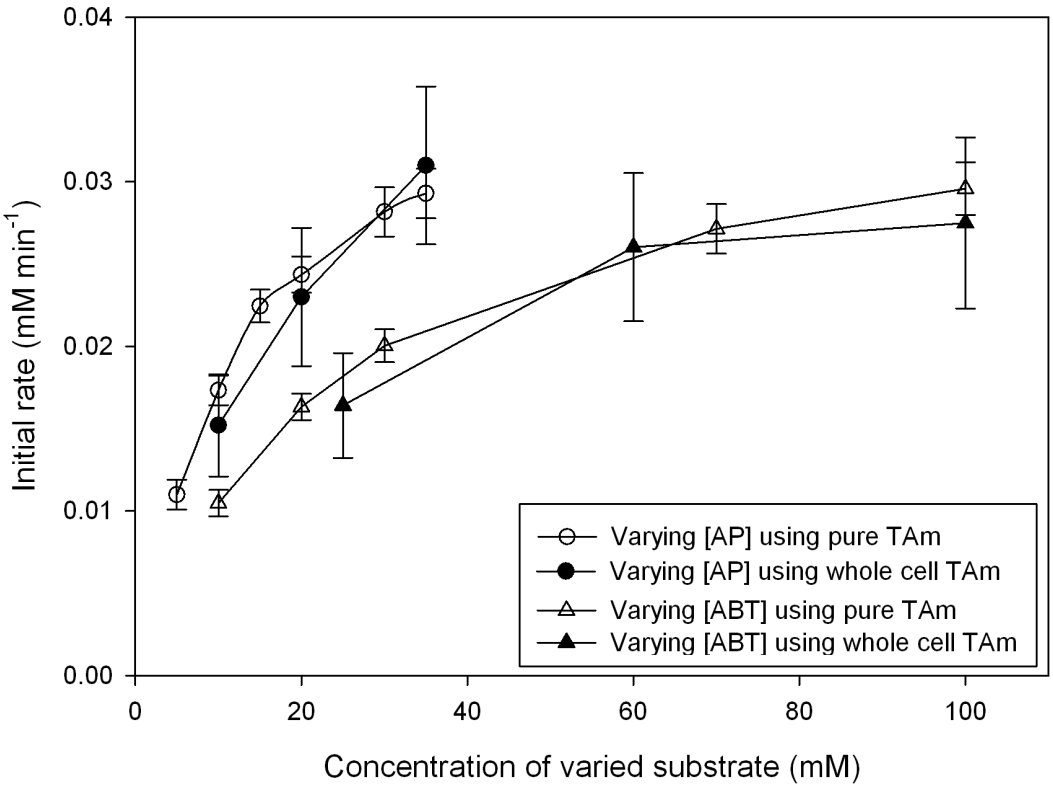

Figure 4.4. Apparent initial rate of the TAm reverse reaction for the synthesis of ABT and MBA as function of the concentration of substrates: (Δ) varying[ABT] while maintaining [AP] fixed at 35 mM using pure enzyme and (▲) TAm in whole cell form ,() varying [AP] while maintaining [ABT] fixed at 100 mM using pure enzyme and (●) TAm in whole cell form. In all experiments 0.2 mg mL^{-1} of TAm in whole cell or pure form were used with 0.2 mM PLP, 30°C and pH 7.5 in 200 mM HEPES. Experiments performed as described in Section 2.8.1. Whole cells produced as described in Section 2.4.2. Purification of the enzyme was performed as described in Section 2.6.2.

As was described with more details in Section 1.5.4.4, TAm requires the coenzyme pyridoxal 5´-phosphate and catalyze enzymatic amino group transfer by a ping-pong bi–bi mechanism (Bulos & Handler 1965; Kuramitsu *et al.*, 1990). It has been reported for TAm bioconversions that a substrate or product can bind an incorrect enzyme form, creating dead end complexes that cannot react further, causing a potentially strong form of inhibition (Bulos & Handler, 1965; Shin & Kim, 1998; Shin & Kim, 2002).

For the CV2025 TAm synthesis of ABT, the presence of abortive complexes in the reaction mechanism was not known, therefore different kinetic models were initially fitted by non linear regression to the experimental initial rate data shown in Figures 4.3 and 4.4. This was necessary to explore the possibility of the formation of different dead end complexes and identify the most suitable preliminary kinetic model. Among all those models, the reaction mechanism which included substrate inhibition by the formation of the complex E-PMP-MBA gave the best statistical fitting (statistical results will be discussed the next paragraph). The resulting King-Altman figure for the selected reaction pathway is represented in Figure 4.5, and the corresponding rate model is derived in Equation 4.1 (Segel, 1975; Shin & Kim, 1998).

A) Overall reaction

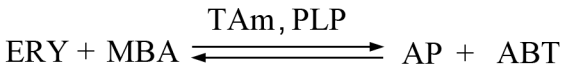

B) King-Altman reaction scheme

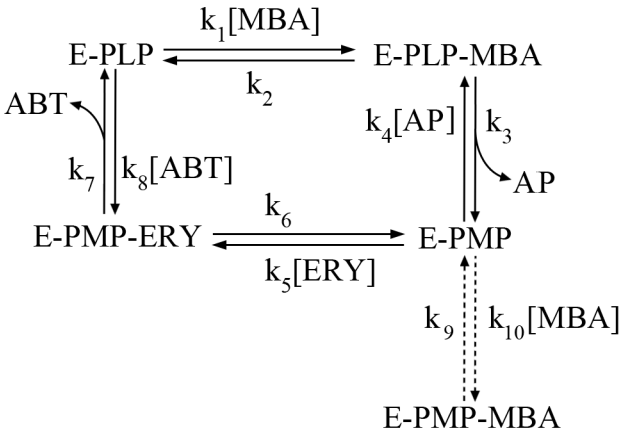

Figure 4.5. Proposed King-Altman figure for the TAm mediated synthesis of ABT. Solid lines arrows represent the basic model without the formation of abortive complexes. The dashed arrows represent the substrate inhibition by the formation of dead end complex E-PMP-MBA.

$$v = \left\{k_f k_r E_{iTAm}\left([MBA][ERY] - \frac{[AP][ABT]}{K_{eq}}\right)\right\}/den \qquad \text{Equation 4.1}$$

$$den = k_r K_{MBA}[ERY] + k_r K_{ERY}[MBA] + k_r[ERY][MBA] + \frac{k_f K_{AP}[ABT]}{K_{eq}} + \frac{k_f K_{ABT}[AP]}{K_{eq}} + \frac{k_f[AP][ABT]}{K_{eq}} + \frac{k_r K_{MBA}[ERY][ABT]}{K_{iABT}} + \frac{k_f K_{ABT}[MBA][AP]}{K_{eq} K_{iMBA}} + \frac{k_f K_{AP}[ABT][MBA]}{K_{iMBAc}} + \frac{k_r K_{ERY}[MBA]^2}{K_{eq} K_{iMBAc}}$$

Where v represents the reaction rate, k_f and k_r represents the catalytic rate constants for the forward and reverse reaction respectively, K_{ERY}, K_{AP}, K_{ABT} and K_{MBA} are the Michaelis constants of ERY, AP, ABT and MBA, K_{iABT} and K_{iMBA} are the inhibition constants of ABT and MBA respectively, K_{iMBAc} is the inhibition constant for the MBA-PMP abortive complex, E_{iTAm} represents the TAm concentration and K_{eq} is the equilibrium constant.

In the absence of products for the forward reaction, Equation 4.1 can be simplified to Equation 4.2:

$$\frac{1}{v} = \frac{1}{k_f E_{iTAm}}\left(1 + \frac{K_{MBA}}{[MBA]} + \frac{K_{ERY}}{[ERY]} + \frac{K_{ERY}[MBA]}{K_{iMBAc}[ERY]}\right) \qquad \text{Equation 4.2}$$

The initial data from Figure 4.3 was fitted using non linear regression to Equation 2 obtaining an R^2 of 0.98 and the sum of squares was of 0.24, which was one order of magnitude below compared to the R^2 of 0.87 and sum of squares of 14.2 for the second best fitting model which did not include substrate inhibition by a dead end complex (Equation 4.2 without including the last two terms).
The preliminary values of the constants k_f, K_{MBA}, K_{ERY} and K_{iMBAc} were 97.2 mM min^{-1}, 0.5, 101.2 and 23.9 mM respectively.

A statistical F-test (Markowski and Markowski, 1990) was performed in order to determine if the addition of the parameter K_{iMBAc} gave a significantly better fit to the data. The result of the F-test was equal to 282.4, which was considerably higher than the critical value of 6.6 from the F distribution tables with false-rejection probability of 0.05, showing that the addition of the parameter K_{iMBAc} was statistically significant.

The plots of reverse initial rate as a function of substrate concentration in Figure 4.4 did not suggest the presence of strong inhibition that could be caused by a dead end complex. This was corroborated by non linear fitting regression, where all the models including the formation of dead end complexes in the reverse reaction failed to give a statistically better fit than the model represented by Equation 4.3, which is a simplification of Equation 4.1 without including products.

$$\frac{1}{v} = \frac{1}{k_r E_{iTAm}}\left(1 + \frac{K_{AP}}{[AP]} + \frac{K_{ABT}}{[ABT]}\right) \qquad \text{Equation 4.3}$$

The initial rate data was fitted to equation 4.3 by non linear regression, and the preliminary parameters of k_r, K_{AP} and K_{ABT} were found to be 13.1 min^{-1}, 19.6 and 39.4 mM respectively. Both non linear regressions for the forward and reverse

reaction had upper and lower bounds of 0.0001 and 2000 and both converged with any arbitrary initial value.

4.3.4 Enzyme stability

An underlying assumption is that the TAm activity should be stable for the duration of the progress curve experiments, which are needed to determine the rest of inhibition and equilibrium constants (Figure 4.1). Good stability of TAm would also demonstrate that the total enzyme concentration was constant during the complete assay; therefore any decrease in the reaction rate could be attributed to inhibition or equilibrium effects and not to irreversible enzyme deactivation.

To test the enzyme stability, the whole cell TAm was incubated with each substrate or product over different incubation times, and the enzyme activity was determined at intervals and plotted as a function of the incubation time in Figure 4.6 (forward reaction activity data was used for substrate incubation tests, and reverse reaction activity for product incubation tests).

No significant decrease in enzyme activity was detected for up to 35 hr of incubation with ERY, ABT and AP. In contrast there was a 10% decrease in initial reaction rate for the whole cell TAm while incubated with MBA. Because improving TAm stability was out of the scope of this project, a maximum of 10% deactivation of enzyme was set as the tolerance limit for the kinetic parameters identification. Therefore the maximum reaction time allowed in all the progress curves was set to be 35 hr.

When incubating the enzyme with MBA, PLP had to be added again so that the enzyme activity would be restored. This was not necessary when incubating the enzyme with ERY, AP or ABT, and the reason could be attributed to a full conversion of PLP to PMP through completion of the first half reaction due to the absence of amino-acceptor, as has been shown previously using the CV2025 TAm (Schell *et al.*, 2009).

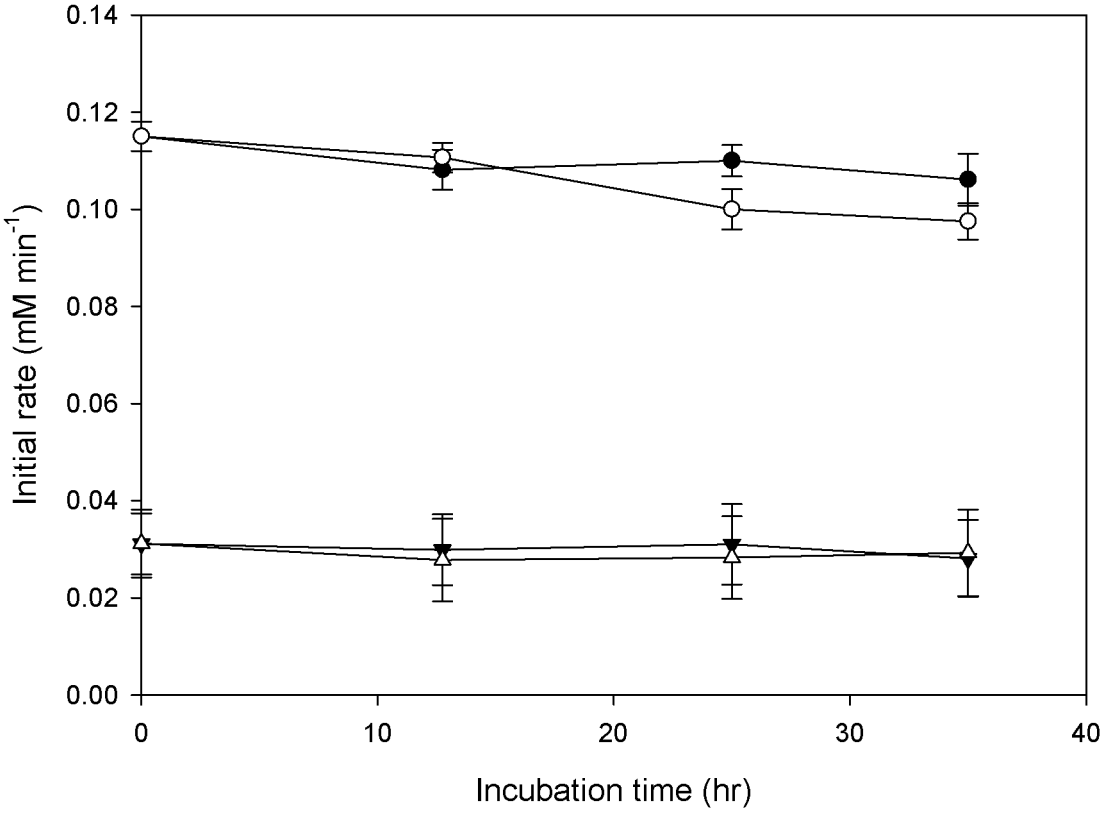

Figure 4.6. Stability experiments using the whole cell TAm biocatalyst: apparent forward initial reaction rates after different times of incubation with (●) 50 mM ERY or (○) 50 mM MBA, and apparent reverse reaction initial rates after different incubation times with(▼) 100 mM ABT or (Δ) 35 mM AP. In all experiments 0.2 mg mL^{-1} of TAm in whole cell form were used with 0.2 mM PLP, 30^{o}C and pH 7.5 in 200 mM HEPES. Reaction conditions for forward reaction were 50 mM equimolar concentration of substrates, and for the reverse reaction 100 mM ABT or 35 mM AP were added to start the reaction. Experiments performed as described in Section 2.8.1. Whole cells produced as described in Section 2.4.2.

4.3.5 Kinetic parameter identification using progress curves

Step 4 in the proposed methodology (Figure 4.1) involved obtaining complete progress curves at higher substrate concentrations, where equilibrium as well as substrate and product inhibition effects would have a stronger weight. A set of 9 progress curves for the forward reaction, each with 12 sampling points at different intervals were obtained to ensure the accuracy of the model fit to the experimental data. This set was complemented with the addition of 3 reverse reaction progress curves, to ensure that the model would fit both forward and reverse reaction profiles. The substrate concentrations chosen are shown in Table 4.1, and included those under which the final bioconversion process might be performed. Also included are experiments at the lower and higher range of the concentration spectrum, to ensure that the inhibition and equilibrium constants would be accurately determined over a range of bioconversion conditions.

Table 4.1. Initial experimental substrate and enzyme concentrations for the 12 progress curves used to obtain the kinetic parameters in Steps 4 and 5 of the methodology described in Figure 4.1. The first 9 progress curves represent forward reaction bioconversions, while the last 3 represent reverse reaction bioconversions.

Progress curve number	**1**	**2**	**3**	**4**	**5**	**6**	**7**	**8**	**9**	**10**	**11**	**12**
[ERY] (mM)	50	70	150	250	300	150	200	10	20	0	0	0
[MBA] (mM)	100	250	250	40	30	15	50	120	200	0	0	0
[AP] (mM)	0	0	0	0	0	0	0	0	0	10	20	40
[ABT] (mM)	0	0	0	0	0	0	0	0	0	120	200	100
E_i (mg ml^{-1})	0.3	0.4	0.3	0.15	0.15	0.15	0.15	0.3	0.45	0.15	0.44	0.3

Initial non linear regressions highlighted the importance of the data points before 60 min of reaction. Those points were crucial involving low products concentration, giving weight to the preliminary parameters K_f, K_r, and the Michaelis constants previously obtained, allowing a better convergence of the optimization. Therefore care was taken to include several points within that time range, in order for the optimization to converge around the vicinity of the preliminary values determined in Section 4.3.3.

The preliminary results of k_f and k_r, of 97.2 and 13.1 min^{-1}, and of K_{MBA}, K_{ERY}, K_{iMBAc}, K_{AP} and K_{ABT} of 0.5, 101.2, 23.9, 19.6 and 39.4 mM respectively obtained in Section 4.3.3 were used as fixed values in the full kinetic model (Equation 4.1). This was done in order to be able to determine the rest of the kinetic constants by non linear regression of the progress curves. The equilibrium constant was calculated simultaneously in the iteration process using the Haldane equation 4.4:

$$K_{eq} = \left(\frac{k_f}{k_r}\right)^2 \frac{K_{ABT}K_{AP}}{K_{MBA}K_{ERY}} \qquad \text{Equation 4.4}$$

The two remaining inhibition constants K_{iERY} and K_{iAP} were calculated using the following Haldane equations:

$$K_{iAP} = \frac{K_{eq}k_r K_{ERY}K_{iMBA}}{k_f K_{ABT}} \qquad \text{Equation 4.5}$$

$$K_{iERY} = \frac{k_f K_{AP}K_{iABT}}{K_{eq}k_r K_{MBA}} \qquad \text{Equation 4.6}$$

The partial equilibrium constant K_1 for the first half reaction, where MBA reacts with E-PLP to produce AP and E-PMP (Figure 4.5) was calculated using Equation 4.7:

$$K_1 = \frac{k_1 k_3}{k_2 k_4} = \frac{K_{iAP}}{K_{iMBA}}$$ Equation 4.7

In the same way, the partial equilibrium constant K_2 for the second half reaction, where E-PMP is converted to E-PLP through the formation of ABT from ERY (Figure 4.5) was obtained using Equation 4.8:

$$K_2 = \frac{k_5 k_7}{k_6 k_8} = \frac{K_{iABT}}{K_{iERY}}$$ Equation 4.8

It should be noted that the global equilibrium constant K_{eq} can also be expressed as the product of the two partial constants as shown in Equation 4.9, and the value obtained should be the same as the one obtained with Equation 4.4.

$$K_{eq} = K_1 K_2 = \frac{[AP]_{eq}[ABT]_{eq}}{[ERY]_{eq}[MBA]_{eq}}$$ Equation 4.9

The global optimization was obtained using the pattern search algorithm available in the `Genetic Algorithm and Direct Search Toolbox' in Matlab (Appendix V) (MathWorks, Natick, MA, USA). Following this approach, the optimization solution was relatively independent of the initial values of the inhibition constants, because only 3 parameters needed to be estimated. The preliminary values of $K_{iMBA,}$ K_{iABT} and K_{eq} were determined to be 0.004 and 2.2 mM and 829.9 respectively. The lower and upper bounds for both non linear regressions were set at 0.0001 and 800, and the optimization was always found to converge to the same result for any given initial value within the bounds.

4.3.6 Reconciliation Step for determination of final kinetic parameter values

The preliminary parameters obtained up to Section 4.3.5 were usually very close to the "true" values, but they still presented some inaccuracies because they were based on the catalytic and Michaelis-Menten constants determined using the simplified kinetic models in Equations 4.2 and 4.3. Any error obtained using such simplified

models in Section 4.3.3 would be propagated to the values of all the next parameters determined in the Section 4.3.5. Therefore in Step 5 of the methodology described in Figure 4.1, the kinetic constants were reconciled by using the corresponding full kinetic model combined with non linear regression of the 12 progress curves, where all the preliminary parameters were used as initial values for the optimization.

The lower and upper bounds were set as 0.1 and 2000 (expect for K_{MBA} and K_{iMBA} where the lower bound was set to 0.01 and 0.0001 respectively), and because the initial estimates were close to the final parameter values, the global optimization was quickly achieved around the vicinity of the initial estimates. The preliminary and "reconciled" kinetic values obtained this way are summarized in Table 4.2, where a description in terms of rate constants of each parameter is also included.

The preliminary and final values were relatively similar and the major difference (33%) was found for the inhibition constant K_{APi}. Such changes to the final values of the kinetic parameters at this point was considered acceptable for a non linear regression approach methodology (Moros *et al*., 1996; Blackmond 2005).

Table 4.2. Initial and final "reconciled" values for the parameters obtained in Step 5 of Figure 4.1 using the full kinetic model represented by Equation 4.1.

Kinetic parameter	Kinetic parameter in terms of rate constants	Initial value	Reconciled value
Catalytic rate constants (min $^{-1}$)			
Rate constant forward reaction: k_f	$\frac{k_3 k_7}{k_3 + k_7}$	97.2	95.1
Rate constant reverse reaction: k_r	$\frac{k_2 k_6}{k_2 + k_6}$	13.1	12
Michaelis-Menten constants (mM)			
Michaelis constant for MBA : K_{MBA}	$\frac{k_7(k_2 + k_3)}{k_1(k_3 + k_7)}$	0.49	0.51
Michaelis constant for ERY : K_{ERY}	$\frac{k_3(k_6 + k_7)}{k_5(k_3 + k_7)}$	101.2	95.5
Michaelis constant for AP : K_{AP}	$\frac{k_6(k_2 + k_3)}{k_4(k_2 + k_6)}$	19.6	16.1
Michaelis constant for ABT : K_{ABT}	$\frac{k_2(k_6 + k_7)}{k_8(k_2 + k_6)}$	39.4	37
Inhibition constants (mM)			
Inhibition constant for MBA: K_{iMBA}	$\frac{k_2}{k_1}$	4.0×10^{-3}	4.0×10^{-3}
Inhibition constant for ERY: K_{iERY}	$\frac{k_6}{k_5}$	0.75	1.0
Inhibition constant for AP: K_{iAP}	$\frac{k_3}{k_4}$	1.2	1.1
Inhibition constant for ABT: K_{iABT}	$\frac{k_7}{k_8}$	2.2	3.1
Inhibition constant for MBA abortive complex: K_{iMBAc}	$\frac{k_9}{k_{10}}$	23.9	24

Equilibrium constants			
Global equilibrium constant	$\frac{k_1 k_3 k_5 k_7}{k_2 k_4 k_6 k_8}$	829.9	**842.9**
Equilibrium constant for the first half reaction : K_1	$\frac{k_1 k_3}{k_2 k_4}$	301	**275**
Equilibrium constant for the second half reaction : K_2	$\frac{k_5 k_7}{k_6 k_8}$	2.9	**3.1**

In order to perform a complete statistical analysis, the full methodology described in Figure 4.1 was also performed using the kinetic model without including substrate inhibition by the formation of dead end complexes (Equation 4.1 without including the last two terms). The final non linear regression performed with this model in Step 5 to reconcile the parameters was not stable and failed to converge successfully. Instead it reached the upper limit for K_{ERY} and showed relatively high discrepancies between the initial and "reconciled" values, presenting a residual of 16.3 compared to 0.55 using the full model of Equation 4.1. A statistical F-test (Markowski and Markowski, 1990) was performed in order to determine if the addition of the parameter K_{iMBAc} gave a significantly better fit to th progress curve data. The result of the F-test was equal to 15.7, which was higher than the critical value of 3.9 from the F distribution tables with false-rejection probability of 0.05, showing that the addition of the parameter K_{iMBAc} was also statistically significant to fit the progress curves.

These statistical results, in addition to those in Section 4.3.3, showed that the kinetic model described by Equation 4.1 presented the best fitting for both initial rate data and the complete progress curves. This finding strongly supports the formation of the abortive complex E-PMP-MBA. Further experiments using LC-MS or other sensitive analytical tools could demonstrate the existence of such complex but those studies were out of the scope of this work as described in Section 1.4.

4.3.7 Validation of the kinetic parameters

In order to validate the kinetic parameters obtained in Table 4.2, experimental and predicted data of reactant concentrations as a function of time were compared. Very good agreement was found for all the concentrations described in Table 4.1 (Appendix VI).

Figure 4.7 shows a set of experimental and model data comparisons, using progress curves from Table 4.1 that were used to determine the kinetic parameters. Figure 4.7a specifically compares experimental ABT data points from different progress curves with the predicted model where excellent agreement was found. Figure 4.7b focuses on the initial period until 60 min where, as described in Section 4.3.5, several key data points were collected.

Figure 4.8 shows the experimental data points of MBA for the 3 reverse progress curves described in Table 4.1, where also excellent agreement was observed between the data and the model.

To further test the kinetic model, Figure 4.9 shows the comparison of model predicted data with an extra set of experimental progress curve data, which was not included in Table 4.1 to establish the kinetic parameters.

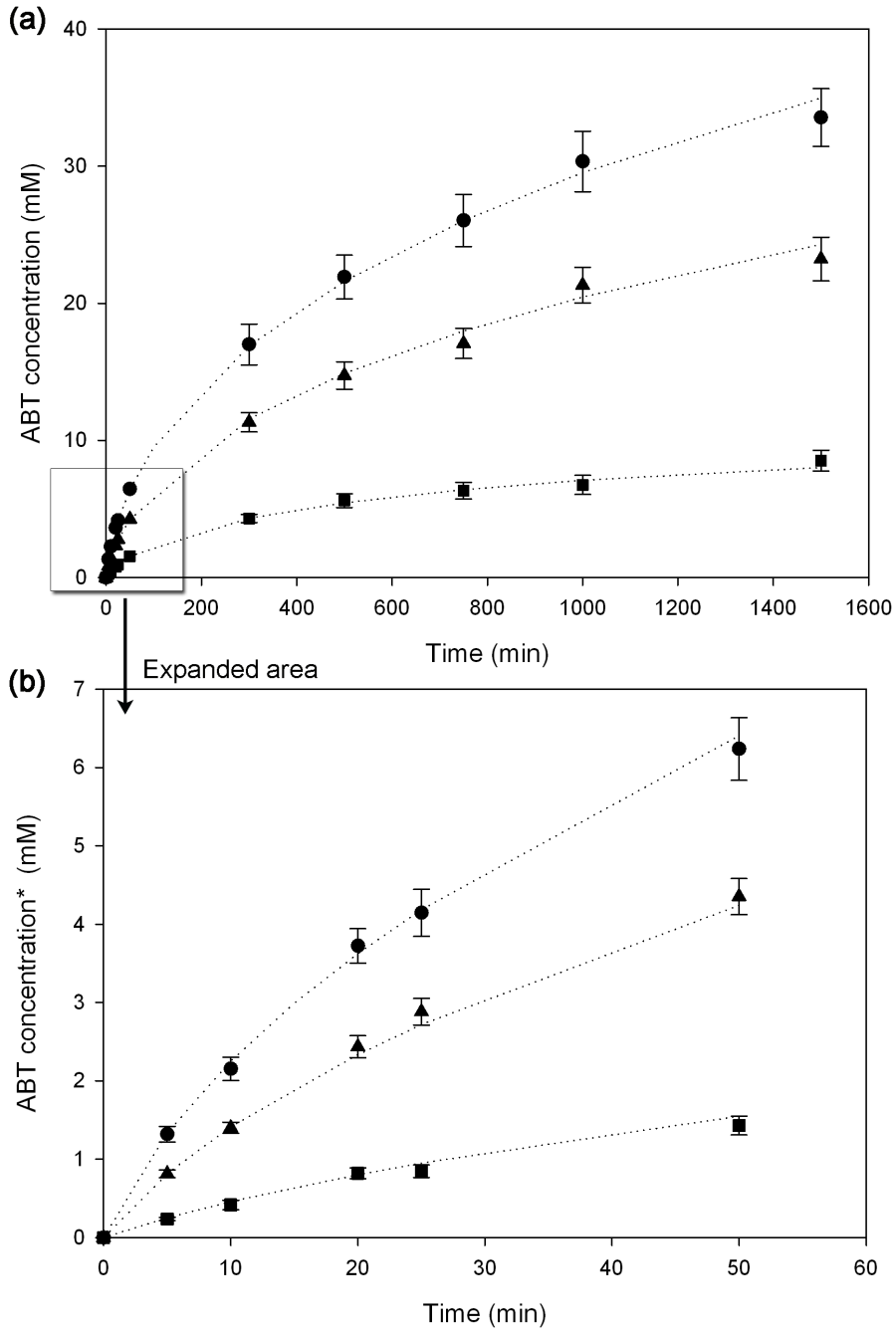

Figure 4.7. Forward reaction experimental and predicted progress curves following (a) [ABT] for the complete length of the bioconversions and (b) [ABT] for the first 50 min of reaction time. The initial substrate concentrations for each progress curve wa●)(150 mM [ERY], 250 mM [MBA] and 0.3 mg mL^{-1} [TAm], (▲) 50 mM [ERY], 100 mM [MBA] and 0.3 mg mL^{-1} [TAm] and (■) 10 mM [ERY], 120 mM [MBA] and 0.3 mg mL^{-1} [TAm]. Dotted lines show model predictions based on Equation 4.1 and final kinetic parameters in Table 4.2. For all the experiments 0.2 mM PLP was used at 30^{o}C and pH 7.5 in 200 mM HEPES buffer. Experiments were performed as described in Section 2.8.1.

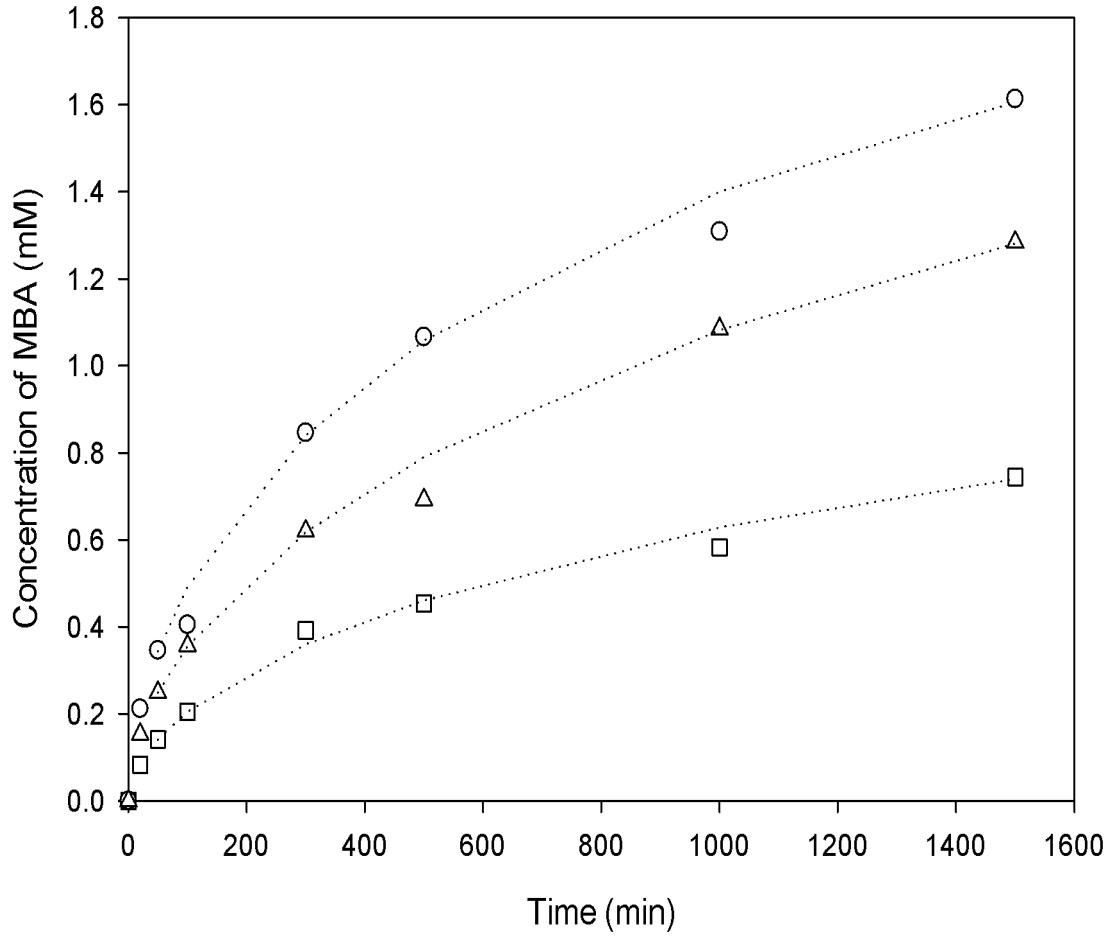

Figure 4.8. Reverse reaction predicted and experimental progress curves following MBA with initial substrate concentrations of (○) 10 mM [AP], 120 mM [ABT] and 0.15 mg m L^{-1} [TAm] (Δ) 20 mM [AP], 200 mM [ABT] and 0.44 mg mL^{-1} [TAm] and (□) 40 mM [AP], 100 mM [ABT] and 0.3 mg mL^{-1} [TAm]. For all the experiments 0.2 mM PLP was used at 30°C and pH 7.5 in 200 mM HEPES buffer. Dotted lines show model predictions based on Equation 4.1 and final kinetic parameters in Table 4.2. Experiments were performed as described in Section 2.8.1.

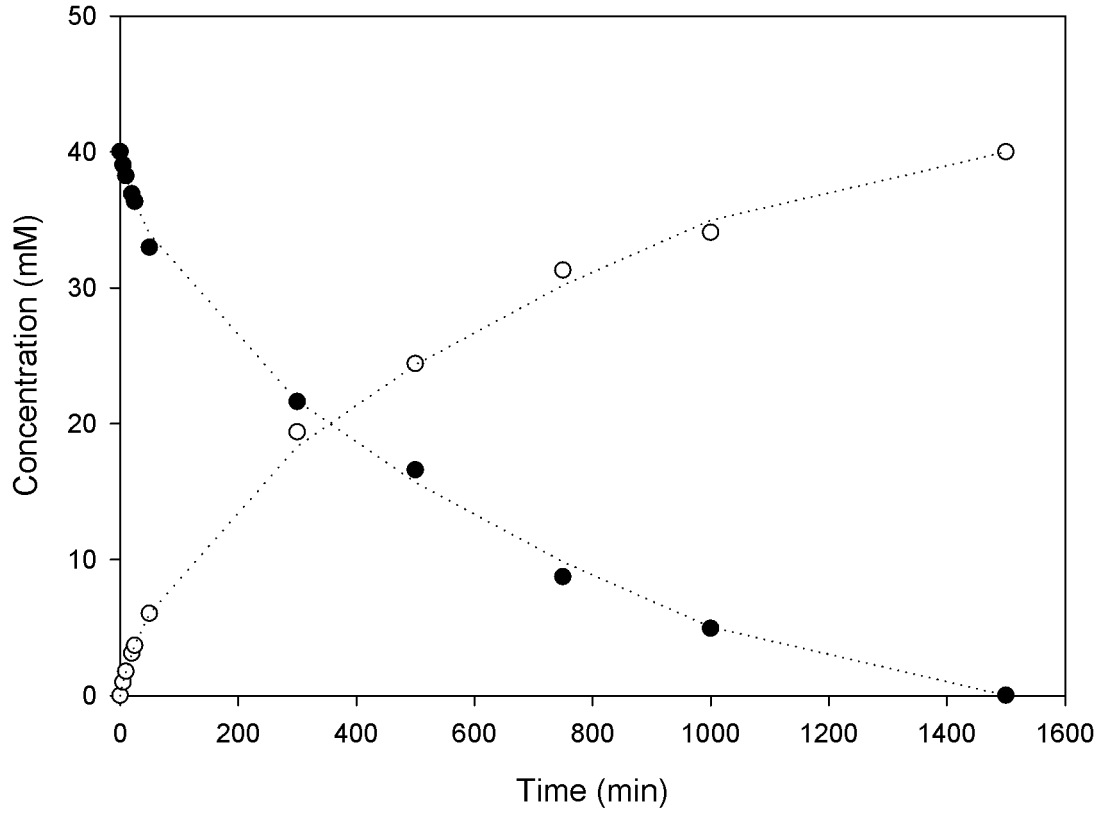

Figure 4.9. Verification of model predictions with an experimental data set not included in the original experimental design. Progress curve following (●) MBA and (○) ABT. Initial [ERY] concentration was 250 mM and MBA was [40] mM, 0.2 mg mL^{-1} of TAm in whole cell form, 0.2 mM PLP, 30^{o}C and pH 7.5 in 200 mM HEPES. Dotted lines show model predictions based on Equation 4.1 and final kinetic parameters in Table 4.2. Experiments were performed as described in Section 2.8.1.

Excellent agreement was found between the experimental values and the model prediction for both the short and longer reaction time scale in Figure 4.7, as well as for the reverse reactions shown in Figure 4.8. In addition, perfect agreement was also found between the independent progress curve which was not used for determining the kinetic parameters and the model predictions, verifying the appropriate determination of the kinetic model (Equation 4.1) and its corresponding parameters (Table 4.2).

4.4 DISCUSSION OF TAM KINETIC PARAMETER RESULTS

4.4.1 Analysis of Michaelis-Menten constants

The Michaelis constant of ERY was 200 times bigger than the one for MBA, while the Michaelis constant of ABT was half compared to the one for AP. In contrast to the reverse reaction, the kinetic parameters of the forward reaction did not follow the general trend where the Michaelis constant of each amino donor were higher than the corresponding amino acceptor (Henson & Cleland, 1964; Christen & Metzler, 1985; Shin & Kim, 1998; Lain-guelbenzu *et al.,* 1991; Lo *et al.,* 2005; Martin *et al.,* 2007).

The value of the Michaelis constant of K_{AP} was determined to be two orders of magnitude higher than K_{MBA}. This result was unexpected due to the similar chemical structures of both compounds containing an aromatic ring and would indicate that the amino group of MBA plays an important role for its high affinity towards the CV2025 TAm. A similar low K_{MBA} and higher K_{AP} value was determined for the ω-TAm from *Vibrio fluvialis* (Shin & Kim, 2002) which shares 38% sequence identity towards the CV2025 TAm (Kaulmann et al., 2007). Interestingly, the opposite result was found for the ω-TAm from *Bacillus thuringiensis,* where the Michaelis constant for MBA and AP were two orders of magnitude higher and lower respectively than the ones determined in this work for the CV2025 TAm (Section 1.5.3.2) (Shin & Kim, 1998).

4.4.2 Analysis of equilibrium constants

The uses of transaminases to synthesize chiral amines have been generally hampered by equilibrium constants near unity or constants which favours the ketone starting material (Taylor *et al*., 1998; Stewart, 2001; Truppo *et al*., 2010). For the conversions studied here however, the value of the partial equilibrium constants K_1 and K_2 for the first and second half reactions were 275 and 3.1 as determined by Equations 4.7 and 4.8 respectively. The high value of K_1 has also been suggested in literature for the synthesis of pyridoxamine 5´-phopsate using CV2025 TAm (Schell *et al*., 2009). The values of K_1 and K_2 lead to a global equilibrium constant of 842 following Equation 4.9, which strongly favoured the asymmetric synthesis of ABT.

In addition, the catalytic constant for the forward reaction was almost one order of magnitude higher than the constant for the reverse reaction. Similar differences in catalytic constants have been found for the ω-TAm from *B. thuringiensis* to produce L-alanine from pyruvate and MBA (Shin & Kim, 1998), yet in general these results are not common among other TAms where k_f and k_r do not differ greatly (Henson & Cleland, 1964; Bulos & Handler, 1965; Christen & Metzler, 1985; Kuramitsu *et al*., 1990; Hayashi *et al.,* 1993; Taylor *et al.,* 1998).

4.4.3 Bottlenecks of the bioconversion

4.4.3.1 Michaelis constant of ERY

A number of bottlenecks need to be solved to reach the full potential of the CV2025 TAm for the asymmetric synthesis of chiral amino alcohols. After evaluating the kinetic constants in Table 4.2, and performing a sensitivity analysis for each parameter (Appendix VII), it was found that one of the key obstacles to improve the amino-alcohol productivity was the high value of K_{ERY} of 96 mM. For similar reaction conditions, Michaelis constants for pyruvate were reported to be one order of magnitude smaller than K_{ERY} using the ω-TAm from *V. fluvialis* and *B. thuringiensis* (Shin & Kim, 1998; Shin, 2002). This result could be explained because the

previously mentioned enzymes, including the CV2025 TAm, belong to the β-Ala:pyruvate transaminases containing a two pocket binding catalytic site, which appears to be evolved for the recognition of pyruvate through a carboxylate trap via a salt bridge and a hydrogen bond (Section 1.5.3.4) (Liu *et al.,* 2004; Cho *et al.,* 2008). Therefore those enzymes present less affinity towards α-ketoglutarate and even less affinity towards ketones which do not contain carboxylic groups (Shin & Kim, 2002; Kaulmann *et al.,* 2007).

The high value of K_{ERY} prevented the enzyme from reaching its full catalytic potential (maximum catalytic rate) at ERY concentrations below 200 mM (Figure 4.3). In contrast, the determined value of K_{MBA} in this work was of 0.5, which was between 1 to 2 orders of magnitude smaller compared to the reported K_{MBA} constants for TAms of *V. fluvialis*, *B. thuringiensis* and *Arthrobacter citreus* (Shin & Kim, 1998; Shin & Kim, 2002; Martin *et al*., 2007).

K_{MBA} was found to be more than 200 times smaller than K_{ERY}, (Table 4.2), and therefore any increase of MBA above 2 mM did not predict to significantly increase the reaction rate and would even cause inhibition and enzyme deactivation (Figures 4.3 and 4.5).

4.4.3.2 Second half reaction

The higher stability of the complex E-PLP-MBA compared to E-PMP-ERY was evidenced by the value of the dissociation constant K_{iMBA} of 4.0×10^{-3} mM, which was 3 orders of magnitude smaller compared to the value of K_{iERY} of 1.0 mM. By analyzing the expressions of the parameters as rate constants in Table 4.2, it can be concluded that the higher values of K_{ERY} and K_{iERY} compared to K_{MBA} and K_{iMBA} make the second half reaction the limiting step of the overall bioconversion. Mutagenesis improving this step would be very beneficial in improving the catalytic rate of the TAm synthesis of ABT.

4.4.3.3 Catalytic constant

The value of the kinetic parameter k_f, which is a function of the forward catalytic constant rates k_3 and k_7, was found to be 97.4 min^{-1}, and as expected, had also a strong influence in the productivity of ABT as determined by the sensitivity analysis (Appendix VII).
This value of k_f was of the same order of magnitude as that reported for a similar ω-TAm using MBA and pyruvate as substrates (Shin & Kim, 1998; Shin & Kim, 2002), but it was found to be several orders of magnitude lower compared with other classes of TAms when used with natural substrates *ex vivo* (Kuramitsu *et al.*, 1990; Markova *et al.,* 2005).

The simulations predicted that using a higher concentration of TAm would lead to significant improvements in the productivity of the bioconversion. Nevertheless as it has been shown in Figure 4.2, the region of linear proportionality between the initial rate and the enzyme concentration faded away after values higher than 0.8 mg mL^{-1}. Therefore experimental progress curves using TAm concentrations above that limit did not correlated well with the predicted results (data not shown).

The catalytic constant of TAm found in this work was 5 and 20 folds smaller than the published catalytic constants for TK D469T and the wild type (Chen et al., 2008, Chen et al., 2009). Those results should be taken in consideration when expression both enzymes in the biocatalyst in order to match their kinetics.

4.4.3.4 Side reactions

Using TAm concentrations above 1 mg mL^{-1} also lead to significant side reactions caused by the whole cells that consumed the substrates and products, affecting the final balance and overall quality of the asymmetric synthesis. One solution to overcome the side reactions is to use pure enzyme instead of whole cells, this has been shown in literature where concentrations one order of magnitude higher of the CV2025 TAm were used successfully without side reactions (Schell *et al.,* 2009).

Another solution to overcome side reactions is to employ non natural ketodiols more stable than ERY like PKD (Scheme 3.2), which is a good target for bioconversion with similar catalytic activity compared to ERY as shown in Chapter 3 (Table 3.2), with the advantage of producing more stable amino alcohols (Smith *et al*., 2010).

4.4.3.5 Product inhibition

Product inhibition in the forward reaction was found to be not so severe compared to other similar ω-TAm bioconversions (Shin & Kim, 1998; Shin & Kim, 2002). In those works, some of the product inhibition constants were found to be one order of magnitude smaller than the value of K_{iAP} and K_{iABT} of 1.1 and 3.1 mM obtained in this work respectively (Table 4.2). A low product inhibition of AP and ABT was also suggested in literature using a TAm from *Pseudomonas aeruginosa* for the asymmetric synthesis of ABT *(*Ingram *et al., 2007)*.

Non-linear fitting suggested that substrate inhibition proceeded through the formation of the dead end complex E-PMP-MBA, which is a common form of inhibition for enzymes that follow a ping pong kinetic mechanism (Segel, 1975). The dissociation constant K_{iMBAd} of the abortive complex was found to be 24 mM (Table 4.2), which is similar to other values found in literature (Henson & Cleland, 1964; Lombardo *et al.,* 1989). Nevertheless it has been shown that this type of inhibition only becomes severe with values of dissociation constants one order of magnitude smaller than the value of K_{iMBAd} (Shin & Kim 1998; Shin & Kim 2002). Although inclusion of the extra parameter K_{iMBAd} was justified by performing an F-Test as well as other statistical analysis (see section 4.2 and 4.5), the sensitivity analysis showed that this inhibition would only become a major bottleneck with values of K_{iMBAc} below ~5 mM (Appendix VII).

4.4.3.6 Reverse reaction

The reverse reaction catalytic constant k_r and the Michaelis constants K_{ABT} and K_{AP} were determined to be 12 min^{-1}, 16 and 37 mM respectively. The sensitivity analysis

showed that those had a smaller impact in the modelling compared to the forward reaction constants. This is explained because the value of k_r was determined to be 8 times smaller compared to k_f. In addition, the relatively high values of K_{ABT} and K_{AP}, and the high equilibrium constant makes the reverse reaction almost negligible, as it can be seen in the low product yield of the reverse progress curves shown in Figure 4.8.

4.4.3.7 Toxicity of MBA towards TAm

Several simulations predicted that high reaction yields of more than 95% should be obtained using high equimolar concentrations of substrates, with the condition that longer reactions times were used. However, the experimental data started to diverge gradually from the predicted model data after longer reaction times (data not shown), probably due to irreversible enzyme inactivation by MBA. As it was shown in Figure 4.6, 10 % of the TAm was deactivated after being incubated for 35 hr with 50 mM MBA. This deactivation percentage was considered negligible for the purposes of determining the kinetic parameters using the methodology of Figure 4.1; but the deactivation may become more significant if longer residence times and also higher concentrations of MBA were used.

TAm inactivation by the amino donor has also been reported in literature (Yun et al., 2004b), and in some cases whole cell TAm biocatalyst have been shown to maintain the TAm more stable versus the inactivation of the amino donor *(*Yun *et al.,* 2004a*)*, which is in agreement with the results found in Chapter 3. Further addition of PLP or TAm (individually) when the reaction stopped did not restore the catalytic activity. In contrast, addition of PLP and TAm (together) after the reaction stopped did restore partially the activity (data not shown), suggesting both enzyme and PLP were degraded after longer reaction times.

4.4.4 Optimum reaction conditions

Taking into account all the previously discussed kinetic and stability results, it was identified that maintaining a high concentration of ERY (more than 250 mM) while minimizing the concentration of MBA proved to enhance the final yield of ABT. Figure 4.10 shows a simulated progress curve along with experimental verification for a reaction with 250 mM of ERY and 40 mM MBA with 0.4 mg mL^{-1} of TAm. In order to compare the effect of each substrate in the bioconversion, a set of experimental data and simulation is also shown using the inverse initial concentrations of 250 mM of MBA and 40 mM ERY, with the same concentration of TAm.

Very good agreement was found in Figure 4.10 between the experimental and predicted data sets. The simulation that considered and excess of ERY predicted a 99% conversion with respect to the limiting substrate MBA in 500 min corresponding to the maximum theoretical yield achievable for the reaction.

In contrast when an excess of MBA was used a final yield of only 37 % mol/mol was predicted and obtained. Using the concentration of 250 mM MBA and 40 mM ERY, the model predicted a final 90% yield in 5500 min, which was one order of magnitude higher than using an excess of ERY. In addition, the experimental ABT yield using an excess of MBA did not increase after 500 min (data not shown), probably due to complete inactivation of the enzyme by the high concentration of MBA. Future work is been performed in applying a systematic statistical approach to determine with more details the optium reaction conditions using the determined kinetic model.

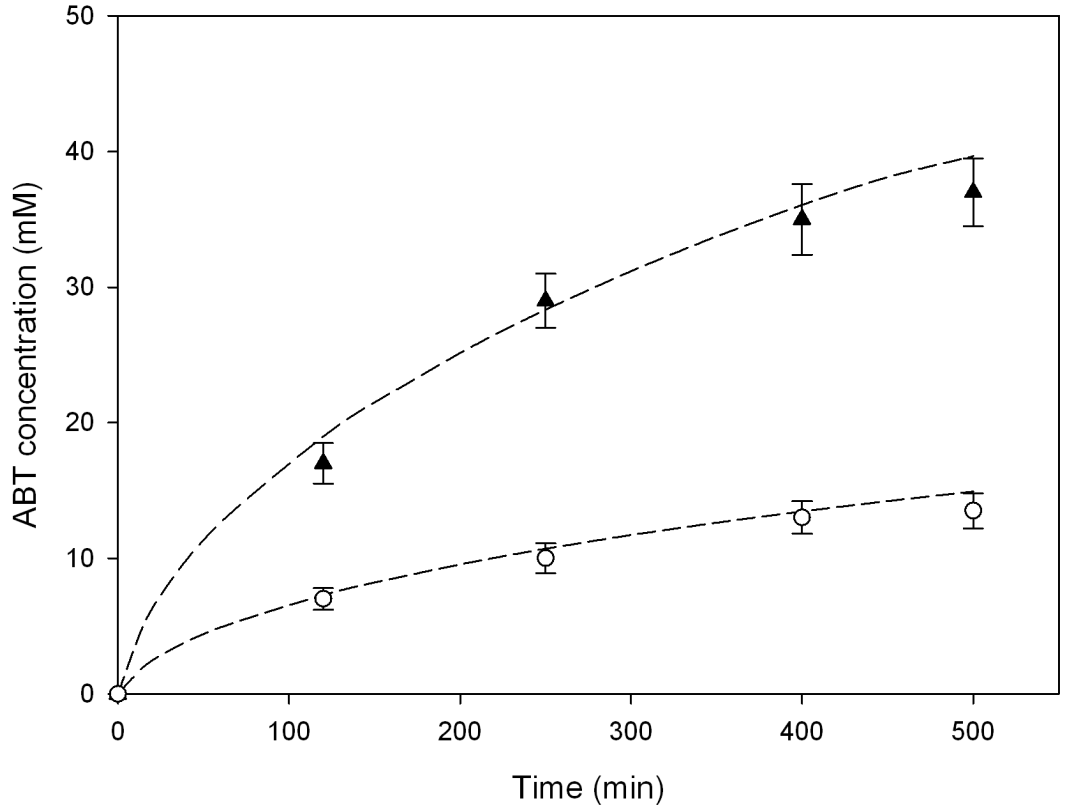

Figure 4.10. **Experimental progress curves and simulations following TAm mediated synthesis of ABT using an initial concentration of(▲) 250 mM ERY and 40 mM MBA and (○) 250 mM MBA and 40 mM ERY. Dotted and dashed lines represent kinetic model predictions based on Equation 4.1 and the parameters listed in Table 4.2. TAm concentration was 0.4 mg mL^{-1} in whole cell form, 0.2 mM PLP, 30°C and pH 7.5 in 200 mM HEPES. Experiments were performed as described in Section 2.8.1.**

4.5 SUMMARY

A microscale standardized methodology was developed, in order to rapidly establish the kinetic parameters of a reversible TAm bioconversion, where the kinetic model was no fully elucidated, in order to optimize the reaction conditions (Figure 4.1).
The hybrid procedure gave strong weight to both the initial rate data to identify a solution in the vicinity of the global minimum, and also to non linear regression methods to determine the exact location of the solution.

The full reaction kinetic model with its corresponding parameters for the TAm mediated synthesis of ABT using whole cells was established (Equation 4.1 and Table 4.2). The kinetic parameters were validated using 12 progress curves including reverse reaction data (Figure 4.7 and 4.8), as well as using a independent experimental data set not involved in the methodology to determine the parameters (Figure 4.9).

The TAm reaction was found to be very suitable for the asymmetric synthesis of ABT, due to the high equilibrium constant of determined of 843 (Table 4.2).

The main bottlenecks of the reaction were found to be the high Michaelis constant of ERY and the low catalytic constant of TAm (Figure 4.3), coupled with the high toxicity of the enzyme towards MBA. Therefore using a low concentration of MBA combined with a high concentration of ERY were considered to be the best reaction conditions, achieving more than 90 % yield in less than 10 hr (Figure 4.10).

Chapter 5 was focused in scaling up the production of the biocatalyst, while rationally controlling the level of expression of TAm and TK, in order to match their kinetic characteristics as discussed in section 4.4.3.3.

5. PRODUCTION OF THE DUAL TK-TAM E. COLI BIOCATALYST AT LABORATORY AND PILOT SCALE [†]

5.1. INTRODUCTION

As discussed in Section 4.4.3.3, the activity of the whole cell TAm was a factor of approximately 20 to 5 times slower than TK for reactions converting both ERY and PKD respectively. An ideal *E. coli* biocatalyst expressing dual TK-TAm activities would need therefore high Tam expression while maintaining a TAm/TK ratio of 5- 20 in order for the overall conversion rates of the two steps to be as similar as possible.

A whole cell *E. coli* biocatalyst with such characteristics was constructed and successfully produced in shake flask fermentations (Section 3.3.3), achieving more than 90% mol/mol yield for the one pot synthesis of amino alcohols (Section 3.3.5).
In principle, multi-step enzymatic conversions in whole cell biocatalysts offer a unique opportunity for synthesis of complex chiral molecules (Santacoloma et al., 2011). However, this opportunity has rarely been exploited beyond research scale. This has been attributed in part to difficulties in scaling-up biocatalyst production while maintaining the appropriate enzymes expression levels and without lowering their operational productivity (Meyer *et al.*, 2007).

In general, the three main scales for fermentation process development are laboratory, pilot plant and production scales. Typical volumetric scale-up ratios between each stage are around 1:10, although lower ratios of about 1:5 have usually been applied

[†] The majority of the results presented in this Chapter were submitted for publication as: Rios-Solis L., P. Morris, A. Odeleye, P. A. Dalby, F. Baganz and G. J. Lye. Scale-up and enzyme expression tuning of an *E. coli* whole cell biocatalyst with a *de novo* engineered pathway. *Biotechnol. Bioeng. Submitted.*

commercially to avoid unexpected performance on scale-up (Ju & Chase, 1992; Votruba & Sobotka, 1992). Factors which could affect biocatalyst performance upon scale-up include: mutation probability, plasmid stability and segregation, pellet formation, pH control agents interference, foam formation, enzyme stability, temperature and aeration gradients and sheer stress among many others (Young, 1979; Reisman, 1993; Humphrey, 1998). Therefore, for industrial application, identification of key issues related to pilot plant scale performance is critical for efficient bioprocess development (Junker, 2004).

5.2. AIM AND OBJETIVES

The aim of this chapter is to scale-up the production of the dual TK-TAm *E. coli* biocatalyst from laboratory to small pilot plant scale whilst maintaining overall biocatalyst productivity. Suitable fermentation conditions will be identified and applied to small pilot scale fermentations, trying if possible to increase enzyme concentration while maintaining the desired TAm/TK ratio. The kinetic performance of the biocatalyst produced at laboratory and pilot scales will be compared. The key objectives of this chapter are thus:

- Scale-up of the whole cell *E. coli* biocatalyst production from shake flask (100 mL) to laboratory (2 L) and small pilot scale (7.5 L) stirred tank fermentors.
- Evaluation of cell growth kinetics and protein expression profiles at different temperatures and induction times.
- Determination of the suitable cell growth conditions to obtain high TAm concentration while maintaining a suitable TAm/TK ratio.
- Comparison of bioconversion kinetic performance of the dual *E. coli* biocatalyst produced at laboratory and pilot scale for the one pot synthesis of APD.

5.3. RESULTS

5.3.1. 2 L fermentation with different temperatures and induction times

The shake flask fermentations of *E. coli* cells double transformed with plasmids pQR801 and pQR412 were previously shown to reach a final biomass concentration of 1.2 g_{DCW} L^{-1} (Figure 3.1), with final TAm and TK concentrations of 0.2 and 0.05 g L^{-1} respectively. In order to increase the total volume of the fermentation, and the overall amount of biocatalyst produced, the fermentation was initially scaled up to a 2 L stirred tank fermentor with a working volume of 1.4 L. The media was LB-glycerol as described in Table 2.1, and the pH, impeller speed and air flow were set to be 7.0, 1200 rpm and 1.4 L min^{-1} (1 vvm) respectively (Section 2.5.1). The biocatalyst used was the *E. coli* BL21-Gold (DE3) cells expressing TK D469E and the CV2025 TAm due to its high activity and *ee* shown for the synthesis of APD (Sections 3.3.3).

The co-expression level of several recombinant enzymes in a single *E. coli* host can be affected by many fermentation factors, such as temperature, media, pH and the time of induction among others (Tolia & Joshua-Tor, 2006). Therefore in this section, in addition to performing a 14-fold scale-up of the fermentation volume, the effects of temperature and time of induction (with 0.1 mM IPTG) were studied for the co-expression of the TK and TAm. Stirred tank bioreactors are more appropriate than shake flasks for such induction studies due to the improved environmental monitoring and control (Humphrey, 1998).

Figure 5.1 shows four growth profiles of the dual *E. coli* strain expressing the *de novo* TK and TAm pathway. Experiments were performed using fermentation temperatures of 30°C and 37°C, with early and late exponential phase induction. Figure 5.2 shows the logged data of DOT, pH, temperature and impeller speed for the fermentations performed at 37°C. The temperature had the largest impact on cell growth rate and final biomass concentration. The cells grown at 37°C presented a specific growth rate of 0.57 and 0.54 h^{-1}, and reached a maximum biomass concentration of 6.6 and 6.8 g_{DCW} L^{-1} for the early

and late induced fermentations respectively (Figure 5.1). The cells grown at 30^{o}C had a specific growth rate of 0.35 and 0.30 h-1, while reaching an 11 and 14% higher biomass concentration than the fermentations at 37^{o}C. The higher biomass obtained at 30^{o}C could be attributed to the better solubility of O_2 at lower temperature, as well to less toxic waste produced by the slower cell metabolism (Shiloach & Fass, 2005). In general the induction time did not have a significant effect in the growth of the cells at both temperatures. This suggests that the synthesis of the recombinant TAm was not a considerable metabolic burden for cell growth (Figure 5.1). The DOT profiles shown in Figure 5.2 suggest that upon early induction both cell growth and enzyme production continued whereas for late induction cell growth largely ceased upon IPTG addition.

Figure 5.3 shows the corresponding profiles for production of TK and TAm for each of the four fermentations described in Figure 5.1. Table 5.1 summarizes the derived growth kinetics parameters and final enzyme concentrations measured in Figures 5.1 and 5.3.

Even though a higher biomass concentration was achieved with the 30^{o}C fermentations, the percentage of TAm expression was higher at 37^{o}C, leading to similar final TAm concentrations of 1.3 and 1.25 g L^{-1} for the fermentations at 37 and 30^{o}C with early induction respectively (Figure 5.3a and 5.3b). These TAm concentrations were 40 and 74 % higher than the corresponding fermentations with late induction, highlighting the relevance of inducing in the early exponential phase to promote the TAm synthesis when the carbon source was still abundant. The final TAm concentration of 0.8 g L^{-1} obtained at 37^{o}C with late induction contrasted with the concentration of 0.3 g L^{-1} at 30^{o}C also with late induction (Figure 5.3c and 5.3d). This could be explained due to the temperature sensitive repressor used in plasmid pQR801 which was constructed using a PET vector (Section 2.3.2); it is well known that this system displays leaky protein expression at higher temperatures (Doublié, 2007).

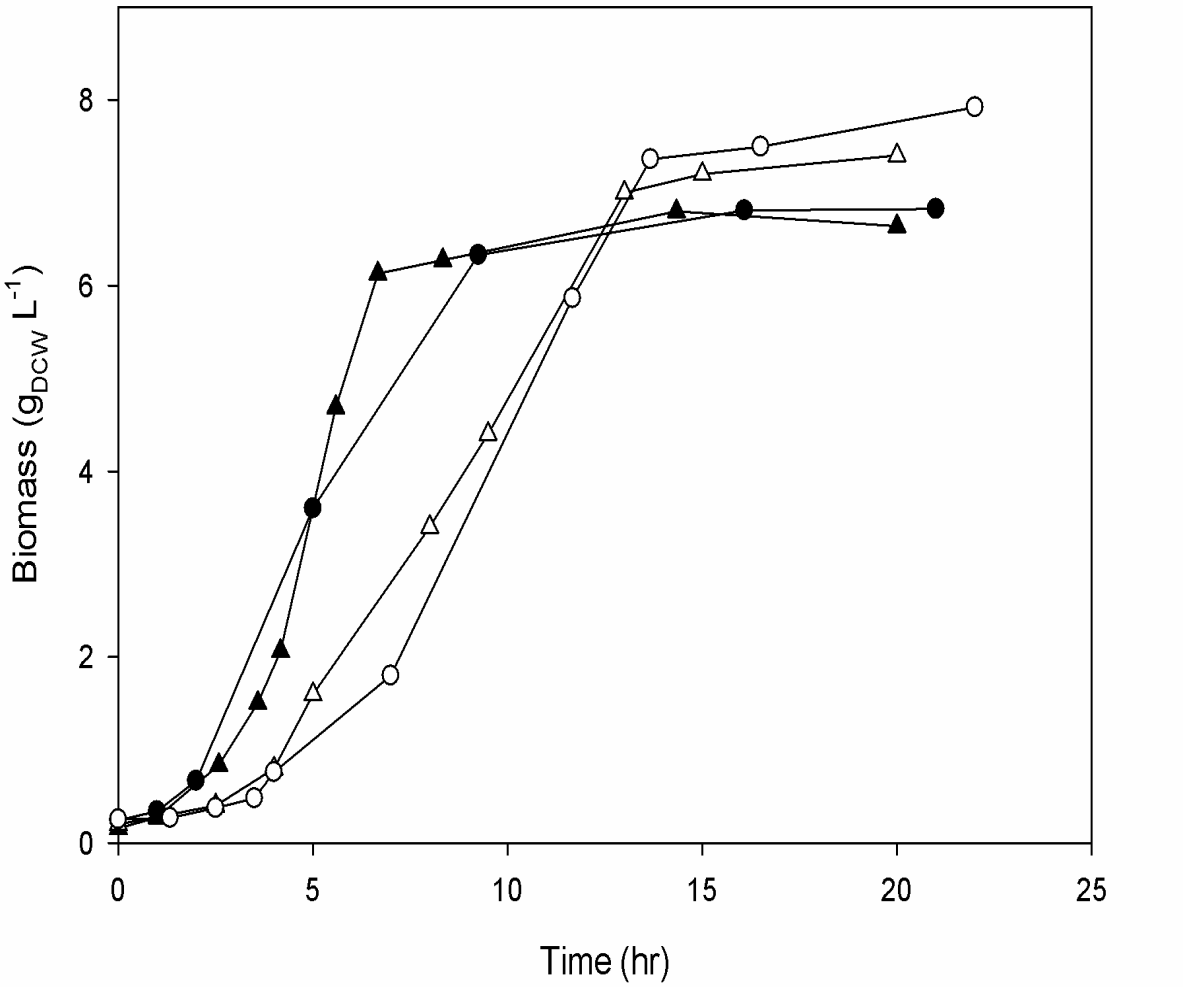

Figure 5.1. Effect of temperature on batch growth profiles for 2 L fermentations of the double transformed *E. coli* BL21-Gold (DE3) cells with plasmids pQR412 and pQR801 constructed as described in Section 2.3.3 and 2.3.5. The temperature was set at 37 ^{o}C (▲) with TAm induction in the early exponential phase after 3.5 hr of growth and (●) with induction in the late exponential phase after 6hr, and at 30 ^{o}C (Δ) with induction in the early exponential phase after 5 hr and (○) induction in the late exponential phase after 11.5 hr. Fermentation conditions were pH 7.0, 1200 rpm and air flow of 1.4 L min^{-1} (Section 2.5.1).

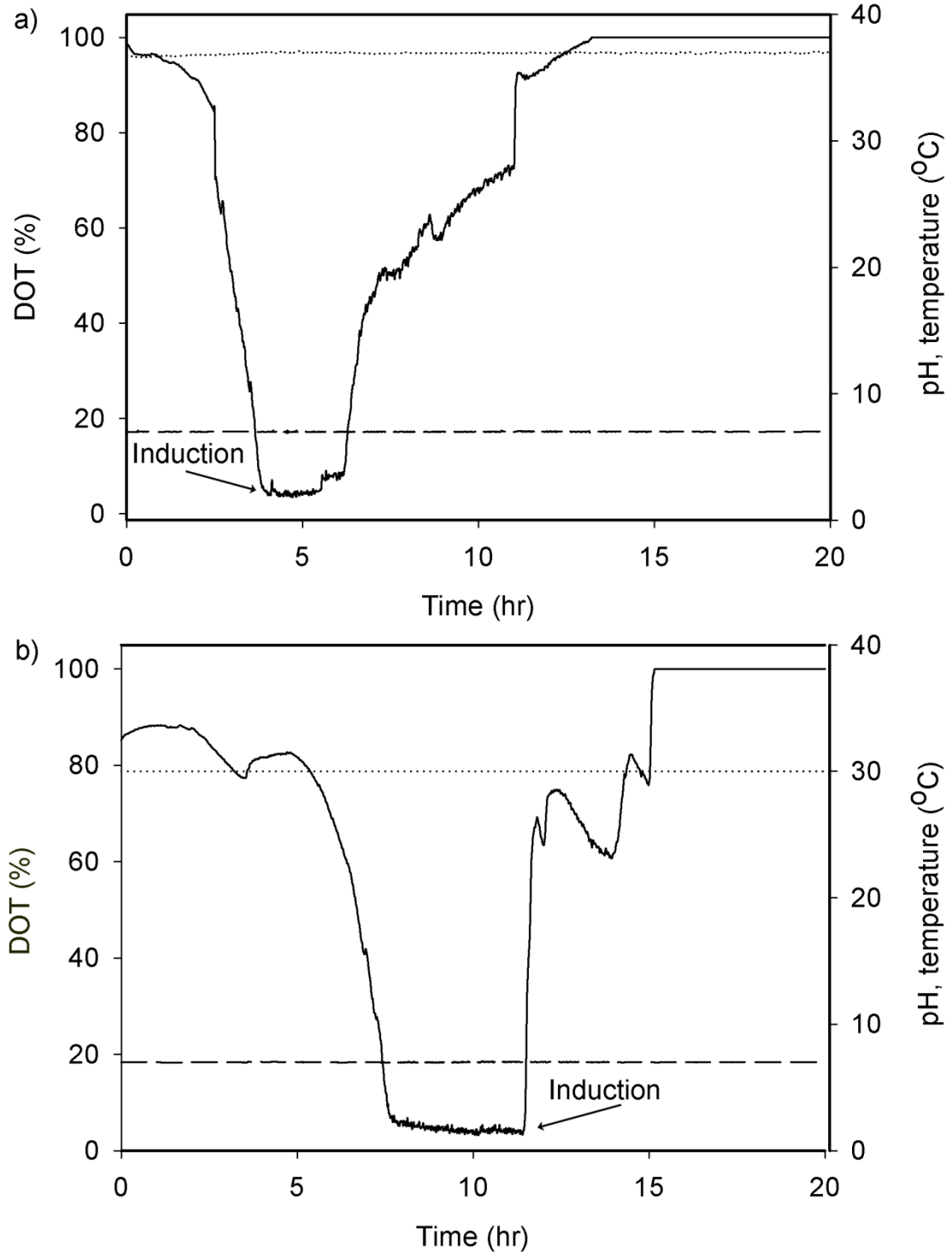

Figure 5.2. **Online measurements of pH (- -), temperature (•••) and DOT(−) for the fermentations shown in Figure 5.1 performed at (a) 37°C with early induction after 3.5 hr of growth and at (b) 30°C with late induction after 11.5 hr. Operating conditions as described in Figure 5.1.**

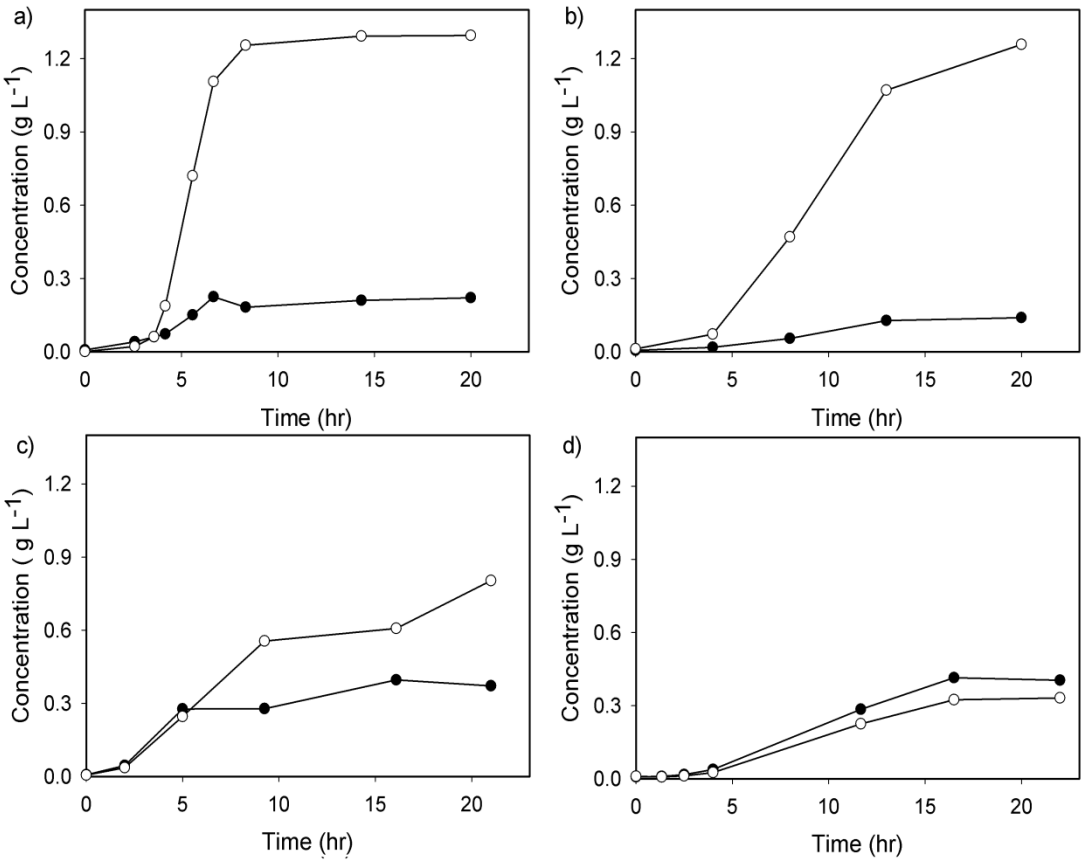

Figure 5.3. **Typical TK (●) and TAm (○) expression profiles for the 2 L fermentations shown in Figure 5.1 performed at 37 °C with (a) induction in the early exponential phase after 3.5 hr growth and (b) at 30°C with induction in the early exponential phase after 5hr, and at 37 °C with (c) induction in the late exponential phase after 6 hr and (d) at 30°C with induction in the late exponential phase after 11.5 hr. The concentration of each enzyme was calculated considering that 50% of the total dry cell biomass of *E. coli* cells were proteins (Watson. 1972), and by obtaining the % of total protein of the corresponding enzyme by SDS-PAGE (Section 2.9.5).**

Table 5.1. Growth and enzyme expression results for the dual *E. coli* biocatalyst produced in shake flasks, 2 L and 7.5 L fermentations as shown in Figures 3.1, 5.1 and 5.4 respectively. When available, the reported error represents one standard deviation of the mean (n=3).

Vessel volume (total)	Temperature (^oC)	Induction time[b]	μ[c] (h^{-1})	Biomass (g_{DCW} L^{-1})	TK (%w/w)	TAm (% w/w)	[TK][d] (g L^{-1})	[TAm][d] (g L^{-1})	TAm/TK ratio
100 mL[a]	37	Early	0.55±0.05	1.5±0.1	8.0±0.9	36.0±3.8	0.06±0.005	0.27±0.04	4.5
2 L	37	Early	0.57	6.6	6.7	39.1	0.22	1.30	5.8
2 L	37	Late	0.54	6.8	8.9	23.5	0.37	0.80	2.6
2 L	30	Early	0.35	7.4	3.8	34.0	0.14	1.26	8.9
2 L	30	Late	0.3	7.9	10.2	8.4	0.40	0.33	0.82
7.5 L	37	Early	0.43±0.07	8. 5±0.5	7.2±1.0	39.0±3.0	0.31±0.05	1.7±0.1	5.5
7.5 L	30	Late	0.36±0.04	9.5±0.4	9.5±0.4	7.6±0.5	0.45±0.03	0.36±0.03	0.80

[a]Results from shake flask fermentations performed in Section 3.3.

[b] Induction time refers to addition of 0.1 mM IPTG for expression of TAm in the early or late exponential phase.

[c] μ refers to the specific growth rate in h^{-1}.

[d]The concentration of each enzyme was calculated considering that 50% of the total dry cell biomass of *E. coli* cells were proteins (Watson. 1972), and by obtaining the % of total protein of the corresponding enzyme by SDS-PAGE (Section 2.9.5).

In Section 3.3.3, it was found that the TK expression in shake flasks of the single transformed *E. coli* host with plasmid pQR412 represented 20% of total protein. This was higher than the TK expression levels summarized in Table 5.1, especially when the TAm expression was predominant (higher TAm/TK ratio). This implied that once induced, the high expression rate of TAm by the T7 RNA polymerase (Section 2.3.3) retarded TK expression which had a constitutive expression (Section 2.3.1). Following this reasoning, the fermentation at 30^{o}C with late induction, which did not leak TAm expression, produced the highest TK concentration and lower TAm/TK ratio of 0.4 g L^{-1} and 0.8 respectively (Figure 5.3d and Table 5.1). This "expression switch" phenomenon has been previously observed and applied to tune enzyme co-expression using PET vectors in *E. coli* hosts (De Marco & De Marco, 2004).

As discussed in Section 4.3, a high TAm/TK ratio is desirable due to the slower bioconversion rate of TAm compared to TK. The fermentation at 30^{o}C with early induction achieved the highest TAm/TK ratio of 8.9 compared to the value of 5.8 obtained with the corresponding fermentation at 37^{o}C. However, the high ratio at 30^{o}C was achieved due to a 43% decrease in TK expression compared to the result at 37^{o}C. This was not desirable for the one pot synthesis of amino alcohols, where a higher TAm/TK ratio is favourable at the expense of producing more TAm, but not at the expense of reducing the TK synthesis. Overall, not only was the TK expression higher at 37^{o}C with early induction, but also the TAm expression was higher, making the biocatalyst produced at 37^{o}C with early induction the most suitable for the multi-step synthesis of amino alcohols.

5.3.2. Scale-up to a 7.5 L fermentor

In Section 5.3.1, it was concluded that the most suitable conditions to produce the dual TK-TAm whole cell *E. coli* biocatalyst for the synthesis of amino alcohols were at 37^{o}C with early induction. This fermentation was therefore scaled-up to a 7.5 L fermentor with a working volume of 5 L. In order to verify the "expression switch" phenomenon

observed in Figure 5.3, the fermentation at 30°C with late induction (maximum TK concentration) was also scaled-up to the 7.5 L fermentor.
The fermentation conditions where the same as Section 5.3.1, expect that the DOT was set to a minimum of 30% through a cascade control of the impeller speed (Section 2.5.2). Figure 5.4 shows the growth profile for the two 7.5 L fermentations.

The fermentation at 37°C had a specific growth rate of 0.43 h^{-1} and a final biomass concentration of 8.5 g_{DCW} L^{-1}, which was 22 % higher than the corresponding 2 L fermentation (Table 5.1). The fermentation at 30°C presented a specific growth rate of 0.36 h^{-1} and a final biomass concentration of 9.5 g_{DCW} L^{-1}, which was 17 % higher than the corresponding 2 L fermentation.

These results were in agreement with the ones found in Section 5.3.1, where the 2 L fermentations at 30°C presented a lower specific growth rate but a higher final biomass compared to the fermentations at 37°C. The higher biomass achieved in the 7.5 L fermentor compared to the 2 L was attributed to better oxygen mass transfer in the larger fermentor, due to the higher level of DOT maintained.

The protein expression concentration of TK and TAm were analyzed over different interval times. Figure 5.5 shows the SDS-PAGE result for different interval samples of the fermentation performed at 37°C with an early induction after 3 hr. A clear increase of TAm and a decrease in TK expression can be observed in the corresponding protein bands after the induction. The expression results have been plotted in Figure 5.6 for both fermentations.

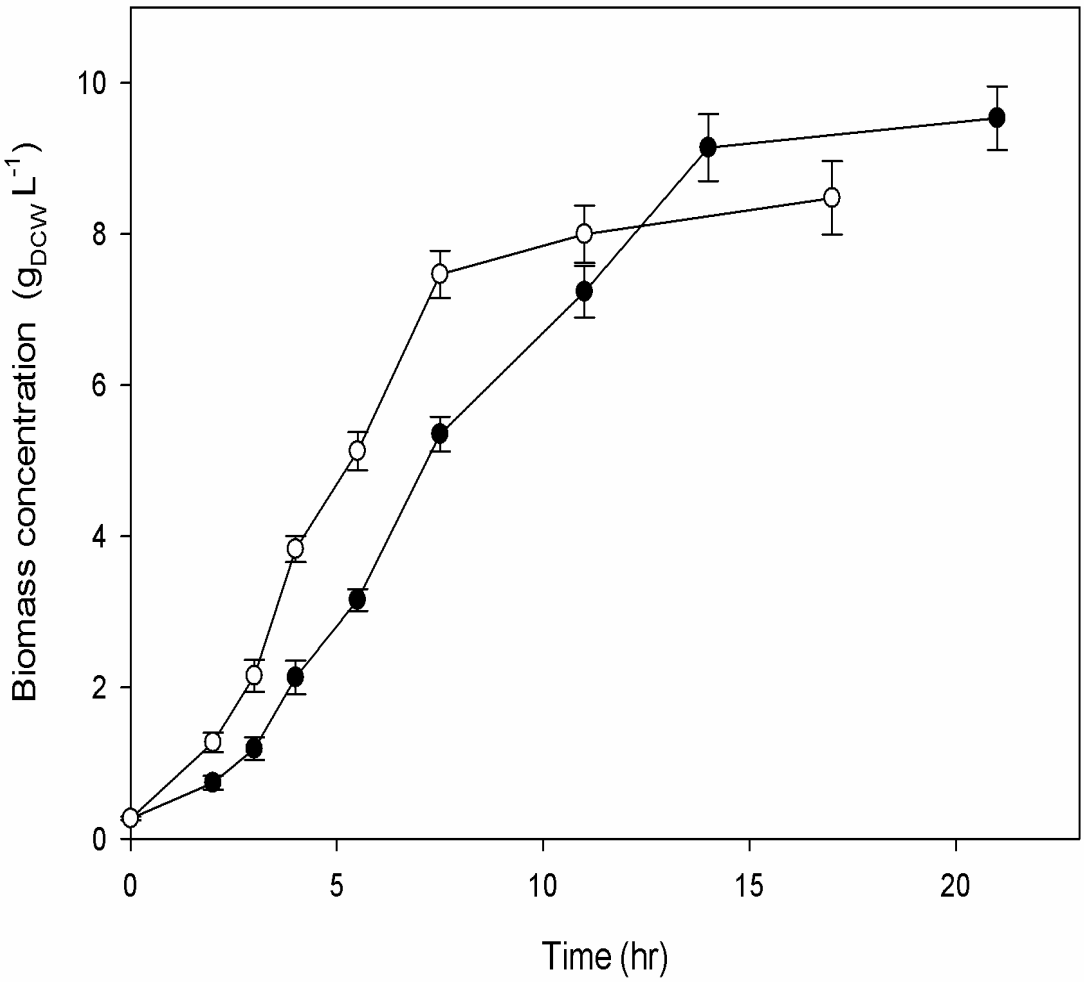

Figure 5.4. Growth profiles for 7.5 L fermentations of the double transformed *E. coli* BL21-Gold (DE3) cells with plasmids pQR412 and pQR801. The temperature was set at 37 °C (○) with induction in the early exponential phase after 3 hr growth, and at 30 °C (●) with induction in the late exponential phase after 11.5 hr of growth. Fermentation conditions were pH 7.0, DOT set to 30% through impeller speed and air flow of 5 L min^{-1} (Section 2.5.2). Error bars represent one standard deviation about the mean (n=3).

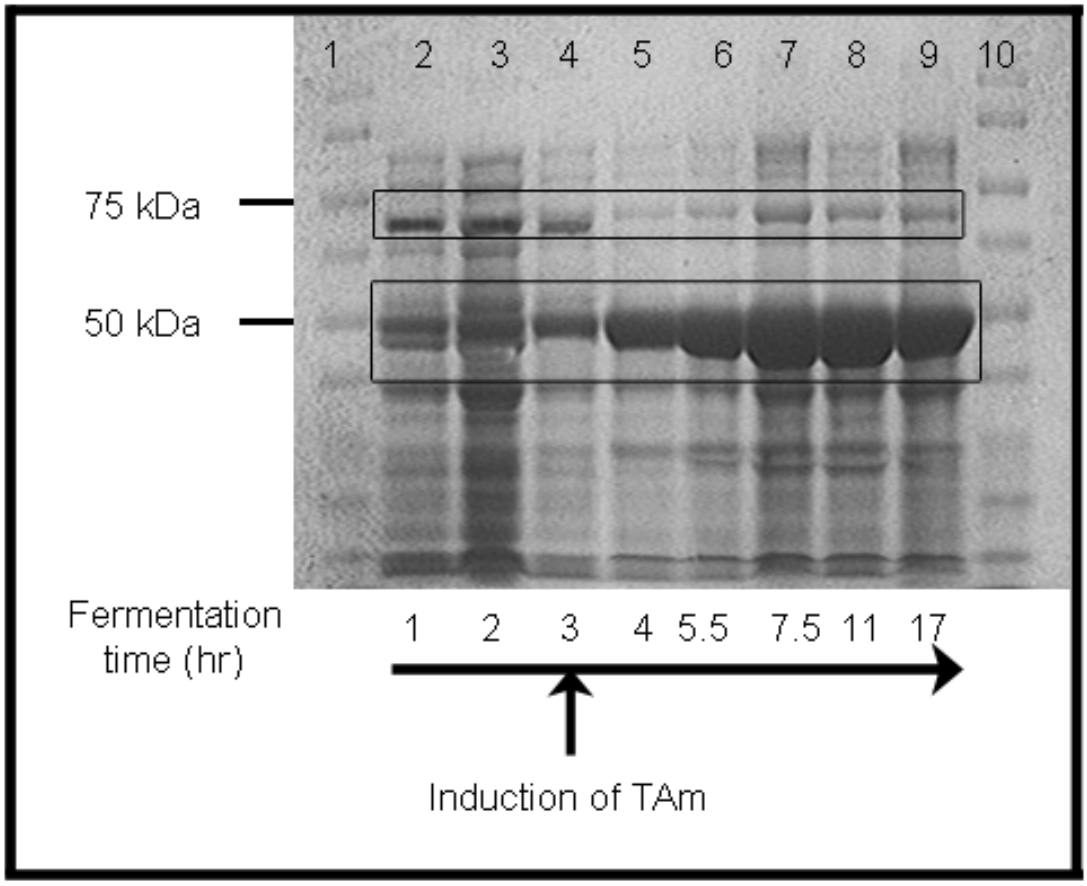

Figure 5.5. SDS-PAGE gel of cellular extracts of the 7.5 L fermentation at 37 °C with induction in the early exponential phase after 3 hr growth shown in Figure 5.4. Bands 1 and 10 are protein markers. Bands 2 to 9 are cellular extracts at different interval times of the fermentation. TK and TAm molecular weight are 72 kDa and 51 KDa respectively. SDS-PAGE gel was prepared as described in Section 2.9.5.

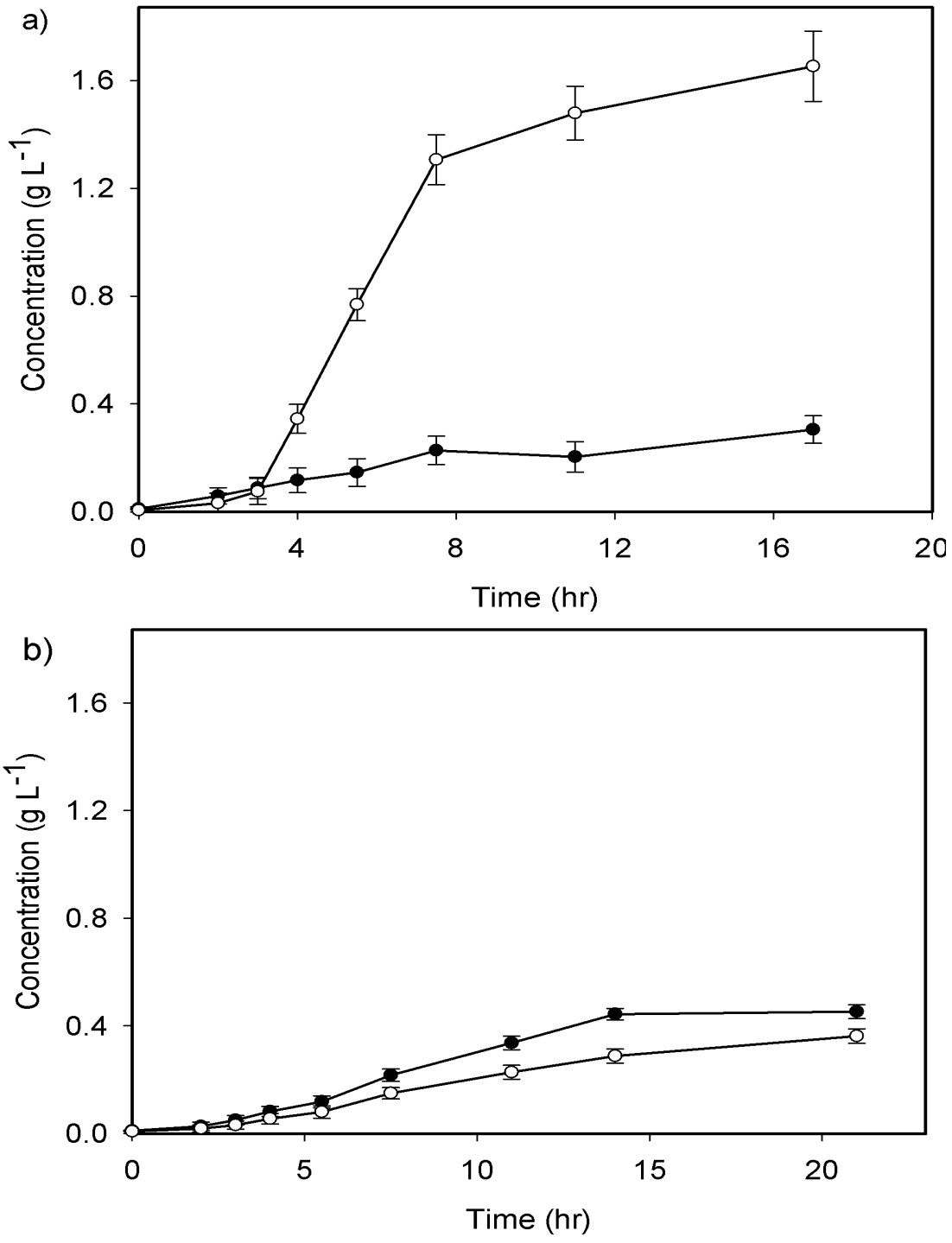

Figure 5.6. **TK (●) and TAm (○) expression profiles for the 7.5 L fermentations shown in Figure 5.4 performed at (a) 37 ^{o}C with induction in the early exponential phase after 3 hr growth and at (b) 30 ^{o}C with induction in the late exponential phase after 11.5 hr. The concentration of each enzyme was calculated as described in Figure 5.3.**

The kinetic growth results and final enzyme concentrations of the 7.5 L fermentations of Figure 5.4 are summarized and compared with the 2 L (Section 5.3.1) and shake flask fermentation results (Section 3.3.3) in Table 5.1 shown in Section 5.3.1. The level of expression of TK and TAm were similar than those achieved in the shake flask and 2 L fermentor, demonstrating the successful scale-up while maintaining the desired TK-TAm expression profile.

The final concentrations of TK and TAm for the fermentation at 37^{o}C with early induction were 5 and 6 folds greater than the shake flask fermentations, and 29 and 24% higher than the corresponding concentrations for the 2 L fermentation (Table 5.1). For the fermentation at 30^{o}C with late induction, the TK and TAm concentrations were 11 and 17% higher than those using the 2 L fermentor.

5.3.3. Comparison of single and dual enzyme expression levels

In the previous Sections the simultaneous expression of TK and TAm enzymes in the duel *E. coli* strain was studied. In addition a series of fermentations were also performed under similar conditions where the expression of TAm was evaluated. The results of these fermentations are included in Appendix VIII.

In general it was found that conditions for the optimum independent TAm expression were the same as in the dual enzyme expressing strain, obtaining a total protein expression of up to 40%.

5.3.4. Kinetic comparison of the laboratory and pilot scale biocatalyst

As illustrated in Table 5.1, the production of the dual TK-TAm *E. coli* biocatalyst was successfully scaled-up 50-fold from sake flask to a small pilot scale (7.5 L) stirred tank fermentor. High levels of both TK and TAm expression were achieved while maintaining a desired TAm/TK ratio greater than 5. Nevertheless it was important to verify the bioconversion kinetics of the biocatalyst produced, as these could have been impacted on

by enzyme stability issues or whole cell integrity problems, which may have arisen during the scale-up process (Junker, 2004). Gradients of temperature and oxygen, shear stress by the impeller and higher mutations probability due to longer fermentations times among other causes could have also affect the quality of the biocatalyst (Reisman, 1993; Humphrey, 1998).

In order to compare the bioconversion kinetic performance of the dual TK-TAm *E. coli* biocatalyst produced at different scales, two microscale one pot syntheses of APD were performed using both biocatalysts as described in Section 2.8.1.

The initial concentration of substrates was 10 mM of PA and HPA, while the cofactors concentrations were 2.4 mM of TTP, 9 mM Mg^{2+} and 0.2 mM of PLP in 200 mM HEPES buffer.

As has been shown in Section 3.3.5, the TK substrate HPA can be aminated by the TAm using MBA, producing serine as a side product and therefore consuming HPA and MBA in an undesirable reaction. To overcome these lose of substrates, the amino donor MBA was subsequently added in the multi-step synthesis after the TK reaction was completed. A stock solution of 300 mM of the amino donor was prepared to be added to the TK-TAm bioconversions. Therefore the volume added of the MBA solution represented only 3% of the original reaction volume, consequently the dilution of substrates and products was considered negligible.

The biocatalyst produced in the laboratory and pilot scale fermentor had slightly different expression of TK and TAm, which represented 8 and 37% of the total protein for TK and TAm in the shake flask fermentation, compared to 7 and 39 % of for the 7.5 L fermentor (Table 5.1). A fixed concentration of 0.4 mg mL^{-1} of TAm was used in both bioconversions. Considering than 50% of the total dry cell biomass of *E. coli* cells were proteins (Watson. 1972), then a final concentration of cell biomass of 2.2 and 2.1 $g_{DCW}\,L^{-1}$ was used of the laboratory and pilot scale biocatalyst respectively. By fixing the TAm

concentration, the TK concentration varied slightly from the two bioconversions, with values of 0.085 and 0.07 mg mL^{-1} for the smaller and larger scale biocatalysts.

Figure 5.7 shows the experimental progress curves for the TK reaction step of the one pot synthesis of APD using both the shake flasks and 7.5 L fermentor biocatalysts. Excellent agreement was found between the experimental data, where the conversion was only marginally faster using the shake flask biocatalyst as expected due to its higher concentration of TK. The TK initial activities were found to be 1.16 and 1.11 μmol min^{-1} mg^{-1} for the biocatalysts produced in the smaller and larger scale fermentations respectively, showing that the TK activity was not affected during the scale-up process. After 7 hours of reaction, final conversions of PKD of 97 and 96 % mol/mol were achieved and no HPA was detected, therefore MBA was added to start the TAm bioconversion.

Figure 5.8 shows the continuation of the progress curves shown in Figure 5.7 for the TAm step in the one pot synthesis of APD, using the laboratory and pilot scale biocatalysts. Again excellent agreement was observed between the TAm experimental data, which presented a specific activity of 9.6×10^{-3} and 9.2×10^{-3} μmol min^{-1} mg^{-1}, and a final conversion of 93 and 92% mol/mol for the laboratory and pilot scale biocatalysts respectively. Those results showed that the activity of TAm was also not affected during the scale-up process.

Tables 5.2 summarize the kinetic results of both bioconversions. Similar activities and final yields of the TK and TAm bioconversions were found for both biocatalysts. This demonstrated that the enzyme stability and kinetic characteristics of the TK-TAm biocatalysts were not affected during the scale-up process.

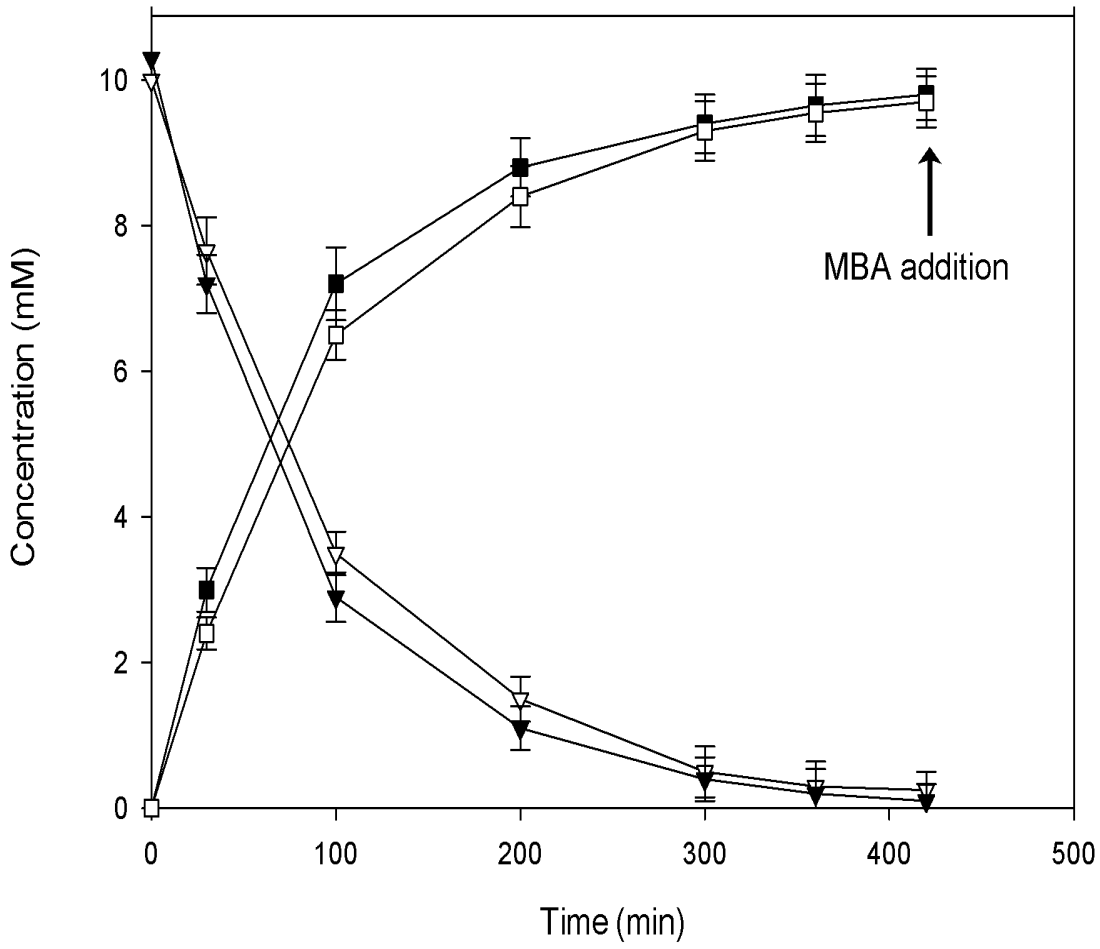

Figure 5.7. Bioconversion kinetics comparison of the dual TK-TAm expressing *E. coli* BL21-Gold (DE3) cells produced at shake flask and 7.5 L fermentor scales. Figure shows TK bioconversion step kinetics in the one pot synthesis of APD following: (■) PKD and (▼) HPA using the laboratory scale biocatalyst, and (□) PKD, and HPA (Δ) using the pilot scale biocatalyst. Reaction conditions: 10 mM [HPA] and [PA], 0.2 mM [PLP], 2.4 mM [TTP], 9 mM [Mg^{2+}], 30 ^{o}C, pH 7.5 in 200 mM HEPES. [TK] was 8.6×10^{-2} and 7.2×10^{-2} mg mL^{-1} for the laboratory and pilot scale biocatalyst respectively. [TAm] was 0.4 mg mL^{-1} for both whole cell biocatalysts. The microscale bioconversions were performed as described in Section 2.8.1. Error bars represent one standard deviation about the mean (n=3).

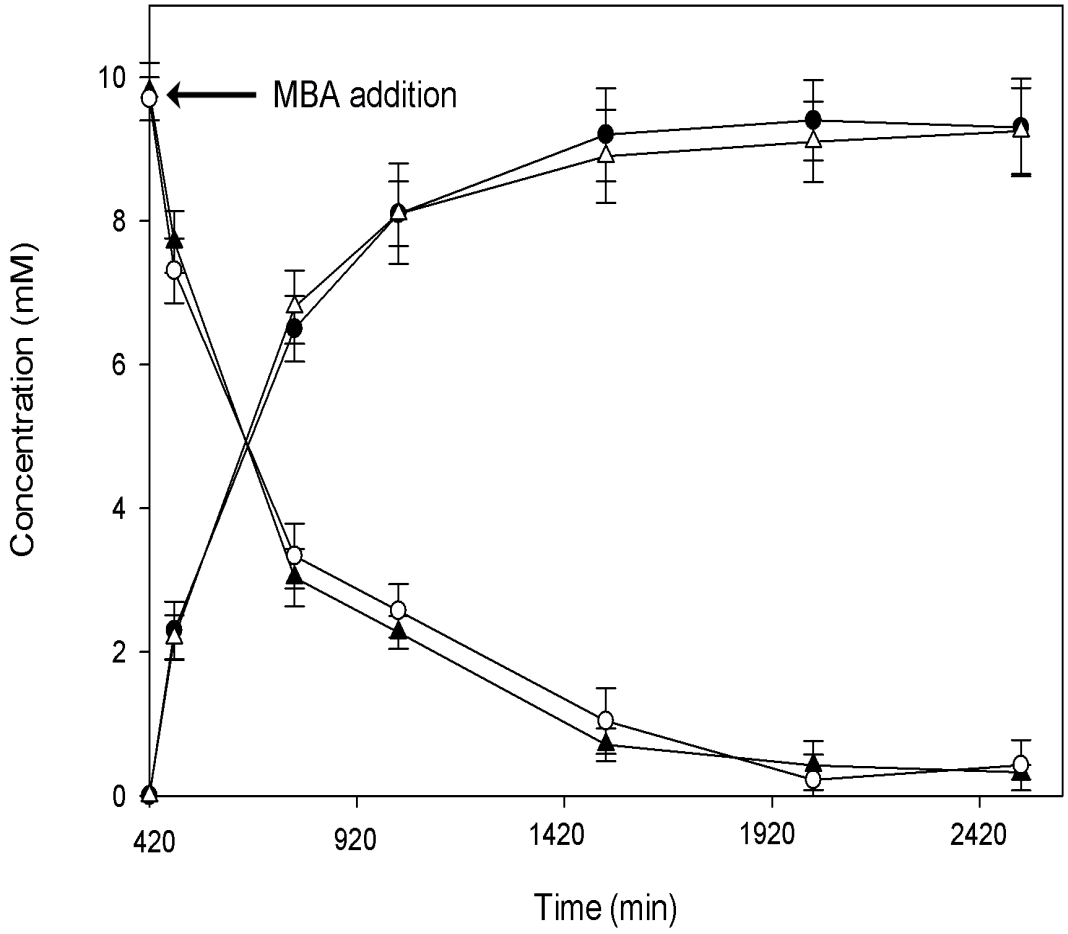

Figure 5.8. Continuation of the one pot synthesis profiles shown in Figure 5.4 using a TK-TAm shake flask and 7.5 L biocatalyst showing the TAm bioconversion step after addition of MBA following: (●) APD and (▲) PKD using the laboratory scale biocatalyst, and (Δ) APD, and PKD (○) using the pilot scale biocatalyst. Reaction conditions: 10 mM [HPA] and [PA], 0.2 mM [PLP], 2.4 mM [TTP], 9 mM [Mg^{2+}], 30 ^{o}C, pH 7.5 in 200 mM HEPES,. [TK] was 8.6×10^{-2} and 7.2×10^{-2} mg mL^{-1} for the laboratory and pilot scale biocatalyst respectively. [TAm] was 0.4 mg mL^{-1} for both whole cell biocatalysts. The microscale bioconversions were performed as described in Section 2.8.1. Error bars represent one standard deviation about the mean (n=3).

Table 5.2. Bioconversion kinetics comparison of the one pot APD synthesis shown in Figures 5.6 and 5.7 using biocatalyst produced at shake flask (Section 3.3.3) and 7.5 L fermentor (Section 5.3.1.2) scales. Microscale bioconversions and the calculation of the kinetic results were performed as described in Section 2.8.1.

Biocatalyst production scale	**Laboratory**	**Pilot scale**
Biomass concentration ($g_{DCW}\ L^{-1}$)	2.2	2.1
TK concentration (mg mL^{-1})	0.086 ± 0.007	0.072 ± 0.009
TK Initial rate (mM min^{-1})	0.10 ± 0.01	0.08 ± 0.009
TK initial specific activity (µmol min^{-1} mg^{-1})	1.2 ±0.1	1.1 ±0.1
TAm concentration (mg mL^{-1})	0.4 ± 0.05	0.4±0.02
TAm initial rate (mM min^{-1})	0.038 ± 0.003	0.037 ± 0.003
TAm initial specific activity (µmol min^{-1} mg^{-1})	0.096 ± 0.014	0.092 ±0.009
Final APD conversion (% mol)	93 ± 6	92 ± 7

5.4. SUMMARY

In summary, an overall scale-up of 50-fold for the production of the dual TK-TAm *E. coli* biocatalyst was performed from shake flasks to a 2 L and then a 7.5 L stirred tank fermentors. The growth kinetics and protein expression profiles at different temperatures and induction times were also investigated (Figures 5.1 and 5.3). The best fermentation conditions were determined to be 37^{o}C with an early exponential phase induction, where the TAm expression was highest (Figure 5.4 and 5.6a). Under those conditions, a 6 fold increase in TK and TAm concentrations were obtained respectively in comparison with the shake flask fermentations, while a suitable TAm/TK ratio of 5 was maintained (Table 5.1).

When used for the one pot synthesis of APD, the bioconversion kinetics of the pilot scale biocatalyst were in excellent agreement with the biocatalyst initially produced at shake flask scale (Figure 5.7 and 5.8). This clearly demonstrates that no lose in either TK or TAm activity occurred during the scale-up process. In the following Chapter, the scale-up of the TK-TAm one pot synthesis will be evaluated, as well as the complete kinetic modelling of the *de novo* engineered pathway for preparative scale bioconversions.

6. SCALE-UP AND MODELLING OF THE DE NOVO ONE-POT SYNTHESIS OF AMINO ALCOHOLS[†]

6.1. INTRODUCTION

A defining feature of the microscale bioprocesses studies, like the ones performed in Chapter 3 and 4, is to inform early stage bioprocess design and to aid predictions of larger scales of operation (Lye et al., 2003; Micheletti & Lye, 2006). However, the scale-up of *in vivo de novo* multi-enzymatic syntheses and the validation of the corresponding microscale data have been poorly explored to date. In part because such systems are difficulty to assemble and model accurately (Meyer et al., 2007).

Microscale, preparative and process scale bioreactors can present differences in fluid dynamics, solvent evaporation, shear stress, mass and heat transfer phenomena, and the methods used for pH control. These can cause significant and often unpredictable discrepancies in the bioconversion behaviour at the different scales (Doig et al., 2002; Micheletti et al., 2006; Nealon et al., 2006; Matosevic et al., 2008).

Therefore the detection of the main complications in the scale-up of the multi-step synthesis is crucial for adequate bioprocess design and implementation (Pollard & Woodley, 2007). Once the direct scale-up of the bioconversion can be guaranteed, mathematical microscale models could be used to predict larger scale synthesis. Such

[†] The majority of the results presented in this Chapter will be submitted for publication as: Rios-Solis L., P. Morris, A. Odeleye, P. A. Dalby, F. Baganz, and G. J. Lye. Scale-up and modelling of *de novo* pathway for the synthesis of chiral amino alcohols. *In preparation.*

models can then be applied in order to evaluate different bioconversion scenarios, and to select the best operating conditions and reactor configurations (Sin et al., 2009; Santacoloma et al., 2011).

6.2. AIM AND OBJECTIVES

The aim of this Chapter is to scale-up and model the one-pot synthesis of amino alcohols using the *de novo* engineering whole cell *E. coli* biocatalyst. In order to do so, the methodology developed in Chapter 4 will be used to establish microscale kinetic models of the synthesis of PKD and APD using the TK D469E and the CV2025 TAm. Subsequently, the microscale TK-TAm multi-step bioconversions of amino alcohols ABT and APD will be scaled-up to preparative synthesis. The models developed using the microscale tools will be then validated for the larger scale syntheses. Finally, using the model predictions, the best bioconversion operating strategies and reactor configuration will be determined and applied. The key objectives of this chapter are thus:

- Determination of the kinetic models for the TK D469E and CV2025 TAm mediated synthesis of PKD and APD respectively.
- Scale-up of the one-pot syntheses of APD and ABT from micro to preparative scale.
- Kinetic modelling of the TK-TAm one-pot syntheses and validation of the kinetic parameters by comparing the experimental and predicted data at the different scales.
- Identification of the best bioconversion conditions and reactor configurations using the predictions of the mathematical models.
- Application of the best reaction conditions to optimize the preparative scale one-pot syntheses of APD and ABT.

6.3. RESULTS

6.3.1. Determination of kinetic parameters

In Chapter 3, using microscale experimentation, the *E. coli* wild type TK and the CV2025 TAm were found to be the best candidates for the one-pot synthesis of ABT, while the mutant TK D469E combined with the CV2025 TAm were selected for the synthesis of APD (Figure 3.7 and 3.8). The kinetic parameters of the TK synthesis of ERY, from GA and HPA, have been reported previously (Gyamerah & Willetts, 1997; Chen et al., 2009), while the full kinetic model of the TAm mediated synthesis of ABT was established in Chapter 4 (Equation 4.1 and Table 4.2).

In contrast the kinetic parameters for the TK D469E catalyzed synthesis of PKD and the subsequent CV2025 TAm mediated synthesis of APD were still unknown. Hence these kinetic parameters were rapidly determined here following the systematic procedure summarized in Figure 4.1. Sections 6.3.1.1 and 6.3.1.2 will focus on the results obtained for the kinetic models, which will be applied in Section 6.3.2 to model the full one-pot synthesis of APD. For more details about the complete set of progress curves used to determine the parameters, and its modelling predictions, refer to Appendix IX and X.

6.3.1.1. Kinetic model of the *E. coli* D469E TK mediated synthesis of PKD

The synthesis of PKD catalyzed by the TK D469E in whole cell form from HPA and PA is an irreversible reaction due to the release of CO_2 as a side product (Scheme 3.2). The bioconversion follows a previously elucidated ping-pong bi-bi mechanism with competitive substrate inhibition, which requires thiamine pyrophosphate and Mg^{2+} as cofactors as was described in Section 1.5.2.3 (Gyamerah & Willetts, 1997; Chen et al., 2008). The full kinetic model can be written as follows in Equation 6.1:

$$\frac{d[PKD]}{dt} = \frac{k_{cat}E_{iTK}[HPA][PA]}{den} \qquad \text{Equation 6.1}$$

$$den = K_{PA}[HPA]\left(1 + \frac{[HPA]}{K_{iHPA}}\right) + K_{HPA}[PA]\left(1 + \frac{PA}{K_{iPA}}\right) + [HPA][PA] + \frac{K_{HPA}}{K_{iPKD}}[PA][PKD] + \frac{K_{HPA}K_{iPA}}{K_{iPKD}}$$

where k_{cat} represents the catalytic rate constant, K_{PA} and K_{HPA} are the Michaelis constants of PA and HPA, K_{iPA}, K_{iHPA} and K_{iPKD} are the inhibition constants of PA, HPA and PKD respectively, and E_{iTK} is the TK enzyme concentration.

Following the methodology illustrated in Figure 4.1, the values of the kinetic parameters were determined here and are summarized in Table 6.1. Figure 6.1 shows the resulting Michaelis-Menten plots, as well as two progress curves used to validate the kinetic parameters. (Refer to Appendix IX for the complete experimental progress curves used to determine the kinetic parameters as well as their modelling predictions).

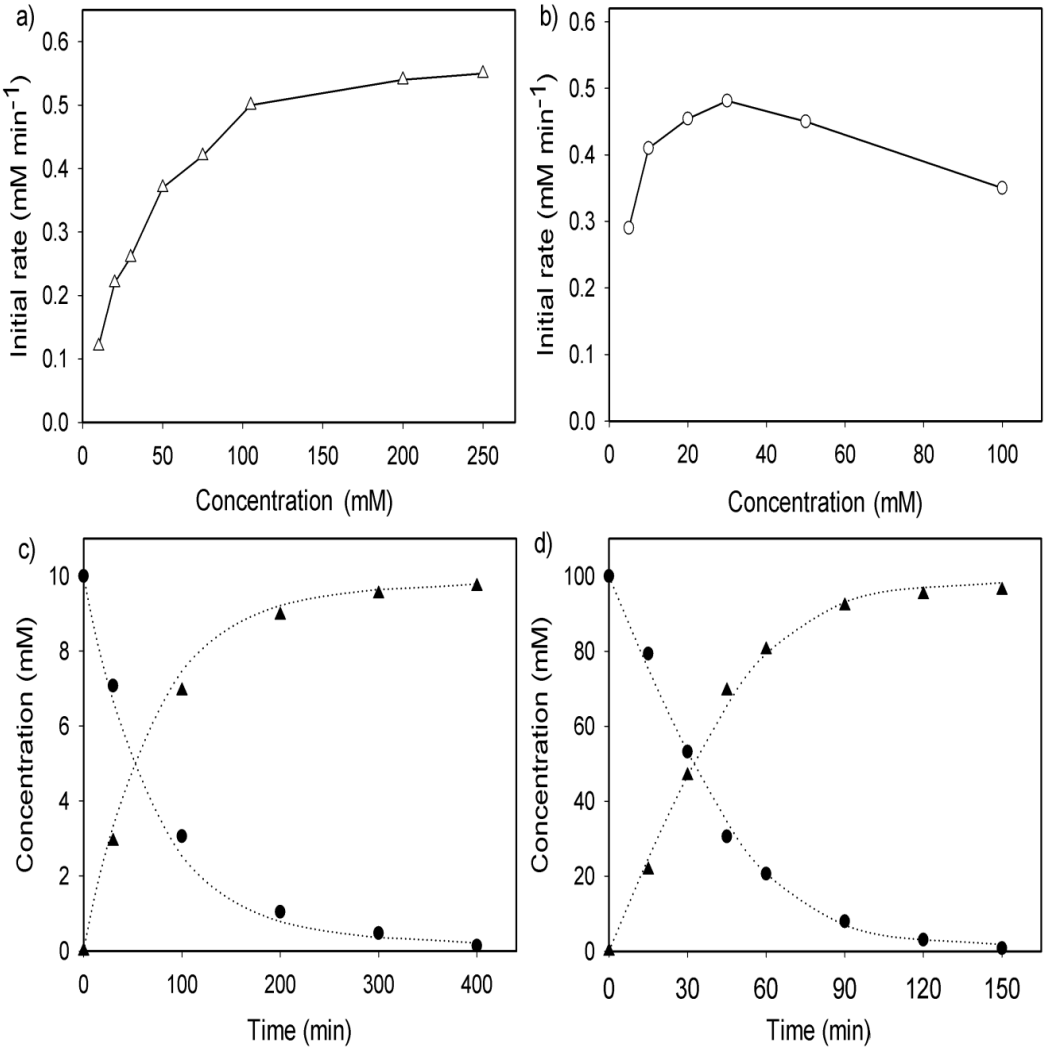

Figure 6.1. **(a) Apparent initial rate of PKD formation using TK D469E as a function of [PA] while maintaining [HPA] fixed at 30 mM, and (b) as a function of [HPA] while maintaining [PA] fixed at 100 mM. For the experiments (a) and (b) [TK] concentration was 0.15 mg mL^{-1} in whole cell form. Experiments (c) and (d) represent typical TK experimental progress curves and model predictions using an initial concentration of (c) 10 mM [PA] and [HPA] and 0.1 mg mL^{-1} [TK] and (d) 100 mM [PA] and [HPA] and 0.4 mg mL^{-1} [TK] following (●) HPA and (▲) PKD. Dotted lines show model predictions based on Equation 6.1 and final kinetic parameters in Table 6.1. For all the experiments TK biocatalyst was used in whole cell form with 2.4 mM [TPP] and 9 mM [Mg^{2+}] at 30°C and pH 7.5 in 50 mM TRIS buffer using microscale experimentation (Section 2.8.1).**

Table 6.1. Experimental values of the apparent kinetic parameters of Equation 6.1 for the synthesis of PKD catalyzed by a whole cell *E. coli* biocatalysts containing the TK mutant D469E. Parameters were obtained following the methodology summarized in Figure 4.1 using microscale experimentation (Section 2.8.1).

Apparent kinetic parameter	Value
Rate constant: k_{cat} (min^{-1})	642.3
Michaelis constant for HPA: K_{HPA} (mM)	5.3
Michaelis constant for PA: K_{PA} (mM)	47.4
Inhibition constant for HPA: K_{iHPA} (mM)	86.7
Inhibition constant for PA: K_{iPA} (mM)	542.2
Inhibition constant for PKD: K_{iPKD} (mM)	886.9

The catalytic constant in Table 6.1 was found to be similar to the previously published value for the synthesis of PKD using *E. coli* TK mutant D469T in lysate form (Chen et al., 2008). It is important to mention that the kinetic parameters of TK D469E in this work were determined at 30°C, while the authors used a temperature of 25°C. Therefore, it could be assumed that at the same temperature, the TK D469T would have a higher catalytic rate constant. Interestingly, both Michaelis constants found in this work are half the value than the ones published for TK D469T.

6.3.1.2. Kinetic model of the CV 20205 TAm mediated synthesis of APD

Following the systematic approach developed in Chapter 4, the kinetic model for the TAm mediated synthesis of APD was elucidated and is represented by Equation 6.2.

$$v = \frac{k_f k_r E_{iTAm}\left([MBA][PKD] - \frac{[AP][APD]}{K_{eq}}\right)}{den} \qquad Equation\ 6.2$$

$$den = k_r K_{MBA}[PKD] + k_r K_{PKD}[MBA] + k_r[PKD][MBA] + \frac{k_f K_{AP}[APD]}{K_{eq}}$$

$$+ \frac{k_f K_{APD}[AP]}{K_{eq}} + \frac{k_f[AP][APD]}{K_{eq}} + \frac{k_r K_{MBA}[PKD][APD]}{K_{iAPD}} + \frac{k_f K_{APD}[MBA][AP]}{K_{eq} K_{iMBA}}$$

where k_f and k_r represents the catalytic rate constants for the forward and reverse reaction respectively, K_{PKD}, K_{AP}, K_{APD} and K_{MBA} are the Michaelis constants of PKD, AP, APD and MBA, K_{iAPD} and K_{iMBA} are the inhibition constants of APD and MBA respectively, E_{iTAm} represents the TAm concentration and K_{eq} is the equilibrium constant.

The kinetic parameters were determined following the procedure represented in Figure 4.1, and their values are summarized in Table 6.2. Figure 6.2 shows the resulting Michaelis-Menten plots, as well as two progress curves used to validate the kinetic parameters. (Refer to Appendix X for the complete experimental progress curves used to determine the kinetic parameters as well as their modelling predictions)

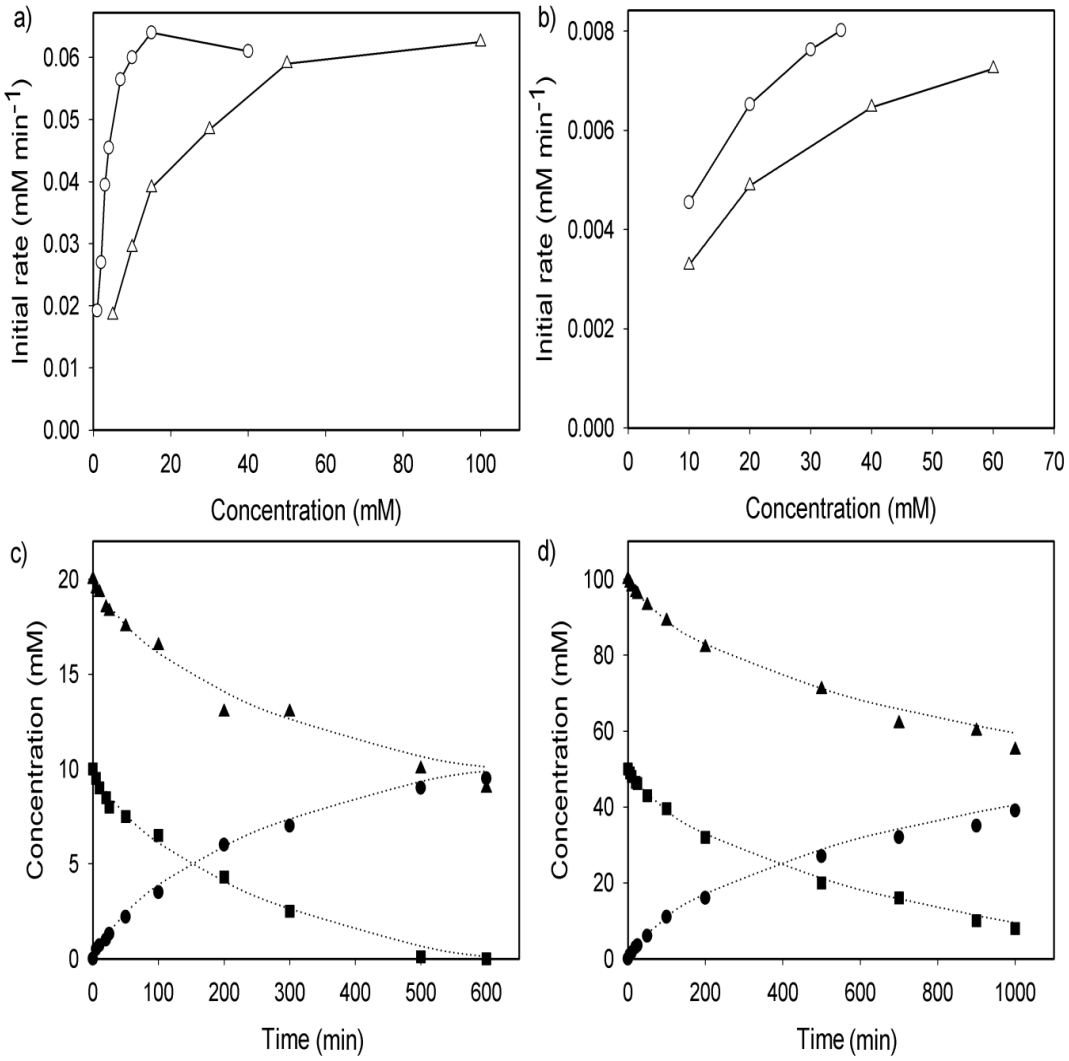

Figure 6.2. **(a) Apparent TAm initial rate of AP for the forward reaction as a function of (○) [MBA] while maintaining [PKD] fixed at 100 mM, and as a function of (Δ) [PKD] while maintaining [MBA] fixed at 10 mM. b) Apparent TAm initial rate of MBA for the reverse reaction as a function of (○) [AP] while maintaining [APD] fixed at 100 mM, and as a function of (Δ) [APD] while maintaining [AP] fixed at 35 mM. For the experiments (a) and (b) [TAm] concentration was 0.3 mg mL^{-1} in whole cell form. Experiments (c) and (d) represent typical experimental TAm progress curves and model predictions using an initial concentration of (c) 20 mM [PKD] and 10 mM [MBA] and 0.2 mg mL^{-1} [TAm] and (b) 100 mM [PKD] and 50 mM [MBA] and 0.3 mg mL^{-1} [TAm] following (●) PKD and (▲) MBA. Dotted lines show model predictions based on Equation 6.2 and final kinetic parameters in Table 6.2. For all the experiments TAm biocatalyst was used in whole cell form with 0.2 mM [PLP] at 30°C and pH 7.5 in 200 mM HEPES buffer using microscale experimentation (Section 2.8.1).**

Table 6.2. Experimental values of the apparent kinetic parameters of Equation 6.2 for the synthesis of APD catalyzed by a whole cell *E. coli* biocatalyst containing the CV2025 TAm. The parameters were obtained following the methodology summarized in Figure 4.1 and using microscale experimentation (Section 2.8.1).

Apparent kinetic parameter	Value
Forward rate constant: kf (min−1)	37.1
Reverse rate constant :kr (min−1)	1.9
Michaelis constant for MBA: KMBA (mM)	1.2
Michaelis constant for PKD: KPKD (mM)	20.4
Michaelis constant for AP : KAP (mM)	17.6
Michaelis constant for APD : KAPD (mM)	23.3
Inhibition constant for MBA: KiMBA (mM)	0.05
Inhibition constant for APD: KiPA (mM)	5.3
Equilibrium constant	6407

The forward catalytic rate constant for the TAm mediated synthesis of PKD was 3-fold smaller than the one for the synthesis of ERY (Table 4.2). In contrast, the Michaelis constant of PKD was 5 times smaller than the one for ERY, while the rest of the constants were in the same order of magnitude as the determined for ERY (Table 4.2 and 6.2). These results indicate that using the same enzyme concentration, the conversion rate of ERY by TAm to ABT would relatively faster than the one of PKD to APD at concentrations above 200 mM. Nevertheless, at concentration below 30 mM, the low Michaelis-Menten constant of PKD compared to ERY would compensate the higher catalytic constant for ERY, giving comparable reaction rates for both amino acceptors.

6.3.2. Scale-up and modelling of the one-pot synthesis of APD

The one-pot synthesis of APD (Scheme 3.2) was scaled-up from 300 µL parallel microwell bioreactors (Section 2.8.1) to a 50 mL working volume laboratory scale stirred bioreactor (Section 2.8.2). This represented a 167-fold increase in volume. Table 6.3 compares the different conditions and bioreactors used for the micro and preparative scale multi-step synthesis.

Table 6.3. Comparison of the different reaction conditions and bioreactors used for the scale-up of the multi-step syntheses from microscale parallel bioreactors (Section 2.8.1) to preparative scale synthesis (Section 2.8.2).

Bioconversion scale	Microscale	Preparative scale
Temperature (^{o}C)	30	30
Temperature control	Under plate heated platform	Circulating water bath
Mixing (rpm)	300	300
Mixing device	Orbital Shaking platform (diameter= 6 mm)	Magnetic stirrer
Working reaction volume	300 µL	50 mL
Reactor vessel	550 µL micro reactors (96 glass microplate)	100 mL glass stirred bioreactor
pH	7.5	7.5
pH control	200 mM HEPES buffer	pH stat with 1M NaOH (aq)

The pH of the preparative scale bioconversion was maintained at 7.5 by the use of automated pH stat addition of 1 M NaOH in comparison to 200 mM HEPES buffer used in the microscale system (Table 6.3). The TAm was shown to be more stable in whole cell form than in lysates (Section 3.3.6), therefore 25 mM HEPES were added to the larger scale bioconversion in order to avoid cell lysis by difference in osmotic

pressure. The temperature was kept constant at 30°C using a circulating water bath in contrast to an "under plate" heated platform used for the microscale experiments (Section 2.8.1 and 2.8.2).

In the case of mixing, previous results reported an increase in transfer rates of substrates for TK bioconversions in the µL scale compared to the mL scale, causing differences up to 40% in the scale-up process (Matosevic et al., 2008). In order to overcome this problem, the authors demonstrated that using a magnetic stirrer at 300 rpm reduced the discrepancies between the larger and small scale results. This mixing system was then chosen for the lab bench vessel in comparison with the orbital shaking platform used for the microscale experiments (Section 2.8.1 and 2.8.2).

For the one-pot synthesis of APD, the microscale bioconversion results obtained in Section 5.3.3 using a shake flask biocatalyst, were used as a reference to compare the scale-up process (Figure 5.6 and 5.7). For the preparative scale synthesis, the TK-TAm biocatalyst produced at the small pilot plant scale using the 7.5 L fermentor (Section 5.3.2) was applied to perform the bioconversion. The concentration of TAm was also fixed at 0.4 mg mL^{-1}; therefore the biomass and the TK concentration were 2.1 g_{DCW} L^{-1} and 0.07 mg mL^{-1} (Table 5.2).

The initial concentration of substrates PA and HPA were 10 mM, and MBA was added after 7 hours of starting the bioconversion, the same was for the microscale synthesis described in Section 5.3.3.

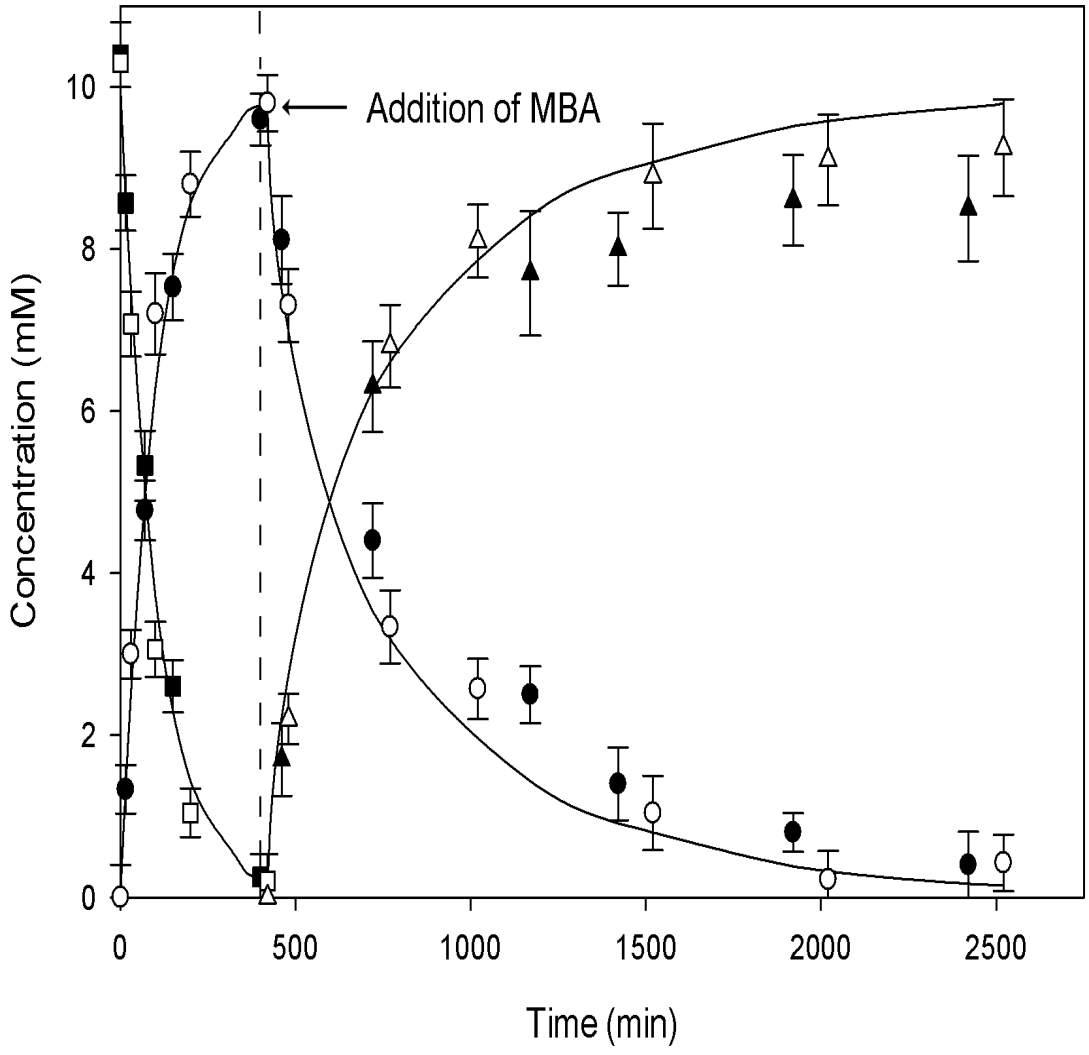

Figure 6.3. **Scale-up and modelling of the whole cell *E. coli* TK-TAm sequential synthesis of APD following: (□) HPA, (○) PKD and (Δ) APD using microscale experimentation (data was obtained from Section 5.3.3), and (■) HPA, (●) PKD and (▲) APD for the preparative scale synthesis (Section 2.8.2). Reaction conditions: 10 mM [HPA] and [PA], 0.2 mM [PLP], 2.4 mM [TTP], 9 mM [Mg^{2+}], 30 ^{o}C, pH 7.5 in 200 mM HEPES. 10 mM MBA was added after 420 min. [TK] and [TAm] were 0.07 and 0.4 mg mL^{-1} respectively for both whole cell biocatalysts. The modelling was performed combining Equations 6.1 and 6.2 with the corresponding kinetic parameters from Table 6.1 and 6.2 and is shown as a solid line. Error bars represent one standard deviation about the mean (n=3).**

Figure 6.3 shows the complete experimental progress curves of the micro and preparative scale bioconversions. Combining equations 6.1 and 6.2, the complete modelling of the one-pot synthesis was also achieved in Figure 6.3.

The microscale results scaled excellently as shown in Figure 6.3, resulting in very similar kinetic profiles after a 166-fold scale-up. The experimental kinetic results from the different scales and the kinetic model predictions are shown in Table 6.4.

Table 6.4. Experimental and predicted apparent kinetic results for the one-pot synthesis of APD shown in Figure 6.3 using microscale experimentation (Section 3.8.1) and a preparative scale bioreactor (Section 3.8.2). The predicted data was obtained using Equations 6.1 and 6.2 with the kinetic parameters from Table 6.1 and 6.2. The calculation of the kinetic experimental results was performed as described in Section 2.8.1.

Apparent kinetic parameter	Model prediction	Microscale data	Preparative scale data
E. coli D469E TK initial specific activity (μmol min^{-1} mg^{-1})	1.1	1.3 ± 0.2	1.2 ± 0.2
CV2025 TAm initial specific activity (μmol min^{-1} mg^{-1})	0.12	0.1 ± 0.01	0.1 ± 0.02
Final APD yield (% mol/mol)	98	93 ±6	85 ± 6.5

The difference in TK and TAm specific activities of both scales were statistically not significant (Table 6.4). This indicates that the biocatalyst did not lose activity in the scale-up process, and also that the preparative scale synthesis did not suffer greater mass transfer limitations compared to the microscale bioconversion.

Excellent agreement was found between the predicted specific activities and the experimental data (Table 6.4), which shows that the mathematical models developed in Section 6.3.1 using microscale data were still valid for preparative scale multi-step

syntheses. After 1500 min of bioconversion, a small difference could be observed between the predicted and experimental data, which was higher than the experimental error, especially for the preparative scale synthesis. This discrepancy could also be detected in the maximum final yield (% mol/mol) of the large scale bioconversion which was 13 and 7% smaller than the predicted and microscale yield. Because the predicted initial specific activities were in agreement with the experimental results of both scales (Table 6.3), and the discrepancies only appeared after 1500 min of reaction time, the difference in the final conversion was attributed to a decrease in stability of TAm, probably caused by the toxicity of MBA as was discussed in Section 4.4.3.7. Also the stirring of the 100 mL bioreactor may have caused lysis of the cells, further reducing the stability of the TAm as was shown in Section 3.3.6. In addition, although APD was a non natural substrate, consumption of APD by the whole cells could also contribute to the difference in final yields, as it has previously been previously shown for similar amino alcohols (Ingram et al., 2007).

An individual TK synthesis of PKD had been successfully scaled-up in a previous work (Smith et al., 2010) obtaining a maximum difference between predicted and experimental data of 30%, which was 2-fold higher than the differences found in this work (Figure 6.3). A previous work scaling up a TAm bioconversion from the µL to mL scale reported a 30% difference in the final yield (% mol/mol), mainly due to pH fluctuations in the small scale system (Truppo et al., 2009). The use of 200 mM HEPES here enabled to maintain the pH of the microscale bioconversion constant, improving the agreement of the results towards the larger scale synthesis.

6.3.3. Scale-up and modelling of the one-pot synthesis of ABT

To be able to model the TK-TAm one-pot synthesis of ABT (Scheme 3.1), the kinetic models of the *E. coli* wild type TK and CV2025 TAm mediated synthesis of ERY and ABT respectively were necessary. The required TAm model was established in Chapter 4 and is represented by Equation 4.1 with the kinetic parameters from Table 4.2. The TK model previously mentioned had been published before (Gyamerah & Willetts, 1997; Chen et al., 2009), and is represented by Equation 6.3 with the corresponding parameters shown in Table 6.5.

$$\frac{d[ERY]}{dt} = \frac{k_{cat}E_{iTK}[HPA][GA]}{den} \qquad \text{Equation 6.3}$$

$$den = K_{GA}[HPA]\left(1+\frac{[HPA]}{K_{iHPA}}\right) + K_{HPA}[GA]\left(1+\frac{GA}{K_{iGA}}\right) + [HPA][GA] + \frac{K_{HPA}}{K_{iERY}}[GA][ERY] + \frac{K_{HPA}K_{iGA}}{K_{iERY}}$$

where k_{cat} represents the catalytic rate constant, K_{GA} and K_{HPA} are the Michaelis constants of GA and HPA, K_{iGA}, K_{iHPA} and K_{iERY} are the inhibition constants of GA, HPA and ERY respectively, and E_{iTK} is the TK enzyme concentration.

Table 6.5. Reported values by Chen et al., (2009) for the kinetic parameters of Equation 6.3 for the synthesis of ERY catalyzed by *E. coli* wild type TK. The parameters reported by the authors were obtained at 25°C and pH 7 using TK in lysate form.

Apparent kinetic parameter	Value
Rate constant: k_{cat} (min^{-1})	2442
Michaelis constant for HPA: K_{HPA} (mM)	18
Michaelis constant for GA: K_{GA} (mM)	16
Inhibition constant for HPA: K_{iHPA} (mM)	40
Inhibition constant for GA: K_{iGA} (mM)	570
Inhibition constant for ERY: K_{iERY} (mM)	536

A 167-fold scale-up of the one-pot synthesis of ABT was performed, from 300 µL parallel micro reactors (Section 2.8.1) to a 50 mL working volume laboratory stirred bioreactor (Section 2.8.2) in a similar way as Section 6.3.2.

The microscale bioconversion was performed using a shake flask biocatalyst (Section 2.4.2 and Figure 3.1), while for the preparative scale synthesis, a wild type TK and TAm biocatalyst was produced using the 7.5 L fermentor (Section 5.3.2). For both biocatalysts, the TK and TAm expression represented on average 39 and 6.5% of the protein when analyzed by SDS PAGE (Section 2.9.5), which were in agreement with the enzyme expression of the biocatalysts summarized in Table 5.1 with the TK D469E.

Due to the higher susceptibility of ERY and ABT to be consumed by whole cell side reactions compared to PKD and APD (Ingram et al., 2007), 25% less biomass concentration was used in the ABT bioconversion in comparison with the synthesis

of APD performed in Section 6.3.2. Therefore the concentration of TK and TAm were 0.06 and 0.3 mg mL^{-1} for both bioconversion scales.

The starting concentration of substrates GA and HPA was 30 mM. Equation 6.3 predicted that after 250 min, the TK bioconversion would reach completion. After this time, MBA was added to a final concentration of 10 mM the same was as in Section 6.3.2. An excess of ERY to MBA 3:1 was maintained in the bioconversion due to the lower TAm Michaelis constant of ERY compared to MBA (Table 4.2). This was done with the aim to speed up the one-pot synthesis and avoid enzyme deactivation by MBA, as well as ABT and ERY degradation by the whole cells.

Figure 6.4 shows the complete experimental progress curve of the micro and preparative scale bioconversions. Combining equations 6.3 and 4.1 with their respective parameters (Table 6.4 and 4.2), the complete modelling of the one-pot synthesis of ABT was also performed and shown in Figure 6.4.

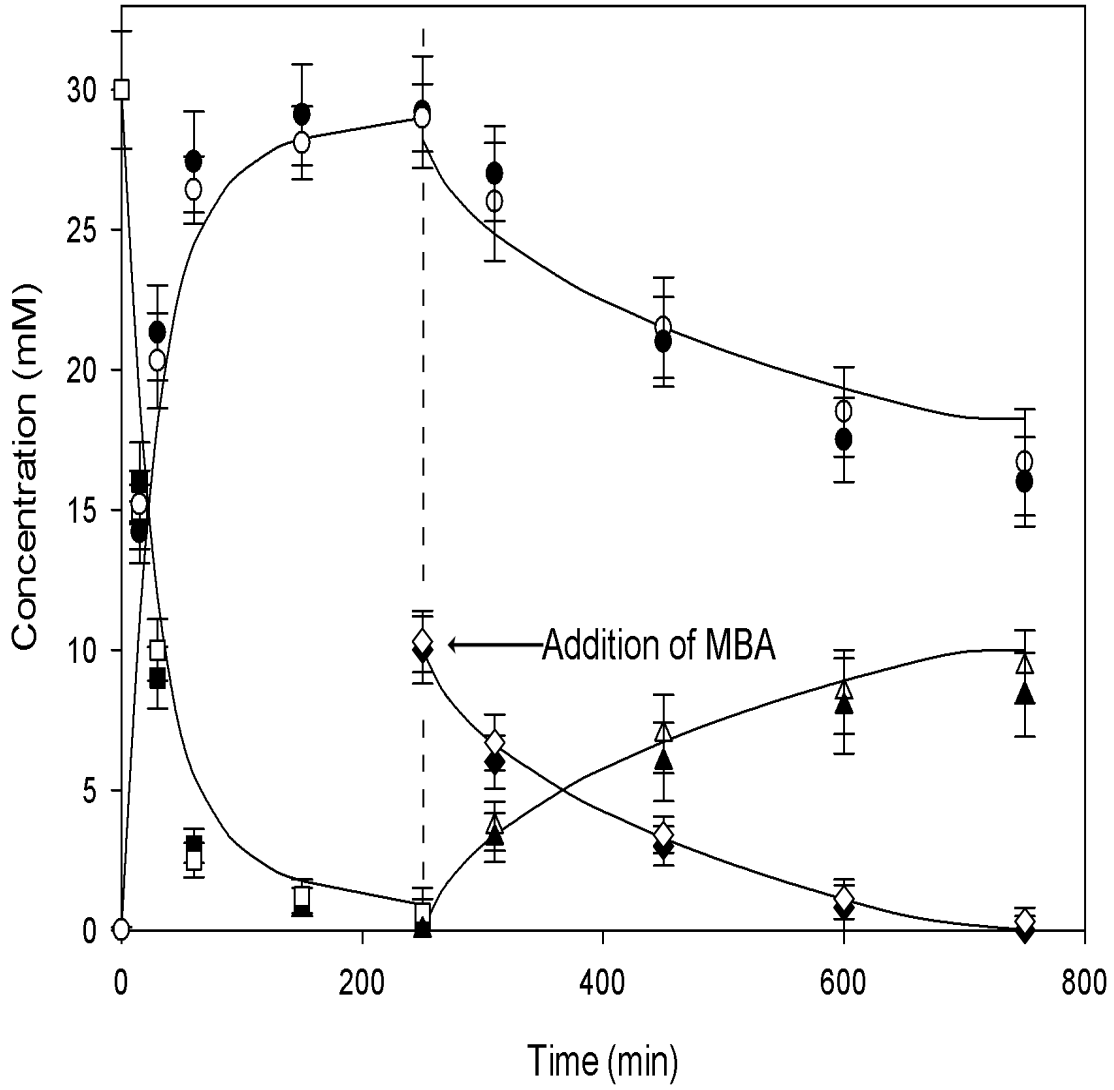

Figure 6.4. **Scale-up and modelling of the whole cell one-pot synthesis of ABT following: (□) HPA, (○) ERY and (Δ) ABT using microscale instrumentation (Section 2.8.1), and (■) HPA, (●) ERY and (▲) ABT for the preparative scale synthesis (Section 2.8.2). Reaction conditions: 30 mM [HPA] and [PA], 0.2 mM [PLP], 2.4 mM [TTP], 9 mM [Mg^{2+}], 30 ^{o}C, pH 7.5 in 200 mM HEPES. 10 mM [MBA] were added after 250 min. [TK] and [TAm] was 0.05 and 0.3 mg mL^{-1} for both whole cell biocatalysts. The modelling was performed combining Equations 4.1 and 6.3 with the corresponding kinetic parameters from Table 4.2 and 6.5 and is shown as solid lines. Error bars represent one standard deviation about the mean (n=3).**

The results from the micro reactors scaled excellently as shown in Figure 6.4, resulting in very similar progress curves between the two scales. The maximum experimental difference for the synthesis of ABT between the two scales was found to be 11%, which was not statistically significant. This demonstrates the microscale experimentation was predictive of the preparative scale multi-step bioconversion of ABT. The kinetic results from the different scales and the model are summarized in Table 6.6.

Table 6.6. Experimental and predicted apparent kinetic results of the one-pot synthesis of ABT shown in Figure 6.4 using microscale experimentation (2.8.1) and a preparative scale bioreactor (Section 2.8.2). The predicted data was obtained using Equations 4.1 and 6.3 with the kinetic parameters from Table 4.2 and 6.5 respectively. The calculation of the kinetic experimental results was performed as described in Section 2.8.1.

Apparent kinetic parameter	Predicted data	Microscale	Preparative scale
Wild type TK initial specific activity (μmol min^{-1} mg^{-1})	1.5	2.0 ± 0.17	1.9 ± 0.22
CV2025 TAm initial specific activity (μmol min^{-1} mg^{-1})	0.19	0.21 ± 0.02	0.18 ± 0.02
Final ABT conversion (% mol/mol)	99	94 ± 9	84 ± 11

A difference of 25% between the TK experimental and predicted specific activity was found (Table 6.6). This was probably due because the TK kinetic model was established at 25^{o}C and pH 7.0 (Chen et al., 2009), instead of 30^{o}C and pH 7.5 which were used for the one-pot synthesis shown in Figure 6.4. The difference was considered acceptable, and good agreement could be concluded between the predicted and experimental data (Figure 6.4), validating the microscale mathematical models for preparative scale multi-step syntheses.

Similar to the one-pot synthesis of APD in Section 6.3.2, the ABT yield (% mol/mol) of the preparative conversion was 10 and 15% smaller than the microscale and predicted model respectively (Table 6.6). Also some consumption of ERY by the whole cell was observed in both scales (Figure 6.4). Nevertheless, by using an excess of 3:1 ERY:MBA, the reaction time to reach completion was reduced by 3 folds compared to an equimolar concentration of 10 mM (Equation 6.3 and Table 6.5). The reduction in time allowed less consumption of ABT and ERY by the whole cells, as well as less inactivation of TAm by MBA. This shows how using the mathematical models, it was possible to design the one-pot synthesis of ABT with 25% less biocatalyst while reaching completion in 3-folds less time than the synthesis of APD (Figure 6.3 and 6.4). This was done in order to minimize the consumption of ERY and ABT by the whole cells.

6.3.4. Selection of the best reactor configuration

6.3.4.1. One-pot synthesis of ABT with fed-batch addition of MBA

After the kinetic models were validated for the preparative scale syntheses of the two different amino alcohols (Section 6.3.2 and 6.3.3), the microscale results could be used to select the best reactor configuration and operating conditions (Sin et al., 2009).

As discussed in Sections 4.4.3.7, MBA was found to be inhibitory to TAm in concentrations above 10 mM, in contrast ERY and PKD did not affect the enzyme stability (Figure 4.6). This limited the yield of the TAm bioconversion in equimolar concentrations above 10 mM as was shown in Figure 3.9. A solution to avoid MBA toxicity was to use a continuous fed-batch addition of the amino-donor. The Michaelis Menten constant of ERY was found to be 97 mM in comparison with the one of MBA of 0.5 mM (Table 4.2). These values predicted that the production rate

of ABT would not be severely affected by maintaining a MBA concentration below 10 mM in the reaction.

Therefore a one-pot synthesis of ABT was performed in preparative scale with fed-batch addition of MBA. The initial volume of the bioconversion was 50 mL, and the pH and temperature were controlled at 7.5 and 30°C the same way as in Section 6.3.1. The initial concentration of HPA and GA was 100 mM, and the concentration of TK and TAm were 0.75 mg mL^{-1} and 0.14 mg mL^{-1} using a whole cell biocatalyst produced in the 7.5 L fermentor (Section 5.3.2).

To model the one-pot synthesis with fed-batch addition of MBA, the TK Equation 6.3 was combined with the following differential equations to model the TAm step:

$$\frac{d[MBA]}{dt} = -R_{MBA} + \frac{FeedRate \times MBAFeed}{Vol} - \frac{[MBA] \times FeedRate}{Vol} \quad \text{Equation 6.4}$$

$$\frac{d[ERY]}{dt} = -R_{ERY} - \frac{[ERY] \times FeedRate}{Vol} \quad \text{Equation 6.5}$$

$$\frac{d[ABT]}{dt} = R_{ABT} - \frac{[ABT] \times FeedRate}{Vol} \quad \text{Equation 6.6}$$

$$\frac{dVol}{dt} = FeedRate \quad \text{Equation 6.7}$$

where R_i (mM min^{-1}) is the kinetic reaction rate of each compound defined by equation 4.2, FeedRate (L min^{-1}) is the rate of MBA solution, MBAFeed (mM) is the concentration of MBA in the feed and Vol (L) is the working reaction volume.
Equation 6.3 predicted that under the previously mentioned conditions, the TK reaction would reach completion after 180 min, at this time MBA was fed continuously using a 300 mM solution (Section 2.8.2).

A varied flow rate of the MBA solution that would match the predicted rate of the consumption of the amino donor by Equation 4.2 would have been desirable (Sayar et al., 2009). Nevertheless, such a programmable pump was not available when this work was performed.

Therefore several simulations were performed using equations 6.4, 6.5, 6.6 and 6.7 to identify an appropriate constant flow rate, which would maximize the reaction rate while maintaining a low concentration of MBA below 10 mM for the maximum possible time. The selected flow rate was found to be 0.31 mL hr^{-1}, which combined with a calculated duration of the fed-batch operation of 53 hr, meant that a total of 5 mmol of MBA would be added to the reaction. This amount of MBA was equivalent to the total number of mmol of ERY that were predicted to be produced by the TK using a solution 100 mM of GA and HPA with an initial working volume of 50 mL. Hence the initial concentration of substrates was 10 folds higher than the concentration used in the previous one-pot synthesis represented in Figures 6.3 and 6.4.

Figure 6.5 shows the experimental progress curves and the predicted data for the amount of each compound (mmol) for the one-pot synthesis of ABT. In order to compare the performance of the different addition modes of MBA, another one-pot synthesis using a single shot addition of 5 mmol of pure MBA (carefully added to allow the system to adjust pH) after 180 min was also performed. The results of this multi-step bioconversion are also shown in Figure 6.5, including its corresponding modelling with Equations 4.1 and 6.3 and the parameters from Table 4.2 and 6.5.

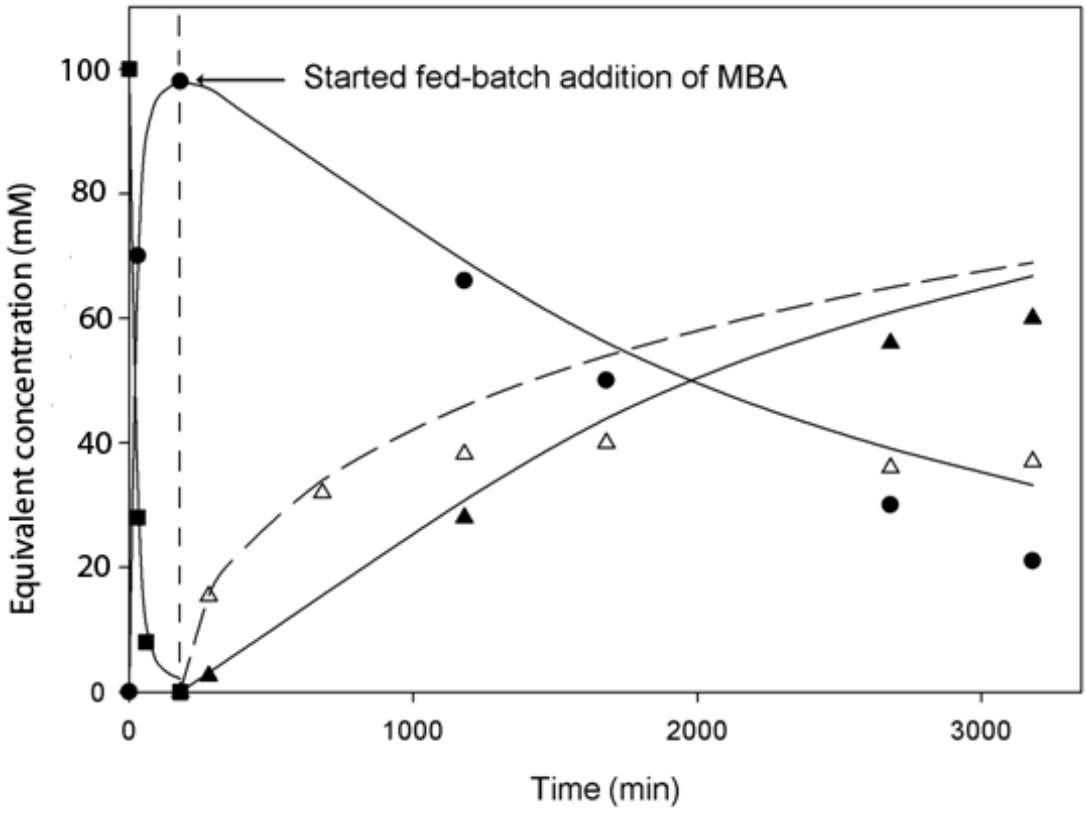

Figure 6.5. **Typical progress curves and modelling of the TK-TAm sequential one-pot synthesis of ABT with continuous fed-batch addition of MBA following the equivalent concentration (reference volume of 50 ml) of: (■) HPA, (●) ERY and (▲) ABT, and with a single shot addition of MBA following (Δ) ABT. The bioconversions were performed using preparative scale experimentation described in Section 2.8.2. Initial reaction conditions : 50 mL working volume, 100 mM [HPA] and [GA], 0.2 mM [PLP], 2.4 mM [TTP], 9 mM [Mg^{2+}], 30 ^{o}C, pH 7.5, 25 mM HEPES. After 180 min, a solution of 300 mM [MBA] was added with a constant flow rate of 0.31 mL hr^{-1} for the fed-batch addition or 5 mmol of pure MBA were added for the single shot addition of the amino donor. [TK] and [TAm] were 0.14 and 0.75 mg ml^{-1} respectively using a whole cell biocatalyst produced in the 7.5 L fermentor (Section 5.3.2). The modelling of the fed-batch bioconversion was performed combining Equations 6.3, 6.4, 6.5, 6.6 6.7 and 4.1 with the corresponding kinetic parameters from Tables 6.5 and 4.2 and is represented by a solid line. The modelling of the TAm step with a single shot addition was performed combining Equations 4.2 and 6.3 with the kinetic parameters from Table 6.5 and 4.2 and is represented by a dashed line.**

Reasonable agreement was again found between the experimental and predicted data for the synthesis with fed-batch addition of MBA shown in Figure 6.5. After 2000 min, the consumption rate of MBA by TAm was overcome by the feed rate of MBA, therefore accumulation of the amino donor above 10 mM started to occur (data not shown). This probably caused deactivation of the enzyme and no further conversion was obtained after 3200 min.

In the multi-step synthesis with a single shot addition of MBA, as Equation 6.3 predicted, the rate of ABT synthesis was initially faster than for the fed-batch bioconversion, resulting in higher ABT yields for the first 1000 min of reaction. Nevertheless, it appears TAm was totally inactivated after 1000 min by the higher concentration of MBA in comparison with the fed-batch bioconversion, and no further production of ABT was quantified after that time. The result was a final conversion yield of 62 % mol/mol for the bioconversion with fed-batch addition, which was 40% higher than the corresponding yield using the one shot addition of MBA.

6.3.4.2. One-pot synthesis of APD with fed-batch addition of IPA

The selection of IPA as amino donor instead of MBA could attenuate the problems of accumulation and toxicity of MBA in the previous fed-batch multi-step synthesis (Section 6.3.4.1). IPA showed great potential in the microscale one-pot synthesis of APD using low concentration of substrates (Figure 3.11). In addition, any excess of IPA could potentially evaporate if the bioreactor was not sealed due to its high volatility (Smith et al., 2010).

A one-pot synthesis of APD was performed with fed-batch addition of IPA in a 50 mL preparative scale bioreactor (Section 2.8.1). The reaction conditions were the same as the multi-step bioconversion performed in Section 6.3.4.1, except that the initial concentration of PA and HPA were 200 mM (20 folds higher than the

concentrations used in the microscale synthesis shown in Figure 3.11 and 6.3). The concentration of TK D469E and the CV2025 TAm were 0.75 and 0.14 mg mL^{-1} using a whole cell biocatalyst produced as described in Section 5.3.2. Using Equation 6.1 and the kinetic parameters from Table 6.1, it was predicted that the TK reaction would reach completion after 10 hr. At that time, a solution of IPA 500 mM was fed continuously to the bioreactor with a flow rate of 0.42 mL hr^{-1} during 48 hr, so that a total amount of 10 mmol of IPA would be added to the vessel, which was equivalent to the total amount of mmol of PKD that were predicted to be produced by the TK reaction.

Figure 6.6 shows the experimental progress curves of the amount of each compound (mmol), as well as the predicted data of the TK step of the preparative scale one-pot synthesis of APD using fed-batch addition of IPA. Perfect agreement was found between the TK experimental and predicted data by Equation 6.1, which validated the TK model for concentrations as high as 200 mM in a preparative scale synthesis.

The TAm bioconversion did not seem to be inhibited by any accumulation of IPA during the 3000 min that the amino donor was fed, suggesting that any excess of IPA was successfully evaporated.

A total volume of IPA solution of 20 mL was added to the bioreactor, leading to a final APD yield of 70% mol/mol. This yield was 3.5 folds higher than the yield obtained under similar batch reaction conditions for a single TAm step bioconversion (Appendix XI). This suggested that IPA could be causing strong inhibition or be toxic to TAm in high concentrations.

Using the selected reaction conditions and reactor configuration, the one-pot synthesis allowed a 6 fold greater yield (% mol/mol) using concentrations 1 order of magnitude higher than a previous 2 step preparative scale batch synthesis of APD (Smith et al., 2010).

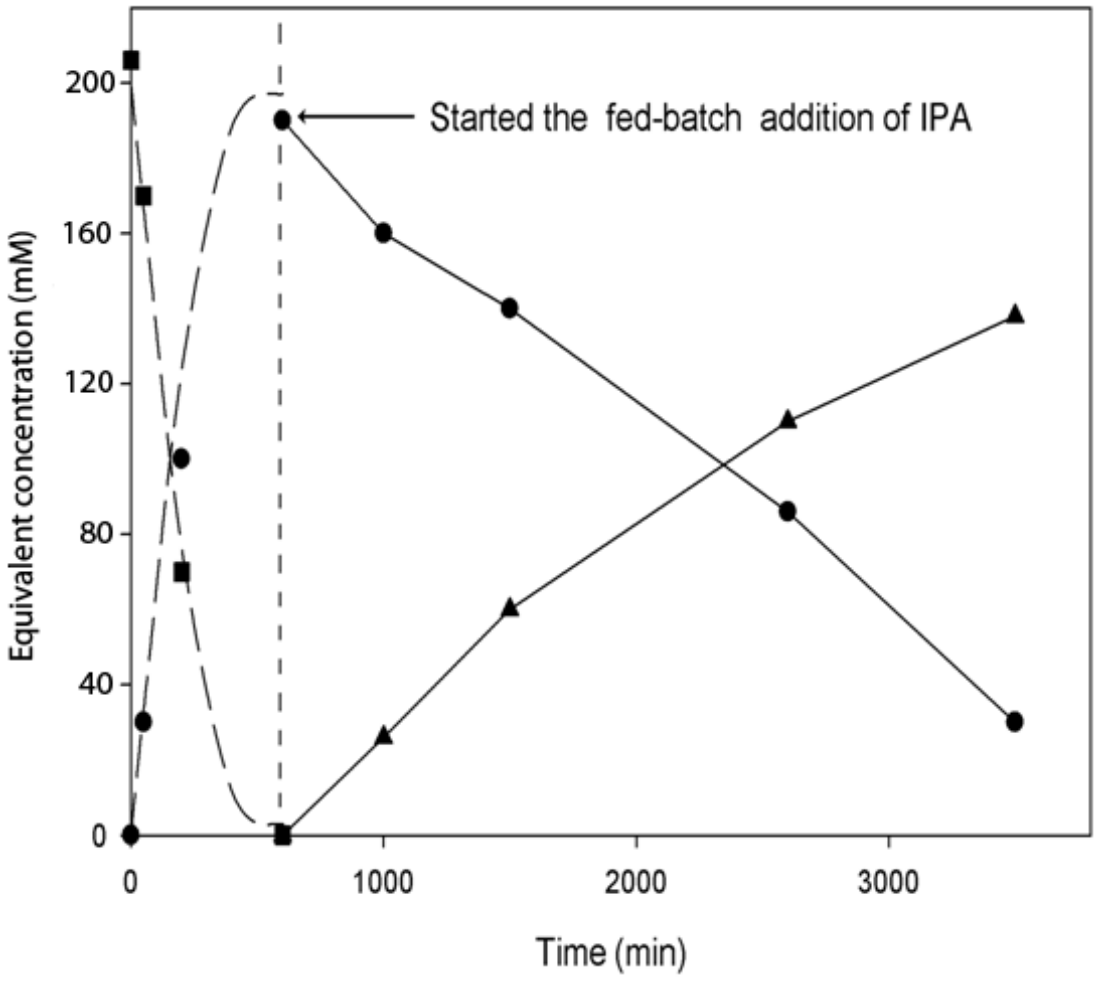

Figure 6.6. **Typical progress curves and modelling of the TK-TAm sequential one-pot synthesis of APD with continuous fed-batch addition of IPA following the equivalent concentration (reference volume of 50 ml) of: (■) HPA, (●) PKD and (▲) APD. The bioconversion was performed using preparative scale experimentation described in Section 2.8.2. Initial reaction conditions: 50 mL working volume, 200 mM [HPA] and [PA], 0.2 mM [PLP], 2.4 mM [TTP], 9 mM [Mg^{2+}], 30 ^{o}C, pH 7.5, 25 mM HEPES. After 600 min, a solution of 500 mM [IPA] was added with a constant flow rate of 0.42 mL hr^{-1}. [TK] and [TAm] were 0.75 and 0.14 mg mL^{-1} respectively using a whole cell biocatalyst produced in the 7.5 L fermentor (Section 5.3.2). The modelling of the TK step was performed using Equation 6.1 with the corresponding kinetic parameters from Table 6.1 and was represented by a dashed line.**

6.4. SUMMARY

In summary, an overall scale-up of 167-fold for the one-pot syntheses of both APD and ABT was performed. The results obtained showed excellent agreement between those obtained at the micro and preparative scales (Figure 6.3 and 6.4).

In order to simulate the multi-step synthesis, the kinetic models for the TK D469E and CV2025 TAm mediated synthesis of PKD and APD were established (Figure 6.1 and 6.2 and Equations 6.1 and 6.2) building on the methodology developed in Chapter 4.

Generation of the relevant kinetic constants enabled modelling for the one-pot bioconversion of both APD and ABT, showing that the methodology could be applied to different bioconversion of substrates and products. In both cases there was excellent agreement between the predicted and experimental data, validating the microscale kinetic models to simulate preparative scale syntheses (Figure 6.3 and 6.4).

Finally, the best bioconversion conditions and reactor configurations have been identified based on the mathematical models generated using microscale experimental data. These led to identification of a reactor with fed-batch addition of the amino donor to be the optimum operating strategy in each case. Under optimal conditions, the one-pot syntheses allowed up to a 6-fold increase in product yield (% mol/mol) (Figure 6.5 and 6.6), using concentrations 1 order of magnitude higher than published preparative scale data (Smith et al., 2010).

The final chapter of this thesis will attempt to put this work in the wider context of industrial bioconversion process design and identify areas where further work is required or improvements can be made.

7. CONCLUSIONS AND FUTURE WORK

7.1. OVERALL CONCLUSIONS

In this study, the design and characterization of *de novo* engineered pathways in a whole cell *E. coli* biocatalyst for multi-step enzymatic syntheses of chiral amino alcohols was achieved. This was facilitated by developing a microscale high-throughput "toolbox", which enabled the efficient evaluation and "mix and match" of the best enzyme candidates, as well as the simulation of the one-pot synthesis to speed-up process development. The toolbox approach was demonstrated for the synthesis of amino alcohols APD (Figure 3.11) and ABT (Figure 3.12), where the best enzyme pairs were found to be the *E. coli* TK mutant D469E and wild type TK combined with the CV2025 TAm respectively using a whole cell biocatalyst.

For this approach to work best the need for early characterization of the kinetics of the individual enzymes in the *de novo* engineered pathway is highlighted. This is necessary in order to rapidly identify the overall bioconversion bottleneck (Figures 3.7 and 3.8). This kinetic data is crucial for early establishment of optimum reaction conditions for the one-pot synthesis which in general needs to favour the rate limiting step of the overall bioconversion.

It was also found that special attention must be taken for the early detection of side reactions that could occur between the different bioconversion steps. A sequential feeding of substrates may be needed to avoid side reactions, as was demonstrated for the case of the amino donor MBA in the one-pot synthesis of ABT (Figure 3.10). Expanding the size of the TK and TAm libraries, by further engineering the enzymes to limit its selectivity towards inappropriate substrates or intermediates, would increase the productivities of the one-pot synthesis strategy.

In principle the microscale toolbox approach could be used to rapidly evaluate any set of enzyme pairs and substrates, which could conceptually be integrated in a multi-step synthesis. It enables the early generation of crucial bioprocess and kinetic data for the effective design of complex bioconversion processes.

For the particular *de novo* engineered pathways studied here, of particular relevance was the early identification and optimization of the critical step of the multi-enzymatic synthesis, which was found to be that catalyzed by TAm (Section 3.3.4). To help optimize this step, a methodology to rapidly establish the full kinetic model and its parameters was developed and integrated in the microscale toolbox.

The creation of a standardized methodology allowed the establishment of the kinetic parameters as a rapid routine procedure, easily applied to all the different enzymes of the *de novo* pathway, requiring less time and resources. It also contributed to a higher transparency of the kinetic parameters identification, facilitating the comparison of the different models.

The key limiting TAm kinetic parameters were found to be the high Michaelis- Menten constant and the low catalytic constant for ABT and APD synthesis respectively (Table 4.2 and 6.2). Also, the high toxicity of the amino donor towards the enzyme was found to limit the final yields of the bioconversion (Section 4.2.4 and 4.3). While saving time and resources through the use of simulations, the early discovery of those bottlenecks was crucial to determine the best reaction conditions and reactor configurations (Section 6.3.4). This kinetic information will also be useful to inform protein engineering strategies to further unlock the potential of the TAm bioconversion.

The modelling results were decisive in the rational design of the whole cell *E. coli* biocatalyst; informing the desired level of expression of each enzyme to match the sequential reaction kinetics. The effect of temperature and induction time was found to be crucial for the relative level of expression of both enzymes. This allowed the scale-up of the production of the *E. coli* biocatalyst to pilot scale obtaining maximum concentrations of TK and TAm, while maintaining a desired TAm/TK ratio of 5 (Figure

5.4 and 5.6a). The capacity to control the relative expression of each enzyme will be critical to harvest the full synthetic potential of *de novo* pathways at industrial scale, increasing productivities and allowing them to be flexible in order to adapt for new substrates and products.

Excellent agreement was found between the kinetic performance of the biocatalysts produced at laboratory and small pilot scale (Figure 5.7 and 5.8), confirming that the integrity of the cells and the stability of the enzymes were maintained during the scale-up process. Further scale-up studies to identify the key issues related with the biocatalyst production will be essential for the efficient bioprocess development to manufacturing scale.

Finally the microscale one-pot syntheses of amino alcohols were modelled and scaled-up 167-fold to a preparative scale. Again, excellent agreement was found between the experimental data at both scales and the predicted data for the one-pot synthesis of ABT (Figure 6.3) and APD (Figure 6.4). Appropriate mixing in the preparative scale synthesis, combined with constant pH and solvent evaporation control in the microscale bioreactors were found to be critical to guarantee successful process scale-up (Section 6.3.2). The main deviations of the experimental data and the model were attributed to TAm instability in the presence of the amino donor (Section 4.3.3.7 and Figure 6.5). In order to predict accurately longer multi-step bioconversions with high concentration of amino donor, the toxic effect of the substrate towards TAm should be taken into account in the mathematical models.

Overall the best reaction conditions and reactor configurations were determined using the microscale models, which resulted in using an excess of the amino acceptor ERY due to its low Michaelis constant (Section 6.3.3), as well as applying a controlled fed batch addition of the amino donor to avoid its toxicity toward the enzyme (Section 6.3.4). Under these optimized conditions, the one-pot syntheses allowed up to a 6-fold increase in yield (% mol/mol) (Figure 6.5 and 6.6), using concentrations 1 order of magnitude higher than previously published preparative scale data (Smith et al., 2010).

We estimate that by applying this microscale systematic approach to design and characterize *de novo* engineered pathways, the industry could make savings of 100 to 1000 times in resources and duration required compared to traditional laboratory scale non systematic methods.

In order to further optimize a multi-step synthesis, the modelling should be combined with an economical analysis. This would allow establishing priorities, and help deciding between increasing the reaction rate at the expense of using an excess of one substrate as was done in this work (Figure 6.4).

The interest of industry towards biocatalysis has been growing not only in the pharmaceutical sector, but also in the production of chemicals and bulk products. The majority of the biocatalytic industrial scale processes nowadays are performed with single enzyme bioconversions due to its simplicity and high productivities. However, it is expected that the biocatalysis of the future will integrate new complexities and configurations such as *in vivo de novo* multi-step enzymatic systems. The methodologies described in this thesis go some way toward helping better characterize and speed up the development of such systems which are generally considered to be difficult to assemble, characterize, and to operate productively at scale.

7.2. FUTURE WORK

The work in this thesis has demonstrated the applicability of microscale tools to design, characterize and optimize *in vivo* multi-step enzymatic syntheses. Future work is required to expand the microscale tools towards downstream and upstream processes. Also further studies need to be done to enable better integration of these microscale approaches with advances in protein engineering, data driven modelling, high-throughput analytical technique and synthetic biology among others. A detailed list of future work recommendations is shown below:

- Future studies are required in the integration of the results of the microscale kinetics models, with the expansion of the TK and TAm libraries by protein engineering. This would result in the development of enzymes variants, with superior catalytic characteristics and improved selectivity, avoiding side reactions between the different bioconversion steps.

- Taking advantage of the expansion of the TK and TAm library, further studies with new substrates, especially with aromatic TK products, which have been shown to be good substrates for ω-TAm, should be performed to produce a new set of high value amino alcohols (Hailes et al., 2009).

- Future studies to expand the microscale toolbox towards the fermentation and biocatalyst manipulation prior to bioconversion, as well as the analytical analysis and downstream processing of the chiral compounds are necessary. In addition modelling of those new operation units would enable the complete simulation of the bioprocess, making the microscale toolbox a very powerful agent for the efficient process development.

- Future automation studies of the microscale toolbox, including the previously mentioned expanded areas, would allow taking advantage of the full potential of the high-throughput nature of the tools.

- In order to take the full advantage of the determined kinetic parameters in Chapter 4, future work is required to apply a systematic statistical methodology to determine the optimum reaction conditions through simulations of the kinetic model .

- As was discussed in Section 4.3.7 and 6.3.4.1, the toxicity of the amino donor, as well as consumption of the substrates and products by whole cell side reactions were found to affect the quality of the modelling. Therefore new studies should be performed to include those effects in the mathematical equations to increase the accuracy of the predictions to a broader range of conditions.

- IPA showed a great potential as an amino donor for the synthesis of amino alcohols (Figure 3.11, 3.12 and 6.6). Further studies to establish its kinetic parameters are necessary. This would allow having more information to optimize the one-pot synthesis of amino alcohols, like designing gradient fed-batch additions of IPA, which would match the consumption of the amino donor by the enzyme as described in Section 6.3.3.

- As discussed in Section 4.4.3.6 the kinetic methodology to obtain the kinetic parameters could be further simplified, eliminating the experimentally difficult step of gathering reverse reaction data, which was shown to have a low impact in the modelling. Genetic algorithms could be a robust tool to assist the establishment of the data driven models.

- The level of TK and TAm expression could be controlled by manipulating the fermentation temperature and induction time of the TAm (Figure 5.3). In order to have a more accurate control of the co-expression, the TK could also be induced instead of being constitutively expressed (Section 2.3.1). Therefore future studies using different compatible methods of induction between the different enzymes are required.

- The final biomass concentration of whole cells containing the *de novo* pathway in this work was 8.5 g_{DCW} L^{-1} (Figure 5.4). Further studies need to be performed in order to increase the final biomass concentration using fed-batch fermentation methods and various feeding strategies.

- The key parameters affecting the scale up of the multi-step bioconversion to preparative scale were established in Section 6.3.2 and 6.3.3. Future studies are necessary to identify the crucial parameters that may affect the performance of the one-pot syntheses at larger pilot plant scale.

- As was found in Section 3.3.6, the whole cell biocatalyst was selected because it improved the stability of TAm. Further studies should be performed in immobilization techniques, which can also improve the stability of the enzyme, while adding the benefit of allowing the enzyme to be recycled and used in a continuous flow bioprocess.

- Studies including economical and environmental factors and constraints should be included in the modelling of the process. This would allow the determination of real optimum conditions that would be required in the manufacturing scale.

8. REFERENCES

Barrett T. A., A. Wu, H. Zhang, M. S. Levy, and G. J. Lye. 2010. Microwell engineering characterization for mammalian cell culture process development. Biotechnology and Bioengineering. **105**:260-75.

Bernard A., and M. Payton. 2001. Fermentation and growth of *Escherichia coli* for optimal protein production. Current Protocols in Protein Science. Ed. Coligan J.E. New York USA.

Bhaskar G. 2004. A short stereoselective synthesis of)(-chloramphenicol and (+)-thiamphenicol. Tetrahedron: Asymmetry. **15**:1279-1283.

Boruwa J., J. C. Borah, S. Gogoi, and N. C. Barua. 2005. A short asymmetric total synthesis of chloramphenicol using a selectively protected 1,2-diol. Tetrahedron Letters. **46**:1743-1746.

Bradford M. M. 1976. A rapid and sensitive method for the quantitation of microgram quantities of protein utilizing the principle of protein-dye binding. Analytical Biochemistry. **72**:248-54.

Brazeau B. J., S. J. Gort, H. J. Jessen, A. J. Andrew, and H. H. Liao. 2006. Enzymatic activation of lysine 2,3-aminomutase from *Porphyromonas gingivalis*. Applied and Environmental Microbiology. **72**:6402-4.

Breuer M., K. Ditrich, T. Habicher, B. Hauer, M. Kesseler, R. Stürmer, and T. Zelinski. 2004. Industrial methods for the production of optically active intermediates. Angewandte Chemie International Edition. **43**:788-824.

Bruggink A., R. Schoevaart, and T. Kieboom. 2003. Concepts of nature in organic synthesis: cascade catalysis and multistep conversions in concert. Organic Process Research & Development. **7**:622–640.

Brunhuber N. M., and J. S. Blanchard. 1994. The biochemistry and enzymology of amino acid dehydrogenases. Critical Reviews in Biochemistry and Molecular Biology. **29**:415-467.

Bulos B., and P. Handler. 1965. Kinetics of beef heart glutamic-alanine transaminase. Journal of Biological Chemistry. **240**:3283.

Burkart M. D. 2003. Metabolic engineering-a genetic toolbox for small molecule organic synthesis. Organic & Biomolecular Chemistry. **1**:1-4.

Caligiuri A., P. D'Arrigo, T. Gefflaut, G. Molla, L. Pollegioni, E. Rosini, C. Rossi, and S. Servi. 2006. Multistep enzyme catalysed deracemisation of 2-naphthyl alanine. Biocatalysis and Biotransformation. **24**:409-413.

Carter O. A., R. J. Peters, and R. Croteau. 2003. Monoterpene biosynthesis pathway construction in *Escherichia coli*. Phytochemistry. **64**:425-433.

Chang T. M. S. 1988. Artificial Cells as Bioreactive Biomaterials. Journal of Biomaterials Applications. **3**:116-125.

Chen B.H., M. Micheletti, F. Baganz, J.M. Woodley, and G.J. Lye. 2009. An efficient approach to bioconversion kinetic model generation based on automated microscale experimentation integrated with model driven experimental design. Chemical Engineering Science. **64**:403-409.

Chen B. H., A. Sayar, U. Kaulmann, P. A. Dalby, J. M. Ward, and J. M. Woodley. 2006. Reaction modelling and simulation to assess the integrated use of transketolase and ω-transaminase for the synthesis of an aminotriol. Biocatalysis and Biotransformation. **24**:449-457.

Chen B. H., E. G. Hibbert, P. A. Dalby, and J. M. Woodley. 2008. A new approach to bioconversion reaction kinetic parameter identification. American Institure of Chemical Engineers Journal. **54**:2155–2163.

Chenault H. K., E. S. Simon, and G. M. Withesides. 1998. Cofactor regeneration for enzyme-catalysed synthesis. Biotechnology Genetic Engineering Reviews. 6:221:270.

Chi Y., S. T. Scroggins, and J. M. J. Fre. 2008. One-Pot Multi-Component Asymmetric Cascade Reactions Catalyzed by Soluble Star Polymers with Highly Branched Non-Interpenetrating Catalytic Cores. Journal of the American Chemical Society. **10**:6322-6323.

Chotani G., T. Dodge, A Hsu, M. Kumar, R. LaDuca, D. Trimbur, W. Weyler, and K. Sanford. 2000. The commercial production of chemicals using pathway engineering. Biochimica et Biophysica Acta. **1543**:434-455.

Chou I. C., and E. O. Voit. 2009. Recent developments in parameter estimation and structure identification of biochemical and genomic systems. Mathematical Biosciences. **219**:57-83.

Cázares A., J. L. Galman, L. G. Crago, M. E. B. Smith, J. Strafford, L. Ríos-Solís, G. J. Lye, P. A. Dalby, and H. C. Hailes. 2010. Non-alpha-hydroxylated aldehydes with evolved transketolase enzymes. Organic & Biomolecular Chemistry. **8**:1301-9.

Dalby P. A., F. Baganz, G. J. Lye, and J. M. Ward. 2009. Protein and pathway engineering in biocatalysis. Chimica Oggi. **27**:18-21.

Doig S. D., S. C. R. Pickering, G. J. Lye, and J. M. Woodley. 2002. The use of microscale processing technologies for quantification of biocatalytic Baeyer-Villiger oxidation kinetics. Biotechnology and bBoengineering. **80**:42-9.

Dowd J., and D.S. Riggs. 1965. A comparison of estimates of Michaelis-Menten kinetic constans from various linear methods. Journal of Biological Chemistry. **240**:863-869

Eisenthal B. R., and Crosnish-Bowden A. 1974. Direct Linear plot-new graphical procedure for estimating enzyme kinetics-parameters. Biochemical Journal **139**:715-720.

Ellis R. J., and D. D. Davies. 1961. Glutamic-oxaloacetic transaminase of cauliflower. 1. Purification and specificity. The Biochemical Journal. **78**:615-23.

Fernandes P. 2010. Miniaturization in biocatalysis. International Journal of Molecular Sciences. **11**:858-79.

Ferrer M., F. Martínez-Abarca, and P. N. Golyshin. 2005. Mining genomes and "metagenomes" for novel catalysts. Current Opinion in Biotechnology. **16**:588-93.

Findrik Z. 2009. Overview on Reactions with Multi-enzyme Systems. Chemical and Biochemical Enginering Quarterly. **23**:545-553.

Fotheringham I. G., N. Grinter, D. P. Pantaleone, R. F. Senkpeil, and P. P. Taylor. 1999. Engineering of a novel biochemical pathway for the biosynthesis of L-2-aminobutyric acid in *Escherichia coli K12*. Bioorganic and Medicinal Chemistry. **7**:2209-13.

Fuhrmann U., E. Bause, G. Legler, and H. Ploegh. 1984. Novel mannosidase inhibitor blocking conversion of high mannose to complex oligosaccharides. Nature. **307**:755-758.

Gernaey K. V., A. E. Lantz, P. Tufvesson, J. M. Woodley, and G. Sin. 2010. Application of mechanistic models to fermentation and biocatalysis for next-generation processes. Trends in Biotechnology. **28**:346-54.

Guérard C., V. Alphand, A. Archelas, C. Demuynck, L. Hecquet, R. Furstoss, and J. Bolte. 1999. Transketolase-Mediated Synthesis of 4-Deoxy-D-fructose 6-Phosphate by Epoxide Hydrolase-Catalysed Resolution of 1,1-Diethoxy-3,4-epoxybutane. European Journal of Organic Chemistry. 3:3399:3402

Gyamerah M., and A. J. Willetts. 1997. Kinetics of overexpressed transketolase from *Escherichia coli JM 107*/pQR 700. Enzyme and Microbial Technology. **20**:127–134.

Hailes HC., P.A. Dalby, and G.J. Lye. 2009. Biocatalytic approaches to ketodiols and aminodiols. Chimica Oggi. **27**:28-31.

Hailes H. C., P. A. Dalby, and J. M. Woodley. 2007. Integration of biocatalytic conversions into chemical syntheses. Chemical Technology. **1066**:1063-1066.

Hecke W. Van, A. Bhagwat, R. Ludwig, J. Dewulf, D. Haltrich, and H. Van Langenhove. 2009. Kinetic modeling of a bi-enzymatic system for efficient conversion of lactose to lactobionic acid. Biotechnology and Bioengineering. **102**:1475-82.

Hecquet L. 1996. Enzymatic synthesis of "natural-labeled" 6-deoxy-L-sorbose precursor of an important food flavor. Tetrahedron. **52**:8223-8232.

Hibbert E. G., F. Baganz, H. C. Hailes, J. M. Ward, G. J. Lye, J. M. Woodley, and P. A Dalby. 2005. Directed evolution of biocatalytic processes. Biomolecular Engineering. **22**:11-9.

Hibbert E. G., T. Senussi, S. J. Costelloe, W. Lei, M. E. B. Smith, J. M. Ward, H. C. Hailes, and P. A. Dalby. 2007. Directed evolution of transketolase activity on non-phosphorylated substrates. Journal of Biotechnology **131**:425-32.

Hibbert E. G., T. Senussi, M. E. B. Smith, S. J. Costelloe, J. M. Ward, H. C. Hailes, and P. A. Dalby. 2008. Directed evolution of transketolase substrate specificity towards an aliphatic aldehyde. Journal of Biotechnology **134**:240-5.

Hobbs G. R., R. K. Mitra, R. P. Chauhan, J. M. Woodley, and M. D. Lilly. 1996. Enzyme-catalyzed carbon-carbon bond formation: Large salce production of *Escherichia coli* transketolase. Journal of Biotechnology. **45**:173- 179.

Humphrey A. 1998. Shake Flask to Fermentor: What Have We Learned? Biochemical Progress. **14**:3-7.

Hussain H. A., and J. M. Ward. 2003. Enhanced Heterologous Expression of Two *Streptomyces griseolus* Cytochrome P450s and *Streptomyces coelicolor* Ferredoxin Reductase as Potentially Efficient Hydroxylation Catalysts. Applied Environmental Microbiology. **69**:373-382.

Hyun Y. L., and V. L. Davidson. 1995. Mechanistic studies of aromatic amine dehydrogenase, a tryptophan tryptophylquinone enzyme. Biochemistry. 34:816-823.

Ingram C. U., M. Bommer, M. E. B. Smith, P. A. Dalby, J. M. Ward, H. C. Hailes, and G. J. Lye. 2007. One-Pot Synthesis of Amino-Alcohols Using a De-Novo

Transketolase and β-Alanine: Pyruvate Transaminase Pathway in *Escherichia coli*. Biotechnology and Bioengineering. **96**:559-569.

Islam R. S., D. Tisi, M. S. Levy, and G. J. Lye. 2008. Scale-up of *Escherichia coli* growth and recombinant protein expression conditions from microwell to laboratory and pilot scale based on matched k_La. Biotechnology and Bioengineering. **99**:1128-39.

Iwasaki A, Y. Yamada, N. Kizaki, Y. Ikenaka, and J. Hasegawa. 2006. Microbial synthesis of chiral amines by (R)-specific transamination with *Arthrobacter sp*. KNK168. Applied Microbiology and Biotechnology. **69**:499-505.

Jiménez-González C., and J. M. Woodley. 2010. Bioprocesses: Modeling needs for process evaluation and sustainability assessment. Computers & Chemical Engineering. **34**:1009-1017.

John A. J. 1995. Pyridoxal phosphate-dependent enzymes. Biochemical Biophysical Acta. **1248**:81-96.

John G. T., and E. Heinzle. 2001. Quantitative Screening Method for Hydrolases in Microplates Using pH Indicators: Determination of Kinetic Parameters by Dynamic pH Monitoring. Biotechnology and Bioengineering. 7:621-627

Ju L., and G. G. Chase. 1992. Bioprocess Engineering Improved scale-up strategies of bioreactors. Bioprocess Engineering **8**:49-53.

Junker B. H. 2004. Scale-up methodologies for *Escherichia coli* and yeast fermentation processes. Journal of Bioscience and Bioengineering. **97**:347-64.

Kajiwara Y., P. J. Santander, C. A. Roessner, L. M. Pérez, and A. I. Scott. 2006. Genetically engineered synthesis and structural characterization of cobalt-precorrin 5A and -5B, two new intermediates on the anaerobic pathway to vitamin B12: definition of the roles of the CbiF and CbiG enzymes. Journal of the American Chemical Society. **128**:9971-8.

Kalaitzakis D., and I. Smonou. 2010. A two-step, one-pot enzymatic synthesis of 2-substituted 1,3-diols. The journal of Organic Chemistry. **75**:8658-61.

Kaldor S. W., V. J. Kalish, J. F. Davies, B. V. Shetty, J. E. Fritz, K. Appelt, J. a Burgess, K. M. Campanale, N. Y. Chirgadze, D. K. Clawson, B. a Dressman, S. D. Hatch, D. a Khalil, M. B. Kosa, P. P. Lubbehusen, M. a Muesing, a K. Patick, S. H. Reich, K. S. Su, and J. H. Tatlock. 1997. Viracept (nelfinavir mesylate, AG1343): a potent, orally bioavailable inhibitor of HIV-1 protease. Journal of Medicinal Chemistry. **40**:3979-85.

Katare S., A Bhan, J. Caruthers, W. Delgass, and V. Venkatasubramanian. 2004. A hybrid genetic algorithm for efficient parameter estimation of large kinetic models. Computers and Chemical Engineering. **28**:2569-2581.

Kaulmann U., K. Smithies, M.E.B. Smith, H.C. Hailes, and J.M. Ward. 2007. Substrate spectrum of ω-transaminase from *Chromobacterium violaceum* DSM30191 and its potential for biocatalysis. Enzyme and Microbial Technology. **41**:628-637.

Koszelewski D., D. Clay, D. Rozzell, and W. Kroutil. 2009. Deracemisation of α-Chiral Primary Amines by a One-Pot, Two-Step Cascade Reaction Catalysed by ω-Transaminases. European Journal of Organic Chemistry. **2009**:2289-2292.

Koszelewski D., M. Garitzer, D. Clay, B. Seisser, and W. Kroutil. 2010. Synthesis of Optically Active Amines Employing Recombinant ω-Transaminases in *E. coli* Cells. ChemCatChem. **2**:73-77.

Koszelewski D., K. Tauber, K. Faber, and W. Kroutil. 2010. omega-Transaminases for the synthesis of non-racemic alpha-chiral primary amines. Trends in Biotechnology. **28**:324-332.

Kwon S., and S. Ko. 2002. Synthesis of statine employing a general syn-amino alcohol building block. Tetrahedron Letters. **43**:639-641.

König S., a Schellenberger, H. Neef, and G. Schneider. 1994. Specificity of coenzyme binding in thiamin diphosphate-dependent enzymes. Crystal structures of yeast transketolase in complex with analogs of thiamin diphosphate. The Journal of Biological Chemistry. **269**:10879-82.

Lineweaver H., and D. **Burk**. 1934. The Determination of enzyme dissociation constants. Journal of American Chemistry Society. **56**:658:666.

Law H. E. M., D. J. Lewis, I. McRobbie, and J. M. Woodley. 2008. Model visualization for evaluation of biocatalytic processes. Food and Bioproducts Processing. **86**:96-103.

Lee K. H., J. H. Park, T. Y. Kim, H. U. Kim, and S. Y. Lee. 2007. Systems metabolic engineering of *Escherichia coli* for L-threonine production. Molecular Systems Biology. **3**:149.

Lee S. Y. 1996. High cell-density culture of Escherichia coli. Trends in Biotechnology. **14**:98-105.

Lee S. K., H. Chou, T. S. Ham, T. S. Lee, and J. D. Keasling. 2008. Metabolic engineering of microorganisms for biofuels production: from bugs to synthetic biology to fuels. Current Opinion in Biotechnology. **19**:556-63.

Li C., L. G. Cao, Y. L. Wang, and E. F. Baril. 1993. Further purification and characterization of a multienzyme complex for DNA synthesis in human cells. Journal of Cellular Biochemistry. **53**:405-19.

Li R., and C. A. Townsend. 2006. Rational strain improvement for enhanced clavulanic acid production by genetic engineering of the glycolytic pathway in *Streptomyces clavuligerus*. Metabolic Engineering. **8**:240-52.

Lombardo M. E., L. S. Araujo, A. A. Juknat, and A. M. Batlle. 1989. Glutamate:4,5-dioxovaleric acid transaminase from *Euglena gracilis*. Kinetic studies. European Journal of Biochemistry. **182**:657-60.

Lye G. J., P. Ayazi-shamlou, F. Baganz, P. A. Dalby, and J. M. Woodley. 2003. Accelerated design of bioconversion processes using automated microscale processing techniques. Trends in Biotechnology. **21**:29-37.

Lye G. J., P. A. Dalby, and J. M. Woodley. 2002. Better Biocatalytic Processes Faster: New Tools for the Implementation of Biocatalysis in Organic Synthesis. Organic Process Research & Development. **6**:434-440.

Macauley-Patrick S., M. L. Fazenda, B. McNeil, and L. M. Harvey. 2005. Heterologous protein production using the *Pichia pastoris* expression system. Yeast. **22**:249-70.

Marco A. D, and V. D. Marco. 2004. Bacteria co-transformed with recombinant proteins and chaperones cloned in independent plasmids are suitable for expression tuning. Journal of Biotechnology. **109**:45-52.

Markowski C. A, E. P. Markowski. 1990. Conditions for the Effectiveness of a Preliminary Test of Variance". The American Statistician **44**: 322–326.

Marques M. P. C., S. Magalhães, J. M. S. Cabral, and P. Fernandes. 2009. Characterization of 24-well microtiter plate reactors for a complex multistep bioconversion: from sitosterol to androstenedione. Journal of Biotechnology. **141**:174-80.

Martin C. H., D. R. Nielsen, K. V. Solomon, and K. L. J. Prather. (2009. Synthetic metabolism: engineering biology at the protein and pathway scales. Chemistry & Biology. **16**:277-86.

Martinez-Torres R. J., J. Aucamp, R. George, and P. Dalby. 2007. Structural stability of *E. coli* transketolase to urea denaturation. Enzyme and Microbial Technology. **41**:653-662.

Matosevic S., M. Micheletti, J. M. Woodley, G. J. Lye, and F. Baganz. 2008. Quantification of kinetics for enzyme-catalysed reactions: implications for diffusional limitations at the 10 ml scale. Biotechnology Letters. **30**:995-1000.

Matosevic S. 2009. Design and characterisation of a prototype immobilised enzyme microreactor for the quantification of multi- step enzyme kinetics. PhD Thesis. University College London.

Matosevic S., N. Szita, and F. Baganz. 2011. Fundamentals and applications of immobilized microfluidic enzymatic reactors. Journal of Chemical Technology and Biotechnology. **86**:325-334.

McArthur G. H., and S. S. Fong. 2010. Toward engineering synthetic microbial metabolism. Journal of biomedicine & biotechnology. Corporation **2010**:459760.

Mehta P. K., and P. Christen. 1994. Homology of 1-aminocyclopropane-1-carboxylate synthase, 8-amino-7-oxononanoate synthase, 2-amino-6-caprolactam racemase, 2,2-dialkylglycine decarboxylase, glutamate-1-semialdehyde 2,1-aminomutase and isopenicillin-N-epimerase with aminotransferases. Biochemical and Biophysical Research Communications. **198**:138-143

Mehta P. K., T. I. Hale, and P. Christen. 1993. Aminotransferases: demonstration of homology and division into evolutionary subgroups. European Journal of Biochemistry. **214**:549-61.

Meyer A., R. Pellaux, and S. Panke. 2007. Bioengineering novel in vitro metabolic pathways using synthetic biology. Current Opinion in Microbiology. **10**:246-53.

Micheletti M., T. Barrett, S.D. Doig, F. Baganz, M.S. Levy, J.M. Woodley, and G.J. Lye. 2006. Fluid mixing in shaken bioreactors: Implications for scale-up predictions from microlitre-scale microbial and mammalian cell cultures. Chemical Engineering Science. **61**:2939-2949.

Micheletti M., and G. J. Lye. 2006. Microscale bioprocess optimisation. Current Opinion in Biotechnology. **17**:611-8.

Mitra R. K., and J. M. Woodley. 1996. A useful assay for transketolase in asymmetric syntheses. Biotechnology Techniques. **10**:167-172.

Monache G. D., and G. Zappia. 1999. A stereocontrolled synthesis of (-)- detoxinine from L -ascorbic acid. Tetrahedron: Asymmetry **10**:2961-2973.

Morbiducci U., A. Tura, and M. Grigioni. 2005. Genetic algorithms for parameter estimation in mathematical modeling of glucose metabolism. Computers in Biology and Medicine. **35**:862-74.

Moros R., H. Kalies, H. Rex, and S. Schaffarczyk. 1996. A genetic algorithm for generating initial parameter estimations for kinetic models of catalytic processes. Computers & Chemical Engineering. **20**:1257–1270.

Morris K. G., M. E. B. Smith, D. Turner Malcolm, J. Nicholas, and others. 1996. Transketolase from *Escherichia coli:* A practical procedure for using the biocatalyst for asymmetric carbon-carbon bond synthesis. Tetrahedron: Asymmetry. **7**:2185–2188.

Muller Y. A., Y. Lindqvist, W. Furey, G. E. Schulz, F. Jordan, and G. Schneider. 1993. A thiamin diphosphate binding fold revealed by comparison of the crystal structures of transketolase, pyruvate oxidase and pyruvate decarboxylase. Structure. **1**:95-103.

Murzin D. 2008. Sustainable chemical technology through catalytic multistep reactions. Chemical Engineering Research and Design. **86**:1002-1010.

Nealon A. J., R. D. O. Okennedy, N. J. Titchener-Hooker, and G.J. Lye. 2006. Quantification and prediction of jet macro-mixing times in static microwell plates. Chemical Engineering Science. **61**:4860-4870.

Niu W., M. N. Molefe, and J. W. Frost. 2003. Microbial Synthesis of the Energetic Material Precursor 1 , 2 , 4-Butanetriol. Biochemistry. **125**:12998-12999.

Payne M. S., K. L. Petrillo, J. E. Gavagan, R. DiCosimo, L. W. Wagner, and D. L. Anton. 1997. Engineering *Pichia pastoris* for biocatalysis: co-production of two active enzymes. Gene. **194**:179-82.

Pfeifer B. A. 2001. Biosynthesis of Polyketides in Heterologous Hosts. Microbiology and Molecular Biology Reviews. **65**:106-118.

Pohl M., G. A Sprenger, and M. Müller. 2004. A new perspective on thiamine catalysis. Current Opinion in Biotechnology. **15**:335-42.

Pollard D. J., and J. M. Woodley. 2007. Biocatalysis for pharmaceutical intermediates: the future is now. Trends in Biotechnology. **25**:66-73.

Prather K. L. J., and C. H. Martin. 2008. De novo biosynthetic pathways: rational design of microbial chemical factories. Current Opinion in Biotechnology. **19**:468-74.

Pósfai G., G. Plunkett, T. Fehér, D. Frisch, G. M. Keil, K. Umenhoffer, V. Kolisnychenko, B. Stahl, S. S. Sharma, M. de Arruda, V. Burland, S. W. Harcum, and F. R. Blattner. 2006. Emergent properties of reduced-genome *Escherichia coli*. Science. **312**:1044-6.

Ranaldi F. 1999. What students must know about the determination of enzyme kinetic parameters. Biochemical Education. **27**:87-91.

Reisman H. B. 1993. Problems in scale-up of biotechnology production processes. Critical Reviews in Biotechnology. **13**:195-253.

Roessner C. A, and A I. Scott. 1996a. Achieving natural product synthesis and diversity via catalytic networking ex vivo. Chemistry & Biology **3**:325-30.

Roessner C. A, and A I. Scott. 1996b. Genetically engineered synthesis of natural products: from alkaloids to corrins. Annual Review of Microbiology **50**:467-90.

Roessner C. A., J. Spencer, N. Stolowich, J. Wang, G. Nayar, P. Santander, C. Pichon, C. Min, M. Holderman, and A. I. Scott. 1994. Genetically engineered synthesis of precorrin-6x and the complete corrinoid, hydrogenobyrinic acid, an advanced precursor of vitamin B12. Chemistry & Biology. **1**:119.

Rokem J. S., A. E. Lantz, and J. Nielsen. 2007. Systems biology of antibiotic production by microorganisms. Natural Product Reports. **24**:1262-87.

Rozwadoska M. D. 1993. An efficient synthesis of S-(+)-amphetamine. Tetrahedron: Asymmetry.**4**:1619-1624.

Rozzell J. D. 1999. Commercial scale biocatalysis: myths and realities. Bioorganic and Medicinal Chemistry. **7**:2253-61.

Römisch W., W. Eisenreich, G. Richter, and A. Bacher. 2002. Rapid one-pot synthesis of riboflavin isotopomers. The Journal of Organic Chemistry. **67**:8890-4.

Santacoloma P., G. Sin, K. Gernaey, and J. M. Woodley. 2011. Multienzyme-catalyzed processes: Next-generation biocatalysis. Organic Process. 203-212.

Sayar N. A, B. H. Chen, G. J. Lye, and J. M. Woodley. 2009. Process modelling and simulation of a transketolase mediated reaction: Analysis of alternative modes of operation. Biochemical Engineering Journal. **47**:10-18.

Sayer C., M. N. Isupov, and J. A Littlechild. 2007. Crystallization and preliminary X-ray diffraction analysis of omega-amino acid:pyruvate transaminase from *Chromobacterium violaceum*. Acta crystallographica. Section F, Structural Biology and Crystallization Communications. **63**:117-9.

Schenk G., R. G. Duggleby, and P. F. Nixon. 1998. Properties and functions of the thiamin diphosphate dependent enzyme transketolase. The International Journal of Biochemistry and Cell Biology. **30**:1297-318.

Schilling C. H., S. Schuster, B. O. Palsson, and R. Heinrich. 1999. Metabolic pathway analysis: basic concepts and scientific applications in the post-genomic era. Biotechnology Progress. **15**:296-303.

Schmid A, J. S. Dordick, B. Hauer, a Kiener, M. Wubbolts, and B. Witholt. 2001. Industrial biocatalysis today and tomorrow. Nature. **409**:258-68.

Schoevaart R., F. V. Rantwijk, and R. A. Sheldon. 2000. A Four-Step Enzymatic Cascade for the One-Pot Synthesis of Non-natural Carbohydrates from Glycerol. Journal of Organic Chemistry. 65:6940-6943.

Schomburg I., A. Chang, C. Ebeling, M. Gremse, C. Heldt, G. Huhn, and D. Schomburg. 2004. BRENDA, the enzyme database: updates and major new developments. Nucleic Acids Research. **32**:D431-3.

Schultheisz H. L., B. R. Szymczyna, L. G. Scott, and J. R. Williamson. 2008. Pathway engineered enzymatic *de novo* purine nucleotide synthesis. ACS Chemical Biology. **3**:499-511.

Scott A. I. 1994. Towards a total, genetically engineered synthesis of vitamin b12. Synlett. 26:**871-874**.

Sheldon R. A. 2008. Enzyme-Catalysed Cascade Reactions, in Ed. Garcia-Junceda E. (Ed). Multi-step Enzyme Catalysis: Biotransformations and Chemoenzymatic Synthesis. Wiley-VCH Verlag GmbH and Co. KGaA , Weinheim, Germany. pp 109-135

Sheldon R. A. 2007. Enzyme Immobilization: The Quest for Optimum Performance. Advanced Synthesis and Catalysis. **349**:1289-1307.

Shiloach J., and R. Fass. 2005. Growing *E. coli* to high cell density--a historical perspective on method development. Biotechnology Advances. **23**:345-57.

Shin J. S., and B. G. Kim. 2001. Comparison of the omega-transaminases from different microorganisms and application to production of chiral amines. Bioscience, Biotechnology and Biochemistry. **65**:1782-1788.

Shin J. S., and B. G. Kim. 1997. Kinetic resolution of alpha-methylbenzylamine with omicron-transaminase screened from soil microorganisms: application of a biphasic system to overcome product inhibition. Biotechnology and Bioengineering. **55**:348-58.

Shin J. S., B. G. Kim, A Liese, and C. Wandrey. 2001. Kinetic resolution of chiral amines with omega-transaminase using an enzyme-membrane reactor. Biotechnology and Bioengineering. **73**:179-87.

Shin J. S., H. Yun, J.-W. Jang, I. Park, and B.-G. Kim. 2003. Purification, characterization, and molecular cloning of a novel amine:pyruvate transaminase from *Vibrio fluvialis JS17*. Applied Microbiology and Biotechnology. **61**:463-71.

Shin J.-S., and B.-G. Kim. 2002. Exploring the active site of amine:pyruvate aminotransferase on the basis of the substrate structure-reactivity relationship: how the enzyme controls substrate specificity and stereoselectivity. The Journal of Organic Chemistry. **67**:2848-2853.

Shin J.-S., and B.-G. Kim. 1998. Kinetic Modeling of ω-Transamination for Enzymatic Kinetic Resolution of a-Methylbenzylamine. Biotechnology and Bioengineering. **60**:534-540.

Shin J. S., and B. G. Kim. 1999. Asymmetric Synthesis of Chiral Amines With ω-Transaminase. Biotechnology and Bioengineering. **65**:206-211.

Shin J. S., and B. G. Kim. (1999). Modeling of the kinetic resolution of α-methylbenzylamine with ω-transaminase in a two-liquid-phase system. Enzyme and Microbial Technology. **25**:426 - 432.

Sin G., J. M. Woodley, and K. V. Gernaey. 2009. Application of modeling and simulation tools for the evaluation of biocatalytic processes: a future perspective. Biotechnology Progress. **25**:1529-38.

Smal J., and P. De Meyts. 1989. Sphingosine, an inhibitor of protein kinase C, suppresses the insulin-like effects of growth hormone in rat adipocytes. Proceedings of the National Academy of Sciences of the United States of America. **86**:4705-9.

Smith M. A., P. J. King, and B. Grimm. 1998. Transient-state kinetic analysis of *Synechococcus* glutamate 1-semialdehyde aminotransferase. Biochemistry. **37**:319-29.

Smith M. E. B., B. H. Chen, E. G. Hibbert, U. Kaulmann, K. Smithies, J. L. Galman, F. Baganz, P. A. Dalby, H. C. Hailes, G. J. Lye, J. M. Ward, J. M. Woodley, and M. Micheletti. 2010. A Multidisciplinary Approach Toward the Rapid and Preparative-Scale Biocatalytic Synthesis of Chiral Amino Alcohols: A Concise Transketolase-/ω-Transaminase-Mediated Synthesis of (2 S ,3 S)-2-Aminopentane-1,3-diol. Organic Process Research & Development. **14**:99-107.

Smith M. E. B., E. G. Hibbert, A. B. Jones, P. A. Dalby, and H. C. Hailes. 2008. Enhancing and Reversing the Stereoselectivity of *Escherichia coli* Transketolase via Single-Point Mutations. Advanced Synthesis & Catalysis. **350**:2631-2638.

Sprenger G. A, U. Schörken, G. Sprenger, and H. Sahm. 1995. Transketolase A of *Escherichia coli K12*. Purification and properties of the enzyme from recombinant strains. European Journal of Biochemistry. **230**:525-32.

Sprenger G. A. 2007. From scratch to value: engineering *Escherichia coli* wild type cells to the production of L-phenylalanine and other fine chemicals derived from chorismate. Applied Microbiology and Biotechnology. **75**:739-49.

Sprenger G. a, and M. Pohl. 1999. Synthetic potential of thiamin diphosphate-dependent enzymes. Journal of Molecular Catalysis B: Enzymatic **6**:145-159.

Stewart J. D. 2001. Dehydrogenases and transaminases in asymmetric synthesis. CurrentOopinion in Chemical Biology. **5**:120-9.

Stitt M., C. Muller, M. Petra, Y. Gibon, P. Carillo, R. Morcuenda. W.R. Scheible, and K. Anee. 2001. Steps towards an integrated view of nitrogen metabolism. Journal of Experimental Botany. **370**-959-970.

Straathof A. J. J., S. Panke, and A. Schmid. 2002. The production of fine chemicals by biotransformations. Current Opinion in Biotechnology. **13**:548-56.

Taylor P. P., D. P. Pantaleone, R. F. Senkpeil, and I. G. Fotheringham. 1998. Novel biosynthetic approaches to the production of unnatural amino acids using transaminases. Trends in Biotechnology. **16**:412-8.

Thiry M., and D. Cingolani. 2002. Optimizing scale-up fermentation processes. Trends in Biotechnology. **20**:103-5.

Tolia N. H., and L. Joshua-Tor. 2006. Strategies for protein coexpression in *Escherichia coli.* Nature Methods. **3**:55-64.

Truppo M. D., J. D. Rozzell, J. C. Moore, and N. J. Turner. 2009. Rapid screening and scale-up of transaminase catalysed reactions. Organic & Biomolecular Chemistry. **7**:395-8.

Truppo M. D., J. D. Rozzell, and N. J. Turner. 2010. Efficient Production of Enantiomerically Pure Chiral Amines at Concentrations of 50 g/L Using Transaminases. Organic Process Research and Development. **14**:234-237.

Tufvesson P., W. Fu, J. S. Jensen, and J. M. Woodley. 2010. Process considerations for the scale-up and implementation of biocatalysis. Food and Bioproducts Processing. **88**:3-11.

Tufvesson P., J. Lima-Ramos, J. S. Jensen, N. Al-Haque, W. Neto, and J. M. Woodley. 2011. Process considerations for the asymmetric synthesis of chiral amines using transaminases. Biotechnology and Bioengineering. **108**:1479-1493.

Turner N. J. 2000. Applications of transketolases in organic synthesis. Current Opinion in Biotechnology. **11**:527-531.

Tyo K. E., H. S. Alper, and G. N. Stephanopoulos. 2007. Expanding the metabolic engineering toolbox: more options to engineer cells. Trends in Biotechnology. **25**:132-7.

Votruba J., and M. Sobotka. 1992. Physiological similarity and bioreactor scale-up. Folia Microbiologica. **37**:331-345.

Watson J. D. 1972. Molecular Biology of the Gene, 2nd ed. Saunders, Philadelphia, PA USA..

Werpy T., and Petersen G. 2004. Top Value Added Chemicals from Biomass Volume I: Results of Screening for Potential Candidates from Sugars and Synthesis. Oak Ridge, TN:US. Department of Energy.

Whitesides G., and C. Wong. 1985. Enzymes as Catalysts in Synthetic Organic Chemistry. Chemie International Edition in English. **24:617-638**

Wikner C., U. Nilsson, L. Meshalkina, C. Udekwu, Y. Lindqvist, and G. Schneider. 1997. Identification of catalytically important residues in yeast transketolase. Biochemistry. **36**:15643-9.

Wilkinson B., and B. O. Bachmann. 2006. Biocatalysis in pharmaceutical preparation and alteration. Current Opinion in Chemical Biology. **10**:169-76.

Wong C. H., S. L. Hagnie, and G. M. Whitesides. 1982. Enzyme-Catalyzed Synthesis of N-Acetyllactosamine with in Situ Regeneration of Uridine 5'-Diphosphate Glucose and Uridine 5'-Diphosphate Galactose. Chemical Communications. **47**:5416-5418.

Woodley J. M. 2006. Choice of biocatalyst form for scalable processes. Biochemical Society Transactions. **34**:301-3.

Woodley J. M. 2008. New opportunities for biocatalysis: making pharmaceutical processes greener. Trends in Biotechnology. **26**:321-7.

Wu C. H., R. Apweiler, A. Bairoch, D. A. Natale, W. C. Barker, B. Boeckmann, S. Ferro, E. Gasteiger, H. Huang, R. Lopez, M. Magrane, M. J. Martin, R. Mazumder, C. O'Donovan, N. Redaschi, and B. Suzek. 2006. The Universal Protein Resource (UniProt): an expanding universe of protein information. Nucleic Acids Research. **34**:187-191.

Yazbeck D. R., C. A Martinez, S. Hu, and J. Tao. 2004. Challenges in the development of an efficient enzymatic process in the pharmaceutical industry. Tetrahedron: Asymmetry. **15**:2757-2763.

Young T. B. 1979. Fermentation scale-up: industrial experience with a total environmental approach. Biochemical Engineering. **326**:165-180..

Yun H., B.-K. Cho, and B.G. Kim. 2004. Kinetic resolution of (R,S)-sec-butylamine using omega-transaminase from *Vibrio fluvialis* JS17 under reduced pressure. Biotechnology and Bioengineering. **87**:772-8.

Yun H., and B.-G. Kim. 2008. Asymmetric Synthesis of (S)-α-Methylbenzylamine by Recombinant *Escherichia coli* Co-Expressing Omega-Transaminase and Acetolactate Synthase. Bioscience, Biotechnology, and Biochemistry **72**:3030-3033.

Yun H., S. Lim, B.-kwan Cho, and B.G. Kim. 2004. ω-Amino Acid: Pyruvate Transaminase from *Alcaligenes denitrificans Y2k-2:* a New Catalyst for Kinetic Resolution of β-Amino Acids and Amines. Applied and Environmental Microbiology **70**:2529-2534.

Zhang H., S. R. Lamping, S. C. R. Pickering, G. J. Lye, and P. A. Shamlou. 2008. Engineering characterization of a single well from 24-well and 96-well microtitre plates. Biochemical Engineering. **40**:138:149

Zhang K., M. R. Sawaya, D. S. Eisenberg, and J. C. Liao. 2008. Expanding metabolism for biosynthesis of nonnatural alcohols. Proceedings of the Academy of Science of United States of America. **105**:20658-20658.

Zimmermann F. T., A. Schneider, U. Schörken, and A. Sprenger. 1999. Efficient multi-enzymatic synthesis of D -xylulose 5-phosphate. Science. **6**:4-7.

APPENDIX I

CALIBRATION PLOT OF BIOMASS IN FUNCTION OF OD_{600}

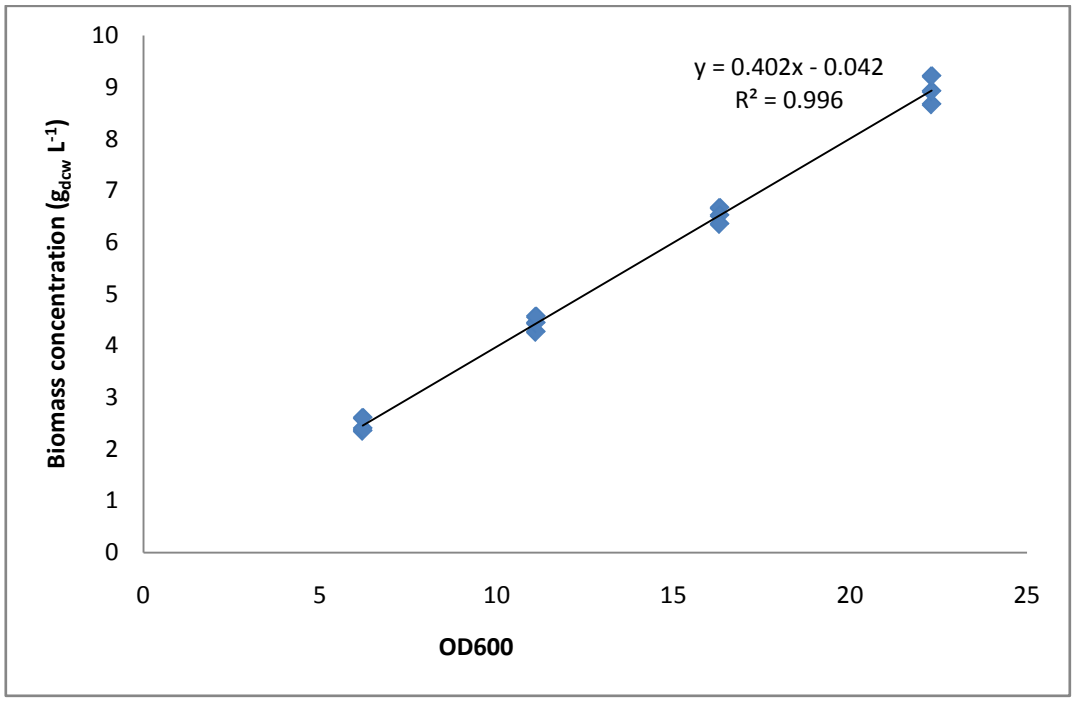

Figure A.I. 1. **Calibration graph of biomass in g_{DCW} L^{-1} as a function of OD_{600} (Section 2.9.2).**

APPENDIX II

BRADFORD ASSAY: CALIBRATION PLOT OF BSA CONCENTRATION IN FUNCTION OF OD_{595}

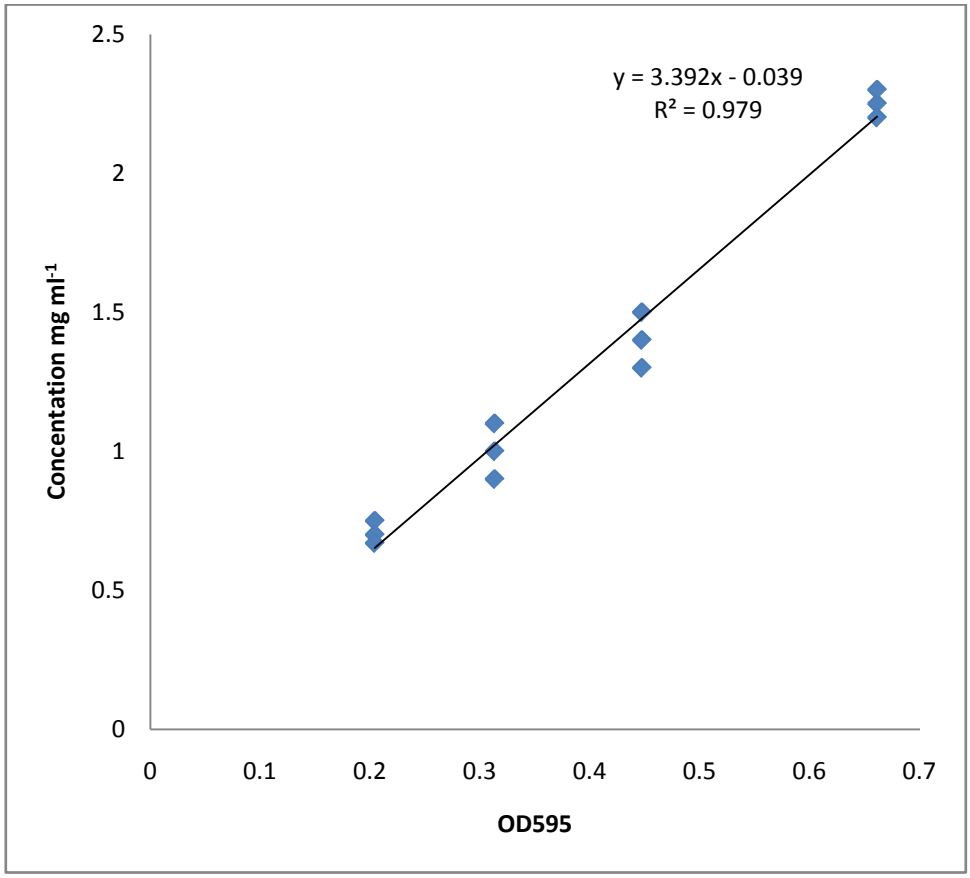

Figure A.II. 1. **Standard graph for Bradford assay of BSA concentration as a function of OD_{595} (Section 2.9.3).**

APPENDIX III

HPLC STANDARD CALIBRATIONS

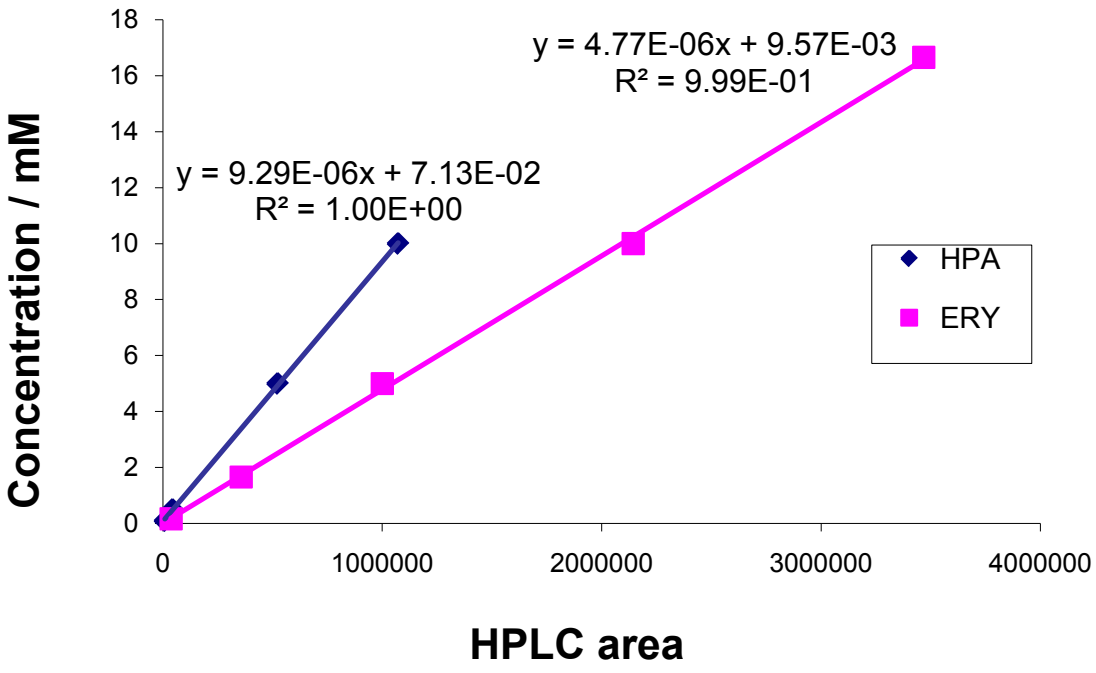

Figure A.III. 1. Calibration graph of ERY and HPA concentration as a function of HPLC area (Section 2.9.6).

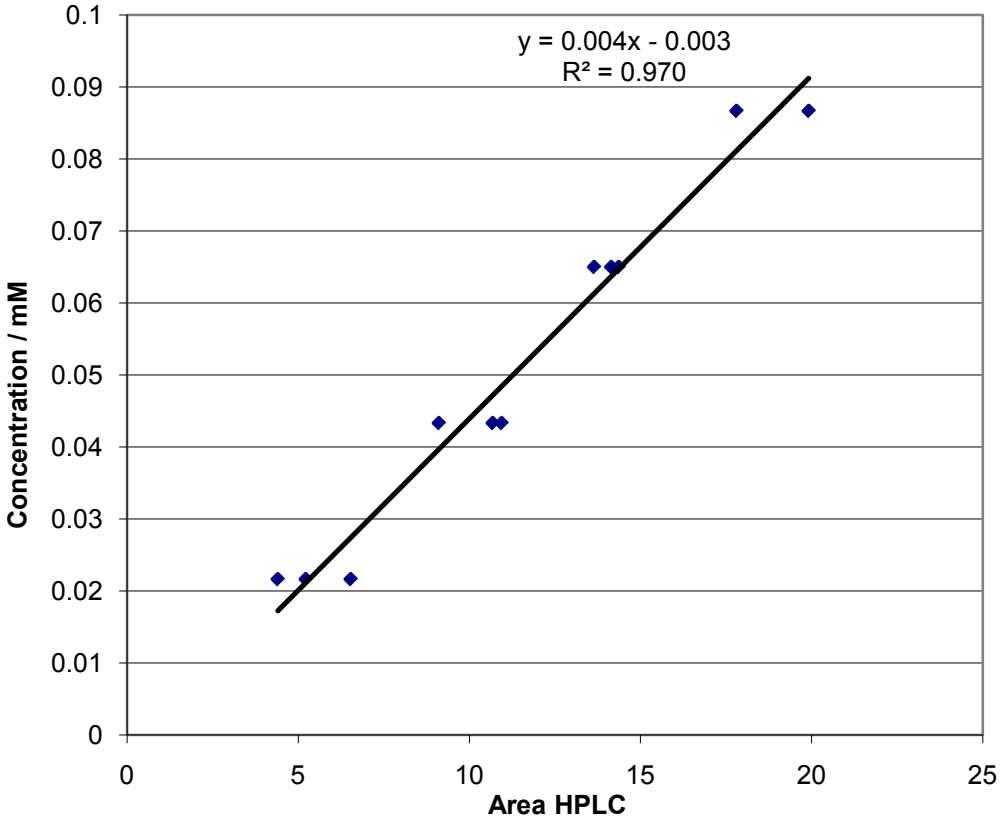

Figure A.III. 2. **Calibration graph of derivatized ABT concentration as a function of HPLC area (Section 2.96).**

APPENDIX IV

TK KINETIC COMPARISON IN WHOLE CELL AND LYSATE FORM

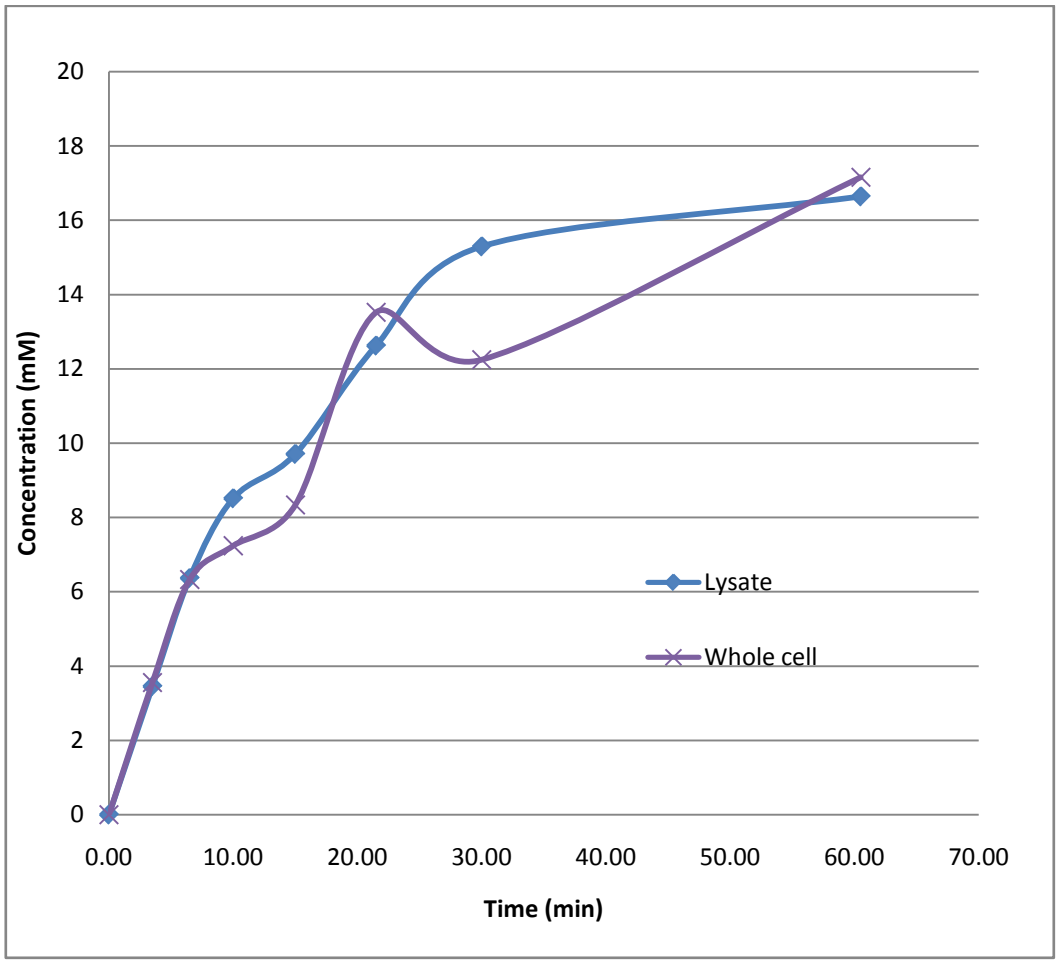

Figure A.IV. 1. ERY production by TK wild type lysate and whole cell at 25°C. Reaction has been performed at 25°C with 0.1 mg ml^{-1} of TK in lysate and whole cell form. [HPA] and [GA] were 50 mM in 50 mM TRIS buffer pH 7. Results show the mean of 2 duplicates.

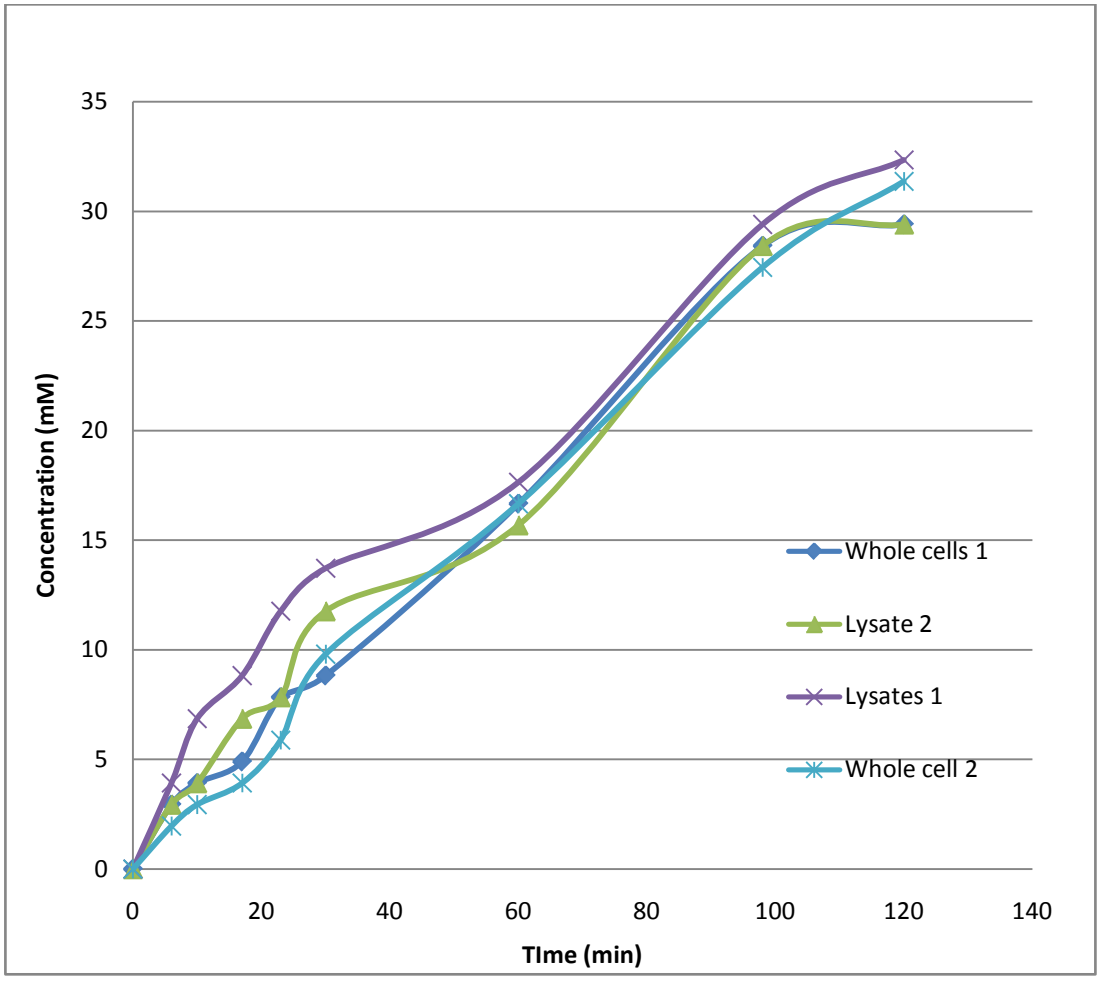

Figure A.IV. 2. Progress curves of the synthesis of ERY at 25°C with TK in lysate and whole cell form. [GA] and [HPA] were 50 mM. Enzyme concentration was 0.1 mg/ml , pH 7.0 with 50 mM TRIS

APPENDIX V

MATLAB PROGRAM FOR KINETIC PARAMETER ESTIMATION

```
function ParaEst

close all
clear all

format bank;

% Intial setup
NumDataSet = 15;                        % Number of progress curves
NumSample(1:NumDataSet) = [12 12 12 12 12 12 12 12 12 12 12 12 12 12
12];
%NumSample(1:NumDataSet) = [6 6 6 8 8 8 8 11 11 11 11 11 11 11 11 11
11 11];

                  % Number of sampling points for each progress
curve

Data_Filename1 = 'InhibitionCurve';  % Data file for Inhibition data
Data_Filename2 = 'P3';   % Data file for progress curves

Result_File = 'Result';          % Result file




% Call the programmes in the software
Result_Filename = strcat(Result_File,'.xls');



[Theta0, Theta] =
PE3(NumDataSet,NumSample,Data_Filename1,Data_Filename2,Result_Filena
me)
```

```
'Kf(1/min),      KERY(mM),      KMBA(mM),     Kr(mM),     KAP(mM),
KEAT(mM),    KdeMBA(mM),    KiMBA(mM),   KiAP(mM)'

StringTitle =
{'Kf(1/min)','KERY(mM)','KMBA(mM)','Kr(mM)','KAP(mM)','KEAT(mM)','Kd
eMBA(mM)','KiMBA(mM)','KiAP(mM)'; ...
    Theta(1) Theta(2) Theta(3) Theta(4) Theta(5)
Theta(6),Theta(7),Theta(8), Theta(9)};



String1 = {'Initial'};
String2 = {'Final'};

xlswrite(Result_Filename, StringTitle,'Parameters','D4');
xlswrite(Result_Filename, String1,'Parameters','C5');
xlswrite(Result_Filename, String2,'Parameters','C6');
xlswrite(Result_Filename, Theta0,'Parameters','D5');
xlswrite(Result_Filename, Theta, 'Parameters','D6');
```

```
function Theta = PE1(Data_Filename)

% Finding preliminary Kcat ka Kb in TK kinetics with initial rate
data

% Intial setup
% Parameter Estimation
    Theta0 = [1 1 1];     % Initial values for Kcat, Ka and Kb
    LB = [0.01 0.001 0.001];            % Lower bound
    UB = [80000 50000 50000];      % upper bound


% Read experimental data
Data = xlsread(Data_Filename);

    CHPA = Data(:,1); %IN our Cases HPA is ERY
    CGA  = Data(:,2); %IN our Cases GA is MBA
    Rate = Data(:,3);
    Ei   = Data(1,4);

    [NumSample,n11] = size(CHPA);



% options group for different optimisers
```

```
    foptions = optimset('MaxIter',200000,'TolFun',1e-9);

    [Theta,Func]= ...
       fmincon(@(x) ObjFunc(x,CHPA,CGA,Rate,Ei,NumSample), ...
                 Theta0,[],[],[],[],LB,UB,[],foptions)

% ======== Objective Function ========
function Func = ObjFunc(C,CHPA,CGA,RateE,Ei,NumSample)
% Objective function called by the main
% DON'T change it

A = 0.0;

for I = 1:NumSample
    y = [CHPA(I) CGA(I)];
    RateC(I)= Kinetics(y,C,Ei);

    A = A + (RateC(I)-RateE(I))^2;

end % for I

Func = A;

% ========  Kinetics Model ========
function R = Kinetics(y,Para,Ei)
% Simplified (no inhibition terms) kinetic model



    Kcat = Para(1);       % Rate constant   [1/min]
    Ka  = Para(2);        % Michaelis constant of ERY  [mM]
    Kb  = Para(3);        % Michaelis constant of MBA   [mM]




% y(1) -- ERY concentration
% y(2) -- MBA  concentration

    Vmax = Kcat*Ei;
    V = Kb*y(1)+Ka*y(2)+y(1)*y(2);
    R = Vmax*y(1)*y(2)/V;
```

```
function [Theta,tspa] =
PE2(NumDataSet,NumSample,NumPara,RatePara,Data_Filename)
format short eng
```

```
counter =1
% Read experimental data
Data = xlsread(Data_Filename);

for I = 1:NumDataSet
    for J = 1:NumSample(I)
        Ei(I,J) = Data(counter,5);
        Time(I,J) = Data(counter,1);
        CHPA(I,J) = Data(counter,2);
        CGA(I,J)  = Data(counter,3);
        CERY(I,J) = Data(counter,4);
        CEAT (I,J)= Data(counter,6);
        counter = counter+1;
    end
end

Lstep = 1;

for I = 1:NumDataSet
    tspa(I) = Time(I,NumSample(I));
end


% Initial values for parameters
    Theta0(1:2) = [0.1 0.1]

    LB(1:2) = [0.00001 0.0001];
    UB(1:2) = [800 800] ;

% Finding optimum parameters

    options =
optimset('Display','iter','MaxFunEvals',1000000,'MaxIter',
1000,'tolx',10E-19,'tolfun', 10E-19,'TolCon',10E-19);



    [Theta,Func]= ...
       fmincon(@(x)
ObjFunc(x,Time,CHPA,CGA,CERY,Ei,CEAT,tspa,NumDataSet,NumSample,RateP
ara), ...
                Theta0,[],[],[],[],LB,UB,[],options)

% ================= Objective Function =================

function Func =
ObjFunc(C,Time,CHPA,CGA,CERY,Ei,CEAT,tspa,NumDataSet,NumSample,RateP
ara)
% Objective function called by the main
% DON'T change it
format short eng

Lstep = 1;
```

```
F = 0.0;
A(NumDataSet) = 0.0;


for I = 1:(NumDataSet)

    tspan = [0:Lstep:tspa(I)];
    B=CHPA (I,1);
    D=CGA (I,1) ;
     E=CERY(I,1);
    G=CEAT(I,1);
    Y0 = [CHPA(I,1),CGA(I,1),CERY(I,1),CEAT(I,1)];

    sol =ode45(@(t,y) TKKine2(t,y,C,Ei(I),RatePara),tspan,Y0);


   Y = deval(sol,Time(I,:));
 % for J = 1:NumSample(I)

%        EHPA(J) = ((B-Y(1,J))/B-((B-CHPA(I,J))/B))^2;
%        EGA(J)  = ((D-Y(2,J))/D-((D-CGA(I,J))/D))^2;
%        if B>D
%     EERY(J) = ((Y(3,J)-CERY(I,J))/(D))^2;
%        EEAT(J) = ((Y(4,J)-CEAT(I,J))/(D))^2;
%        else
%        EERY(J) = ((Y(3,J)-CERY(I,J))/(B))^2;
%        EEAT(J) = ((Y(4,J)-CEAT(I,J))/(B))^2;

%       end
%      A(I) = A(I) + EHPA(J) + EGA(J) + EERY(J)+ EEAT(J) ;




 for J = 2:NumSample(I)
     EHPA(J) = (((Y(1,J))-CHPA(I,J))/Y(1,J))^2;
 EGA(J) = (((Y(2,J))-CGA(I,J))/Y(2,J))^2;
 EERY(J) = (((Y(3,J))-CERY(I,J))/Y(3,J))^2;
 EEAT(J) = (((Y(4,J))-CEAT(I,J))/Y(4,J))^2;
 A(I) = A(I) + EHPA(J) + EGA(J) + EERY(J)+ EEAT(J) ;

 end

  F = F + A(I) ;% for J;
end

Func = F;
return
```

```
% ========  Kinetics Model ========
function dy = TKKine2(t,y,RC,Ei,RatePara)
% PingPong Bi-Bi mechanism for reaction:
kf = RatePara(1);    % Rate constant   [1/min]
KmA = RatePara(2);     % Michaelis constant of ERY  [mM]
KmB = RatePara(3);     % Michaelis constant of MBA   [mM]
kr=RatePara(4);
KmP=RatePara(5);
KmQ = RatePara(6);
KiBs = RatePara (7);
KiB = RC(1);
KiQ= RC(2);
%KiQ = (kf/kr)*(kf/kr)*KmQ*KmP*KiB*KiA/(KmB*KmA*KiP);



[M,N]=size(y);
RealZero = 1.0e-18;
for I = 1:M
    if (y(I) <= RealZero)
        y(I) = RealZero;
    end
end


dy = zeros(M,1);

KEQ = (kf/kr)*(kf/kr)*KmP*KmQ/(KmA*KmB);


d3=(kf*Ei*kr*Ei*(y(1)*y(2)-
(y(3)*y(4))/(KEQ)))/(kr*Ei*KmB*y(1)+kr*Ei*KmA*y(2)+kr*Ei*y(1)*y(2)+k
f*Ei*KmP*y(4)/(KEQ)+kf*Ei*KmQ*y(3)/(KEQ)+...
  kf*Ei*y(3)*y(4)/(KEQ)+kr*Ei*KmB*y(1)*y(4)/KiQ
+kf*Ei*KmQ*y(2)*y(3)/(KEQ*KiB)...
+kr*Ei*KmA*y(2)*y(2)/(KiBs*KEQ)+kf*Ei*KmP*y(2)*y(4)/(KiBs));
%last line contains the extra terms for the model with substrate
inhibition


dy(1) =- d3;
dy(2) = -d3;
dy(3) = d3;
dy(4) = d3;




return
```

```
function [Theta0, Theta] = PE3(NumDataSet,NumSample, ...
    Data_Filename1,Data_Filename2,Result_Filename)

format short eng

% Intial setup
NumPara2 = 2;         % Number of parameter to be estimated (for Ki)
NumPara3 = 9;         % Number of parameter to be estimated (for
complete model)
NumComponent = 4;     % Number of Reaction component, here is HPA,
GA, ERY
%n=0
%for P = 0.1:0.5:10
%n=n+1
Theta1 = PE1(Data_Filename1);

RatePara = Theta1;

[Theta2,tspa] =
PE2(NumDataSet,NumSample,NumPara2,RatePara,Data_Filename2)



Theta0 = double(([Theta1 Theta2]))
KEQ=
Theta0(1)/Theta0(4)*Theta0(1)/Theta0(4)*Theta0(5)*Theta0(6)/(Theta0(
2)*Theta0(3))
KiERY= Theta0(1)*Theta0(5)*Theta0(9)/(KEQ*Theta0(4)*Theta0(3))
KiAP=KEQ*Theta0(4)*Theta0(2)*Theta0(8)/(Theta0(1)*Theta0(6))
K1=Theta0(8)/KiAP
K2=Theta0(9)/KiERY
Lstep = 1

% Read experimental data
Data = xlsread(Data_Filename2);
counter =1;
for I = 1:NumDataSet
    for J = 1:NumSample(I)
        Time(I,J) = Data(counter,1);
        CHPA(I,J) = Data(counter,2);
        CGA(I,J)  = Data(counter,3);
        CERY(I,J) = Data(counter,4);
        Ei(I)     = Data(counter,5);
        CEAT(I,J)     = Data(counter,6);
        counter =counter+1;
    end
end

for I = 1:NumDataSet
    Conc(I,1,:) = CHPA(I,:);
```

```
    Conc(I,2,:) = CGA(I,:);
    Conc(I,3,:) = CERY(I,:);
    Conc(I,4,:) = CEAT(I,:);

    % Finding optimum parameters
  %  psoptions =
psoptimset('Display','iter','MaxFunEvals',2000000,'MaxIter',2000000,
'TolFun',1e-12);
  % [Theta,Func]= ...
   %   patternsearch(@(x) ObjFunc(x,Ei,Time,Conc,NumDataSet,...
    %
NumComponent,NumSample,tspa),Theta0,[],[],[],[],LB,UB,[],psoptions);
end

% Initial values for parameters


LB(1:NumPara3) = [0.1 0.1  0.01 0.1 0.1  0.1  0.1 0.00001  0.001 ];
 UB(1:NumPara3) = [8000 8000 8000 8000 8000 8000 8000 80000  800  ]
;



options =
optimset('Display','iter','MaxFunEvals',10000,'MaxIter',400,'tolx',1
0E-12,'tolfun', 10E-12,'TolCon',10E-12);
%'UseParallel','always','algorithm', 'interior-
point')%'AlwaysHonorConstraints','bounds','DerivativeCheck','on','Fu
nValCheck','on'); % ,'MaxIter', 10);



[Theta,Func]= ...
       fmincon(@(x) ObjFunc(x,Ei,Time,CHPA,CGA,CERY,CEAT,NumDataSet,
...

NumComponent,NumSample,tspa),Theta0,[],[],[],[],LB,UB,[],options)



KEQ=
Theta(1)/Theta(4)*Theta(1)/Theta(4)*Theta(5)*Theta(6)/(Theta(2)*Thet
a(3))
KiERY= Theta(1)*Theta(5)*Theta(9)/(KEQ*Theta(4)*Theta(3))
KiAP=KEQ*Theta(4)*Theta(2)*Theta(8)/(Theta(1)*Theta(6))
%Parameter(1:20) =1
%result(1:20)=1
%Parameter(n) = (P)
%result (n)=(Func)
%end
%Sensitivity_File = 'Sensitivity';          % Result file

%Sensitivity_Filename = strcat(Sensitivity_File,'.xls');
```

```
%String1 = {'Parameter'};
%String2 = {'Residual'};

%xlswrite(Sensitivity_Filename,Parameter ,'Parameters','D5');
%xlswrite(Sensitivity_Filename, String1,'Parameters','C5');
%xlswrite(Sensitivity_Filename, String2,'Parameters','C6');
%xlswrite(Sensitivity_Filename,result,'Parameters','D6');

% ======== Plotting the result comparison ========
NC = Theta;
Lstep = 1;


for I = 1:NumDataSet
   tspan = [0:Lstep:tspa(I)];
    Y0 = [CHPA(I,1),CGA(I,1),CERY(I,1),CEAT(I,1)];

   W=I;


    [t,y] =ode45(@(t,y) TKKine3(t,y,NC,Ei(I)),tspan,Y0);

 figure(I)

    plot(Time(I,:),CHPA(I,:),'ro','LineWidth',2)
    hold on
    plot(Time(I,:),CGA(I,:),'md','LineWidth',2)
    plot(Time(I,:),CERY(I,:),'bs','LineWidth',2)
    plot(t,y(:,1),'r-','LineWidth',2)
    plot(t,y(:,2),'m-','LineWidth',2)
    plot(t,y(:,3),'b-','LineWidth',2)
    hold off

    xlabel('Time (min)','fontsize',14, 'fontweight','bold')
   ylabel('Concentration (mM)','fontsize',14, 'fontweight','bold')
    set(gca, 'fontsize',14, 'fontweight','bold', 'LineWidth',2);
    legend('ERY)','MBA','ABT','Location','best');

%    for J = 1:NumSample
%        fprintf(fid, '%6.2f %12.8f %12.8f %12.8f %12.8f\n', ...
%            Time(I,J),YY(1,J),YY(2,J),YY(3,J),YY(4,J));
%    end
end


% Write experiment data, model prediction and residuals into data
file
for I = 1:NumDataSet
    tspan = [0:Lstep:tspa(I)];
    Y0 = [CHPA(I,1),CGA(I,1),CERY(I,1),CEAT(I,1)];
```

```
    [t,y] =ode45(@(t,y) TKKine3(t,y,NC,Ei(I)),tspan,Y0);


    sol =ode113(@(t,y) TKKine3(t,y,NC,Ei(I)),tspan,Y0);


    Y = deval(sol,Time(I,:));

    Residual1(I,:) = CHPA(I,:) - Y(1,:);
    Residual2(I,:) = CGA(I,:)  - Y(2,:);
    Residual3(I,:) = CERY(I,:) - Y(3,:);
    Residual4(I,:) = CEAT(I,:) - Y(4,:);

    for J = 1:NumSample(I)
        T1(J+(I-1)*NumSample(I)) = Time(I,J);
        C1(J+(I-1)*NumSample(I)) = CHPA(I,J);
        Y1(J+(I-1)*NumSample(I)) = Y(1,J);
        R1(J+(I-1)*NumSample(I)) = Residual1(I,J);

        C2(J+(I-1)*NumSample(I)) = CGA(I,J);
        Y2(J+(I-1)*NumSample(I)) = Y(2,J);
        R2(J+(I-1)*NumSample(I)) = Residual2(I,J);

        C3(J+(I-1)*NumSample(I)) = CERY(I,J);
        Y3(J+(I-1)*NumSample(I)) = Y(3,J);
        R3(J+(I-1)*NumSample(I)) = Residual3(I,J);

        C4(J+(I-1)*NumSample(I)) = CEAT(I,J);
        Y4(J+(I-1)*NumSample(I)) = Y(4,J);
        R4(J+(I-1)*NumSample(I)) = Residual4(I,J);
    end
end% I

StringMatrix = {'Time', 'HPA-E', 'HPA-P', 'Residual-1', 'GA-E', ...
    'GA-P', 'Residual-2', 'ERY-E',  'ERY-P', 'Residual-3'};

xlswrite(Result_Filename,StringMatrix,'Comparison','A1');

DataMatrix = [T1;C1;Y1;R1;C2;Y2;R2;C3;Y3;R3;C4;Y4;R4];

xlswrite(Result_Filename, DataMatrix,'Comparison','A2');

% ================= Objective Function ==================
function Func = ObjFunc(CC,Ei,Time,CHPA,CGA,CERY,CEAT, ...
                        NumDataSet,NumResp,NumSample,tspa)
format short eng
Lstep = 1;
F = 0.0;
MaxNum = max(NumSample(1:NumDtaSet));
A(NumDataSet) = 0.0;
```

```
for I = 1:NumDataSet
    tspan = [0:Lstep:tspa(I)];
      Y0 = [CHPA(I,1),CGA(I,1),CERY(I,1),CEAT(I,1)];
 B=CHPA (I,1);
    D=CGA (I,1);
    E=CERY(I,1);
    G=CEAT(I,1);
W=I;


    sol =ode45(@(t,y) TKKine3(t,y,CC,Ei(I)),tspan,Y0);


    Y = deval(sol,Time(I,:)) ;
%
%  for J = 1:NumSample(I)

%        EHPA(J) = ((B-Y(1,J))/B-((B-CHPA(I,J))/B))^2;
%        EGA(J)  = ((D-Y(2,J))/D-((D-CGA(I,J))/D))^2;
%        if B>D
%        EERY(J) = ((Y(3,J)-CERY(I,J))/(D))^2;
%        EEAT(J) = ((Y(4,J)-CEAT(I,J))/(D))^2;
%        else
%       EERY(J) = ((Y(3,J)-CERY(I,J))/(B))^2;
%        EEAT(J) = ((Y(4,J)-CEAT(I,J))/(B))^2;

%        end
%        A(I) = A(I) + EHPA(J) + EGA(J) + EERY(J)+ EEAT(J) ;


 for J = 1:NumSample(I)
     EHPA(J) = (((Y(1,J))-CHPA(I,J))/Y(1,J))^2;
 EGA(J) = (((Y(2,J))-CGA(I,J))/Y(2,J))^2;
 EERY(J) = (((Y(3,J))-CERY(I,J))/Y(3,J))^2;
 EEAT(J) = (((Y(4,J))-CEAT(I,J))/Y(4,J))^2;
 A(I) = A(I) + EHPA(J) + EGA(J) + EERY(J)+ EEAT(J) ;

 end

 F = F + A(I);
end
Func = F;

return
```

```
% ========  Kinetics Model ========
function dy = TKKine3(t,y,RC,Ei)

% PingPong Bi-Bi mechanism for reaction:

% PingPong Bi-Bi mechanism for reaction:
kf = RC(1);    % Rate constant   [1/min]
KmA = RC(2);     % Michaelis constant of HAP  [mM]
KmB = RC(3);     % Michaelis constant of GA   [mM]
kr=RC(4);
KmP = RC(5);
KmQ = RC(6);
KiBs= RC(7);
KiB =RC(8);
KiQ = RC(9);

[M,N]=size(y);
RealZero = 1.0e-18;
for I = 1:M
    if (y(I) <= RealZero)
        y(I) = RealZero;
    end
end



dy = zeros(M,1);

KEQ = (kf/kr)*(kf/kr)*KmP*KmQ/(KmA*KmB);


d3=(kf*Ei*kr*Ei*(y(1)*y(2)-
(y(3)*y(4))/(KEQ)))/(kr*Ei*KmB*y(1)+kr*Ei*KmA*y(2)+kr*Ei*y(1)*y(2)+k
f*Ei*KmP*y(4)/(KEQ)+kf*Ei*KmQ*y(3)/(KEQ)+...
  kf*Ei*y(3)*y(4)/(KEQ)+kr*Ei*KmB*y(1)*y(4)/KiQ
+kf*Ei*KmQ*y(2)*y(3)/(KEQ*KiB)...
+kr*Ei*KmA*y(2)*y(2)/(KiBs*KEQ)+kf*Ei*KmP*y(2)*y(4)/(KiBs));
%last line contains the extra terms for the model with substrate
inhibition


dy(1) =- d3;
dy(2) = -d3;
dy(3) = d3;
dy(4) = d3;


return
```

APPENDIX VI

PROGRESS CURVES WITH MODEL PREDICTIONS FOR THE TAM SYNTHESIS OF ABT USING MBA AS AMINO DONOR

Table A.VI.1 **Initial experimental substrate concentrations for the 12 progress curves used to obtain the kinetic parameters in Steps 4 and 5 of the methodology described in Figure 4.1 for the synthesis of ABT using TAm whole cells. The first 9 progress curves represent forward reaction bioconversions, while the last 3 represent reverse reaction bioconversions. The concentration of PLP was 0.2 mM at 30°C and pH 7.5 in 200 mM HEPES for all the progress curves.**

Progress curve N°	1	2	3	4	5	6	7	8	9	10	11	12
[ERY] (mM)	50	70	150	250	300	150	200	10	20	0	0	0
[MBA] (mM)	100	250	250	40	30	15	50	120	200	0	0	0
[AP] (mM)	0	0	0	0	0	0	0	0	0	10	20	40
[ABT] (mM)	0	0	0	0	0	0	0	0	0	120	200	100
E_i mg mL^{-1}	0.3	0.44	0.3	0.15	0.15	0.15	0.15	0.3	0.45	0.15	0.44	0.3

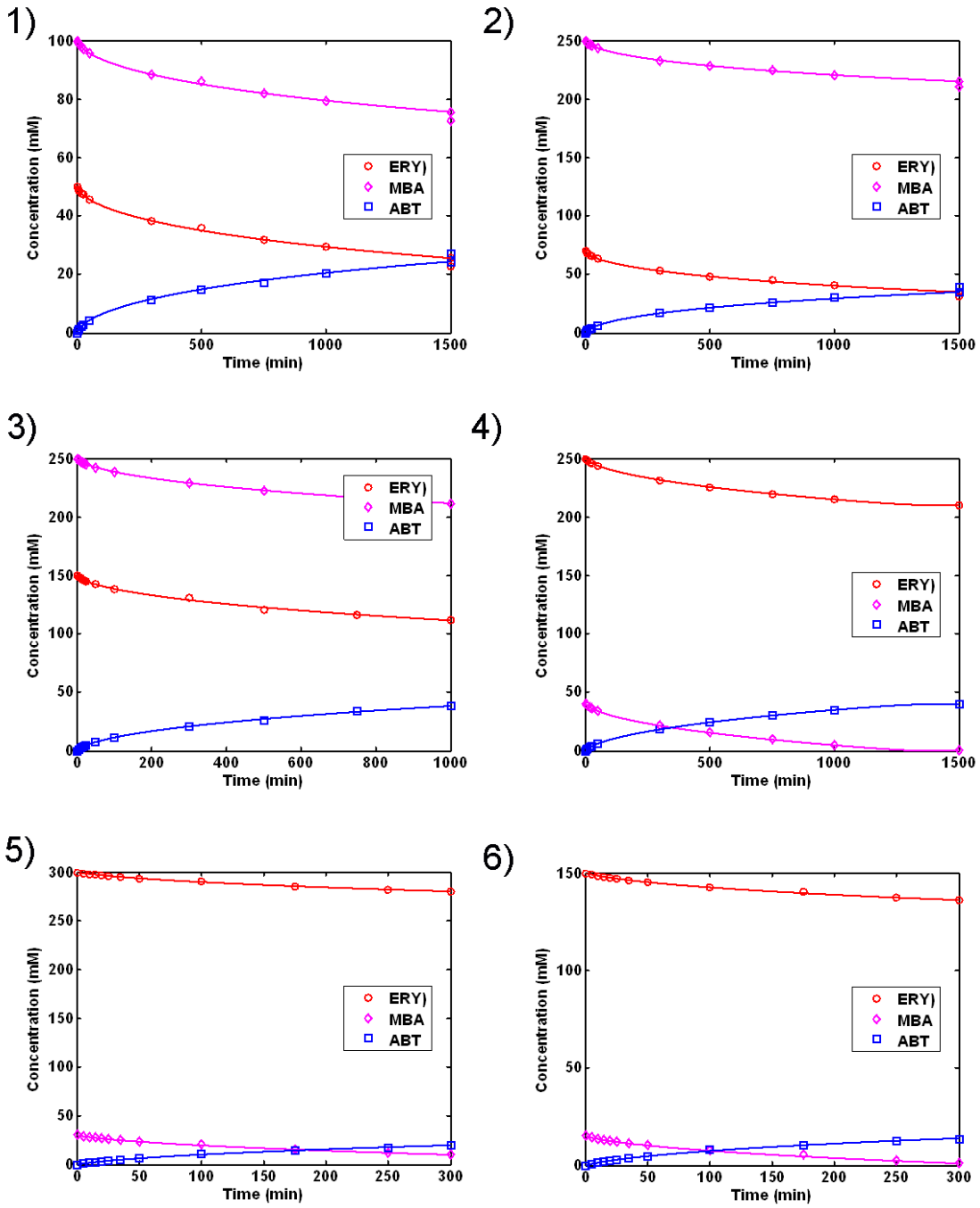

Figure A.VI. 1. Progress curves of whole cell TAm mediated synthesis of ABT from substrates ERY and MBA. The number of each graph relates with the initial concentrations of substrates and enzyme described in Table A.VI.1. Modelling was performed with Equation 4.1 and the parameters from Table 4.2 and is shown in solid lines.

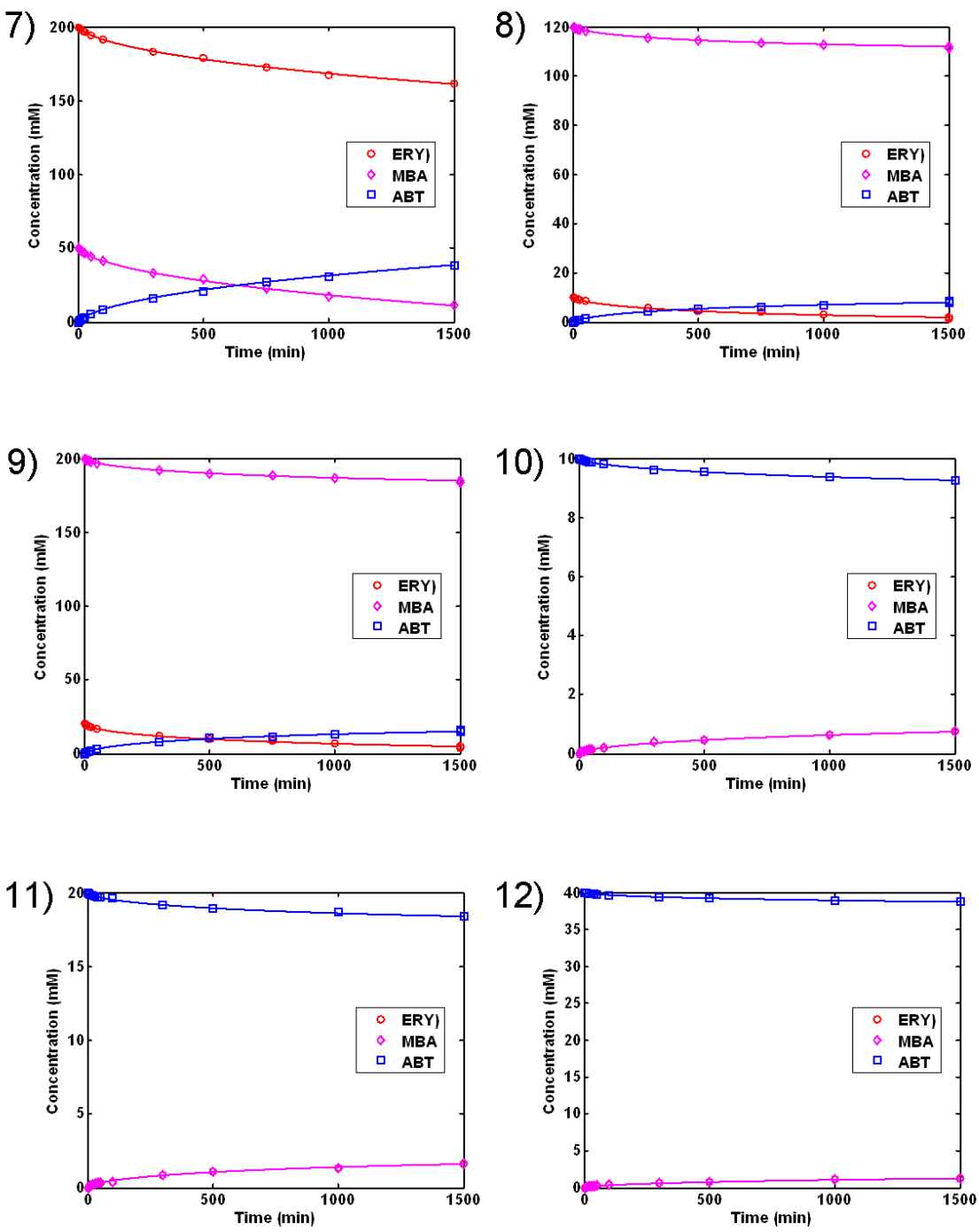

Figure A.VI. 2. **Progress curves of whole cell TAm mediated synthesis of ABT from substrates MBA and ERY (continuation from Figure A.VI.1). The number of each graph relates with the initial concentrations of substrates and enzyme described in Table A.X.1. Modelling was performed with Equation 4.1 and the parameters from Table 4.2 and is shown in solid lines.**

APPENDIX VII

SENSITIVITY ANALYSIS OF THE KINETIC PARAMETERS OF THE TAM MEDIATED SYNTHESIS OF ABT

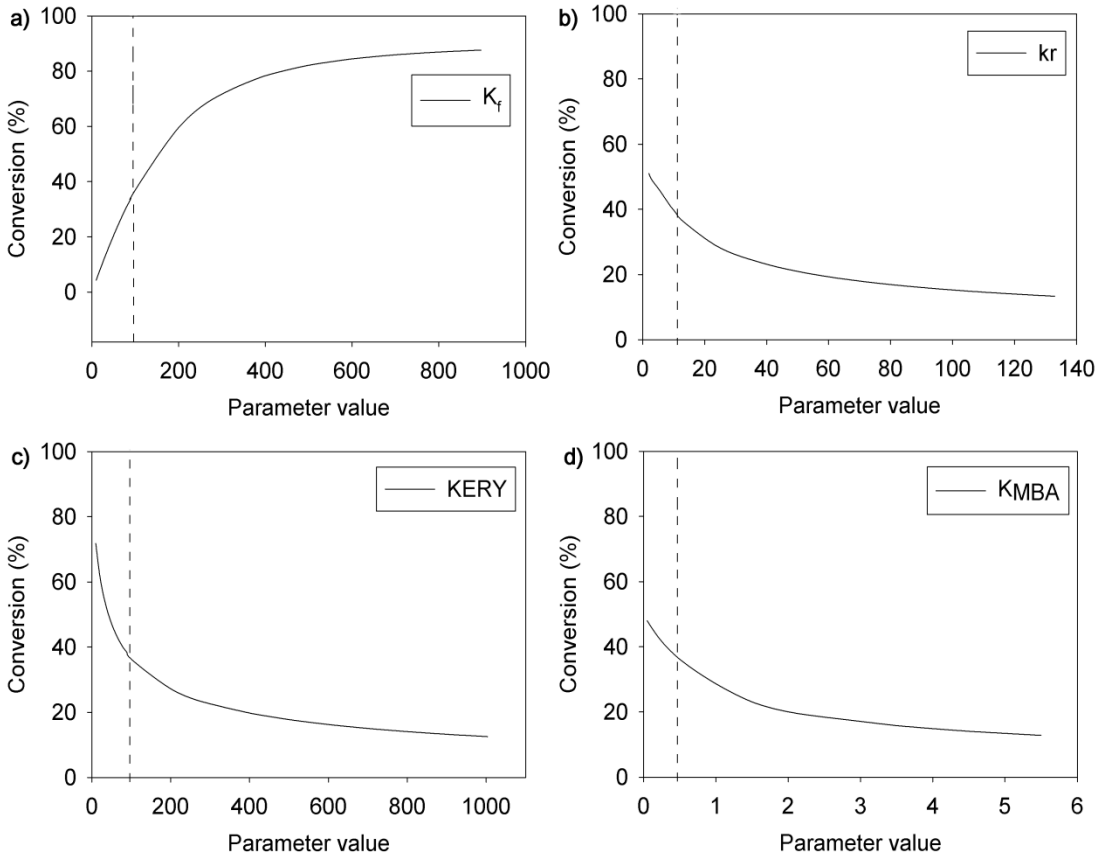

Figure A.VII.1. **Effect of the parameter value of (a) k_f, (b) k_r, (c) K_{ERY} and (d) K_{MBA} in the simulated yield of ABT (% mol/mol) considering a 24 hr reaction using 100 mM equimolar of [MBA] and [ERY] and 0.3 mg ml^{-1} of TAM. Equation 4.1 was used with the parameters from Table 4.2, and the parameters were varied increasing and decreasing 10-fold their values. The sensitivity results are discussed in Section 4.4.3.**

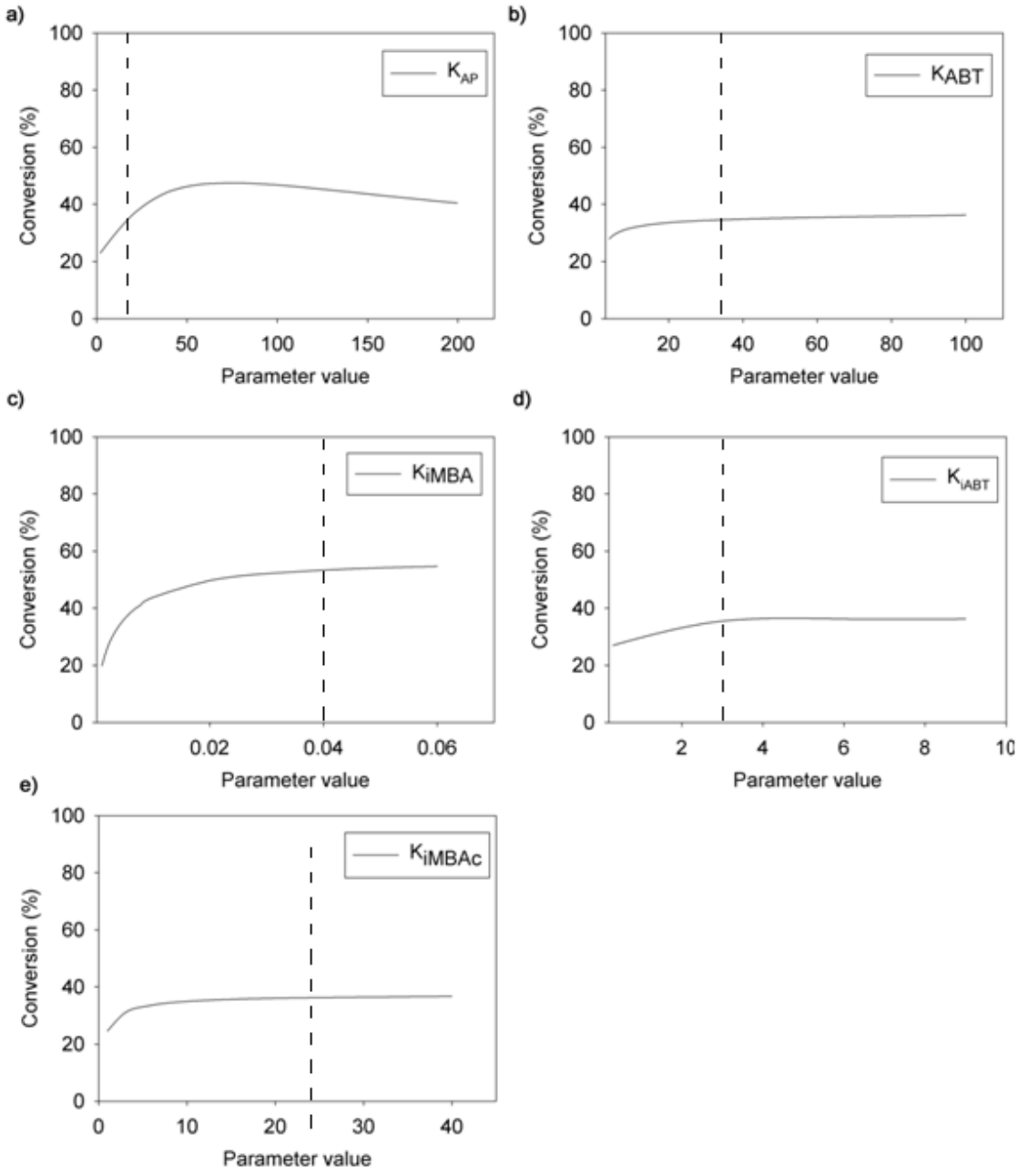

Figure A.VII. 2. Effect of the parameter value of (a) k_{AP}, (b) k_{ABT}, (c) K_{iMBA}, (d) K_{iABT} and (e) K_{iMBAc} in the simulated yield of ABT (% mol/mol) considering a 24 hr reaction using 100 mM equimolar of [MBA] and [ERY] and 0.3 mg ml^{-1} of TAM. Equation 4.1 was used with the parameters from Table 4.2 (original values indicated with a dashed line), and the parameters were varied increasing and decreasing 10-fold their values. The sensitivity results are discussed in Section 4.4.3.

APPENDIX VIII

PILOT PLANT FERMENTATION OF E. COLI CELLS OVEREXPRESSING TAM

VIII. TRANSAMINASE PILOT SCALE FERMENTATIONS

VIII.I Fermentation with one single pulse addition of glycerol

The shake flask fermentation of *E. coli* single induced with plasmid pQR801 to express TAm shown in Figure 3.1 reached a final biomass of 1.8 g_{DCW} L^{-1} and a final TAm concentration of 0.36 g L^{-1}. In order to increase the total volume of the reaction and the final yield of TAm, the fermentation was scaled up to a 7.5L New Brunswick fermentor (BioFlo 110, New Brunswick, Hertfordshire, UK) with a working volume of 5L. (For more details about the characteristics of the fermentor see Section 2.5.2 of the Materials and Methods). The temperature and pH were the same as for the shake flask fermentations of Figure 3.1, which were 37^{o}C, pH 7.0 and the DOT was set to be maintained to a minimum of 80% through a cascade control of the impeller speed. The selected media was LB-glycerol which initially only contained 3g L^{-1} of glycerol. One single shot addition of pre-sterilized 25 grams of glycerol was made to the fermentor after 5.0 hours. Figure VIII.1 shows the cell growth curve of the fermentation while figure VIII.2 shows the profiles of DOT, rpm of the impeller, pH and temperature.

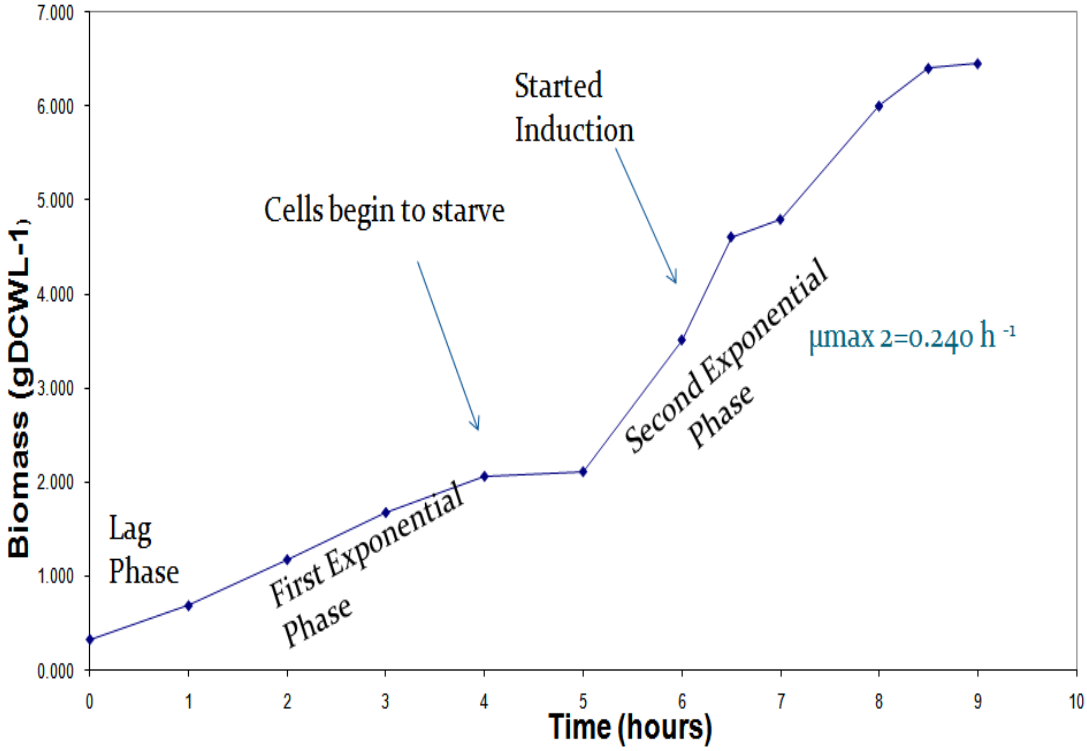

Figure VIII.1. Growth profile of *E. coli* cells overexpressing TAm for the fermentation with single shot addition of glycerol as described in Section VIII.1.

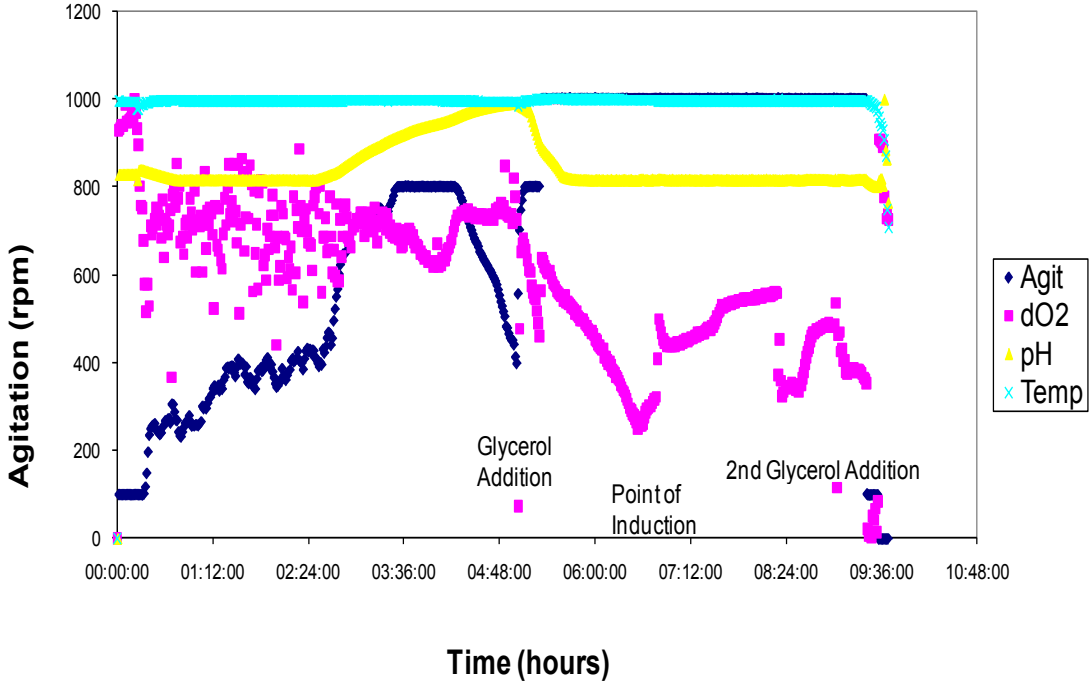

Figure VIII.2. Logged pH, DO2, temperature and agitation speed for the *E. coli* fermentation of Figure VIII.1

The fermentation presented a first exponential phase with a specific growth rate of 0.36 hr^{-1} which ended after 4 hours of fermentation when the cells reached the first stationary phase, which correlated with a sharp decrease in the speed impeller after 4 hours (Figure VIII.2), due to decrease in metabolic activity of the cells. Therefore after 5 hours, 25 g of glycerol were added, which correlated with an immediate increase in the impeller speed and a steady decrease in DOT, leading to second exponential growth phase with a specific growth rate of 0.24 hr^{-1} which ended after 9 hours of fermentation when the cell reached the second stationary phase with a final biomass 6.4 g_{DCW} L^{-1}. Figure VIII.3 shows the SDS PAGE gels for cellular extracts taken at different time intervals.

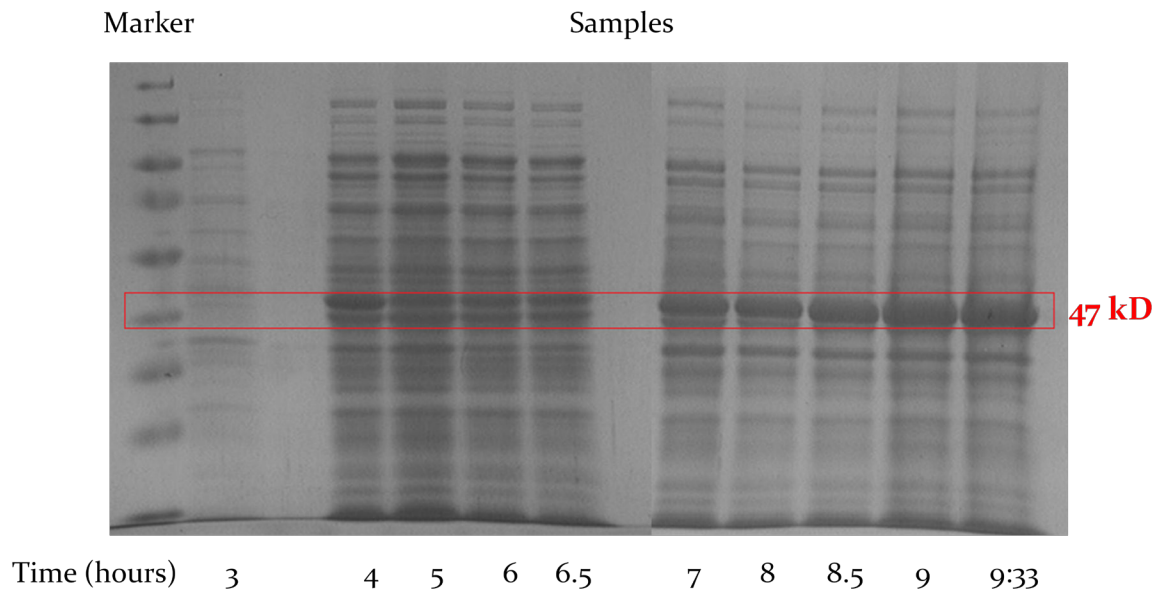

Figure VIII.3. SDS PAGE gel of the cellular extracts at different intervals of time of the fermentation shown in Figure VIII.1

The cells were induced after 6.5 hours, which correlated with a sharp increase in enzyme synthesis as can be seen in Figure VIII.3 The final TAm expression represented 40% of the total protein, which was similar to the level of expression obtained in shake flasks, however due to the higher biomass concentration achieved in the 7.5L fermentor, the final TAm concentration was found to be 1.3 g L^{-1}, which represented a 3.5 improvement compared to the shake flask fermentations of Chapter 3.

VIII.II. Fermentation with continuous fed batch feeding of glycerol

In order to increase the biomass and enzyme yield obtained in the fermentation described in Appendix Section VIII.I, a continuous fed-batch fermentation of TAm was performed in a 2L fermenter (Adaptive Biosystems, London, England) as described in Sections 2.5.1 and 2.5.3. The temperature and pH were controlled at 37^{o}C and pH 7.0, the media was LB with 5 g L^{-1} of glycerol, and the speed impeller was fixed at 1100 rpm. Figure VIII.4 shows the growth curve over time while Figure VIII.5 illustrates the DOT, pH, temperature and impeller speed profiles of the fermentation.

After 8 hrs of growth, when the carbon source was depleted which correlated with the DOT reaching 100%, glycerol was added in a continuous fed batch mode with increasing rates as described by Equation 2.1 in Section 2.5.3, maintaining a specific growth rate of 0.3. The fermentation reached a final biomass of 24 g L^{-1} after 43 hrs, and figure VII.6 shows the SDS PAGE gels for cellular extracts taken at different time intervals.

Induction was performed after 15 hr, where a sharp increase in enzyme synthesis could be observed in Figures 5.7 and 5.8 reaching a final TAm yield of 4.8 g L^{-1}, which represented a 4X and 13X improvement compared to the fermentation with a single shot addition of glycerol and the shake flask fermentation respectively of Chapter 3.

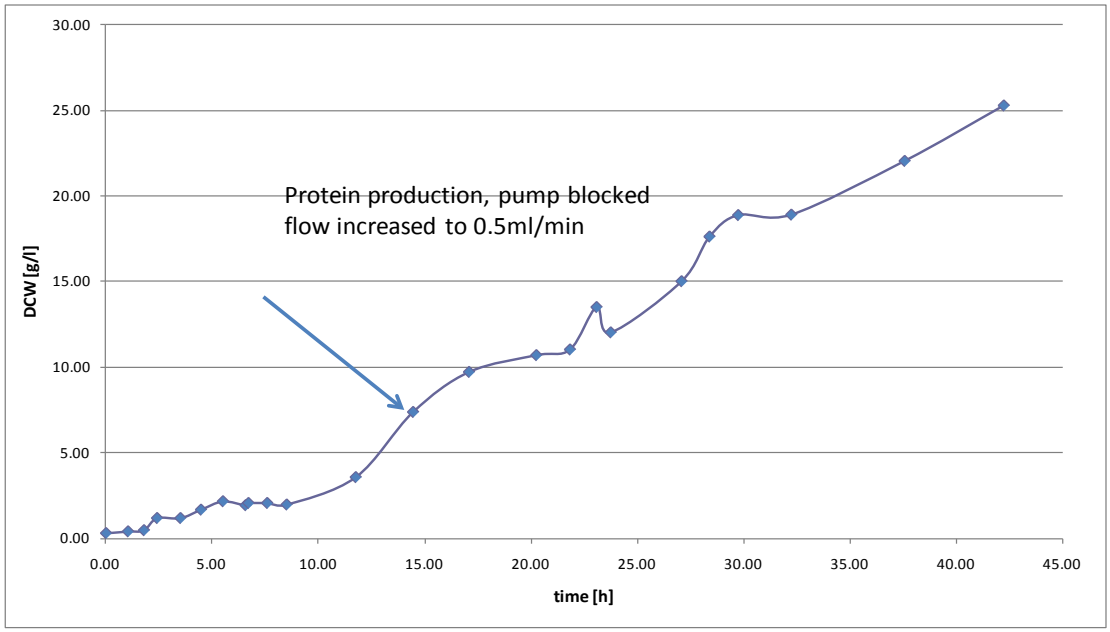

Figure VII.4. Growth curve as a function of time for the fed batch fermentation of *E. coli* cells with plasmid pQR801 as described in Section 2.8.3.

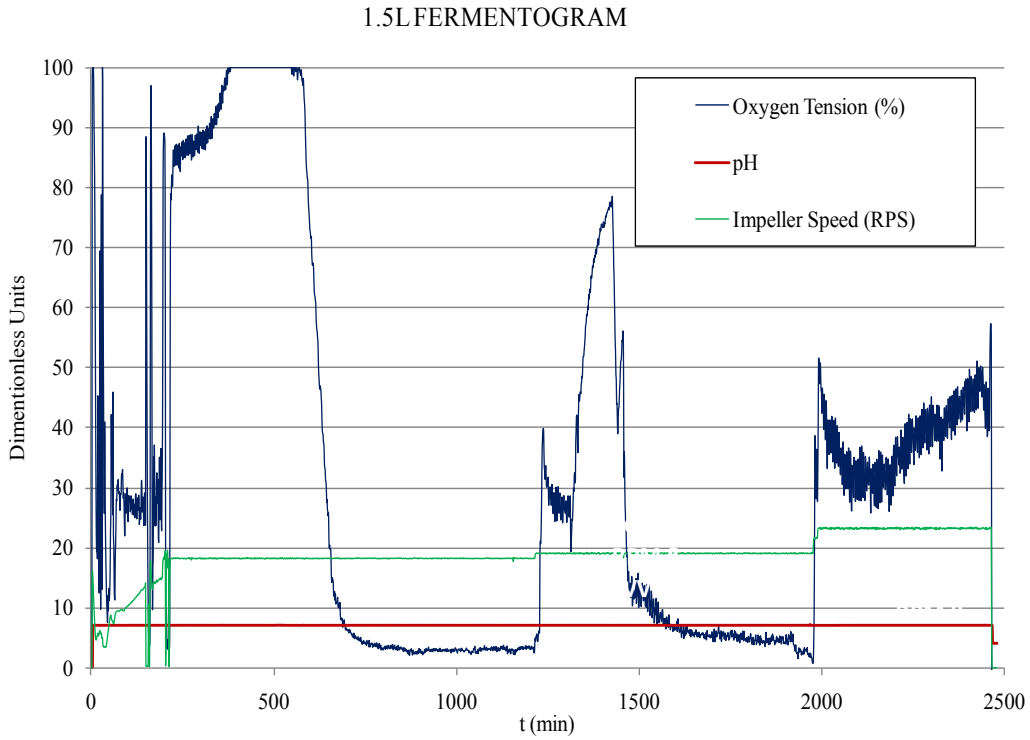

Figure VII.5. **Logged pH, temperature, DOT and RPM for the fed batch fermentation of Figure VII.4**

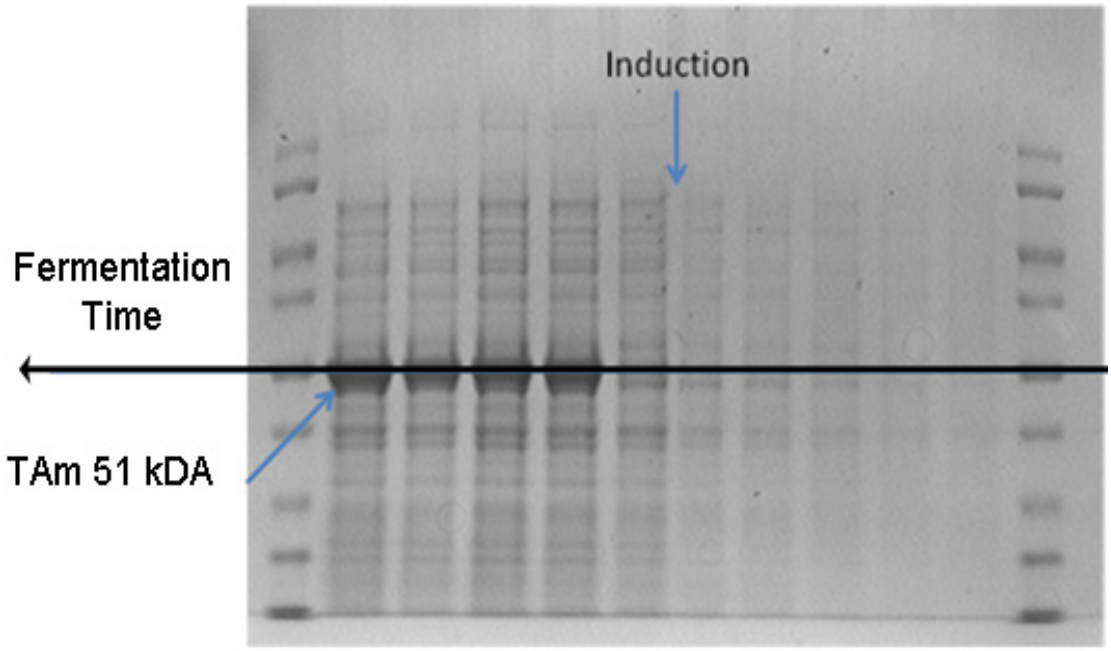

Figure VIII.6. **SDS PAGE gel for different interval samples of the fermentation shown in Figure VIII.5. (Note that time increases from right to left).**

APPENDIX IX

PROGRESS CURVES WITH MODEL PREDICTIONS FOR THE TK D469E SYNTHESIS OF PKD

Table A.IX.1. Initial experimental substrate and enzyme concentrations for the 9 progress curves used to obtain the kinetic parameters in Steps 4 and 5 of the methodology described in Figure 4.1 for the synthesis of PKD using TK D469E whole cells. The concentration of TPP and Mg^{2+} was 2.4 and 9 mM respectively at 30^{o}C in 50 mM TRIS buffer pH 7.5.

No Progress curve	1	2	3	4	5	6	7	8	9
[HPA] (mM)	100	130	150	230	100	150	200	300	300
[GA] (mM)	130	170	200	300	50	110	140	200	270
E_i mg ml^{-1}	0.3	0.3	0.3	0.4	0.5	0.5	0.6	0.6	0.6

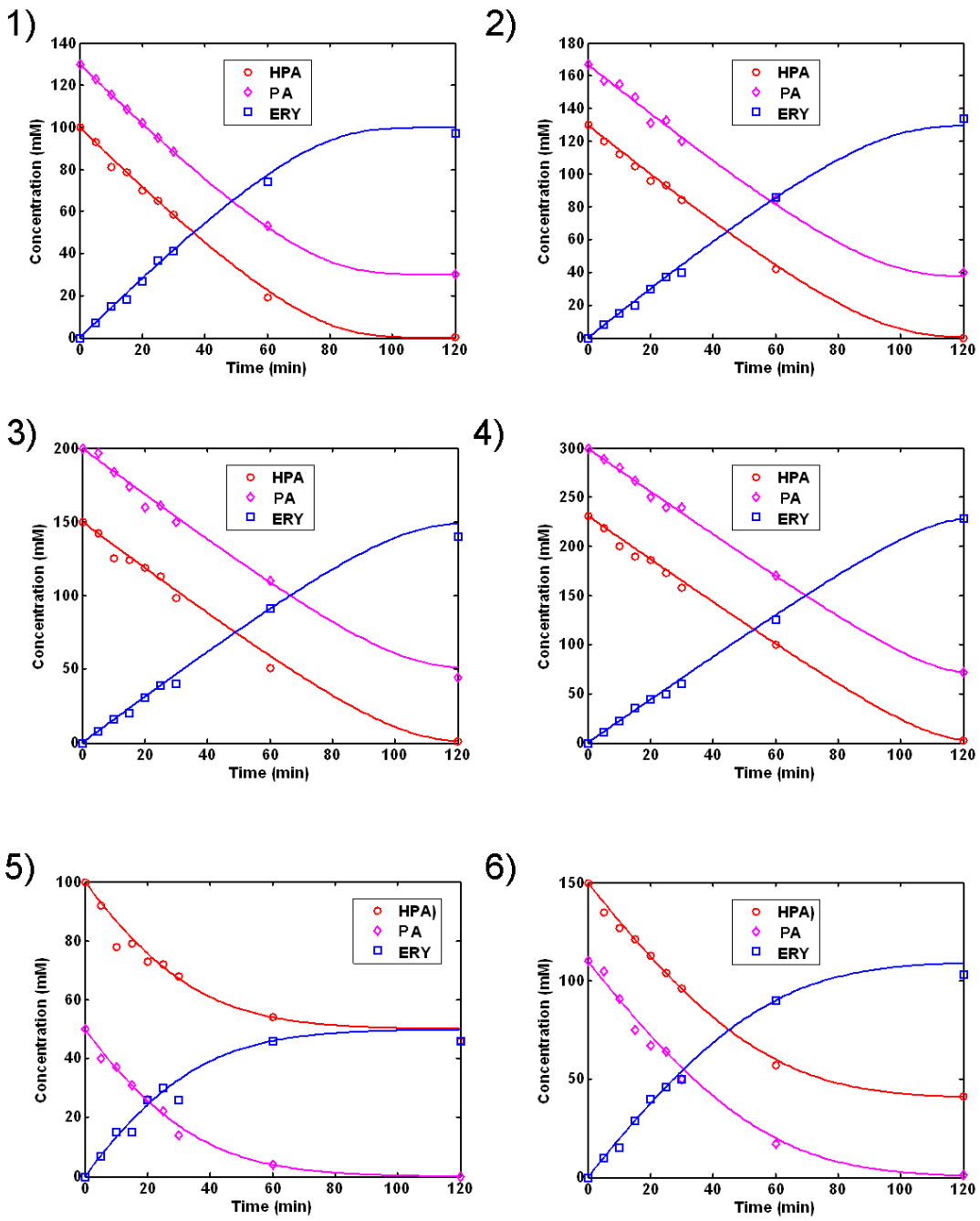

Figure A.IX.1. **Progress curves of whole cell TK D469E mediated synthesis of PKD from substrates PA and HPA. The number of each graph relates with the initial concentrations of substrates and enzyme described in Table A.IX.1. Modelling was performed with Equation 6.1 and the parameters from Table 6.1 and is shown in solid lines.**

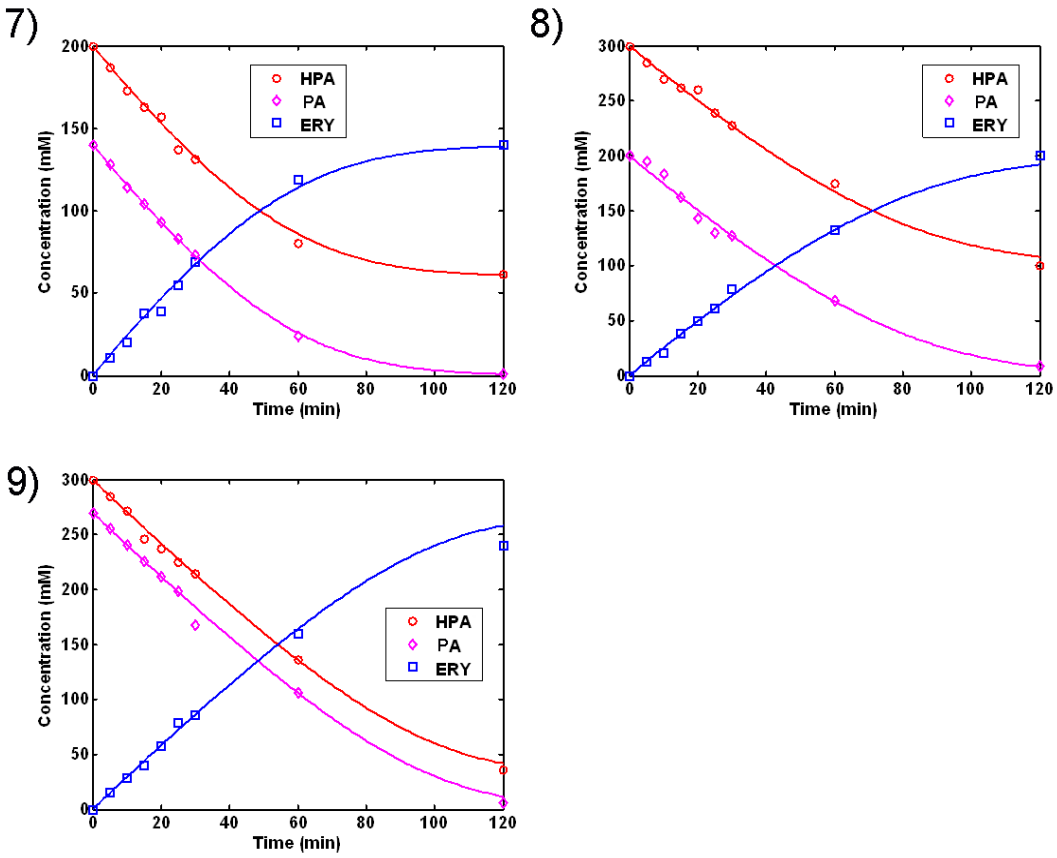

Figure A.IX. 2. Progress curves of whole cell TK D469E mediated synthesis of PKD from substrates PA and HPA (continuation from Figure A.IX.1). The number of each graph relates with the initial concentrations of substrates and enzyme described in Table A.IX.1. Modelling was performed with Equation 6.1 and the parameters from Table 6.1 and is shown in solid lines.

APPENDIX X

PROGRESS CURVES WITH MODEL PREDICTIONS FOR THE TAM SYNTHESIS OF APD

Table A.X. 1. Initial experimental substrate and enzyme concentrations for the 9 progress curves used to obtain the kinetic parameters in Steps 4 and 5 of the methodology described in Figure 4.1 for the synthesis of APD using CV2025 TAm whole cells. The concentration of PLP was 0.2 mM at 30°C and pH 7.5 in 200 mM HEPES for all the progress curves.

No progress curve	1	2	3	4	5	6	7	8	9
[PKD] (mM)	50	70	100	250	300	150	200	300	10
[MBA] (mM)	100	250	250	40	30	15	50	200	120
E_i mg ml^{-1}	0.3	0.4	0.3	0.15	0.15	0.15	0.15	0.6	0.3

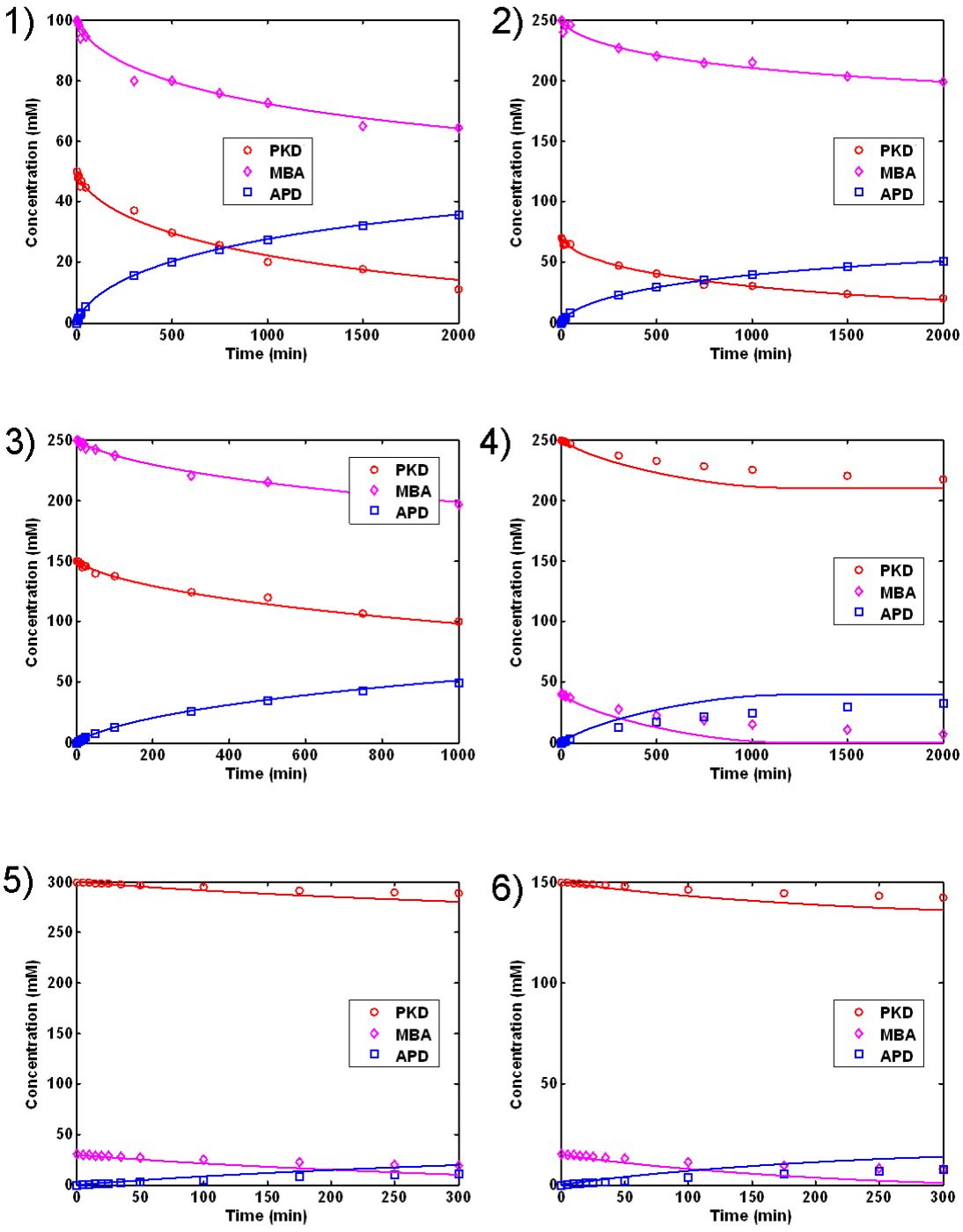

Figure A.X.1. **Progress curves of whole cell TK mediated synthesis of APD from substrates PKD and MBA. The number of each graph relates with the initial concentrations of substrates and enzyme described in Table A.X.1. Modelling was performed with Equation 6.2 and the parameters from Table 6.2 and is shown in solid lines.**

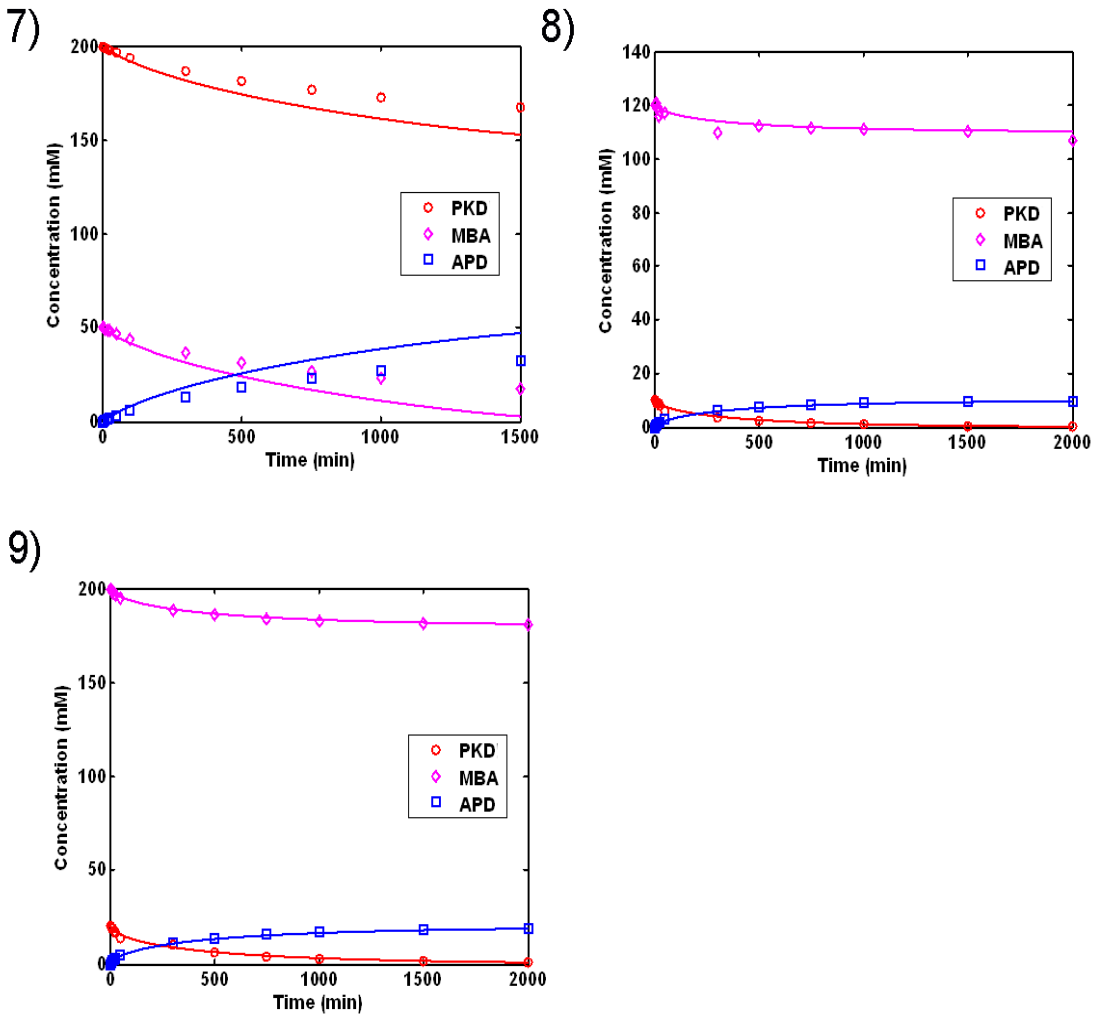

Figure A.X.2. **Progress curves of whole cell TK mediated synthesis of PKD from substrates PKD and MBA (Continuation from Figure A.X.1). The number of each graph relates with the initial concentrations of substrates and enzyme described in Table A.X.1. Modelling was performed with Equation 6.2 and the parameters from Table 6.2 and is shown in solid lines.**

APPENDIX XI

PROGRESS CURVES OF THE TAM MEDIATED SYNTHESIS OF ABT AND APD USING IPA AS AMINO DONOR

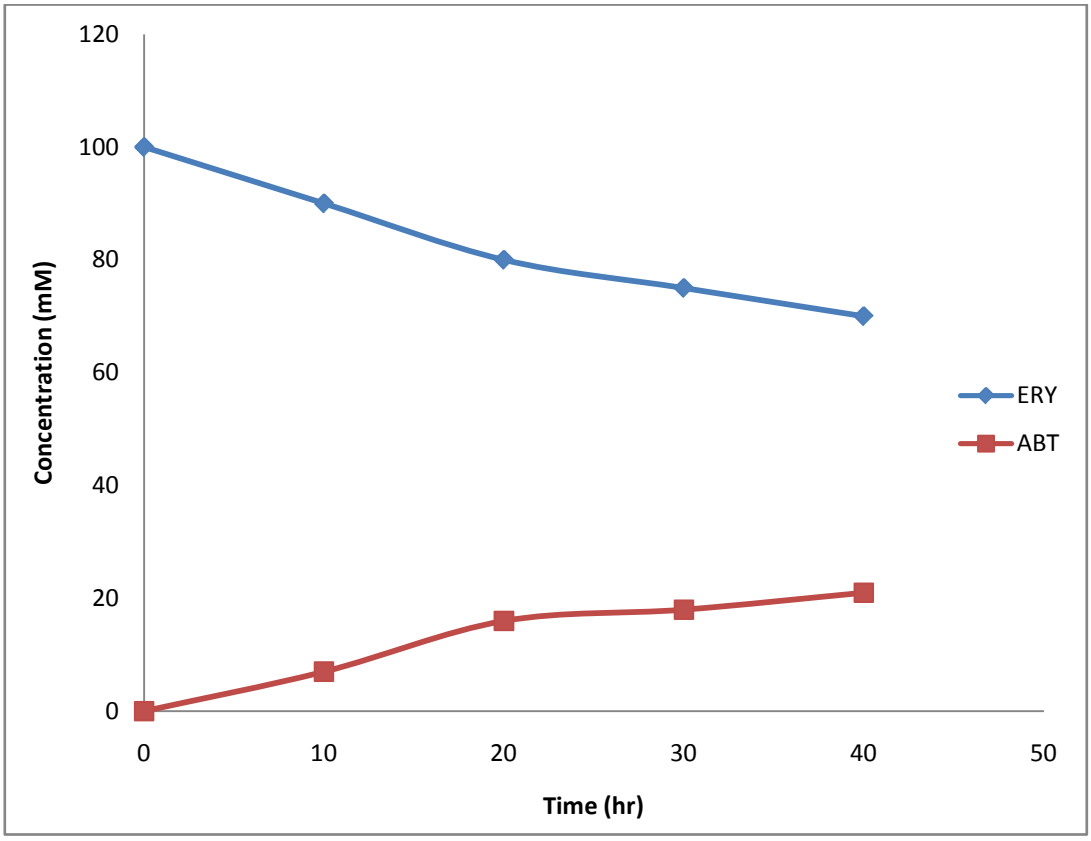

A.XI. 1. TAm mediated synthesis of ABT with IPA as amino donor. ERY and IPA were 100 mM, 0.3 mg ml^{-1} of TAm in whole cell form, pH 7.5 in 200 mM HEPES buffer at 30^{o}C. Bioconversions performed as described in Section 2.8.1.

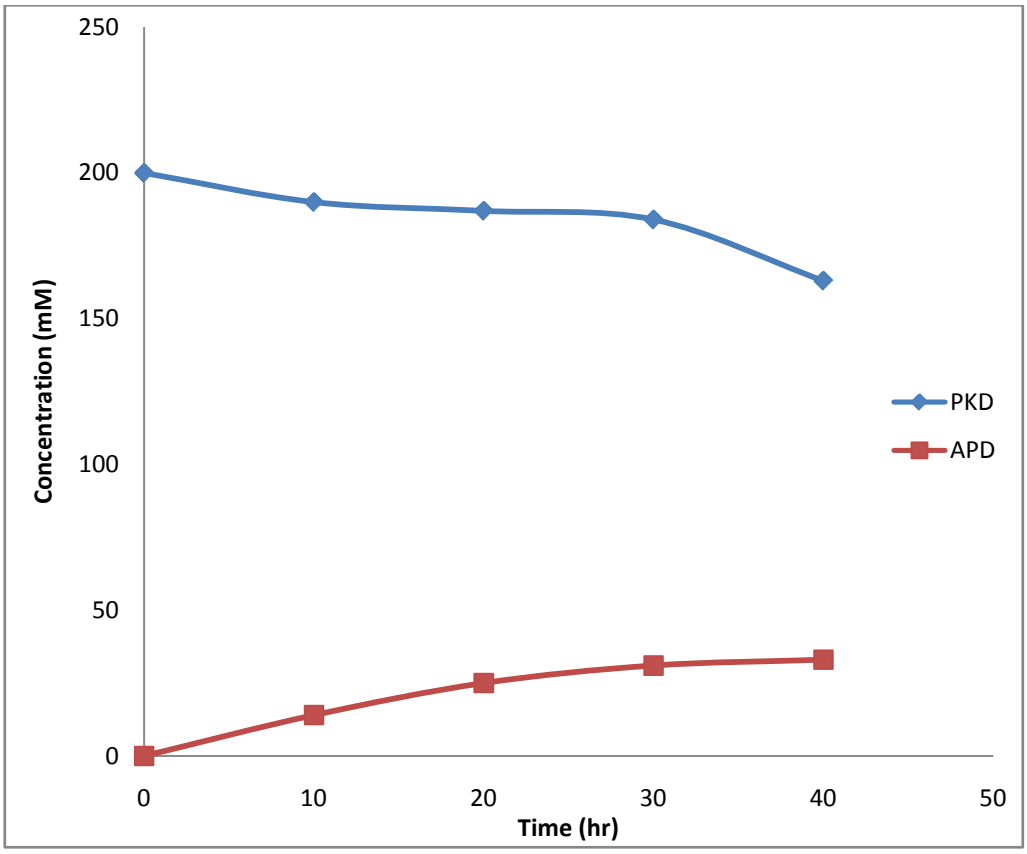

A.XI. 2. TAm mediated synthesis of APD with IPA as amino donor. PKD and IPA were 200 mM, 0.3 mg ml-1 of TAm in whole cell form, pH 7.5 in 200 mM HEPES buffer at 30°C. Bioconversion performed as described in Section 2.8.1.

APPENDIX XII

LC–ECI–MS CHROMATOGRAMS

LC-ECI-MS analysis was carried out on reaction mixture with ABT produced from a single TAm bioconversion using MBA and ERY as subtrates (Figure A.XI.1), and from dual TK-TAm reaction (Scheme 3.1). Results were compared with previous ABT MS-MS standards (Matosevic, 2009).

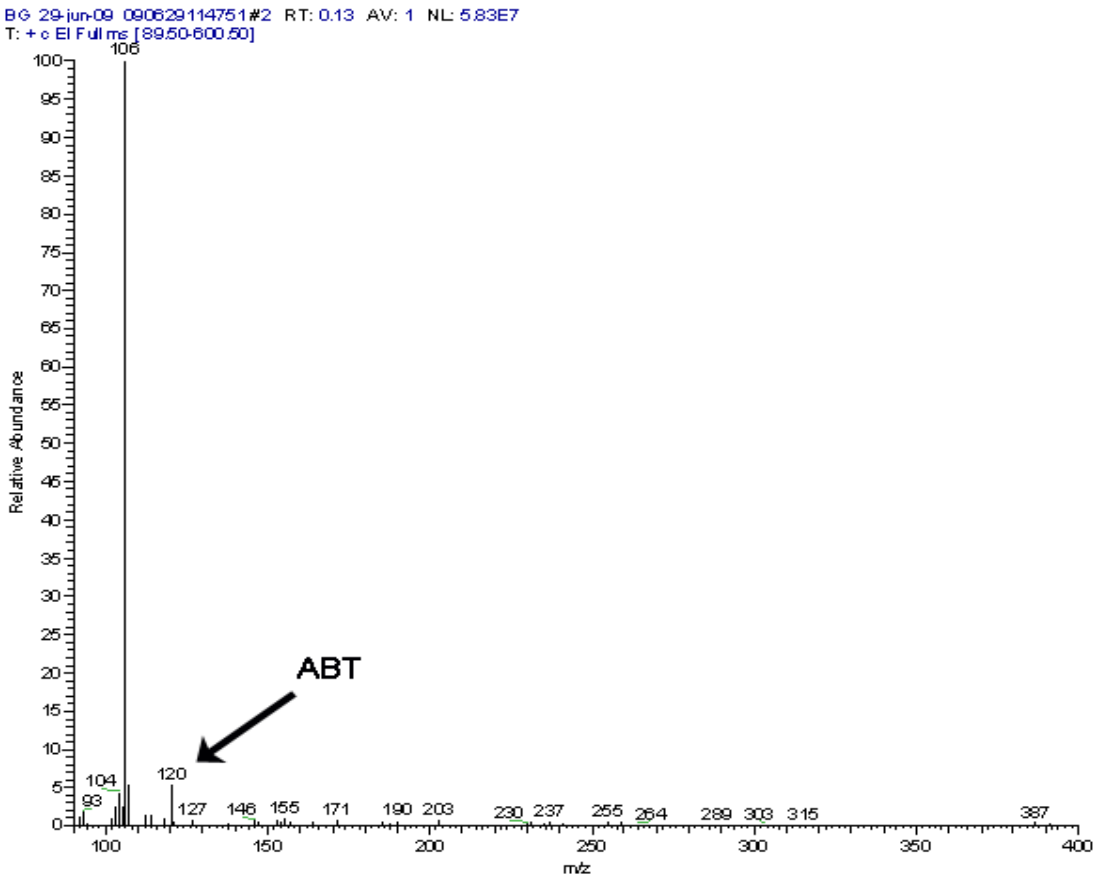

Appendix A.XII. 1. LC-ECI-MS analysis for reaction mixture with ABT produced from individual TAm bioconversion using ERY and MBA as substrates (Section 2.9.7).

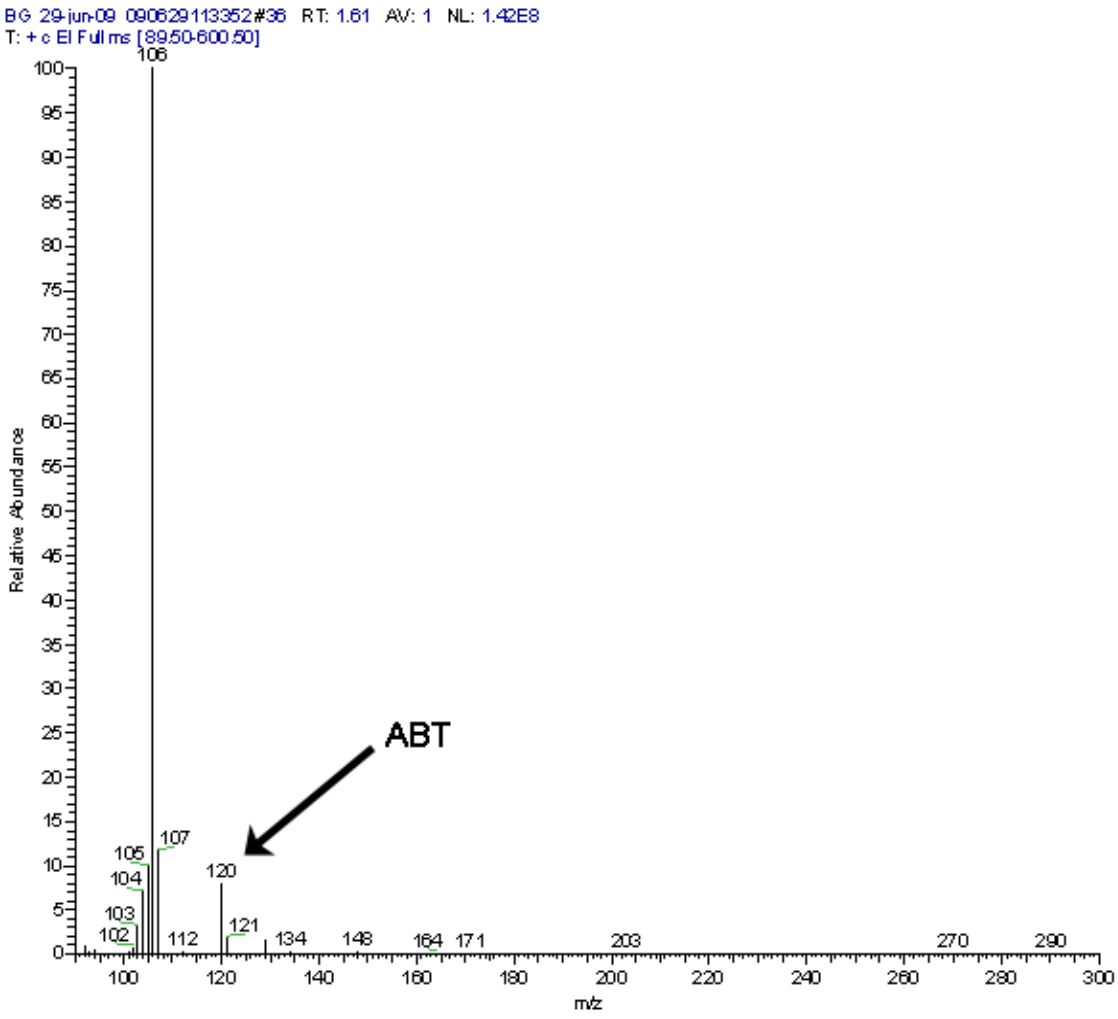

Appendix A.XII. 2. LC-ECI-MS analysis for reaction mixture with ABT produced from dual-TK-TAm multi-step bioconversion (Scheme 3.1) (Section 2.9.7).